

ÉCOLE DOCTORALE des sciences de la vie et de la santé (ED 414)

Génétique Moléculaire, Génomique, Microbiologie (GMGM)

UMR 7156, Université de Strasbourg/CNRS

THÈSE présentée par :

Carmen LÁZARO SÁNCHEZ

soutenue le : **04 décembre 2024**

pour obtenir le grade de : **Docteur de l'université de Strasbourg**

Discipline/ Spécialité : Toxicologie et biologie de l'environnement

**Microbial degradation of dichloromethane in aquifers:
diversity, community dynamics
and stability of the function
in response to changes in physicochemical parameters**

THÈSE dirigée par :

Mme MULLER Emilie

Chargée de recherches, Université de Strasbourg

RAPPORTEURS :

M. CHAPLEUR Olivier

Chargé de recherche, INRAE Anthony

M. MARTIN-LAURENT Fabrice

Directeur de recherche, INRAE Dijon

AUTRES MEMBRES DU JURY :

Mme ARSENE-PLOETZE Florence

Professeure, Université de Strasbourg

Acknowledgments

This research was funded by the doctoral school ‘École des sciences de la vie et la santé’ (ED 414) of the University of Strasbourg, and it was part of the EC2CO-DéGra program. All the work was carried out within the research unit “Génomique Moléculaire, Génétique et Microbiologie” (UMR 7156 - CNRS), where I was warmly welcomed from the start. I would like to take this opportunity to thank all the members for their support over these years.

I would like to thank the jury members for accepting evaluating this PhD thesis: Olivier Chapleur, Fabrice Laurent-Martin and Florence Arsène-Ploetze. I also extend my gratitude to the members of the CSI commission that helped me during the course of my thesis: Claudine Bleykasten-Grosshans and Valérie Geoffroy.

I am immensely grateful to my thesis supervisor, Emilie Muller. Thank you for your empathy, kindness, and full support over these three years (plus two years pre-thesis). Thank you for always finding the bright side of things and guiding me toward it when I was lost in frustration during the (many) challenges we faced in this project. Over this long journey of supervision, you guided me through the fascinating world of microbial ecology, sharing with me your passion for this field – a gift for which I am deeply thankful.

I want also to express my gratitude to the other members in the AIME team. To Stephane, thank you for giving me the first opportunity to join this lab and the guidance and help you offer me since then. To Catherine, Ethan, Françoise, and Thierry, thank you for always being ready to help, for your countless advices, and for your kindness over these years. It was a pleasure working with all of you. And lastly but certainly not least, a huge thank you to my two officemates, Enrico and Lucile, for always bringing ‘a bit’ of fun to the lab and for always being available for laughing about our stressful days. Enrico, thank you for bringing your South-European energy to the lab, your passion for having fun with science, and for always ‘forcing’ us, asocial people, to eat and drink together. Lucile, thank you for your immense generosity (tu es trop chooouuuuu), your warm friendship, the endless daily gossip, and, most importantly, your always delicious cakes and cookies (I will definitively miss them!).

I am also very grateful for the help provided by Gwenaël Imfeld and Benoit Guyot, from the ITES team. To Gwenaël, thank you for the scientific discussions and all the support you have provided me over all these years, especially for giving me the opportunity to use the GC-MS for this work. To Benoit, thank you for your constant willingness to help and your patience with all the issues we faced with the GC-MS (and sorry for all the syringes that were broken!).

Aside from my team members and collaborators, during the 6 years I lived in Strasbourg, I have been lucky to meet some amazing people that will be always a part of my journey here. Even though most have already moved on to exciting new paths, I just want to thank them for making this adventure more fun and fuller of kindness: Sara, Mauricio, Paula, Jordi, Jana,

Tetyana, PO, Mouna, Matéo, Anouk, Adrien, Domitille, Maria, Marine, Victoria, Patricio, Solène, Nikita, Carmen, Gauthier, Pia and Marion.

The most special and heartfelt thank you goes to my little *estrasburguiense* family, who always made me feel at home and provided me a safe and ‘sunny’ net of support and love in the sometimes cloudy environment of this city. Lúlu, thank you for being my first and best friend (bffff), and for instilling in me your passion for the DCM (what dcmito joined, only dcmito can break). Dani, my fav roomie, thank you for always being there and for listening to my endless, muddle, and most of the time useless stories. And Gil, o meu companheiro de vida, thank you for your patience, your infinite support, and for always making me laugh. I admire you with all my heart. A los tres, subiría y bajaría la montaña eternamente con *vosotros*, pero solo si acaba en un abrazo infinito que trascienda kilómetros, fronteras y tiempos.

Y para acabar, quiero agradecer a mis cuatro pilares de vida, papá, mamá, Pedro y Teresa, por vuestro apoyo incondicional a pesar de la distancia. A mis hermanos, gracias por haberme inspirado durante toda mi vida, tanto a nivel académico como a nivel personal, sin lo cual no sería la persona que soy hoy. A mis padres, gracias por acompañarme, ayudarme, y dejarme siempre volar, y por ser el lugar seguro y lleno de amor al que siempre volver cuando estoy perdida. Sin vosotros, sin duda, esto no habría sido posible.

Table of contents

Acknowledgments	i
List of figures	ix
List of tables	xv
Abbreviations	xvii
Chapter I - General introduction	1
I.1 Dichloromethane	3
I.1.1 Properties and environmental distribution	3
I.1.2 Remediation of DCM	7
I.1.3 Microbial utilisation of DCM	9
I.1.3.1 Aerobic biodegradation of DCM.....	10
I.1.3.2 Anaerobic biodegradation of DCM	13
I.2 DCM biodegradation in aquifers.....	16
I.2.1 What is an aquifer	17
I.2.2 Impact of disturbances in the environment	19
I.2.3 Impact of water level fluctuations on DCM biodegradation	24
I.3 Aims and general approach.....	26
I.3.1 Thesis aim and research questions	26
I.3.2 General approach	26
Chapter II - Materials and Methods	29
II.1 Chemicals and reagents.....	32
II.2 Culture media	32
II.3 Microbial inocula and cultivation.....	33
II.3.1 Pure bacterial strains.....	33
II.3.2 Natural microbial community	34
II.4 Analytical methods	35
II.4.1 Gas chromatography (GC).....	35
II.4.1.1 GC-FID	35
II.4.1.2 GC-FID-MS.....	36
II.4.2 Oxygen measurements.....	37

II.4.3 pH measurements	37
II.4.4 Optical Density (OD ₆₀₀) measurements.....	37
II.5 Molecular biology methods.....	37
II.5.1 DNA	37
II.5.1.1 DNA extraction.....	37
II.5.1.2 DNA quantification.....	38
II.5.1.3 PCR	38
II.5.1.4 Agarose gel electrophoresis	39
II.5.1.5 PCR products purification and sequencing	39
II.5.1.6 <i>In silico</i> analysis of the sequenced PCR products	39
II.5.2 RNA.....	41
II.5.2.1 RNA extraction	41
II.5.2.2 RNA quantification	42
II.5.2.3 Determination of RNA quality	42
II.6 Bacterial community analysis.....	43
II.6.1 16S ribosomal RNA (rRNA) gene amplicon sequencing.....	43
II.6.1.1 Illumina NovaSeq 6000 platform.....	43
II.6.1.2 Illumina NextSeq 2000 platform	44
II.6.2 Data pre-processing	44
II.6.3 Data normalization and transformation.....	44
II.6.4 Metabarcoding data analysis	45
II.6.4.1 Alpha-diversity analyses.....	45
II.6.4.2 Beta-diversity analyses.....	45
II.7 <i>Hyphomicrobium</i> sp. GJ21 transcriptome.....	46
II.7.1 Whole-transcriptome sequencing	46
II.7.2 RNA-seq reads quality control.....	47
II.7.3 RNA-seq reads mapping to the reference genome	47
II.7.4 Quantification of number of reads per annotated gene.....	47
II.7.5 Analysis of the differential gene expression.....	48

Chapter III - Impact of water content and oxygen status on a DCM-degrading microbial community	49
III.1 Introduction.....	51
III.2 Materials and Methods.....	52
III.2.1 Laboratory microcosms' set up and experimental design	52
III.2.1.1 Inoculum.....	52
III.2.1.2 Laboratory microcosms with different water content	52
III.2.1.3 Laboratory microcosms with different oxygen status.....	53
III.2.1.4 Summary of the laboratory microcosms' set up	55
III.2.2 Monitoring of DCM degradation.....	57
III.2.3 Molecular biology analysis	57
III.2.3.1 DNA extraction from sand matrix.....	57
III.2.3.2 Primer design.....	57
III.2.3.2 Biomarker genes detection and <i>in silico</i> analyses	58
III.2.3.3 16S rRNA gene amplicon sequencing and data analysis	59
III.3 Results	59
III.3.1 DCM degradation kinetics	59
III.3.1.1 Impact of water content.....	60
III.3.1.2 Impact of oxygen status	62
III.3.2 Presence of biomarker genes for DCM biodegradation	66
III.3.3 Composition of the microbial community.....	68
III.3.3.1 Microcosms with different water content	68
III.3.3.2 Microcosms with different oxygen status	72
III.4 Discussion	77
III.4.1 Impact of water content on DCM degradation kinetics and microbial community composition	77
III.4.2 Impact of oxygen status on DCM biodegradation kinetics and microbial community composition	78
III.4.3 Limitations and improvements of the experimental design	80
III.5 Conclusion	81
Supplementary information - chapter III	83

Chapter IV - Method development and optimisation	87
IV.1 Introduction	89
IV.2 Stabilité des conditions d'oxygénation	900
IV.2.1 Stabilité de la condition oxygène et volume de matrice	90
IV.2.2 Stabilité de la condition anoxique.....	91
IV.3 Sélection de l'inoculum.....	92
IV.4 Sélection de la matrice artificielle.....	94
IV.4.1 Matrice de billes de verre sodo-calcique	94
IV.4.1.1 Maintien du pH	94
IV.4.1.2 Biodégradation du DCM en présence de la matrice artificielle.....	95
IV.4.2 Matrice de billes en verre/zirconium.....	96
IV.4.2.1 Maintien du pH	96
IV.4.2.2. Biodégradation du DCM en présence de la matrice artificielle	97
IV.5 Détermination de la capacité de rétention d'eau des matrices artificielles en fonction de leur diamètre.....	98
IV.6 Optimisation de la quantité de matrice artificielle à utiliser pour l'extraction d'ADN	100
IV.6 Limites de détection (LOD) et quantification (LOQ)	101
IV.7. Résumée des paramètres choisis	104
Chapter V - Impact of matrix granulometry on the response of a DCM-degrading microbial community to water content and oxygen status.....	105
V.1 Introduction.....	107
V.2 Materials and Methods	108
V.2.1 Set up of laboratory microcosms	108
V.2.2 Experimental design.....	110
V.2.3 Monitoring of DCM concentrations	111
V.2.3.1 Data treatment	111
V.2.4 Molecular biology analysis	112
V.2.4.1 DNA extraction	112
V.2.4.2 Detection of biomarkers and <i>in silico</i> analyses	112
V.2.4.3 16S rRNA gene amplicon sequencing and data analysis	112

V.3 Results.....	113
V.3.1 DCM degradation kinetics depending on experimental conditions	113
V.3.2 Presence of biomarker genes for DCM biodegradation	117
V.3.3 Analysis of microbial community composition in relation to experimental conditions	119
V.3.3.1 Impact of physicochemical parameters on microbial taxonomical composition.....	119
V.3.3.2 Impact of physicochemical parameters on the richness, evenness and diversity.....	127
V.3.3.3 Impact of physicochemical parameters on beta-diversity.....	130
V.3.3.4 Correlation between physicochemical parameters and bacterial community composition.....	134
V.4 Discussion	141
V.4.1 Impact of physicochemical parameters on DCM degradation kinetics and microbial community composition.....	141
V.4.2 Response of DCM-degrading microbial community to a change in oxygen status.....	145
V.5 Conclusions	146
Supplementary information - chapter V	149
Chapter VI - Effect of oxygen concentration on <i>Hyphomicrobium</i> sp. GJ21 gene expression.....	151
VI.1 Introduction	153
VI.2 Materials and methods	155
VI.2.1 Cultivation of the model strain <i>Hyphomicrobium</i> sp. GJ21.....	155
VI.2.1.1 Characterisation of growth.....	155
VI.2.1.2 Preparation of cultures for RNA extraction	155
VI.2.2 Molecular biology analysis.....	157
VI.2.2.1 RNA extraction from <i>Hyphomicrobium</i> sp. GJ21 cultures.....	157
VI.2.3 RNA characterization.....	157
VI.2.4 Whole transcriptomics sequencing and data analysis.....	157
VI.3 Results	158
VI.3.1 Growth monitoring of <i>Hyphomicrobium</i> sp. GJ21.....	158

VI.3.2 Quantification of gene expression	159
VI.3.3 Differential gene expression in response to oxygen concentration	160
VI.4 Discussion.....	167
VI.5 Conclusions.....	169
Supplementary data - Chapter VI.....	171
Chapter VII - General conclusions and perspectives.....	173
VII.1 Conclusions.....	175
VII.2 Experimental limitations	177
VII.3 Perspectives.....	179
VII.3.1 Characterisation of ecological niches and DCM-degrading taxa	179
VII.3.2 Importance of matrix grain size vs. porosity and converging to on-site conditions	181
VII.3.3 Exploration of the role of PQQ under anoxic conditions	182
VII.3.4 Other future perspectives	183
References	188
Annexe I	211
Annexe II	227

List of figures

Figure I.1. Major reported sources of DCM emission in the environment	3
Figure I.2. Two main DCM degradation pathways in the human liver	5
Figure I.3. Anthropogenic DCM emissions to the atmosphere	6
Figure I.4. Former industrial site of Themeroil and well locations	9
Figure I.5. Proposed co-metabolic pathways for enzymatic DCM degradation	10
Figure I.6. Proposed metabolic pathway for DCM utilization as sole carbon and energy source in the model strain <i>M. extorquens</i> DM4	11
Figure I.7. Comparison of the <i>dcm</i> genes of <i>Hyphomicrobium</i> sp. MC8b, <i>H. denitrificans</i> ATCC 51888 and <i>Hyphomicrobium</i> sp. GJ21 with those in the model strain <i>M. extorquens</i> DM4	12
Figure I.8. Example of a CSIA dual plot for the degradation of DCM	13
Figure I.9. Proposed metabolic pathways for DCM utilization as growth substrate under anoxic conditions	14
Figure I.10. <i>mec</i> cassettes and close homologs identified in the genomes of the known anaerobic DCM-degrading bacteria strains and populations	15
Figure I.11. Proposed pathway for the initial steps of DCM transformation under anoxic conditions in <i>D. formicoaceticum</i> strain EZ94	16
Figure I.12. Overview of the aquifer system	18
Figure I.13. Gradients of physicochemical parameters and microbial community characteristics established from the unsaturated to the saturated zone	19
Figure I.14. Disturbance types	20
Figure I.15. Possible outcomes of microbial community responses to a disturbance in terms of the function of interest and taxonomic diversity over time	22
Figure I.16. GLF effects on soil microbial community and geochemical components	23
Figure I.17. Study of the impact of GLF on DCM degradation and microbial community composition in laboratory-scale aquifers	25
Figure I.18. Research questions	28

Figure II.1. Picture of laboratory culture systems	34
Figure II.2. Preparation of microcosms with the natural microbial community inoculum	35
Figure II.3. Quality assessment of the total RNA using the Agilent RNA 6000 Nanopore Assay	43
Figure II.4. Workflow for the microbial community analysis	46
Figure II.5. Workflow for the analysis of the whole-transcriptome sequencing data	48
Figure III.1. Experimental set-up to investigate the impact of water content on DCM-degrading microbial populations	53
Figure III.2. Experimental set-up to investigate the impact of oxygen concentration on DCM-degrading microbial populations	55
Figure III.3. Impact of the water content on the DCM degradation	61
Figure III.4. Impact of the oxygen status on DCM degradation	64
Figure III.5. Phylogenetic tree of the <i>dcmA</i> sequences recovered from the microcosms with different water content or oxygen status	68
Figure III.6. Family-level relative abundances at the beginning and at the end of the experiment of microcosms exposed to different water content	70
Figure III.7. Microbial community diversity indices of microcosms exposed to different water content	71
Figure III.8. Principal Coordinate Analysis plot derived from clr-transformed abundance data at the genus-level phylotype in the environmental samples exposed to different water contents	72
Figure III.9. Family-level relative abundances at the beginning and at the end of the experiment in microcosms exposed to different oxygen statuses	74
Figure III.10. Microbial community diversity indices of microcosms exposed to different oxygen statuses	75
Figure III.11. PCA plot derived from clr-transformed abundance data at the genus-level phylotypes in the environmental samples exposed to different oxygen statuses	76

Figure IV.1. Aperçu synthétique des questionnements techniques pour la détermination de la configuration expérimentale de la prochaine expérience	90
Figure IV.2. Stabilité de la condition oxiqne dans les vials de 20 mL	91
Figure IV.3. Test de maintien des conditions hermétiques en fonction du montage des microcosmes	92
Figure IV.4. Dégradation microbienne du DCM en fonction de l'origine de l'inoculum environnemental	93
Figure IV.5. Maintien du pH au cours du temps dans les différents milieux SGW après contact avec la matrice artificielle de verre sodocalcique à différente granulométrie	95
Figure IV.6. Dégradation du DCM au cours du temps en fonction de la granulométrie de la matrice de verre sodocalcique	96
Figure IV.7. Maintien du pH au cours du temps dans les milieux SGW après contact avec la matrice artificielle de billes de verre/zirconium à différente granulométrie	97
Figure IV.8. Dégradation du DCM au cours du temps en fonction de la granulométrie de la matrice artificielle de verre/zirconium	98
Figure IV.9. Détermination de la capacité de rétention d'eau (CRE) de chaque matrice artificielle	99
Figure IV.10. Concentration d'ADN extraite pour chaque taille de billes en fonction de la masse de billes échantillonnées	100
Figure IV.11. Courbes d'étalonnage déterminant les limites de détection (LOD) et quantification (LOQ) par condition expérimentale	103
Figure IV.12. Réponses apportées aux questionnements initialement posées suite aux développements méthodologiques présentés dans ce chapitre	104
Figure V.1. Preparation of the initial inoculum according to the type of microcosm	109
Figure V.2. Experimental design	111
Figure V.3. DCM degradation depending on matrix grain size and water content in different oxic conditions before and after the disturbance	116
Figure V.4. Relative abundances at the family-level at To, T-bef and T-aft in the abiotic controls	120

Figure V.5. Relative abundances at the family-level at To, T-bef and T-aft in the biotic controls	121
Figure V.6. Relative abundances at the family-level at To, T-bef and T-aft in the environmental samples before the disturbance	124
Figure V.7. Relative abundances at the family-level at To, T-bef and T-aft in the environmental samples after the disturbance	126
Figure V.8. Microbial community diversity in the environmental samples depending on the grain size matrix	127
Figure V.9. Microbial community diversity in the environmental samples before the disturbance as a function of oxygen status	128
Figure V.10. Microbial community diversity in the environmental samples after the disturbance as a function of oxygen status	129
Figure V.11. Microbial community diversity in the environmental samples as a function of water content	130
Figure V.12. PCA plot derived from clr-transformed abundance data of the genus-level phylotypes in the environmental samples at the beginning of the experiment and before the disturbance and at the end of the experiment	131
Figure V.13. PCA plot derived from clr-transformed abundance data of the genus-level phylotypes in the environmental samples before disturbance across matrix grain sizes	132
Figure V.14. PCA plot derived from clr-transformed abundance data of the genus-level phylotypes in the OO and AA environmental sample microcosms before disturbance and at the end of the experiment across matrix grain sizes	133
Figure V.15. PCA plot derived from clr-transformed abundance data of the genus-level phylotypes in the environmental samples at the end of the experiment across matrix grain sizes	134
Figure V.16. Heatmap displaying the Spearman correlation coefficients between the relative abundance of specific genera before the disturbance and the physicochemical parameters as well as the observed degradation rate	137
Figure V.17. Heatmap displaying the Spearman correlation coefficients between the relative abundance of specific genera after the disturbance and the physicochemical parameters as well as the observed degradation rate	138
Figure V.18. Relationship between soil water content and microbial activity	143

Figure VI.1. Respiratory chains during denitrification and aerobic respiration	154
Figure VI.2. Preparation of <i>Hyphomicrobium</i> sp. GJ21 cultures for RNA extraction	156
Figure VI.3. <i>Hyphomicrobium</i> sp. GJ21 growth curves under oxic or anoxic conditions	158
Figure VI.4. Growth curve of the <i>Hyphomicrobium</i> sp. GJ21 cultures and harvesting points for total RNA extraction under oxic and anoxic conditions	159
Figure VI.5. Venn diagram of the core and specific transcriptomes as a function of the oxygen status	160
Figure VI.6. Heatmap plot based on the Euclidean distances among samples in terms of gene expression	161
Figure VI.7. Volcano plot of the differentially expressed genes in <i>Hyphomicrobium</i> sp. GJ21 when exposed to oxic conditions compared to anoxic conditions	164
Figure VI.8. Genomic regions containing several genes found in the top 20 most overexpressed genes under anoxic conditions	165
Figure VI.9. Genomic region containing genes found in the top 20 most overexpressed genes under oxic conditions	166
Figure VII.1. Visual summary of the conclusions obtained during this PhD work	177
Figure VII.2. Characterisation of matrix impact	182

List of tables

Table I.1. Physicochemical properties, environmental behaviour, and toxicology data of DCM	4
Table II.1. Summary of the experimental work associated to the experimental chapters .	31
Table II.2. Composition of the defined media M3Clo and SGW	32
Table II.3. Oligonucleotides and PCR parameters	40
Table II.4. PCR programs used	41
Table II.5. Parameters used for filtering and trimming demultiplexed raw data in DADA2 pipeline	44
Table III.1. Summary of the laboratory microcosms' set up	56
Table III.2. Newly designed primer pairs for amplifying the loci of the <i>dcm</i> cluster	58
Table III.3. DCM half-life during each pulse at each tested water content in the abiotic controls, biotic controls and environmental samples	62
Table III.4. DCM half-life during each pulse depending on the oxygen status in the abiotic controls, biotic controls and environmental samples	65
Table III.5. Presence of <i>dcmA</i> and <i>mecE-F</i> genes biomarkers for the DCM degradation in microcosms with different water content, or oxygen statuses	67
Table IV.1. pH du milieu SGW avant et après contact avec la matrice artificielle en verre sodo-calcique à différente taille de billes	94
Table IV.2. Récapitulatif des CRE et volumes à rajouter en fonction de la granulométrie de la matrice artificielle	99
Table V.1. Summary of microcosms' set up according to the initial experimental conditions	109
Table V.2. Detection of <i>dcmA</i> and <i>mecE-F</i> biomarkers for DCM degradation before the disturbance	118

Table V.3. Detection of <i>dcmA</i> and <i>mecE-F</i> biomarkers for the DCM degradation at the end of the experiment	118
Table V.4. Indicator species in the environmental samples along the experiment	139
Table VI.1. Summary of reads per sample of reads obtained before and after trimming, reads that aligned to the <i>Hyphomicrobium</i> sp. GJ21 genome and reads that mapped to predicted genes	160
Table VI.2. Differentially expressed genes in each COG category and functional group	162
Table VI.3. Differentially expressed genes whose expression was at least doubled in one of the oxygen concentrations compared to the other one	163
Table VI.4. Top 20 most overexpressed genes in <i>Hyphomicrobium</i> sp. GJ21 under anoxic conditions compared to oxic conditions	165
Table VI.5. Top 20 most overexpressed genes in <i>Hyphomicrobium</i> sp. GJ21 under oxic conditions compared to anoxic conditions.	166

Abbreviations

aLRT: Approximate likelihood-ratio test

ANOVA: Analysis of variance

ASV: Amplicon sequence variant

BLAST: Basic local alignment search tool

clr: centered-log ratio

COG: Cluster of orthologous groups

CSIA: Compound specific isotope analysis

DCM: Dichloromethane

DNA: Deoxyribonucleic acid

DMSO: Dimethyl sulfoxide

FC: Fold change

GC-FID: Gas chromatography equipped with a flame ionization detector

GC-FID-MS: Gas chromatography equipped with a flame ionization detector and coupled with a mass spectrometer

GLF: Groundwater level fluctuations

LNAPL: Light Non-Aqueous Phase Liquids

MNA: Monitored Natural Attenuation

MUSCLE: Multiple sequence comparison by log-expectation

M₃Cl₀: *Methylobacterium* mineral medium without chloride

NA: Nutrient Agar

OD₆₀₀: Optical density at 600 nm

PAH: Polycyclic aromatic hydrocarbons

PCA: Principal component analysis

PCR: Polymerase chain reaction

ppm: parts per million

PQQ: Pyrroloquinoline quinone

RIN: RNA Integrity Number

RISA: Ribosomal Intergenic Spacer Analysis

RNA: Ribonucleic acid

SGW: Simulated ground water

Chapter I

General introduction

I.1 Dichloromethane

I.1.1 Properties and environmental distribution

Dichloromethane (DCM), also known as methylene chloride, is an organochloride compound whose chemical formula is CH_2Cl_2 . This compound can originate from natural sources, such as mangroves (Kolusu et al., 2018), volcanic eruptions (Schwandner et al., 2013), biomass combustion (Rudolph et al., 1995), rocks weathering from near-surface and deep subsurface (Mulder et al., 2013), or by micro- and macro-algae (Blackman et al., 1992; Kolusu et al., 2017) (**Figure I.1**). However, the majority of DCM in the environment is the result of anthropogenic emissions (Simmonds et al., 2006). Since its first synthesis by Regnault in 1839, DCM found wide usage as an industrial solvent because of its physico-chemical properties (**Table I.1**): it is colourless, highly volatile and mixes well with water and several organic solvents. From its applications, DCM is used primarily as an extraction and synthesis solvent in the pharmaceutical industry and in the production of polycarbonate plastics. Minor applications include the use of DCM as an extraction solvent in the food industry, for example to remove caffeine from coffee and tea and to extract spices and beer hops, as well as in the manufacture of various commercial products, such as paint strippers and varnishes, degreasing and cleaning agents, and biocides. This extensive use has resulted in significant releases of DCM into the environment, which, due to its toxic and persistent nature, poses problems for human health and the environment itself.

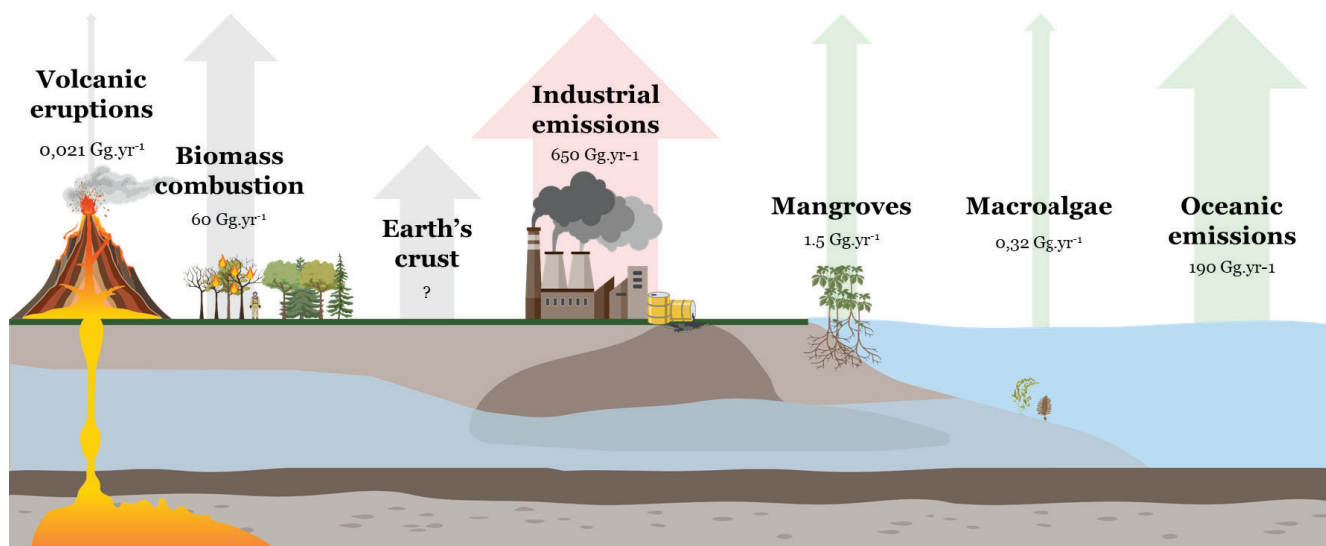


Figure I.1. Major reported sources of DCM emission in the environment. The quantity of DCM emitted by each source (Gg=thousands of tons) per year (yr) is based on data from Gribble (2023) and Kolusu et al. (2018). Green arrows represent biotic sources, grey arrows represent abiotic sources and red arrow represents anthropogenic sources. The size of the arrows indicates the magnitude of DCM emissions.

Table I.1. Physicochemical properties, environmental behaviour, and toxicology data of DCM.

Characteristics	Data ^a
Physicochemical properties	
Name and abbreviation	Dichloromethane (DCM)
Synonymous name	Methylene chloride
Formula	CH ₂ Cl ₂
Molar mass (g.mol ⁻¹)	84.9
Density (g.L ⁻¹)	1.3
Melting temperature (°C)	-96.6
Boiling temperature (°C)	39.7
Solubility at 20°C (g.L ⁻¹)	13.0
Octanol/water partition coefficient (log P _{ow})	1.25
Sorption coefficient distribution (log K _{oc})	1.3 to 1.4
Vapor pressure at 20°C (Kpa)	47
Henry's constant at 20°C (Pa.m ³ .mol ⁻¹)	270
Environmental behaviour	
Half-life in atmosphere	150 days (McCulloch, 2017)
Half-life in water	From weeks to several years (Radding et al., 1977; Zoeteman et al., 1980)
Distribution per compartments (%)	Atmosphere: 99.04 Water: 0.96 Soil and sediments: <0.01
Toxicology data	
Toxicity	Potentially carcinogenic (2A)

^a Data obtained from INERIS except otherwise indicated

In the last decades, toxicological studies have highlighted the potential carcinogenic properties of DCM in humans (Benbrahim-Tallaa et al., 2014), with documented effects on the brain, liver, and kidneys (Schlosser et al., 2015). Consequently, in 2008, the European Union classified DCM as a Category 2 substance, pointing to its suspected carcinogenic effect to humans (proposal COM(2008) 80 final - 2008/0033 (COD)). Furthermore, in 2014, the International Agency for Research in Cancer (IARC) classified DCM in Group 2A, which includes compounds that are probably cancerogenic for humans (Benbrahim-Tallaa et al., 2014). The primary route of DCM exposure in humans is through inhalation (DiVincenzo & Kaplan, 1981), with skin absorption also being of substantial risk (Stewart & Dodd, 1964). Once in the body, DCM is mainly metabolized in the liver, where two metabolic pathways have been identified (**Figure I.2**). The first one, involving the cytochrome P450, is a high affinity, low capacity pathway (threshold of 200 ppm; DiVincenzo & Kaplan, 1981) that results in the oxidation of DCM to carbon monoxide, whose binding to haemoglobin reduces the oxygen-carrying capacity of the blood (Shusterman et al., 1990). The second metabolic pathway is a

low affinity, high capacity pathway (Reitz et al., 1988) catalysed by a specific glutathione S-transferase, GSTT1, and consists of the conjugation of DCM to glutathione. This process results in the formation of two reactive intermediates, S-chloromethyl glutathione and then formaldehyde, which are involved in the genotoxicity and carcinogenicity of DCM (Hashmi et al., 1994). This toxicity has been demonstrated not only in humans, but also by a variety of assays in mammals *in vivo*, in mammalian cells *in vitro*, and in bacteria (Dekant et al., 2021). In general, DCM toxicity has been shown to be organism-dependent: as the toxicity is primarily derived from the metabolism of DCM, the organisms that do not metabolize it effectively are less susceptible, as it is the case with individuals lacking functional alleles for the GSTT1 (Schlosser et al., 2015; Warholm et al., 1994). In July 2024, the Environmental Protection Agency adopted a rule to ban the production and distribution of DCM for all consumer applications, while also restricting its industrial and commercial uses to ensure that DCM no longer presents an unreasonable risk for health (EPA, 2024).

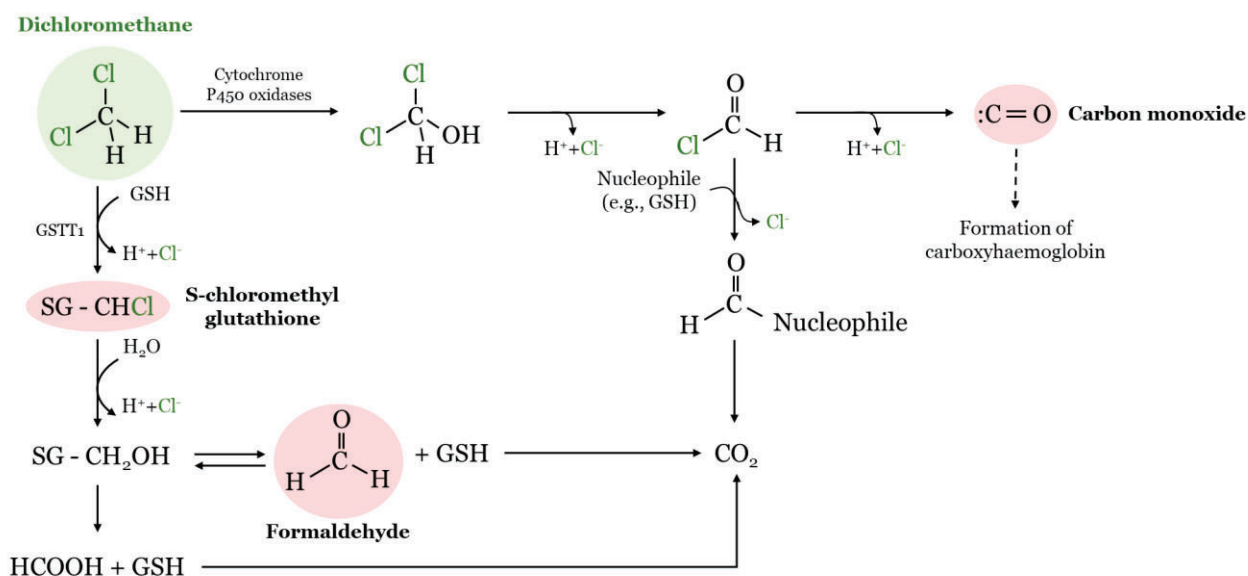


Figure I.2. Two main DCM degradation pathways in the human liver. The first pathway, involving the cytochrome P450, consist of the oxidation of DCM to carbon monoxide, which binds to haemoglobin and reduce its oxygen carrying capacity due to the formation of carboxyhaemoglobin. The second pathway, catalyzed by the glutathione S-transferase GSTT1, results in the formation of two reactive intermediates, S-chloromethyl glutathione and formaldehyde, which are involved in the genotoxicity and carcinogenicity of DCM. Adapted from: [INERIS](#)

In the environment, due to its high volatility, DCM is mainly found in the atmosphere, where it is considered to be the most abundant chlorinated compound. Global DCM emissions to the atmosphere have been estimated at ~1.1 Tg per year by 2020 ([WMO, 2022](#), Bednarz et al., 2023). In a study examining DCM emissions to the atmosphere in China, Feng and colleagues reported that, by 2016, most of these emissions came from its use as a foam agent and as an industrial solvent (more than 40% of total emissions each) (Feng et al., 2018) (**Figure I.3-a.**).

In the atmosphere, DCM is degraded by reaction with hydroxyl radicals, resulting in the release of chlorine radicals (Cl \cdot), which contribute to the photocatalytic destruction of the ozone layer. With an atmospheric half-life of less than 6 months, DCM was thought to have little effect on the stratospheric ozone depletion and was therefore not regulated under the Montreal Protocol (Layer, 1988). However, recent studies have shown that these types of compounds also play an important role in increasing atmospheric chlorine concentrations (Bednarz et al., 2023). Indeed, it is thought that if DCM emissions continue to rise, as it is the case in Asia (**Figure I.3-b.**), this could delay the recovery of the ozone layer by 5 to 30 years, depending on future emissions scenarios (i.e., whether the emissions continue to increase or stabilize at 2019 levels) (An et al., 2021; Hossaini et al., 2017).

A small proportion of DCM (<1 %) is also released into water bodies where the solvent hydrolysis is highly dependent on the environmental conditions. In surface water, the half-life of DCM generally ranges from weeks to several years (Zoeteman et al., 1980), while in groundwater, estimates varies from ~18 months to ~700 years depending on temperature and pH conditions (Dilling et al., 1975; Radding et al., 1977). Hence, DCM is considered a recalcitrant compound in water bodies, especially in groundwater, where volatilization is limited ((Mabey & Mill, 1978); US EPA, 1987).

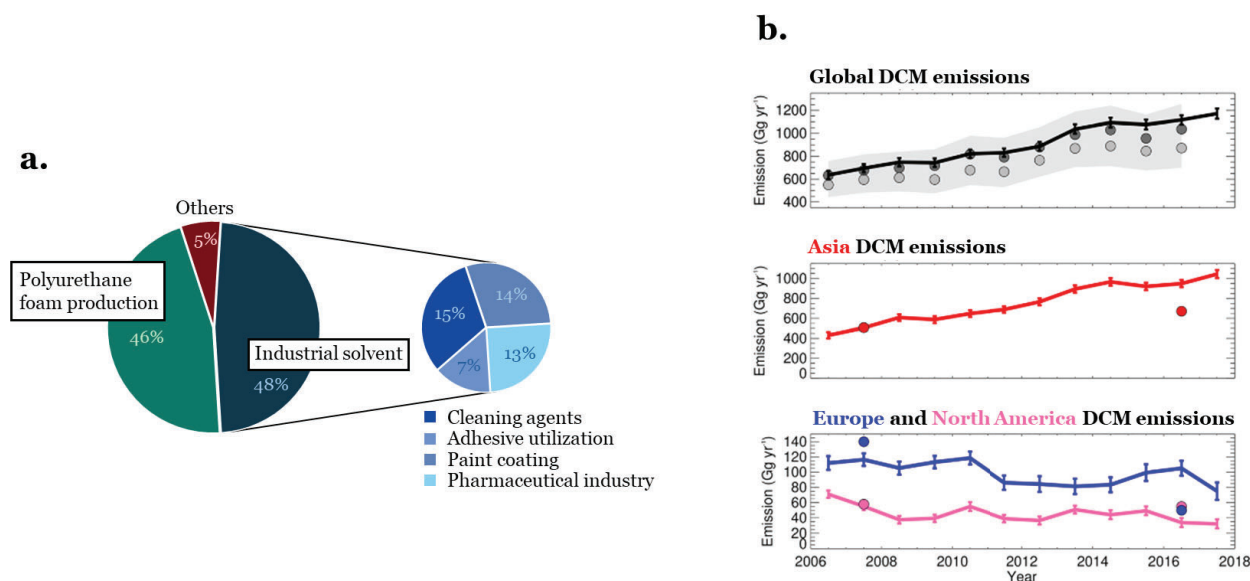


Figure I.3. Anthropogenic DCM emissions to the atmosphere. **a.** DCM emissions by industrial sectors in China for 2016. Data from (Feng et al., 2018). **b.** Evolution of annual DCM emissions over a 12-year period globally, in Asia, and in Europe and North America (from top to bottom). The lines represent observed DCM emissions over the years. The circles represent estimated industrial emissions based on a global industry database of dichloromethane production and production capacity. Figure adapted from Claxton et al. (2020).

Due to its toxicity, persistence and bioaccumulation in surface and subsurface water, DCM was included in the first list of priority pollutants in 1979 (Keith & Telliard, 1979). That same year, the European Council classified the group of organohalogenes, including DCM, as priority pollutants in groundwater under the Council Directive 80/68/EEC. More recently, in 2001, the European Parliament added DCM to the list of priority substances in the domain of the water (Decision 2455/2001/CE) for which measures must be adopted aiming “at the cessation of emissions, discharges and losses into water”. In line with this, the European Union has banned the manufacture, supply and use of paint strippers containing ≥ 0.1 % of DCM since 2012 ([European Chemical Agency, 2012](#)).

I.1.2 Remediation of DCM

Despite recent environmental and health legislation aim at reducing the use of DCM, current production volumes and emissions to the environment remain significant, especially to subsurface waters, and a vast number of sites are considered as polluted. Therefore, various approaches have been developed to remove organohalides, including DCM, from this type of polluted sites. The most commonly used methods include physicochemical approaches, such as air stripping and aeration, adsorption and chemical oxidation, as well as biological remediation (Shestakova & Sillanpää, 2013). Air stripping and aeration, terms often used interchangeably, refer to a process in which a liquid is brought into contact with a gas, allowing undesirable substances in the liquid phase to be carried away by the gas (Huang & Shang, 2006). The resultant off-gas can be treated, when necessary, using granular activated carbon, which adsorbs the airborne volatile organic compounds (VOCs). This method is highly efficient for removing VOCs in general (up to 99%), notably for DCM removal (up to 95%). Adsorption methods rely on the use of various adsorbent materials (e.g., activated carbon and polymer resins). Novel adsorbents derived from industrial and agricultural waste materials, such as linseed and wheat bran, have shown a removal efficiency of 70-90% of DCM across a wide pH range (pH 1 to pH 11), making them promising options for industrial water remediation (Adachi et al., 2001, 2005; Shestakova & Sillanpää, 2013). Chemical oxidation strategies involve the injection of oxidants, such as ozone or persulfate, directly into the polluted site (groundwater or soil) to degrade the organic pollutants *in situ* (Watts & Teel, 2006). This process is typically less efficient for DCM removal than the previous ones due to the low reactivity of DCM with these compounds, achieving only 18-19% removal efficiency (Ward et al., 2005).

Biological remediation, also referred to as bioremediation, is an alternative to physicochemical approaches. It relies on the transformation of hazardous compounds, such as DCM, into non- or less-toxic substances using biological agents. Supervised bioremediation methods for pollution removal depend on microorganisms that are either introduced deliberately (bioaugmentation) or naturally present *in situ* (monitored natural attenuation, or

MNA). Additionally, nutrients and electron acceptors (e.g., oxygen, nitrate, etc.) can be added to the contaminated sites to enhance microbial activity (biostimulation) (Kensa, 2011). The bioaugmentation method has yielded contrasted results, as its effectiveness is highly dependent on the microbial inoculum's ability to adapt to on-site conditions, particularly the new biotic and abiotic context it encounters. Thus, for successful bioaugmentation, it is possible to protect the inoculum from adverse circumstances (e.g., through encapsulation), and to predict its ecological selectivity/specificity, whether it will occupy a metabolic niche not utilized by the indigenous microbiota (El Fantroussi & Agathos, 2005). The biostimulation method has the advantage of working with indigenous microbial communities that are already adapted to the specific environmental context on-site. However, this method is also subjected to contrasted results in achieving remediation objectives, often due to challenges in delivering the additives to the contaminated site and making them available for microbial communities *in situ* (Henry, 2010). Additionally, biostimulation may also promote the growth of competing bacteria, which can hinder the activity of the degrading strains. Finally, the MNA is an integrative approach aiming at understanding and qualitatively documenting naturally occurring processes, including biodegradation, dispersion, dilution, volatilisation, sorption, and stabilisation of pollutants at the contaminated site (Parsons, 2009). Its success depends on the contaminant type and its physico-chemical properties, as well as the site's hydrogeology and necessitate the control of the source. This method has been applied in Europe (Declercq et al., 2012) and North America ([Government of Canada, 2021](#)) for the remediation of various compounds *in situ*, including chlorinated solvents (McGuire et al., 2004). For example, in France, MNA was implemented from 2011 to 2018 in the former industrial site of Themeroil (Varenes-le-Gran, Saône-et-Loire; GPS coordinates, 46.701141 N, 4.843919 E; **Figure I.4**), which consist of a heavily contaminated groundwater containing a mixture of pollutants, with chlorinated solvents being the major pollutants (Hermon et al., 2018).

In general, bioremediation methods are considered more eco-friendly, cost-effective, and efficient compared to physico-chemical approaches (DeWeerd et al., 1998; Tyagi et al., 2011). These methods have been applied to the remediation of contaminated sites, including the treatment of petroleum-hydrocarbon, other recalcitrant hydrocarbons in soil, and chlorinated solvents (Agnello et al., 2016; Curiel-Alegre et al., 2022; Lv et al., 2018). In the case of DCM, MNA has been commonly used, though with mixed results. To effectively apply bioremediation approaches *in situ*, it is thus crucial to characterize both the individual processes involved in the natural attenuation of DCM (**section I.1.3**) and the impact of hydrogeochemical parameters and variations occurring *in situ* on the indigenous microbial community (**section I.2**).

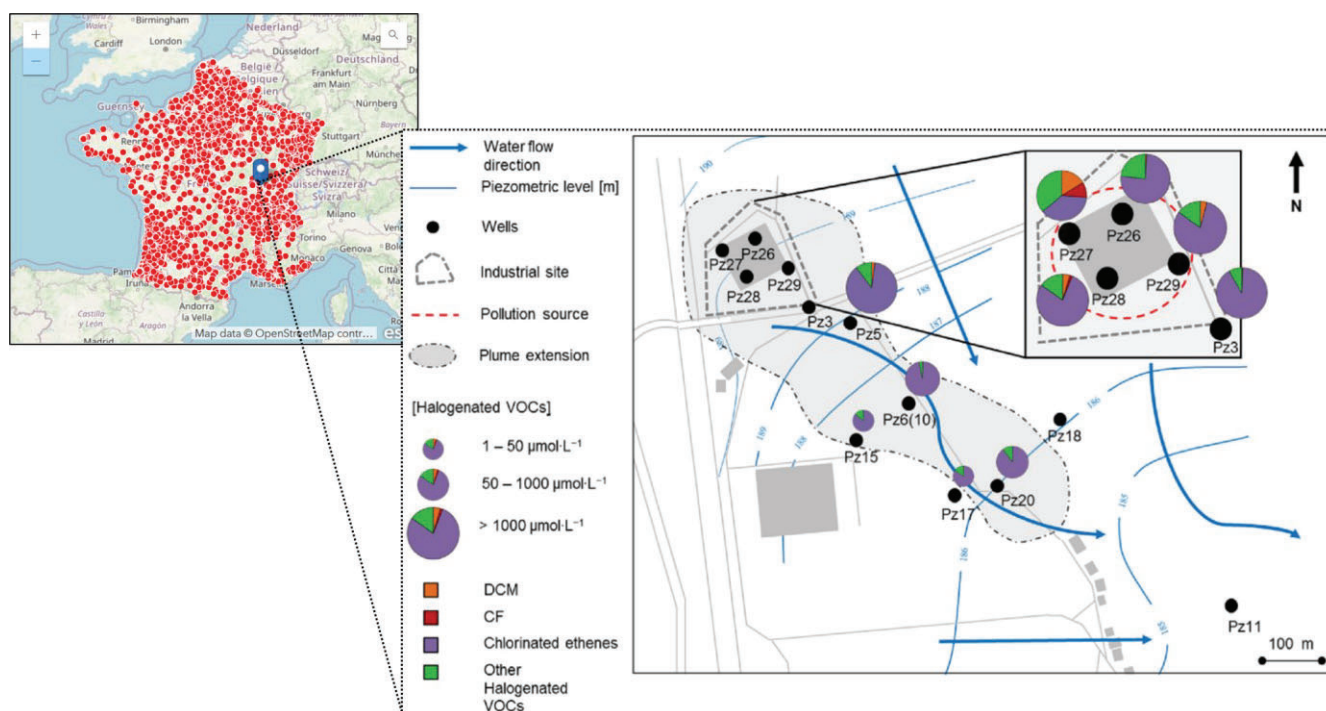


Figure I.4. Former industrial site of Themeroil (Varenes-le-Grand, France) and well (Pz) locations. The red points in the map indicate the referenced polluted sites in France ([Basesol](#) - Base de données du Ministère de l'Écologie et du Développement Durable), with Themeroil site indicated in blue. Adapted from Hermon (2017).

I.1.3 Microbial utilisation of DCM

Microbial DCM biodegradation has been described under both aerobic (**section I.1.3.1**) and anaerobic conditions (**section I.1.3.2**), with several characterized pathways. However, not all of them support microbial growth. For example, under aerobic conditions, the pathway involving the haloalkane dehalogenase Dh1A, an enzyme with a broad substrate range, allows the degradation of DCM through a hydrolytic reaction, yet there is no evidence of bacterial growth associated with this pathway (Muller et al., 2011a) (**Figure I.5**). During this process, a reactive intermediate, the chloromethanol, is produced, which may have toxic effects on the bacterial host. Another example of aerobic co-metabolic DCM degradation is the monooxygenase-based pathway, where DCM is oxidized without serving as growth substrate. This pathway results in the production of the reactive acylchloride, a toxic compound for bacterial growth (Green, 1997; Muller et al., 2011a) (**Figure I.5**). In the following sections, we will focus on the microbial pathways allowing the use of DCM as sole carbon and energy source under aerobic (**section I.1.3.1**) and anaerobic (**section I.1.3.2**) conditions.

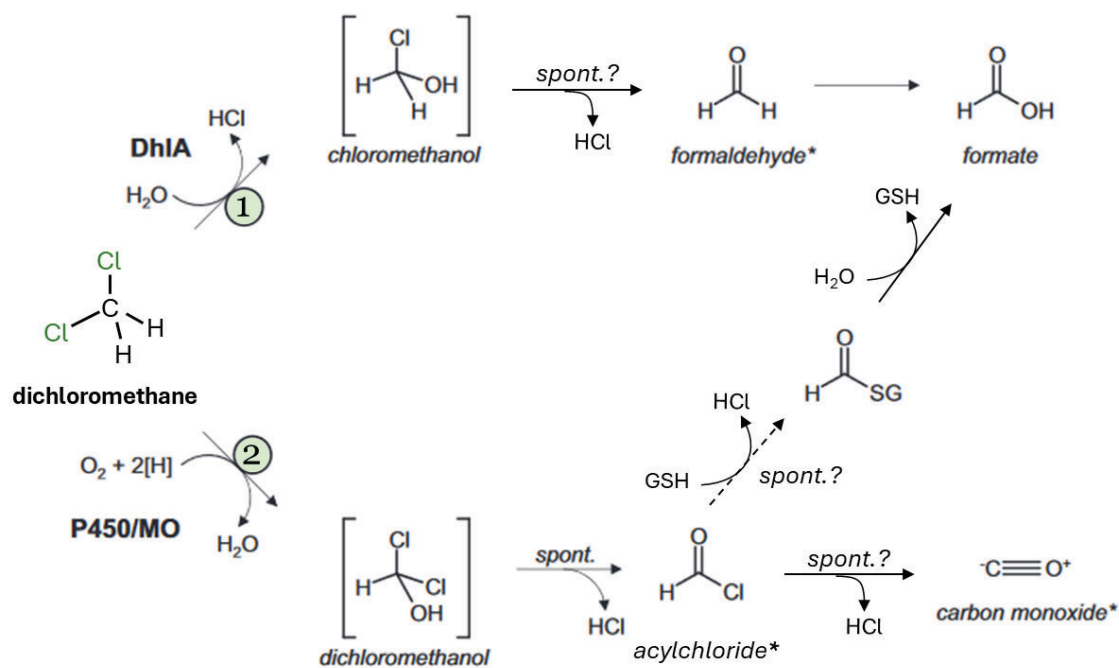


Figure I.5. The two proposed co-metabolic pathways for enzymatic DCM degradation. There is no evidence of microorganisms using DCM as growth substrate in these pathways. Spont: spontaneous, abiotic reaction. Square brackets indicate reactive reaction intermediates, and asterisk indicate compounds known to be toxic. Dashed arrows indicate reactions that have not been reported in the specific context of DCM degradation. **(1)** The haloalkane dehalogenase (DhIA) pathway, in which DCM is hydrolysed to produce formate; **(2)** The monooxygenase-based pathway (P450/MO), in which DCM is oxidized to produce formate or carbon monoxide. Adapted from Muller et al. (2011a).

I.1.3.1 Aerobic biodegradation of DCM

The only pathway characterized to date that allows DCM to be used as sole carbon and energy source under aerobic conditions involves the DCM dehalogenase DcmA, a specific glutathione S-transferase that catalyses the conversion of DCM to formaldehyde and 2 molecules of HCl (**Figure I.6**). This pathway was first elucidated in aerobic methylotrophic bacteria (Leisinger et al., 1994; Stucki et al., 1981; Vuilleumier, 2002) and has since been found both in gram positive and negative bacteria, encoded on chromosome or on plasmids, in isolates from polluted or pristine environments. In the DCM-degrading model strain *Methylobacterium extorquens* DM4, this pathway is encoded by a *dcm* catabolic cluster composed of 4 genes: (i) *dcmA*, encoding for the DCM dehalogenase DcmA; (ii) *dcmR*, encoding for the transcriptional factor DcmR that regulates the *dcmA* gene expression (Maucourt, 2019); and (iii)-(iv) *dcmB* and *dcmC*, encoding for two proteins (DcmB and DcmC) of unknown function (Muller et al., 2011a; Vuilleumier et al., 2009). To cope with the genotoxic effects of the short-lived intermediates and intracellular hydrochloric acid produced during the enzymatic transformation of DCM, bacteria using **this** pathway possess other adaptations. This includes having a more efficient DNA repair system (Firsova et al., 2005; Kayser et al., 2000), as well as an enhanced detoxification system, to extrude Cl⁻ and respond to the solvent stress imposed

by DCM (Michener et al., 2014; Muller et al., 2011b; Torgonskaya et al., 2011). Previous work has shown that without these adaptations, strains are unable to grow with DCM even in the presence of an active DCM dehalogenase (Kayser et al., 2002; Muller et al., 2011b).

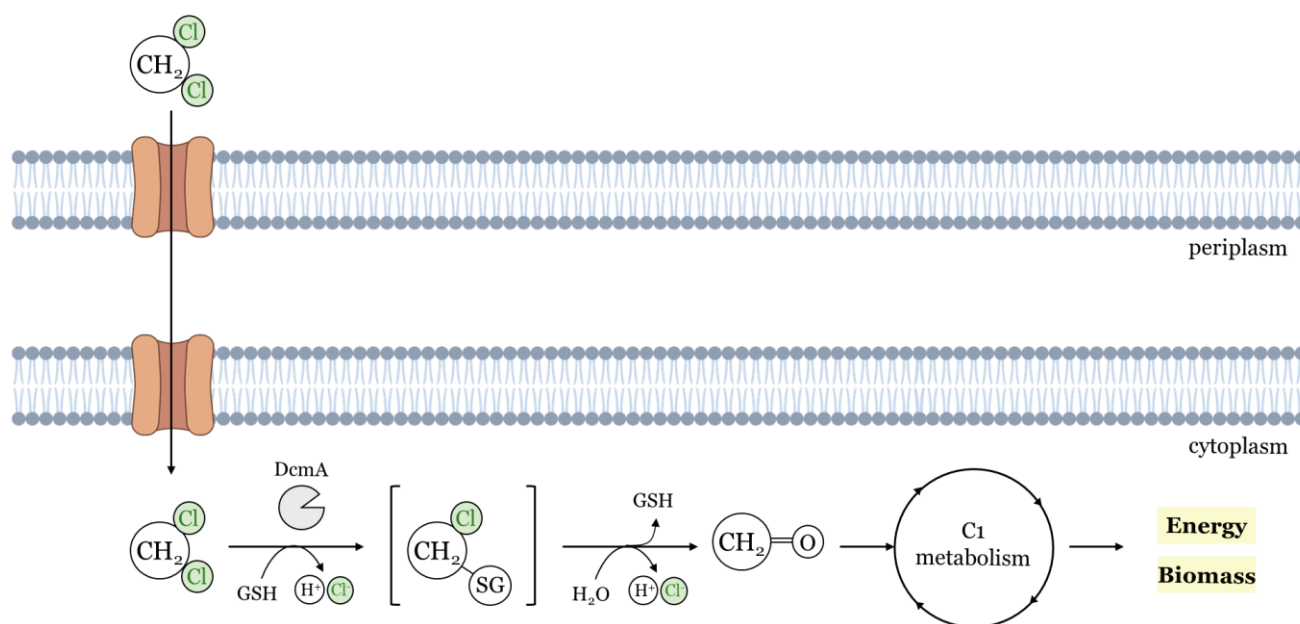


Figure I.6. Proposed metabolic pathway for DCM utilization as sole carbon and energy source in the model strain *M. extorquens* DM4. Once in the cytoplasm, DCM is hydrolysed by the DCM dehalogenase DcmA to formaldehyde (CH₂O) and 2 molecules of HCl. S-chloromethyl glutathione (between brackets) is a genotoxic reactive intermediate. The formaldehyde is used as central intermediate in the methylotrophic serine cycle (C1 metabolism) for energy and biomass production. GSH: glutathione; SG: glutathionyl.

In general, the DCM dehalogenase DcmA is highly conserved in terms of sequences at both nucleic and amino acid levels in most bacteria that use DCM as a carbon and energy source under aerobic conditions. This, together with the fact that the *dcm* cluster is typically flanked by transferases and insertion sequences, supports the hypothesis of its horizontal transfer within the bacterial world (Vuilleumier et al., 2009). However, there are exceptions to this high degree of conservation. For example, the DcmA protein in *Methylophilus* sp. DM11 shows the most divergent amino acid sequence compared to the model strain *M. extorquens* DM4 (58.4% of identity at the DNA-level encoding for a 267 amino acid long protein compared to 288 amino acids for all other known sequences) (Firsova et al., 2010). Another example is found in the DCM-degrading strain *Hyphomicrobium* sp. MC8b, which presents a highly divergent set of *dcm* genes. This strain was first isolated from a DCM-degrading biofilter (Ergas et al., 1994) and, despite being closely related to other DCM-degrading *Hyphomicrobium* strains utilizing the DcmA pathway, the *dcmA* gene was undetectable by both Southern-blot and PCR-based approaches (Nikolausz et al., 2005). However, through a pan-proteomic approach, we demonstrated that the strain *Hyphomicrobium* sp. MC8b did contain and express the DCM dehalogenase DcmA, the DcmR and the DcmB proteins, while DcmC remained undetected

(Hayoun et al., 2020). These findings were further confirmed by genome sequencing, which revealed that in *Hyphomicrobium* sp. MC8b, the structure of the *dcm* cluster (unusual arrangement, with *dcmC* being a relic), its intergenic regions (a 54% reduction in the region between the *dcmR* and *dcmA* genes), the surrounding genes (absence of IS elements flanking the *dcm* genes), and the nucleotide sequences of the *dcm* genes (88%, 83% and 84% identity for *dcmA*, *dcmR*, and *dcmB* genes, respectively) differ significantly from the model strain *M. extorquens* DM4 (**Figure I.7**).

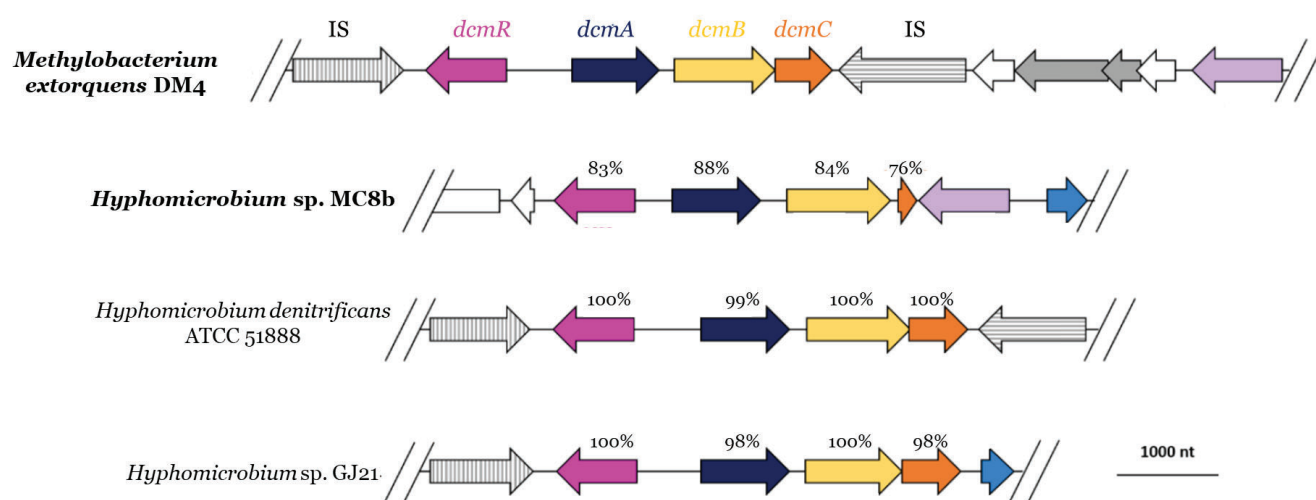


Figure I.7. Comparison of the *dcm* genes of *Hyphomicrobium* sp. MC8b, *H. denitrificans* ATCC 51888 and *Hyphomicrobium* sp. GJ21 with those in the model strain *M. extorquens* DM4. Homologous genes are shown in the same colour, along with the percentage of identity to *M. extorquens* DM4 at the nucleotide level. Transposase genes are shown in grey, with homologous genes displaying the same pattern. Adapted from Hayoun et al. (2020).

Even though the DCM dehalogenase pathway is typically found in strictly aerobic strains, the DcmA-related biodegradation of DCM has also been reported under nitrate-reducing conditions. Examples include the *Acinetobacter* sp. strain DCM (Freedman et al., 1997), and facultatively methylotrophic bacteria belonging to the *Hyphomicrobium* genus, such as the strains *Hyphomicrobium* sp. DM2, GJ21, KDM2, and KDM4 (Kohler-Staub et al., 1995; Nikolausz et al., 2005). This unique feature is possible due to the ability of these strains to use nitrate as an alternative electron acceptor. Among them, *Hyphomicrobium* sp. GJ21, isolated from environmental samples contaminated with halogenated compounds (Ottengraf et al., 1986) and which genome was fully sequenced in 2017 (Bringel et al., 2017), has been extensively used as a model strain for DCM degradation in bioreactor studies (Bailón et al., 2007; Diks et al., 1994) and aquifer laboratory microcosms (Hermon et al., 2018).

Finally, among the DCM-degradation strains reported to use DCM as the sole carbon and energy source under aerobic conditions, several are reported to be missing the *dcmA* gene. These include *Flavimonas* sp. P3310 and *Chryseobacterium* sp. G31 (Kawata et al., 2000), *Ralstonia metallidurans* PD11 (Miyake-Nakayama et al., 2006), *Mycobacterium* sp. GD11 and GD23 (Yu et al., 2006), *Lysinibacillus sphaericus* wh22 (Wu et al., 2009), *Albibacter*

methylovorans DM10 (Doronina et al., 2001), *Enterobacter amnigenus* ESB-23 and *Aminobacter aminovorans* ESB-4 (Osuna et al., 2008), *Pandoraea pnomenusa* LX-1 (Yu et al., 2014), and *Rhodococcus* sp. EH831 (Lee et al., 2010). Given that none of these strains have been sequenced yet, two possibilities may explain the lack of *dcmA* detection: either these strains have an alternative, yet undescribed, pathway for DCM utilisation, or, as in the case of *Hyphomicrobium* sp. MC8b, they harbor the same DcmA pathway but with excessive sequence divergence from the known sequences, making them difficult to detect with the current universal primer pairs. In this context, an alternative approach to the pan-proteomic strategy or full genome sequencing that can help revealing the presence or absence of the DcmA pathway is the compound-specific isotope analysis (CSIA). This technique relies in changes in stable isotope ratios (e.g., $^{13}\text{C}/^{12}\text{C}$) of organic compounds undergoing a (bio)degradation reaction. Generally, molecules containing light isotopes (e.g., ^{12}C) are preferentially degraded compared to those with heavy isotopes (e.g., ^{13}C). This results in a change in the isotope ratio of the remaining compound, which is specific of the transformation/enzymatic pathway (Elsner & Imfeld, 2016) (**Figure I.8**). Thus, CSIA can provide evidence for different microbial degradation pathways even in the absence of biomolecular data.

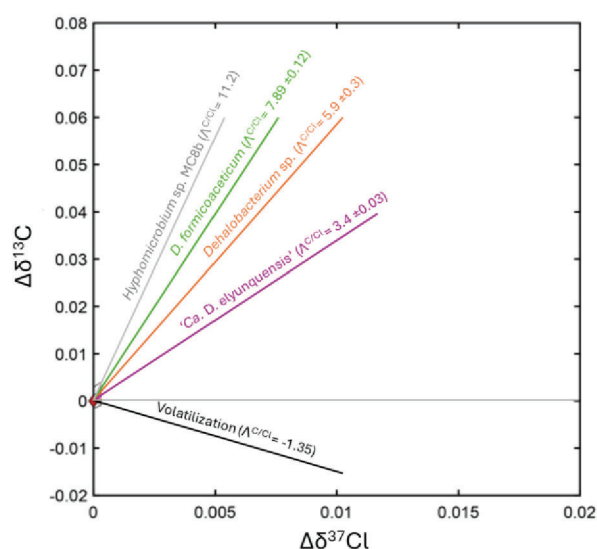


Figure I.8. Example of a CSIA dual plot ($\Delta\delta^{13}\text{C}$ vs. $\Delta\delta^{37}\text{Cl}$) for the degradation of DCM. Each line corresponds to the linear regression derived from the reported $\Delta\text{C}/\text{Cl}$ values, which are specific to the transformation pathways in the strains *Hyphomicrobium* sp. MC8b (grey), *Dehalobacterium formicoaceticum* (green), *Dehalobacterium* sp. (orange), and ‘*Candidatus* Dichloromethanomonas elyunquensis’ (pink). The black line represents 99% of DCM volatilization. Figure adapted from Prieto-Espinoza et al. (2021).

I.1.3.2 Anaerobic biodegradation of DCM

Compared to aerobic conditions, the DCM metabolism under strictly anaerobic conditions is less well understood. To date, two main pathways have been identified in bacterial populations from the family *Peptococcaceae* (*Firmicutes* phylum), that allow DCM to be used as a growth substrate: a mineralization pathway and two variants of a fermentative pathway.

The mineralization pathway has only been shown in ‘*Candidatus Dichloromethanomonas elyunquensis*’ and involves the complete mineralization of DCM to CO_2 , H_2 and inorganic chloride (Chen et al., 2020a; Kleindienst et al., 2017) (**Figure I.9-a.**). This process requires the presence of H_2 -consuming partner populations (i.e., hydrogenotrophic methanogens and homoacetogens) to consume the produced H_2 , as it has a strong inhibitory effect on DCM degradation (Chen et al., 2017). On the other hand, the fermentative pathway was firstly described in the bacterial isolate *Dehalobacterium formicoaceticum* strain DMC (Mägli et al., 1996) and consists of the conversion of DCM to a 1:2 molar ratio of formate and acetate (Mägli et al., 1998; Trueba-Santiso et al., 2020) (**Figure I.9-b.**). This pathway is dependent on a Co(I) corrinoid and tetrahydrofolate. Furthermore, ‘*Candidatus Formimonas warabiya*’ strain DCMF, isolated from anaerobic enrichment cultures, is capable of fermenting DCM to acetate (Holland et al., 2021; Kleindienst et al., 2017) (**Figure I.9-c.**). A key difference between strain DMC and strain DCMF is that the latter appears to further metabolize formate and ‘recycle’ the resulting CO_2 for acetogenesis, explaining the difference in the observed end-products during DCM degradation by the two strains.

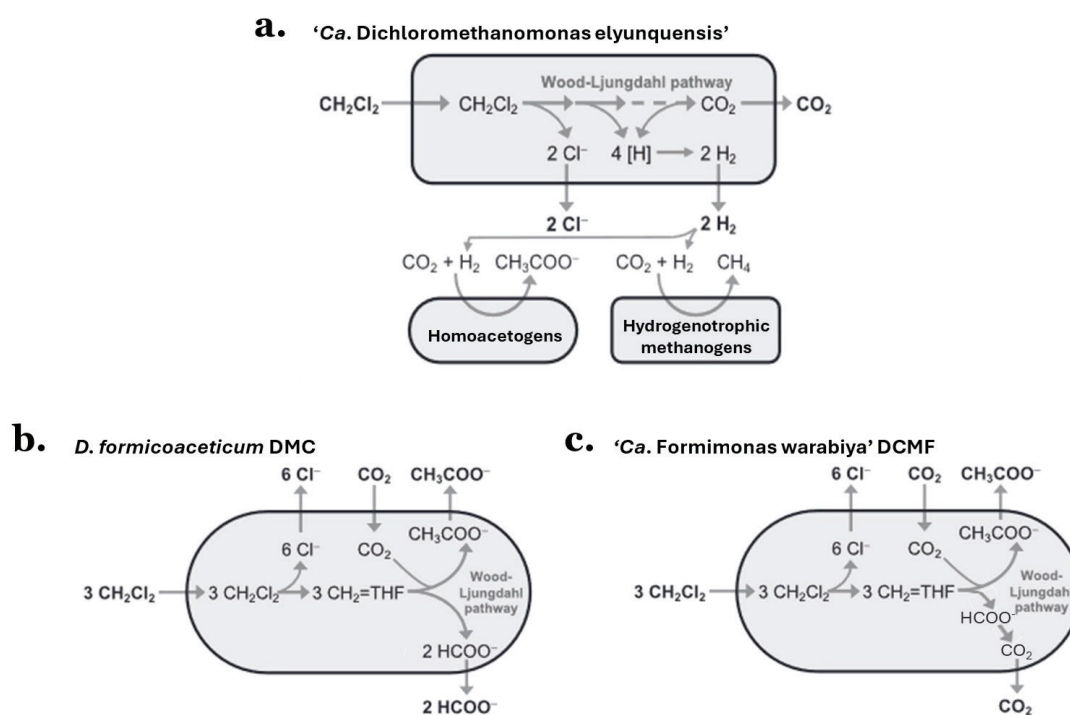


Figure I.9. Proposed metabolic pathways for DCM utilization as growth substrate under anoxic conditions. Two pathways have been proposed: mineralization (**a**) and fermentation (**b** and **c**). **a.** DCM is completely mineralized to CO_2 by ‘*Ca. Dichloromethanomonas elyunquensis*’, which is associated with H_2 -consuming partner populations. These partner populations use the inhibitory H_2 as a growth substrate, leading to the production of methane and acetate. **b.** DCM is degraded to acetate and formate (in a 1:2 molar ratio) by *D. formicoaceticum* DMC. **c.** DCM is degraded to acetate and CO_2 by ‘*Ca. Formimonas warabiya*’ DCMF. The only difference from the fermentative pathway of *D. formicoaceticum* DMC is that in this case, the formate is completely metabolized to CO_2 . Adapted from Chen et al. (2020a) and Holland et al. (2021).

In recent comparative genomics studies, Murdoch and colleagues identified a genomic cluster, named the *mec* cassette (for methylene chloride catabolism) and comprising 10 genes from *mecA* to *mecJ*, which was suspected to be involved in the DCM transformation in anoxic conditions (Murdoch et al., 2022). This genomic cluster was detected in all genomes and metagenomes of known anaerobic DCM-degrading bacteria, including the strains and bacterial populations mentioned above, but has not been found in other phylogenetically related bacteria (**Figure I.9**). The importance of these cluster during DCM degradation under anoxic conditions was supported by three (meta)proteomic studies done with ‘*Ca. Formimonas warabiya*’ DCMF, *D. formicoaceticum* strain EZ94 and a DCM-degrading enrichment culture, all of which demonstrated that proteins encoded by the *mec* cassette were highly expressed under these conditions (Bulka et al., 2024; Holland et al., 2022; Wasmund et al., 2023).

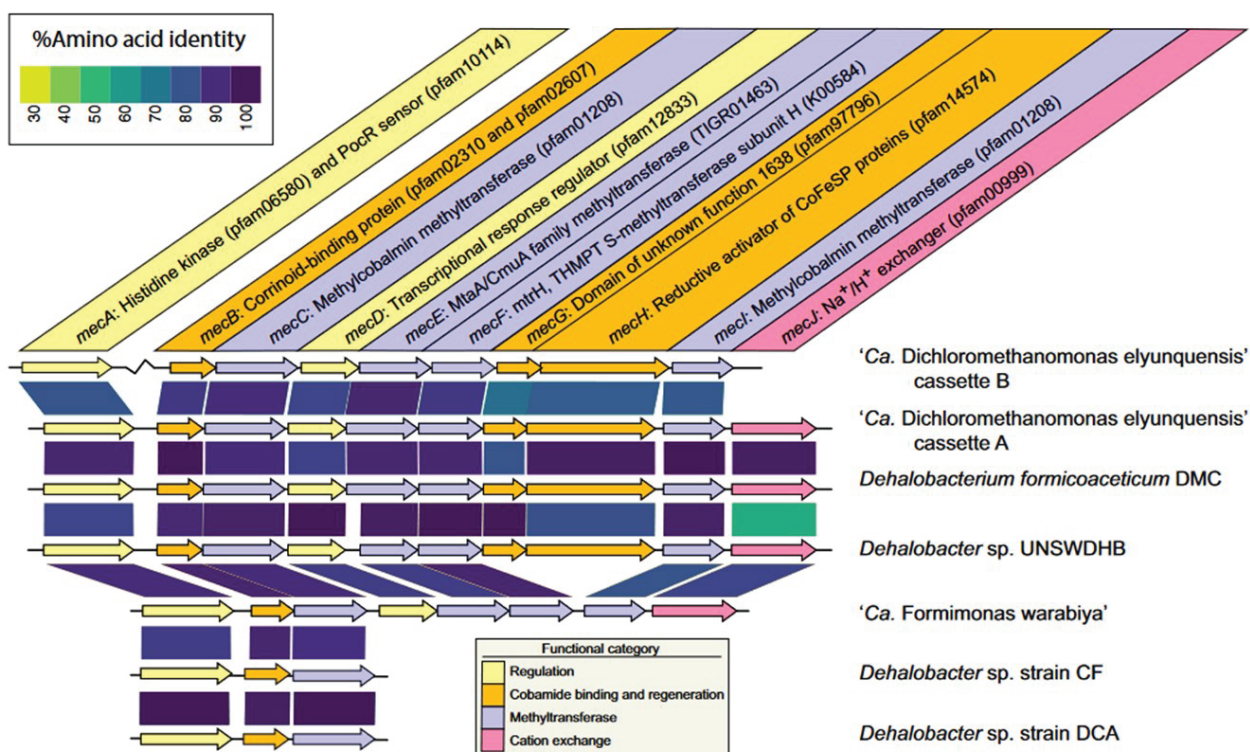


Figure I.10. *mec* cassettes and close homologs identified in the genomes of the known anaerobic DCM-degrading bacteria strains and populations. Homologous genes are color-coded by function, and the links between homologs are coloured according to percentage of amino acid identity. The specific functions of each gene (indicated in the coloured rectangles in the upper part of the schema) were inferred from functional annotation data bases. Figure reproduced from Murdoch et al. (2022).

In September of this year, Soder-Walz and colleagues investigated the DCM fermentation process in *D. formicoaceticum* strain EZ94 and revealed that among all the proteins encoded by the *mec* cassette, MecE, MecB and MecC were the central enzymes involved in the anaerobic DCM degradation (Soder-Walz et al., 2024). In particular, enzymatic activity assays showed that only when these three enzymes were present, the complete transformation of DCM was achieved. Additionally, through *in silico* protein structure predictions, specific functions of these three proteins were assigned: MecE and MecC act as two methyltransferases (I and II,

respectively), while MecB is a cobalamin-dependent enzyme that forms a stable complex with MecE, that is essential for the demethylation activity of MecE. The pathway proposed by the authors is shown in **Figure I.11**.

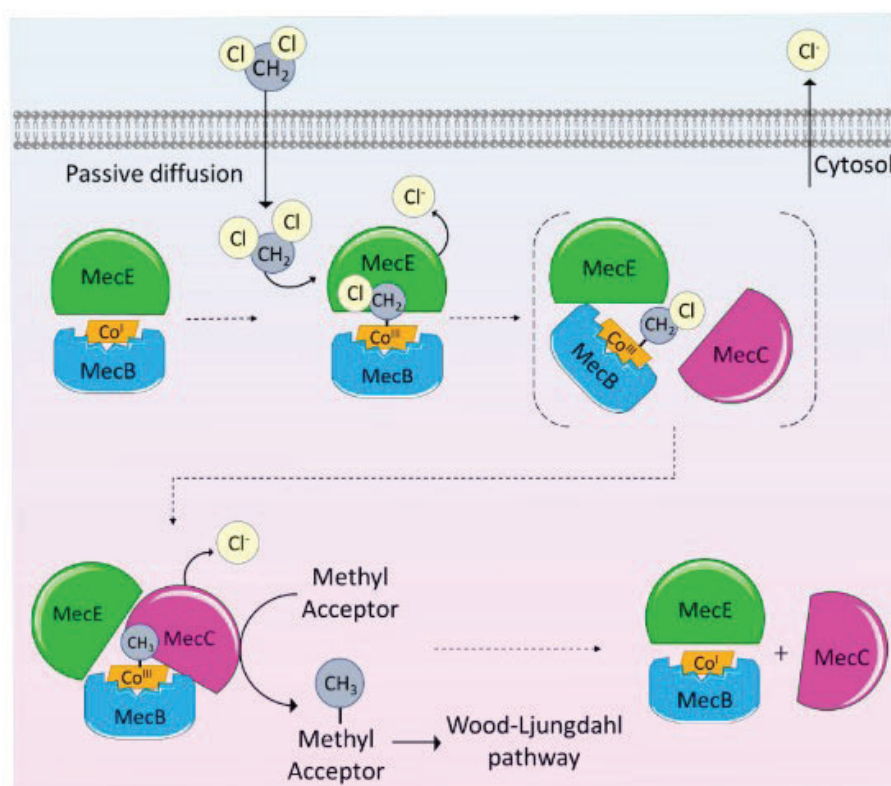


Figure I.11. Proposed pathway for the initial steps of DCM transformation under anoxic conditions in *D. formicoaceticum* strain EZ94. Once DCM enters the cytoplasm, it binds to the MecEB heterodimer. The cobalamin(I) in MecB initiates a nucleophilic attack on the chloromethyl group of DCM, resulting in the formation of a chloromethyl-cobalamin (III) bound, with a chloride (Cl^-) released by the methyltransferase MecE. Next, the second methyltransferase, MecC, attacks the methyl group of the chloromethyl-cobalamin (III) in MecB, leading to the released of the second Cl^- . The final methyl group is suggested to be transferred to a methyl acceptor, such the tetrahydrofolate via MecF (not shown in the schema), from which it will enter the Wood-Ljungdahl pathway. Figure reproduced from Soder-Walz et al. (2024).

I.2 DCM biodegradation in aquifers

Groundwater aquifers hold most of the available fresh water on Earth, and are an integral step of the natural water cycle. In Europe, around 65% of drinking water comes from groundwater and 75% of Europeans rely on it for their water supply ([EEA Report No 7/2018](#)). However, as mentioned in the Directive 2006/118/EC, groundwater is not only the largest body of freshwater in the European Union, but also the most vulnerable to chemical pollution. Among the pollutants, the widespread production of chlorinated solvents has led to significant groundwater contamination. In particular, by 2013, these compounds were detected in 19% of

polluted subsurface sites in France ([Commissariat Général au Développement Durable, 2013](#)). Additionally, in the U.S, DCM has been reported to be present in at least 30% of the subsurface sites managed by the Superfund program of the United States Environmental Protection Agency (U.S EPA)(Koenig et al., 2015).

To effectively apply microbial-based remediation strategies for the removal of DCM from contaminated aquifers, it is important to understand the factors behind the successes and failures of these bioremediation approaches. Studying the microbial metabolisms responsible for DCM degradation in the laboratory is essential for understanding the mechanisms involved in these processes. However, most of these studies do not consider the inherent complexity of the endogenous microbial communities or the variations in the physicochemical conditions to which these communities are exposed *in situ*. Consequently, results obtained in the laboratory are not always replicable in the field. Therefore, in parallel with the study of pure cultures in the laboratory, it is necessary to design experiments that include the natural hydrogeological and biogeochemical conditions of aquifers.

I.2.1 What is an aquifer

An aquifer is a subsurface body of rock or sediment with sufficient porosity and permeability to store groundwater and allow its movement. Based on their connection to the land surface, aquifers can be categorized in two groups: confined and unconfined (**Figure I.12-a.**). Confined aquifers are water-saturated aquifers that are separated from upper layers and the atmosphere by layers of low permeability material. Unconfined aquifers, on the other hand, are partially or completely filled aquifers whose upper water surface is exposed to the land surface. These types of aquifers are therefore more susceptible to climatic conditions and any type of surface contamination.

Unconfined aquifers are traditionally separated into three distinct and dynamic layers based on moisture content: the unsaturated zone, the saturated zone and the capillary fringe (**Figure I.12-b.**). The unsaturated zone, also known as the vadose zone, is the layer between the land surface and the water table (i.e., the level at which groundwater is found). In this zone, the pore spaces of the matrix contain both water and air. The saturated zone, also known as phreatic zone, lies below the water table, where all pore spaces are completely filled with water. Finally, the capillary fringe, situated between the unsaturated and saturated zone, consists of groundwater that seeps up from the water table by capillary action, partially filling the pores. This zone is considered a hotspot for subsurface activity, playing a crucial role in both physicochemical processes and microbial activity (Smith et al., 2018). The extent of the capillary fringe is highly dependent on the water holding capacity (WHC) of the sediment matrix. The WHC is the amount of water held by the matrix against the force of gravity and is primarily controlled by the matrix grain size. Soils with smaller particles, such as clay (>0.002 mm), have a larger surface area and thus retain more water than soils with larger particles, such as sand (~2 mm). As a result, aquifer sediments with finer grain sizes form a higher

capillary fringe and thus concern a larger volume of sediments, than the ones with larger grain sizes (**Figure I.12-c.**).

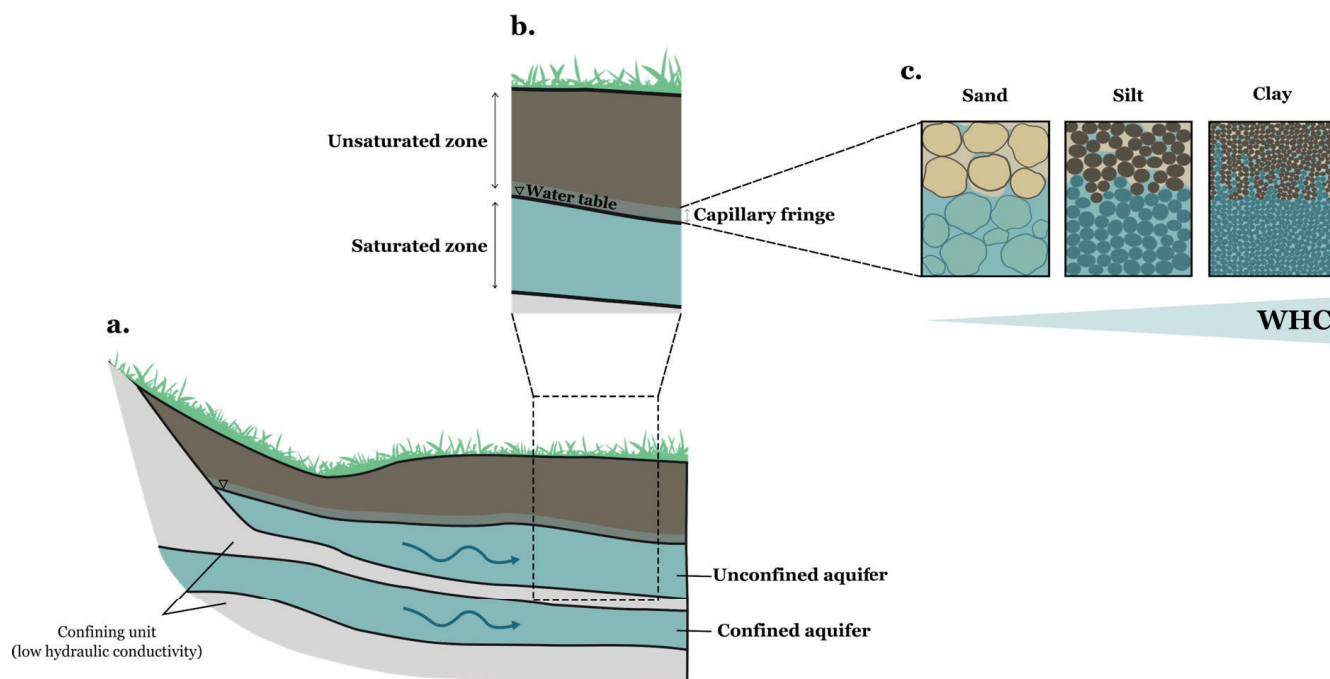


Figure I.12. Overview of the aquifer system. **a.** Based on the connection to land surface, two types of aquifers exist in the environment: confined aquifers, which are separated from the atmosphere through confining units, and unconfined aquifers, which are exposed to the land surface. The blue arrows represent the flow of groundwater. The inverted triangle indicates the water table of the aquifer. **b.** Unconfined aquifers consist of three dynamic layers based on their moisture content: saturated zone, which is located below the water table and where soil pores are full of water; the unsaturated zone, which lies above the water table and where soil pores contain both water and air; and the capillary fringe, situated between the saturated and unsaturated zone and where groundwater seeps up from the water table by capillarity. **c.** The volume of the capillary fringe varies depending on the sediment type of the aquifer, following the WHC of the soil. In general, finer grain soils have a higher WHC, resulting in a larger capillary fringe.

Gradients of physicochemical conditions are established from the unsaturated to the saturated zone (**Figure I.13**). These gradients control the characteristics and properties of the microbial communities in each layer (Fierer et al., 2003b). For example, the natural gradient of decreasing total nitrogen, organic carbon, and oxygen concentration with depth creates an oligotrophic (i.e., resource-limited) and anoxic environment within the saturated zone (Smith et al., 2018). Additionally, the high interconnectivity between matrix particles due to water saturation in this layer leads to microbial communities in the saturated zone being dominated by a few taxa that are best adapted to these conditions (Zhou et al., 2002). This results in lower diversity and biomass in the saturated zone compared to the upper layer (Brewer et al., 2019; Fierer et al., 2003b). On the other hand, the higher microbial density and diversity in the unsaturated zone is also attributed to the heterogeneity of the habitats (e.g., large variation in

availability of water and nutrients, notably carbon sources, and temperature fluctuations), maintained by an uneven and patchy distribution of resources (Or et al., 2007). This, combined with the fragmentation of the aqueous phase in this zone, promotes the coexistence of taxa. Moreover microorganisms generally form surface-attached microcolonies and biofilms (Or et al., 2007). The capillary fringe has its own specific microbial community, probably involved in the observed rich catalytic diversity of this intermediary layer. A lower diversity and some dominant adapted populations are observed in this layer due to the frequent redistribution of nutrients, gas and other resources (Bougon et al., 2012).

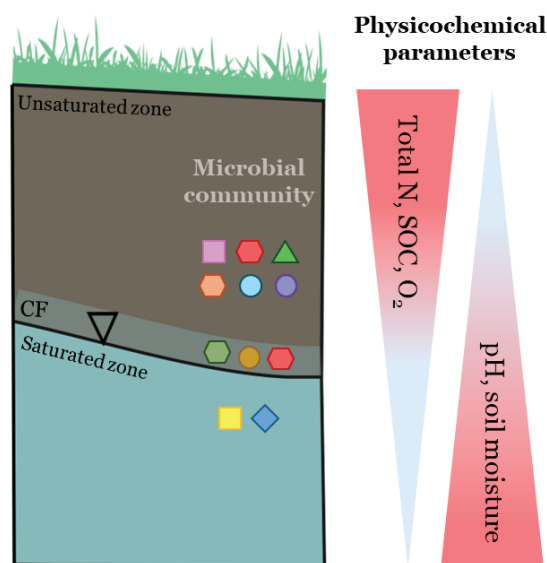


Figure I.13. Gradients of physicochemical parameters and microbial community characteristics established from the unsaturated to the saturated zone. Total nitrogen, soil organic carbon (SOC) and oxygen concentrations decrease with depth, while pH and soil moisture follow an opposite pattern, increasing with depth. These physicochemical gradients lead to changes in the microbial community composition across the different layers of the aquifer: microbial biomass and diversity decrease with depth. In the saturated zone, due to the high environmental connectivity, only taxa highly adapted to the oligotrophic conditions dominate the microbial community. In contrast, the unsaturated zone, characterized by an uneven distribution of resources, hosts a more heterogeneous microbial community. The capillary fringe (CF) has its own specific microbial community, characterized by a high catalytic activity. The inverted triangle indicates the water table of the aquifer. Adapted from Sheng et al. (2021).

I.2.2 Impact of disturbances in the environment

Many definitions of an ecological disturbance are used in the literature, some of them even using the word ‘disturbance’ interchangeably to refer to both the events that cause, and the consequences of, ecological change. Traditionally, Rykiel defined a disturbance as “an event (physical force, agent or process), either abiotic or biotic, that causes a perturbation in an ecological component or system (Rykiel Jr, 1985)”. For White and Pickett, a disturbance is “a discrete event in time that disrupts ecosystem, community, or population structure or changes resources, substrate availability, or the physical environment” (White, 1985). Plante proposed

an alternative definition of disturbance for the specific use in microbial ecology, describing it as “a casual, unpredictable event that causes direct removal of living biomass, thereby altering community structure” (Plante, 2017). More recently, Graham and colleagues aimed for a broader, more adaptable definition that could be applied to across various studies and spatiotemporal scales. They describe a disturbance event as “the occurrence of a driver whereby a force, either biotic or abiotic, generates a deviation from the local, prevailing background conditions” (Graham et al., 2021). In the following of this thesis dissertation, “disturbance” will refer to a discrete or continuous biotic or abiotic event that disrupts any ecological, environment or resource component, altering directly or indirectly the microbial community structure and/or activity. With this definition, I aimed to incorporate key elements associated with the concept of disturbance in the literature, while also emphasizing its effect on microbial community function by including changes in activity. In addition, disturbances are typically classified as either pulses or presses depending on their duration (Bender et al., 1984). Pulses disturbances are discrete, short-term events, whereas presses are long-term or continuous (Shade et al., 2012) (**Figure I.14**). From this point forward, we will focus on pulse disturbances, which are expected to also increase in frequency along to the ongoing gradual temperature rise due to associate changes (e.g., extreme weather events related to climate change) (Graham et al., 2021).

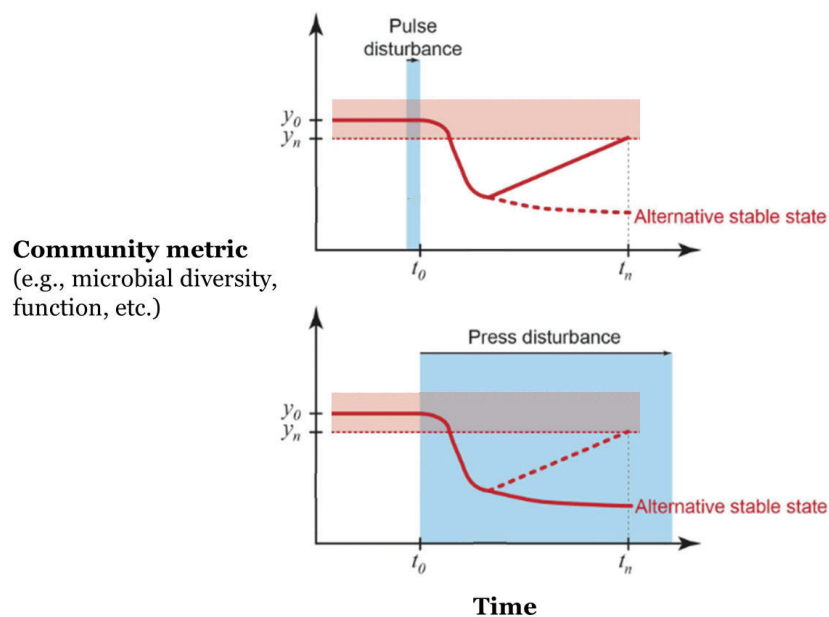


Figure I.14. Disturbance types. Two types of disturbances are found in the environment based on their duration: pulses disturbances, which are discrete events, and press disturbances, which are long-term or continuous events. Following a disturbance, the community may either return to its initial state or shift to an alternative stable state. y_0 corresponds to the value of the community metric of interest (e.g., microbial diversity, function activity, etc.) at t_0 . y_n corresponds to the value of the community metric of interest after a time n (t_n). The light red area indicates the 95% confidence interval around the mean of y_0 and the temporal variation. Adapted from Shade et al. (2012).

Following a disturbance, different outcomes of the microbial community are possible. In this thesis, and following the recent literature review of Hellal and colleagues, the possible responses of the microbial community will be addressed in terms of its activity (Hellal et al., 2023). The first case scenario occurs when the microbial community maintains the set of considered activities or functions after a disturbance, with or without a loss of taxa. In this context, the microbial community can be considered resistant to the disturbance, if it withstands the disturbance, or resilient, if it takes a moment to recover its previous activity level after the disturbance (**Figure I.15-a.**). The ability of the microbial community to maintain its function despite the loss of some taxa involved in the studied activity indicates functional redundancy, meaning different organisms can perform similar metabolic functions (Louca et al., 2018). The second possibility is that the microbial community loses its activity after a disturbance. In this case, the community can be considered sensitive, if the activity is lost immediately after the disturbance, or tolerant, if the activity is less performant or gradually lost after the disturbance (**Figure I.15-b.**). In both of these cases, this can come along with the abrupt or gradual loss of the taxa responsible for the function. Finally, a third case scenario, not described in the review of Hellal and colleagues, occurs when the activity of the microbial community emerges after the disturbance, with or without a change in taxonomical diversity (**Figure I.15-c.**). This phenomenon has been linked to the latent microbial functional diversity, which consists of a pool of dormant microbial taxa that “resuscitate” after the disturbance, filling newly available niches in the environment (Shade, 2023; Smith et al., 2022). The concept of latent microbial functional diversity is closely related to the idea of niches. An environmental niche is defined as the set of environmental conditions (comprising biotic and abiotic factors) in which a specie can persist, utilize resources and thus impact its environment (Malard & Guisan, 2023). In this context, latent microbial functional diversity only appears when the conditions align with the ecological requirement (i.e., environmental niche) of the taxon.

Commonly studied disturbances in the environment include changes in the temperature (Hamdi et al., 2011), fire (Allison et al., 2010), desiccation and drying-rewetting cycles (Fierer et al., 2003a; McKew et al., 2011), freeze-thaw cycles (Stres et al., 2010), land management (Jansa et al., 2003), and anthropogenic contamination (Macdonald et al., 2011; Noyer et al., 2023). In aquifers, a frequent environmental disturbance is groundwater level fluctuations (GLF), which consists of changes in the water table due to external factors, such as evapotranspiration, precipitation, and groundwater withdrawal (Wu et al., 2020; Zhang et al., 1998). The significance of GLF in aquifers is growing, as climate change and global shifts in precipitation patterns, frequency, and seasonal temperatures are expected to increase the occurrence of this phenomenon (Zhou et al., 2020).

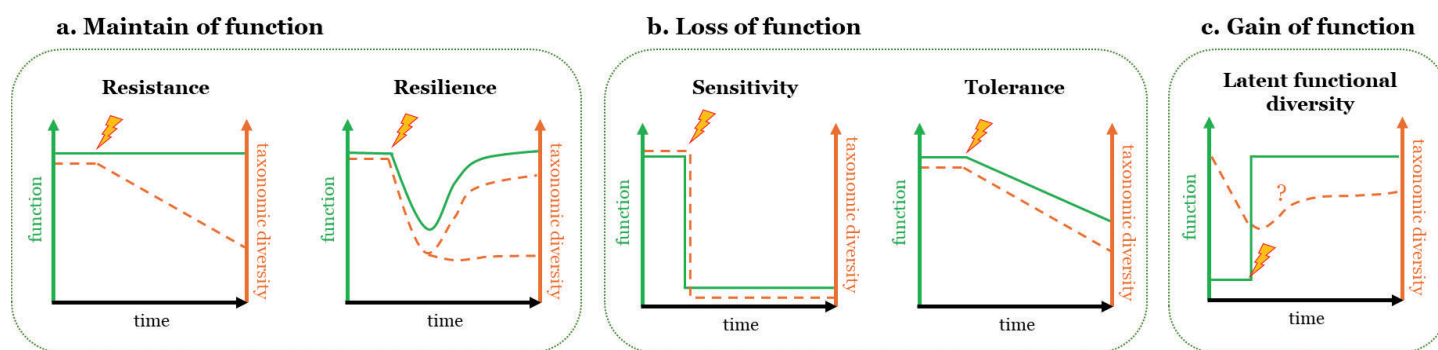


Figure I.15. Possible outcomes of microbial community responses to a disturbance (lightning) in terms of the function of interest (solid green line, left y-axis) and taxonomic diversity (dashed orange line, right y-axis) over time (x-axis). **a.** The function is maintained. Two responses are possible: resistance, when the microbial community withstands the disturbance at the functional level, potentially losing taxonomic diversity; and resilience, when the microbial community temporarily loses the function and taxonomic diversity, but may or may not recovers over time. **b.** The function is lost. Two responses are possible: sensitivity, when microbial community immediately loses both the function and taxonomic diversity after the disturbance; and tolerance, when the microbial community has a reduced performance or gradually loses both the function and taxonomic diversity over time. **c.** The function is gain, which consist of the latent microbial functional diversity, when the microbial community ‘recovers’ its function after the disturbance. The taxonomic diversity may or may not change over time. Adapted from Hellal et al. (2023).

GLF results in the formation a fluctuating zone between the continuously saturated and continuously unsaturated zone, characterized by temporal variations in the water saturation, redox state (e.g. O₂ concentration), and other geochemical components (e.g. nutrients, organic carbon) (Haberer et al., 2012; Wei et al., 2024). These variations have an impact on the microbial community by impacting population-level metabolisms and interactions (**Figure I.16**). For example, as the water table rises, the gas diffusion in the GLF zone is reduced and oxygen concentration decreases, leading to changes in the microbial metabolic patterns as microorganisms need to use alternative electron acceptors (e.g. nitrate, iron), promoting different populations in the area (Peralta et al., 2014; Wei et al., 2024). Changes in water saturation can also alter the specific composition of microbial communities directly, by selecting for microbes that can survive frequent changes in water potential (i.e., availability of water as a resource) (Fierer et al., 2003a), or indirectly, by altering other parameters such as nutrient availability (Allison et al., 2007; Cruz-Martínez et al., 2012). In general, GLF impose a selective pressure in the microbial community and favour microorganisms that possess metabolic plasticity and redox tolerance mechanisms (Rosenberg & Freedman, 1994).

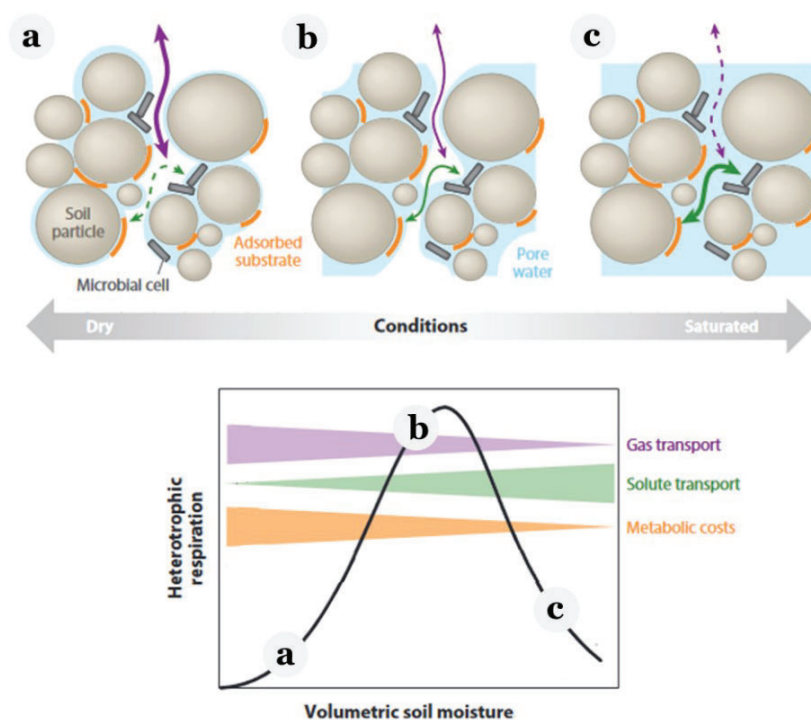


Figure I.16. GLF effects on soil microbial community and geochemical components. Grey rectangles represent microbial cells, and orange lines represent substrates adsorbed onto soil particles (brown circles). Purple arrows represent gas diffusion and green arrows represent nutrient diffusion. The bottom panel shows the relationship between soil respiration (y-axis) and soil moisture (x-axis), which results from the combined effects of diffusion and physiological/biochemical processes. Adapted from Schimel (2018)

Apart from influencing the microbial community composition, GLF has also been shown to impact microbial activity. For example, in a fluctuating water-table soil column experiment, Rezanezhad and colleagues observed an increase in microbial oxidation of organic carbon in the fluctuating zone compared to the other zones in the column (Rezanezhad et al., 2014). This was attributed to a combination of varying redox conditions and favourable soil moisture. Similarly, Pronk and colleagues, reported an enhancement in microbial organic carbon degradation in fluctuating conditions and stated that it was primarily linked to a metabolically more active microbial community, driven by redox variations, rather than a distinct microbial composition (Pronk et al., 2020). In the context of polluted aquifers, GLF have been shown to significantly impact the biodegradation of various compounds, with contrasted results. For example, experiments comparing steady-state conditions and water-level fluctuations demonstrated increase biodegradation rates of compounds such as light non-aqueous phase liquids (LNAPL; Dobson et al., 2007; Gupta et al., 2019) and alkanes (Liu et al., 2022). These observations have been associated with the role of GLF in enhancing oxygen diffusion, replenishing micronutrients, and removing accumulated reaction by-products from the biodegradation process (Cavelan et al., 2022). Moreover, in the case of LNAPLs, this process is further enhanced by the increased availability of these compounds to microorganisms,

resulting from the LNAPLs spreading during GLF (Gupta et al., 2019). Conversely, An and colleagues demonstrated that increased GLF cycles inhibited the natural attenuation of petroleum hydrocarbons in sandy-loam columns due to the formation of an anaerobic environment, which is generally unfavourable for the biodegradation of these type of compounds (An et al., 2024). Interestingly, this effect was not observed in sand columns, where oxygen concentrations were maintained after the GLF cycles. They conclude that soil texture (i.e. the proportion of clay, silt, and sand in a sample) may be a critical factor in determining the inhibitory effects of GLF on petroleum hydrocarbon attenuation in the vadose zone.

I.2.3 Impact of water level fluctuations on DCM biodegradation

The impact of GLF on DCM biodegradation in contaminated aquifers is challenging to study due to the lack of accurate long-term monitoring and the limited spatial and temporal resolution, which are inherent limitations in subsurface field studies (Zhang & Furman, 2021). A complementary approach to address these knowledge gaps involves the use of laboratory-scale experimental set-ups that can integrate and/or decouple different variables. Among these, microcosms are simplified ecosystems of various size and complexity that mimic natural ecosystems under controlled conditions. This strategy allows for better extrapolation to field conditions and improves the understanding and modelling of natural microbial interactions (Pritchard & Bourquin, 1984).

Previous work involved two meter-scale laboratory aquifers to study the impact of GLF on the DCM degradation metabolism and the associated microbial community (Prieto-Espinoza et al., 2021). During the experiment, contaminated groundwater coming from the multi-contaminated aquifer under the former industrial site of Themeroil (**Figure I.4**, Hermon et al., 2018) and anaerobically stored was pumped into the laboratory-scale aquifers, either with a constant flow (steady-state water table condition) or with periodic changes in the flow causing the water table to rise up and drop overtime, mimicking GLF (fluctuating condition) (**Figure I.17-a.**). These fluctuations, as observed in the field, induced changes in the water saturation of the fluctuating zone and also altered its redox status. This was evidenced by an increase in O_2 concentration in the fluctuating zone each time the water table decreased (**Figure I.17-b.**). Furthermore, these changes in O_2 concentration were maintained after the water table rose, which was suggested to be linked with air entrapment in the matrix. The study showed that DCM dissipation was significantly higher under fluctuating conditions compared to steady-state conditions (95% vs. 42% of DCM removal). Using the CSIA method, this dissipation was shown to be mainly driven by biodegradation and associated with changes in the bacterial community composition (**Figure I.17-c.**). Following these observation, Prieto-Espinoza and colleagues developed a multi-phase flow reactive transport model to identify the main drivers of the observed enhanced DCM biodegradation during the fluctuating conditions. They pointed out the importance of the capillary fringe in this process and highlighted the potential key role of heterotrophic bacteria populations in regulating redox conditions across

the fluctuating zone, as well as in the production of CO_2 , a by-product of importance for anaerobic DCM degraders using fermentative pathways and the Wood Ljungdahl pathway.

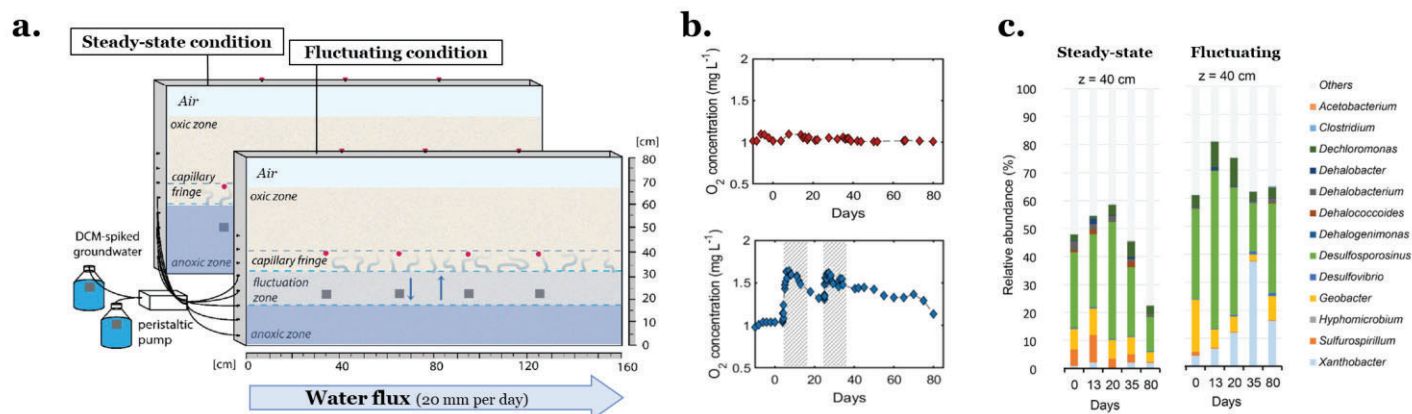


Figure I.17. Study of the impact of GLF on DCM degradation and microbial community composition in laboratory-scale aquifers. **a.** Overview of the laboratory-scale systems. Each laboratory aquifer was filled with sterile sand, and groundwater from a multi-contaminated aquifer at the former industrial site of Themerol was introduced using a constant water flux (steady-state condition), or a fluctuating water flux (fluctuating conditions), mimicking GLF. The large light blue arrow indicates the direction of the water flux. Red circles correspond to sampling ports ($z=40$), where water samples were collected from inside the aquifer. Grey squares represent to the O_2 sensors used to measure dissolved O_2 concentration inside the aquifers ($z=25$). **b.** Dissolved O_2 concentration (mg/L) over time (days) in the laboratory aquifers under steady-state conditions (red) or fluctuating conditions (blue). Measurements were done in the fluctuating zone using the O_2 sensors ($z=25$). The grey area in the graph indicates the period when the water table was maintained at low level. **c.** Relative abundance (%) of bacterial genera associated in the literature with dechlorination (in colour) found in the laboratory aquifers under steady-state conditions (left) and fluctuating conditions (right). The analysis was performed using the water samples collected at $z=40$ (red circles in panel **a.**), with extracted DNA sequenced using 16S rRNA gene amplicon sequencing. Adapted from Prieto-Espinoza et al. (2021).

This study highlighted the importance of GLF in promoting DCM biodegradation in aquifers. However, despite the simplification offered by working with laboratory-scale aquifers, the system remained complex, resulting in several limitations. One major challenge was isolating the individual impact of the various parameters that change during GLF. For instance, the model proposed by Prieto-Espinoza and colleagues emphasized the key role of redox conditions during GLF (Prieto-Espinoza et al., 2023). However, it did not address the impact of the changes in the soil moisture within the fluctuating zone, which, as mentioned earlier, can impact resource availability and gas diffusion, thereby influencing the microbial composition and activity (**Figure I.16**). Another limitation of working with laboratory scale aquifers was that DCM concentration was sampled from the headspace of the system and from specific sampling points across it, making it problematic to determine whether DCM biodegradation was uniformly enhanced throughout the system or confined to specific areas with unique characteristics; e.g. the fluctuating one and/or the saturated zone. Lastly, working

with laboratory-scale aquifers also presented several technical limitations. For instance, to study the hydrogeochemical parameters and microbial community within the system, pore water samples were collected directly from multiple sampling ports located across the aquifers throughout the experiment. Thus, each sampling event may have caused slight alterations to the sand matrix structure, potentially changing the environment inside the aquifers, and to the environmental parameters, notably by drying out the matrix around the sampling port. Additionally, the DNA recovered from these pore water samples was very low, which limited the further analysis of the microbial community.

I.3 Aims and general approach

I.3.1 Thesis aim and research questions

This PhD thesis aims to investigate the impact of key physicochemical parameters during GLF on a DCM-degrading microbial community. In particular, three parameters, considered to play a major role in this phenomenon, were studied: water content, oxygen concentration, and soil granulometry. An integrative approach, including DCM concentration measurements, search of DCM-degrading activity biomarkers, and microbial diversity analysis, was used to examine and compare the behaviour of a DCM-degrading microbial community at both the activity and composition levels, depending on the environmental parameters to which it was exposed. A secondary aim was to assess the response of both the DCM-degrading microbial community and the model strain *Hyphomicrobium* sp. GJ21, a known facultatively anaerobic strain, when exposed to a disturbance consisting of a change in oxygen concentration. The response to the disturbance was studied at the community level, through the analysis of the activity and composition of the microbial community, and at the individual strain level, through the analysis of transcriptomic changes.

This PhD project targets the following research questions (**Figure I.18**):

- What is the impact of water content and oxygen status on the activity and composition of a DCM-degrading microbial community?
- Can soil granulometry change how water content and oxygen level impact the activity and composition of a DCM-degrading microbial community?
- What is the response of a DCM-degrading microbial community to a change in oxygen concentration?
- How does a change in oxygen concentration impact the gene expression of the facultatively anaerobic DCM-degrading strain *Hyphomicrobium* sp. GJ21?

I.3.2 General approach

Three different laboratory set up experiments were chosen to address these questions, which are presented in **chapters III, V and VI**. The experimental approaches and analysis methods

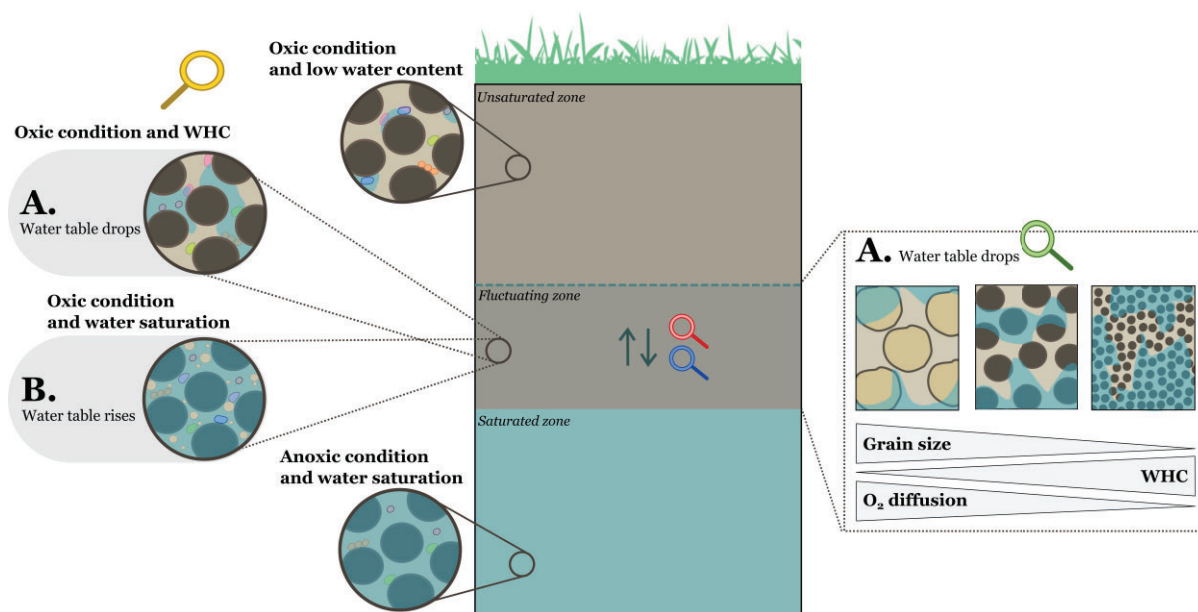
used in this work are presented in **chapter II**, while **chapter IV** details the optimization of the laboratory set up done during this PhD work.

In detail, **Chapter III** examines the impact of water content or oxygen status on the activity and composition of a DCM-degrading microbial community. To do so, laboratory microcosms were set up in 160 mL serum bottles filled with a sand matrix inoculum derived from two multi-contaminated laboratory aquifers that demonstrated DCM biodegradation activity (Prieto-Espinoza et al., 2021). These microcosms were exposed to different water contents under oxic conditions, or different oxygen statuses under saturated water conditions, and DCM was added over time through several spikes. To assess DCM degrading activity, DCM concentration was periodically monitored, while the microbial community composition was analyzed using 16S rRNA gene amplicon sequencing on DNA extracted from the sand matrices.

In **Chapter V**, the influence of soil granulometry on the activity and composition of a DCM-degrading microbial community exposed to specific water content and oxygen concentrations was studied. To do so, an optimised set up of laboratory microcosms in 20 mL glass vials was used (**chapter IV**). These microcosms were filled with (or without) artificial matrices of different grain sizes and exposed to various combinations of water content and oxygen concentrations, with DCM added over time through several spikes. Similar to chapter III, DCM-degrading activity was assessed by monitoring DCM concentration periodically, while the microbial community composition was analyzed using 16S rRNA gene amplicon sequencing on DNA extracted from the artificial matrices. Additionally, the response of the microbial community to a disturbance, consisting of a change in oxygen concentration, was studied from both the activity and composition perspectives using the same approaches as before: DCM concentration monitoring and metabarcoding of the 16S rRNA genes.

Chapter VI investigates the gene expression of the facultatively anaerobic DCM-degrading strain *Hyphomicrobium* sp. GJ21 when exposed to different oxygen levels. Laboratory cultures of this model strain were established under oxic and anoxic conditions, and mRNA sequencing was performed to explore the transcriptomic profiles in each condition.

Finally, a general synthesis of the main findings of the thesis, along with their implications for research perspectives, is presented in **Chapter VII**.



Research questions

-  What is the impact of water content and oxygen status on a DCM degrading community?
-  Can soil granulometry change the impact of water content and oxygen level on the DCM degrading community?
-  What is the response of a DCM-degrading microbial community to a change in oxygen concentration?
-  How does a change in oxygen concentration impact the gene expression of *Hyphomicrobium* sp. GJ21?

Figure I.18. Research questions.

Chapter II

Materials and Methods

In this second chapter, the materials and methods are grouped by topic or application. For the sake of clarity and improved readability, **Table II.1** summarizes the specific experimental set-up and analytical strategies used in the three main experimental chapters.

Table II.1. Summary of the experimental work associated to the experimental chapters.

	Chapter III	Chapter V	Chapter VI
Culture media	SGW	SGW	M ₃ Clo
Bacterial inocula	Natural microbial community	Natural microbial community	Pure strain
Experimental design	Microcosms in 160 mL serum bottles	Microcosms in 20 mL glass vials	Cultures in 160 mL serum bottles
Analytical methods	GC-FID	GC-FID-MS	OD ₆₀₀ measurements
	Oxygen measurements	Oxygen measurements	Oxygen measurements
Sequencing methods	16S rRNA gene amplicon sequencing - Illumina NovaSeq 6000	16S rRNA gene amplicon sequencing - Illumina NextSeq 2000	Total RNA sequencing - Illumina NextSeq 2000
Data analysis	Microbial community profiling	Microbial community profiling	Differential gene expression (DESeq2)
	Alpha-diversity metrics	Alpha-diversity metrics	
	PCA	PCA Correlation analysis	

II.1 Chemicals and reagents

All used chemicals and reagents were of the required purity and purchased from Euromedex, QIAGEN, Sigma-Aldrich, Thermo Fisher Scientific, New England Biolabs and ROTH. Salt-free oligonucleotides were purchased lyophilized from Eurofins.

II.2 Culture media

Two mineral media were used to culture the dichloromethane-degrading strains and microbial consortia: “*Methylobacterium* Mineral Medium without chloride”(M3Clo; modified from Roselli et al., 2013) and “Simulated Ground Water” (SGW; Dybas et al., 1995). The composition of the media is given in **Table II.2**. For solid media, agar (15 g/L) was added to the main mineral solution prior to autoclaving (121°C, 21 min) .

Table II.2. Composition of the defined media M3Clo and SGW.

Composition	Formula	M3Clo	SGW
		g/L	g/L
Monopotassium phosphate	KH ₂ PO ₄	2.9	0.8
Disodium phosphate	Na ₂ HPO ₄	5.1	2
Magnesium sulfate heptahydrate	MgSO ₄ ·7H ₂ O	0.1	0.15 ^a
Ammonium sulfate	(NH ₄) ₂ SO ₄	0.2	-
Sodium nitrate	NaNO ₃	-	1.6
Sodium carbonate	Na ₂ CO ₃	-	0.16 ^a
Sodium metasilicate pentahydrate	Na ₂ SiO ₃ ·5H ₂ O	-	0.35 ^a
Calcium nitrate tetrahydrate	Ca(NO ₃) ₂ ·4H ₂ O	0.025 ^b	0.0125 ^b
Trace elements solution	M3Clo	1 mL ^b	-
	SGW	-	1 mL ^b

^a Separately autoclaved and added from a 100X stock solution

^b Separately autoclaved and added from a 1000X stock solution

For M3Clo and SGW media, 1 mL of Ca(NO₃)₂·4H₂O was added after autoclaving from sterile stock solutions at 1000X (25 g/L and 12.5 g/L, respectively). For SGW media, 10 mL of sterile stock solutions at 100X of Na₂CO₃ (16 g/L), Na₂SiO₃·5H₂O (35 g/L) and MgSO₄·7H₂O (15 g/L) were added after separate autoclaving preventing precipitation.

Trace elements, prepared as 1000x stock, were sterilized by filtration (0.2 µm, Minisart, Thermo Fisher Scientific) and added to the heat-sterilised main saline medium. The M3Clo trace element stock solution was prepared in a final volume of 100 mL, by adding 0.5 mL H₂SO₄ (95%) and 1 g Fe(II)SO₄·7H₂O to 19.5 mL ultrapure water, followed by the addition of 10 mL of

each of the following stock solutions: 10 g/L $\text{MnSO}_4 \cdot \text{H}_2\text{O}$, 2.7 g/L $\text{Na}_2\text{MoO}_4 \cdot 7\text{H}_2\text{O}$, 1 g/L H_3BO_3 , 4.1 g/L $\text{CuSO}_4 \cdot 5\text{H}_2\text{O}$, 5.27 g/L $\text{ZnSO}_4 \cdot 7\text{H}_2\text{O}$, 1 g/L NH_4VO_3 , 2.5 g/L $\text{Co}(\text{NO}_3)_2 \cdot 6\text{H}_2\text{O}$, 1 g/L $\text{NiSO}_4 \cdot 6\text{H}_2\text{O}$. The SGW trace element stock solution was prepared in a final volume of 100 mL by adding 0.5 mL H_2SO_4 (95%) to 19.5 mL ultrapure water, followed by the addition of 10 mL of each of the following stock solutions: 10 g/L $\text{Fe}(\text{II})\text{SO}_4 \cdot 7\text{H}_2\text{O}$, 10 g/L $\text{MnSO}_4 \cdot \text{H}_2\text{O}$, 2.5 g/L $\text{Na}_2\text{MoO}_4 \cdot \text{H}_2\text{O}$, 1 g/L H_3BO_3 , 2.4 g/L $\text{CuSO}_4 \cdot 5\text{H}_2\text{O}$, 5.27 g/L $\text{ZnSO}_4 \cdot 7\text{H}_2\text{O}$, 2 g/L $\text{CoSO}_4 \cdot 7\text{H}_2\text{O}$, 1.07 g/L $\text{NiSO}_4 \cdot 7\text{H}_2\text{O}$.

To visually detect pH acidification caused by the hydrochloric acid produced during DCM degradation, solid media can be supplemented with bromothymol blue (BBT) from a stock solution (100x) to a final concentration of 0.08 g/L. The indicator colour shifts from blue to yellow in response to this acidification.

II.3 Microbial inocula and cultivation

II.3.1 Pure bacterial strains

Hyphomicrobium sp. GJ21 (Bringel et al., 2017) was cultured in M3Clo or SGW liquid and solid media from laboratory cryostocks. In the work described in **chapters III** and **V**, *Hyphomicrobium* sp. GJ21 was used as a model strain for DCM degradation. In these chapters, the strain was inoculated into the microcosms at the equivalent of 5% (v/v) from a preculture in SGW liquid medium with an OD_{600} of 0.1, following the protocol of Hermon and colleagues (Hermon et al., 2018). The precultures were done in 250 mL airtight flasks (erlenmeyer transformed with a screw thread, closed with screw caps with valves, Mininert; **Figure II.1-a.**). In the work described in **chapter VI**, *Hyphomicrobium* sp. GJ21 was cultured in 160 mL serum bottles with M3Clo liquid medium and sealed with 20 mm grey butyl rubber stoppers and crimp caps (**Figure II.1-b.**). Cultures were set in oxic (natural atmosphere) or anoxic conditions (replacement of the gas phase by H_2/N_2 (5%/95%)) at 1 atm and addition of KNO_3 at 20 mM from a heat-sterilized stock solution at 1 mM). In these cultures, DCM was added as a carbon source at a final concentration of 8 mM by adding the adequate volume from a stock solution of DCM at 25 mM, and cultures were incubated at 30°C with shaking (120 rpm). For growth in M3Clo solid medium, 1.4 mM of DCM was added to hermetically closed glass jars containing the solid cultures, which were then incubated at 30°C (**Figure II.1-c.**).

Methylobacterium extorquens DM4 (Vuilleumier et al., 2009) and *Hyphomicrobium* sp. MC8b (Hayoun et al., 2020) were grown in M3Clo liquid and solid media from laboratory cryostocks under oxic conditions. For growth in liquid media, the strains were cultured in 250 mL airtight flasks. DCM was added as a carbon source to a final concentration of 10 mM (v/v) from the pure solution, and the cultures were incubated at 30°C with shaking (120 rpm). For growth in solid medium, 1.4 mM of DCM was added to hermetically closed glass jars containing the solid cultures prior to incubation at 30°C.

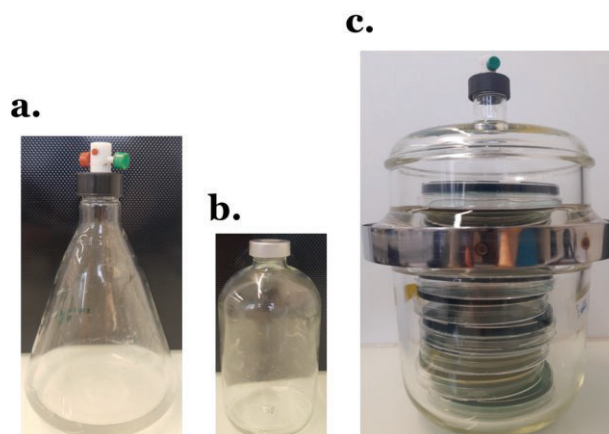


Figure II.1. Picture of laboratory culture systems. Liquid cultures of pure strains were done in **a.** 250 mL airtight flasks and **b.** 160 mL serum bottles. Solid cultures of pure strains were incubated in **c.** hermetically closed glass jars.

II.3.2 Natural microbial community

In the work described in **chapters III** and **V**, we used as inoculum a natural microbial community derived from the solid phase (quartz sand of 0.4 - 0.6 mm) of a previous experiment in laboratory-scale aquifers (Prieto-Espinoza et al., 2021). This natural microbial community was originally derived from a groundwater sample collected from the source zone of a well-characterized multi-contaminated aquifer located in the former industrial site of Themeroil (Vareannes-le-Grand, GPS coordinates: 46.701141 N, 4.843919 E; Piezometer 28, Hermon et al., 2018). The groundwater was kept under a constant N_2 -flux to maintain anoxic condition and used as inflow for the laboratory-scale aquifers, which were previously filled with sterile quartz sand (0.4-0.6 mm). At the end of the experiment conducted by Prieto-Espinoza and colleagues, the sand was collected and stored in two different ways for further use in our experiment: either it was saturated in contaminated water and kept at 4°C, or it was collected from cores in sterile polyethylene tubes (\varnothing : 5 cm) coming from the laboratory-scale aquifers and drained from its liquid phases before preservation at -20°C.

In **chapter III**, 100-140 g of the sand was used as inoculum and mixed with different volumes of SGW liquid media (see **Table III.1**) in 160 mL serum bottles sealed with 20 mm diameter grey butyl rubber stoppers (Interchim) and 20 mm diameter aluminium crimp caps (Supelco). DCM was added as a carbon source to a final concentration of 1 mM and microcosms were incubated at 25°C under oxic or anoxic conditions (**Figure II.2**).

In **chapter V**, we first prepared 18 precultures by mixing, per culture, 40 g of the sand with 50 mL of SGW liquid medium in 160 mL serum bottles sealed with 20 mm diameter grey butyl rubber stoppers and crimp caps, 9 under oxic conditions and 9 under anoxic conditions. DCM was added as a carbon source to a final concentration of 1 mM and the precultures were incubated at 25°C. After DCM degradation, the liquid phases coming from either the oxic or anoxic precultures were collected and pooled (\approx 450 mL per oxygen concentration). These

liquid phases were stored at 4°C and used as inocula in the microcosms prepared in 20 mL glass vials with 15 g of an artificial matrix. The microcosms were sealed (SG2 Silicon, PreSens GmbH) on the vial rim before placing a 20 mm magnetic crimp caps butyl-PTFE (Advion Interchim Scientific) and set under oxic or anoxic conditions. DCM was added as a carbon source to a final concentration of 1 mM, and microcosms were incubated at 25°C (**Figure II.2**).

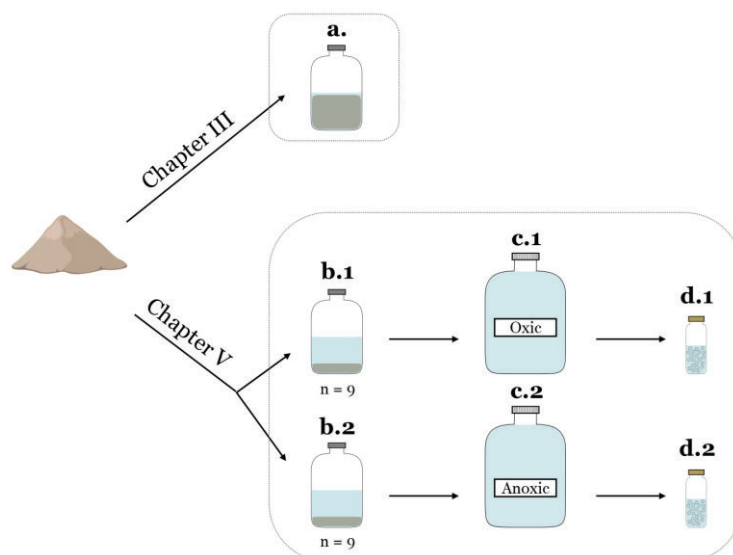


Figure I.2. Preparation of microcosms with the natural microbial community inoculum. In **chapter III**, microcosms were prepared in 160 mL serum bottles (**a.**) by mixing 100-140 g of sand from previous laboratory-scale aquifers with different volumes of SGW liquid media. 1 mM DCM was added as carbon source. In **chapter V**, precultures were prepared in 160 mL serum bottles by mixing 40 g of the same sand with 50 mL of SGW liquid media either under oxic (**b.1**; n=9) or anoxic (**b.2**; n=9) conditions. 1 mM DCM was added as carbon source. After DCM degradation, the liquid phases of the oxic (**c.1**) and anoxic (**c.2**) precultures were collected, pooled and stored at 4°C. Microcosms were prepared in 20 mL glass vials by mixing 15 g of an artificial matrix and different volumes of these liquid phases under oxic (**d.1**) or anoxic (**d.2**) conditions.

II.4 Analytical methods

II.4.1 Gas chromatography (GC)

DCM is a highly volatile compound which equilibrates between the liquid and gas phases at room temperature according to Henry's Law. In this work, DCM was directly quantified from the gas phase of the microcosms using two types of gas chromatographs (GC): a gas chromatograph connected to a flame ionization detector (GC-FID) or a GC-FID coupled to a mass spectrometer (GC-FID-MS).

II.4.1.1 GC-FID

In the work described in **chapter III**, DCM concentration was measured using a CP3800 gas chromatograph connected to a flame ionization detector (GC-FID; Agilent Technologies

France SAS). Headspace samples of 100 μL were collected from each microcosm manually with a gas-tight 1750 syringe (Hamilton Bonaduz AG) and injected into the GC column (CP-Sil 5 CB, length 15 m, diameter 0.25 mm, film thickness 0.25 μm ; Varian). Priming of the syringe was systematically carried out before sampling by purging 3 times the syringe with the headspace. The volatile compound was separated by isothermal elution at 32°C for 1 min, followed by a linear gradient of temperature increase to 220°C at 20°C/min. The injector and detector were maintained at 220°C in splitless mode, and 300°C, respectively. Nitrogen was used as the carrier gas at a flow rate of 2 mL/min. A hydrogen generator (Hydrogen generator PGH₂, DBS) provided the necessary combustible for the FID. The analysis time per sample is of 4 min 30 sec, with a peak corresponding to the eluted DCM at 1 min 50 sec. Peak areas were analyzed using the Galaxie Workstation software (Varian).

After the addition of DCM, an equilibration time of 3 hours was respected for DCM to distribute between the liquid and gas phases of the microcosms before the initial measurement of DCM concentration (T₀). Periodic measurements were then taken over time. The relative DCM concentration at each time point was calculated using the equation below, where the peak area at T₀ was used as the reference of the maximum value (100%). Values greater than the T₀ were set to 100%.

$$[\text{DCM}]_{\text{relative}}(\%) \text{ at timepoint } n = \frac{\text{Peak area at timepoint } n}{\text{Peak area at } T_0} \times 100$$

II.4.1.2 GC-FID-MS

During the work described in **chapter V**, DCM concentration was measured by a gas chromatograph (GC, Trace 1300, Thermo Fisher Scientific) equipped with a flame ionization detector (FID) and coupled with a mass spectrometer (MS, ISQ®, Thermo Fisher Scientific). Headspace samples of 200 μL were collected from each microcosms after 30 sec of automatic shaking using an autosampler (TriPlus RHSTM, Thermo Fisher Scientific) and injected into the GC column (DB-624, length 30 m, diameter 0.25 mm, film thickness 1.4 μm). The volatile compound was separated by isothermal elution at 50°C for 2 min, followed by a linear gradient of temperature increase to 230°C at 30°C/min. Injector and detector were set at 240°C in split mode (split ratio 1:10) and 250 °C, respectively. Helium was used as the carrier gas at a flow rate of 1.5 mL/min. The analysis time per sample is 5 min, with a peak corresponding to the eluted DCM at 2 min 50 sec. Peak areas were analyzed with the Xcalibur software (Thermo Fisher Scientific). DCM calibration curves were prepared similarly as the experimental microcosms, with the same matrix and headspace volume (see details in **section IV.6**).

After the addition of DCM, an equilibration time of 3 hours was respected for DCM to distribute in the different phases of the microcosms before making a first measurement of DCM concentration. Daily measurements were then performed using an automated sequential program, which included blanks and calibration points alongside the samples. The two

calibration points (0 mM and 1 mM) were measured to account for machine drift and normalize the peak areas of the samples, allowing for the calculation of DCM concentration at each timepoint using the below equation. Values higher than the 1 mM calibration point were set at 1 mM.

$$[\text{DCM}](\text{mM}) = \frac{\text{Peak area sample}}{\text{Peak area calibration point 1 mM}}$$

II.4.2 Oxygen measurements

Oxygen concentration was periodically monitored during all experiments using non-invasive optical sensor spots (SP-PSt3-YAU, Presens Unisens) attached in the upper part of the inner transparent surface of microcosms and cultures. Measurements were done with a fibre optic meter (Fibox, detection limit 15 ppb, Presens Unisens) connected to a 2 mm polymer optical fibre (POF, Presens Unisens). The POF transfers excitation light to the optical sensor spot from the outside through the wall, and the sensor response back to the meter. Signals were analyzed using the Fibox 3 version 6.02 software (Presens Unisens) and reported in ppm. Atmospheric oxygen concentration is approximately 8 ppm (~20% v/v), while anoxic conditions were defined as below 0.5 ppm (~ 1% v/v).

II.4.3 pH measurements

pH was measured using a pH microelectrode pHemonal[®] MIC220 (VWR) connected to the pH cyberscan 520 pH (Thermo Fisher Scientific). The pH meter was calibrated in standard solutions of pH 4, 7 and 10 before use.

II.4.4 Optical Density (OD₆₀₀) measurements

Optical Density at 600 nm (OD₆₀₀) was measured to monitor the growth of the pure strain *Hyphomicrobium* sp. GJ21. A 1 mL sample was taken from the cultures at different time points through the septum using a sterile syringe and needle, then transferred to a cuvette. The OD was measured using a spectrophotometer Jenway 7315 UV-Visible at 600 nm wavelength. The culture media was used as blank before each measurement.

II.5 Molecular biology methods

II.5.1 DNA

II.5.1.1 DNA extraction

DNA from pure strains was prepared using the MasterPure[™] Complete DNA and RNA Purification kit (Epicentre) following manufacturer's instruction from cell pellets.

Total DNA was also extracted from the microcosms matrix in **chapters III** and **V** using the DNeasy PowerWater kit (Qiagen) according to the manufacturer's instructions. Briefly, 1 g of the matrix was insert into a 5 mL "PowerWater Bead Pro Tube", and 1 mL of the "Solution PW1", previously warmed to 55°C, was added. The tubes were then vortex (Vortex Genie 2, Scientific Industries Inc.) at maximum speed (speed 10) for 5 min, and centrifuged at 4000 g for 1 min. The supernatant (~800 µL) was recovered in a clean 2 mL collection tube and centrifuge at 13 000 g for 1 min at room temperature. Avoiding the pellet, the supernatant (~800 µL) was transferred to a clean 2 mL collection tube and 200 µL of "Solution IRS" were added. The tube was then briefly vortexed and incubated on ice (4°C) for 5 min. Next, the tube was again centrifuged at 13 000 g for 1 min, the supernatant (~800 µL) was recovered in a new 2 mL collection tube, and 650 µL of "Solution PW3", previously warmed at 55°C, were added to the tube, which was briefly vortexed. 650 µL of the resultant solution were loaded onto a "MB Spin Column" that was centrifuged at 13 000 g for 1 min. The flow-through was discarded and this step was repeated till the solution was completely processed (on average, this step was repeated a total of 3 times). Next, the "MB Spin Column" was placed into a clean 2 mL collection tube and 650 µL of "Solution PW4", previously shake, were added. The tube was centrifuged at 13 000 g for 1 min. The flow-through was discarded and 650 µL of ethanol were added, and the tube was centrifuged again. After discarding the flow-through, the tube was centrifuged at 13 000 g for an additional 2 min to remove residual ethanol. Finally, the "MB Spin Column" was placed into a clean 2 mL collection tube and 50 µL of ultrapure water were added to elute the DNA. Following centrifugation at 13 000 g for 1 min, the flow-through was recovered and re-passed through the "MB Spin Column" to maximize DNA elution. The recovered DNA was quantified and stored frozen at -20°C until further use.

II.5.1.2 DNA quantification

DNA concentrations were quantified by the Qubit® 2.0 Fluorometer with the Qubit® dsDNA HS Assay kit (Thermo Fisher Scientific). 5 µL of the DNA samples were added to 195 µL of a working solution (mix of buffer and reagent (200X) from the kit at a 199:1 ratio) and incubated at room temperature for 3-5 min before measurement. DNA concentration in each sample was determined by comparison with Qubit® standard DNA solutions from the kit (0 and 10 ng/µL) that were prepared adding 10 µL to 190 µL of the working solution and that were measured before the experimental samples.

II.5.1.3 PCR

Amplification reactions of DNA were done using the primers and the programs presented in **Table II.3** and **Table II.4**. For Ribosomal Intergenic Spacer Analysis (RISA; (Ranjard et al., 2000)), PCR reactions were performed in a final volume of 25 µL, and contained 1 µL DNA template at 20 ng/µl excepted when mentioned, ITSF and ITSr primers at 0.4 µM final concentration each, 0.1 mM dNTP mix, 0.024 U DreamTaq polymerase (5 U/µL, Thermo Fisher Scientific), 1X DreamTaq Green Buffer containing 20 mM MgCl₂. Other PCR amplification reactions were carried out in a final volume of 10 µL, and contained 1 µL DNA

template at 20 ng/ μ l excepted when mentioned otherwise, each primer (**Table II.3**) at 0.5 μ M final concentration, 0.2 mM dNTP mix, 0.02 U Phusion polymerase (2 U/ μ L, Thermo Fisher Scientific), 1X Phusion HF or GC buffer containing 1.5 mM MgCl₂. All PCRs were made in Biometra TOne 96 Thermocycler (Analytikjena).

II.5.1.4 Agarose gel electrophoresis

After amplification, PCR products were subjected to electrophoresis using 1% (w/v) agarose gel in TAE 1X buffer (Euromedex) and ethidium bromide at 2 mg/ μ L. Before loading the gel, 1X TriTrack loading dye (Thermo Fisher Scientific) was added in each sample when needed. A DNA ladder was also loaded in the gel to determine the size of the products of interest (GeneRuler 1 kb Plus DNA Ladder, Thermo Fisher Scientific). Gels were run for 45 min at 90V before visualizing the PCR products under UV-light (Transilluminateur Herolab, E.A.S.Y Win32 software).

II.5.1.5 PCR products purification and sequencing

The PCR products corresponding to the gene *dcmA* were Sanger sequenced (outsources at Eurofins genomics). To do so, the PCR products or the bands on agarose gel corresponding to the correct size of this gene were recovered and purified using the “NucleoSpin Gel and PCR Clean-Up” kit (Macherey-Nagel) according to the manufacturer’s instructions. The purified amplicons were then quantified by Qubit® as described above, concentration adjusted to fit the guidelines and sequenced with the Sanger method by Eurofins using customized primers (**Table II.3**) following the company’s instructions.

II.5.1.6 *In silico* analysis of the sequenced PCR products

Obtained sequences coming from the PCR products were screened to keep only high confidence bases. The *dcmA* gene sequences obtained from the natural microbial community were compared to the reference sequences from *Methylobacterium extorquens* DM4 (Metdi2656), *Hyphomicrobium* sp. GJ21 (HYPGJv1_31561), *Hyphomicrobium* sp. MC8b (HYPMC8B_v1_1632) and *Hyphomicrobium denitrificans* ATCC 5188 (Hden_0711) using the Global Alignment tool in BLAST (Zhang et al., 2000). Reference strain sequences were extracted from the MicroScope platform of Genoscope (Vallenet et al., 2020). Sequences were then analysed in fasta format using the “Nucleotid BLAST” (BLASTn) tool available in the NCBI platform. A phylogenetic tree was constructed with all *dcmA* gene sequences using the phylogeny.fr platform in one-click mode (Dereeper et al., 2008).

Table II.3. Oligonucleotides and PCR parameters.

Target	Primer name	Sequences (5' ... 3') ^a	Size (bp)	PCR parameters (T _a , polymerase, buffer) ^b	Reference
16S-23S rRNA intergenic region ^c	ITSF	GTCGTAACAAGGTAGCCGT	889 ^d	55°C, DreamTaq ⁱ , Green buffer	(Cardinale et al., 2004)
	ITSR	GCCAAGGCATCCACC			
<i>rps</i> gene	Pro314F	CCTACGGGNBGCASCAG	439 ^e	58°C, Phusion ^g , HF buffer	(Takahashi et al., 2014)
	Pro805R	GACTACNVGGGTATCTAATCC			
<i>dcmA</i> gene	Forw <i>dcmA</i> Univ	CGCCGACATCTGGATCG	930	60°C, Phusion, GC buffer	Lázaro Sánchez (section III.2.3.2)
	Rev <i>dcmA</i> Univ	YGGCCCTCYTTCTCAA			
	SG1	GCCTACTTTATCATCCGGCG			
<i>dcmA</i> gene	<i>dcmA</i> GJ21/DM4/ATCC51888-R	ATCGAAGGAATGCGATGAAC	961	62°C, Phusion, GC buffer	Lázaro Sánchez (section III.2.3.2)
	<i>dcmA</i> _MCb8b_uniqueF	GGCAGGCCAGTCTACAGAAG			
	<i>dcmA</i> _MCb8b_uniqueR	TACACGGGCAACGGAGC			
HYPDCMNEW_v1_20300 ^h	GJ21fi	TGCTGCTCACCCCTGTCTTTC	1197	60°C, Phusion, HF buffer	Bringel (not published)
	GJ21r2	GTGCTGCTGTGAGGGGATT			
<i>mec</i> cluster	<i>mecE</i> 828F	ACCATAATTGTCTTTTGTGCCYCAG	726	58°C, Phusion, HF buffer	Murdoch et al., 2022
	<i>mecF</i> 641R	GCAAGGATADCCATAITTTGTCTTT			

^a Nomenclature IUPAC (N = all bases; B = C or G or T; S = G or C; V = A or C or G; Y = C or T)

^b T_a: annealing temperature

^c Region between the genes coding the small (16S) and the large (23S) subunits of ribosomal

^d Size of the region between the small (16S) and the large (23S) subunits of ribosomal sequences of *Hyphomicrobium* sp. GJ21. Variable size depending on the strains

^e Size of the hypervariable region V3-V4 of *Hyphomicrobium* sp. GJ21. Variable size depending on the strains

^f DreamTaq DNA Polymerase (5U/μL); Thermo Fisher Scientific

^g Phusion High-Fidelity DNA Polymerase (2U/μL); Thermo Fisher Scientific

^h Gene coding for a protein of unknown function, unique to *Hyphomicrobium* sp. GJ21 in comparison to other strains studied during my work

Table II.4. PCR programs used.

Step	RISA ^a amplification	Other amplifications	Cycles
Initial denaturation	95 °C for 3 min	98°C for 2 min	1
Denaturation	95 °C for 45 sec	98°C for 30 sec	30
Annealing	55 °C for 1 min	T _a for 30 sec ^b	
Extension	72 °C for 45 sec	72°C for 1 min 15 sec	
Final extension	72 °C for 7 min	72°C for 3 min	1

^a RISA: Ribosomal Intergenic Spacer Analysis

^b T_a: annealing temperatures specified in **Table II.3**.

II.5.2 RNA

II.5.2.1 RNA extraction

Total RNA was extracted from *Hyphomicrobium* sp. GJ21 liquid cultures harvested in the mid-exponential phase (OD₆₀₀ ~0.066 to 0.122) by centrifugation (8 500 rpm for 20 min at room temperature) using the “Monarch Total RNA Miniprep Kit” (New England Biolabs) according to the manufacturer’s instructions for “Tough-to-Lyse Samples”. All the following centrifugation steps were realised at 16 000 g for 30 sec, except when mentioned so. Briefly, pellets were first submitted to an enzymatic lysis by adding 300 µL of 1 mg/mL lysozyme prepared in DEPC-treated water. After incubation at 25°C for 5 min, the solution was transferred to a 2 mL RNase-free microfuge tube and 600 µL of “RNA Lysis Buffer” were added. The tube was vortex vigorously for 10 sec and centrifuged for 2 min. 800 µL of the supernatant were loaded to a “gDNA Removal Column” fitted with a collection tube and centrifuged. An equal volume of ethanol 95% (~800 µL) was added to the flow-through and mix thoroughly by pipetting. The mixture was then loaded to a “RNA Purification Column” placed in a clean collection tube and centrifuged. The flow-through was discarded and 500 µL of “RNA Wash Buffer” was added onto the column. After centrifugation, the flow-through was again discarded and 80 µL of a mixture of “DNase I” (5 µL) with “DNase I Reaction Buffer” (75 µL) was added. The tube was then incubated for 15 min at room temperature. Next, 500 µL of “RNA Priming Buffer” was added on top of the column and centrifuged. The flow-through was discarded and 500 µL of “RNA Wash Buffer” was added. After centrifugation and discarding again the flow-through, another 500 µL of “RNA Washer Buffer” were added and the column was centrifuged for 2 min. The column was then transferred to a RNase-free tube and 50 µL of Nuclease-free ultrapure water was added onto the column. Following a centrifugation step, the flow-through was recovered and re-passed through the column to optimise the elution of RNA. A 5 µL aliquot of the eluted total RNA was prepared and stored frozen at -20°C for subsequent quality analysis. The other 45 µL total RNA was stored frozen at -80°C until depletion, library preparation and sequencing.

II.5.2.2 RNA quantification

Total RNA concentrations were quantified by the Qubit® 2.0 Fluorometer with the Qubit® RNA HS Assay kit (Thermo Fisher Scientific). 5 µL of the RNA samples were added to 195 µL of a working solution (mix of buffer and reagent (200X) from the kit at a 199:1 ratio) and incubated at room temperature for 3-5 min before measurement. RNA concentration in each sample was determined by comparison with the Qubit® standard RNA solution (10 ng/ µL) and DEPC-treated water (0 ng/ µL). These standards were prepared adding 10 µL to 190 µL of the working solution and were measured before the experimental samples

II.5.2.3 Determination of RNA quality

The quality of the total RNA extracted was assessed using the “Agilent RNA 6000 Nano Assay”, according to the manufacturer’s instructions. This method is based on the electrophoretic separation of RNAs on a microchip and subsequent detection via laser-induced fluorescence detection. To prepare the gel and the gel-dye mix, 550 µL of “RNA 6000 Nano gel matrix” was firstly loaded into a spin filter and centrifuged at 1 500 g for 10 min. Aliquots of 65 µL of filtered gel were prepared into 0.5 mL RNase-free microfuge tubes and conserved at 4°C. In parallel, the “RNA 6000 Nano dye concentrate” was equilibrated to room temperature for 30 min, vortexed, and 1 µL of dye was added into a 65 µL aliquot of filtered gel. The solution was vigorously vortex and centrifuged at 13 000 g for 10 min. The gel-dye mix was then loaded to a “RNA 6000 Nano chip” (**Figure II.3-a.**), previously placed on the chip priming station (**Figure II.3-b.**). To do so, 9 µL of gel-dye mix were pipetted in the dedicated well. The chip priming station was closed, and the plunger was pressed to be held by the clip. After 30 sec, the pressure by released by opening the clip according to manufacturer recommendations before the chip priming station was open. Next, we pipetted 9 µL of gel-dye mix in the wells marked G and 5 µL of “RNA 6000 Nano marker” in all the other wells. A volume of 1 µL of the RNA samples were added in the numbered sample wells as well as 1 µL of a prepared ladder in the well marked so. Finally, 1 µL of “RNA 6000 Nano Marker” was pipetted in each unused sample well, if any. Once prepared, the chip was vortexed in an IKA vortexer at 24 000 rpm for 1 min and placed in the “Agilent 2100 bioanalyzer” and analysed using the “RNA 6000 Nano assay” with the software “2100 Expert Software”. This software generates an electropherogram that provides a visual assessment of the quality of each RNA sample and calculates its RIN value (RNA Integrity Number), a standardized measure of total RNA quality ranging from 10 (highly intact RNA) to 1 (completely degraded RNA) (**Figure II.3-c.**).

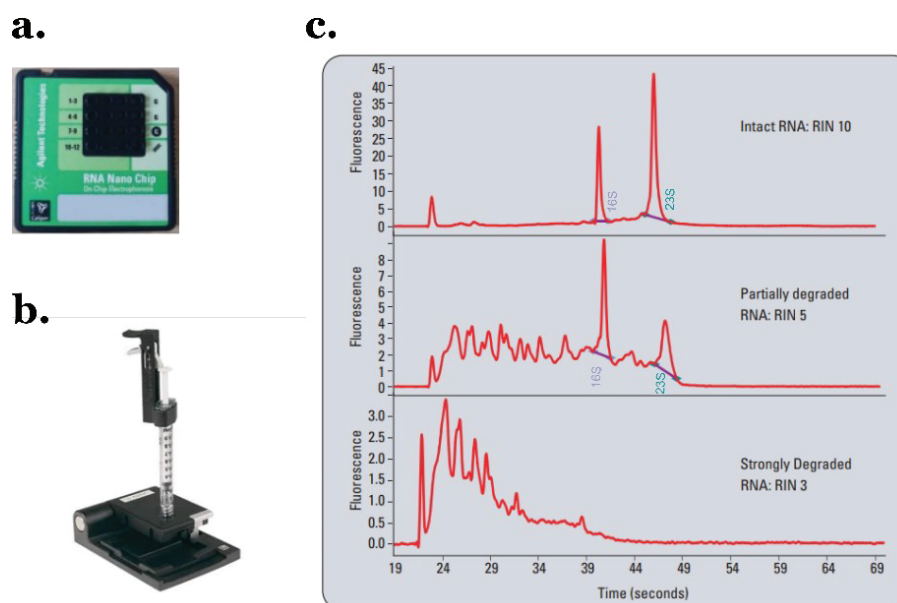


Figure II.3. Quality assessment of the total RNA using the Agilent RNA 6000 Nanopore Assay. **a.** Microchip (“RNA 6000 Nano chip”) within which the gel matrix is prepared and used for separating the RNAs based on their size. **b.** Chip priming station used to load the gel into the microchip. **c.** Examples of samples electropherograms with different RIN values depending on the quality of the total RNAs. The X-axis represents time and the Y-axis represents the fluorescence. Adapted from Mueller et al. (2004).

II.6 Bacterial community analysis

II.6.1 16S ribosomal RNA (rRNA) gene amplicon sequencing

The diversity of the hypervariable V3-V4 regions of the 16S rRNA genes from the natural microbial community in the extracted DNA was amplified and sequenced. The data generation was outsourced. Illumina NovaSeq 6000 platform was used during the experiments described in **chapter III**, and Illumina NextSeq 2000 platform was used in the experiments described in **chapter V**. The **Figure II.4** summarizes the general steps followed for the analysis of the data.

II.6.1.1 Illumina NovaSeq 6000 platform

PCR amplicons were prepared using the primers 341F (5'-CCTAYGGGRBGCASCAG-3') and 806R (5'-GACTACNNGGTATCTAAT-3') carrying adapters. Barcoded amplicon sequencing (2x250 bp paired end) was performed using Sequencing by Synthesis (SBS) technology by the Illumina NovaSeq 6000 platform. Demultiplexed raw data were trimmed, filtered and denoised using the DADA2 pipeline (Callahan et al., 2016). The obtained sequences were clustered at 100% identity to obtain Amplicon Sequence Variants (ASVs). Each ASV was annotated with the QIIME2 platform (Bolyen et al., 2019) and the Silva database (version 138, November 2022), before the data was released to us (Novogene, Cambridge).

II.6.1.2 Illumina NextSeq 2000 platform

PCR amplicons were prepared using the primers Forward (5'-CCTACGGGNGGCWGCAG-3') and Reverse (5'-GACTACHVGGGTATCTAATCC-3'). Barcoded amplicon sequencing (2x300 bp paired end) was performed using the Illumina NextSeq 2000 platform (LCSB genomic platform, University of Luxembourg). Demultiplexed raw data was released to us. The data was then trimmed, filtered and denoised following the DADA2 R package (Callahan et al., 2016) according to the pipeline tutorial found at benjjneb.github.io/dada2/tutorial.html. The specific parameters used for the trimming and filtering steps in our analyses are detailed in **Table II.5**. The obtained treated sequences were clustered at 100% identity to obtain Amplicon Sequence Variants (ASVs). Each ASV was annotated with the Silva database (version 138, May 2024).

Table II.5. Parameters used for filtering and trimming demultiplexed raw data in DADA2 pipeline.

Steps	R parameter	Objective
Filtering	maxN=0	Removal of reads with more than 0 ambiguous bases (N)
	maxEE=c(2,4)	Removal of forward and reverse reads with a maximum of 2 and 4 expected errors, respectively
Trimming	truncLen=c(280,230)	The forward reads are truncated to a length of 280 bases and the reverse reads to a length of 230 bases
	truncQ=2	Reads with an average quality score of less than 2 are truncated at the first position
	trimLeft=c(21,21)	Removal of the first 21 bases from both forward and reverse reads, where primer sequences are found

II.6.2 Data pre-processing

The first step before starting the analysis of the 16S rRNA gene amplicon sequencing data was to unify this data into an integrated format that could be used in the different analyses. To do so, the phyloseq R package (McMurdie & Holmes, 2013) was used, which imports the data coming from the output files of the DADA2 and QIIME2 pipelines (ASV and taxonomy tables), as well as the data of the experimental conditions, and merge it as a multi-component class called the “phyloseq” class. This class can then be used as the sole input data, simplifying the commands in the different analyses that will follow afterwards.

II.6.3 Data normalization and transformation

The compositional aspect of the 16S rRNA gene amplicon sequencing data arises from inherent biases in the technique, leading to a lack of sample independence and the emergence of spurious correlations (Gloor et al., 2017). Therefore, when working with this type of data, it is necessary to normalize and transform the data prior to undertaking any statistical analysis.

One of the most recommended methods in the literature is the centered log-ratio (CLR) transformation. This method transforms the compositional data into their log-ratio representation by using the geometric mean of all ASVs as the denominator. This allows the relationship between ASVs to be captured, restoring the independence among samples and making the data ready to be used in multivariate analyses (Yerke et al., 2024). However, this transformation also has its limitations, particularly due to the sparsity of the 16S rRNA amplicon sequencing data. To overcome this issue, after the transformation, we replaced the negative values with 0. The negative values are the result of low-abundance (or rare) ASVs.

II.6.4 Metabarcoding data analysis

To characterise the bacterial community from the 16S rRNA gene amplicon sequencing data we used alpha- and beta-diversity analysis. Alpha-diversity describes the diversity within the samples, giving insights about the species richness (number of taxa) and the evenness (relative abundance of those taxa), while the beta-diversity examines the differences or dissimilarities in terms of composition between the samples.

II.6.4.1 Alpha-diversity analyses

Three indices were used to characterize the alpha-diversity in the samples: the Chao1 index, that estimates the number of taxonomic unit (ASV here) in a community, the Pielou's evenness index, that measures how evenly the taxonomic units (ASV) are distributed in the community, and the Shannon-Wiener index, that is an equitability measure that reflects both the number of taxonomic unit (ASV) and their relative abundance (Kim et al., 2017; Whittaker, 1972). All indices were calculated using the phyloseq R package and plotted using the ggplot2 R package (Wickham, 2016). Statistical analyses of significance, i.e. ANOVA followed by post-hoc Tukey HSD test, were performed using the stats R package (R Core Team, 2023).

II.6.4.2 Beta-diversity analyses

To examine the compositional dissimilarities between samples, a Principal Component Analysis (PCA) was performed using the microViz R package (Barnett et al., 2021). This package allows for the use of the Aitchison distance, which is equivalent to the Euclidean distance, but is calculated on taxonomic unit counts (in our case, at the genus taxonomical level) subjected to a CLR transformation. The Aitchison distance has the advantage of being insensitive to differences in sampling depth, meaning that the addition of more data (i.e. more sequencing reads) will not make two samples appear less distant (Quinn et al., 2018).

The PCA is a multivariate analysis that projects a high-dimensional dataset into a reduced space by extracting the most informative characteristics that explain the variation of the dataset (principal components) and representing them in a two-dimensional scale plot (Bro & Smilde, 2014). Each data point representing a sample is positioned in the PCA plot based on its projection onto the principal components, reflecting how it is defined by the variation present in the data set. Samples that are close together have similar features, while those that

are further apart have greater variation of them. This information can help to identify clusters of samples in the dataset.

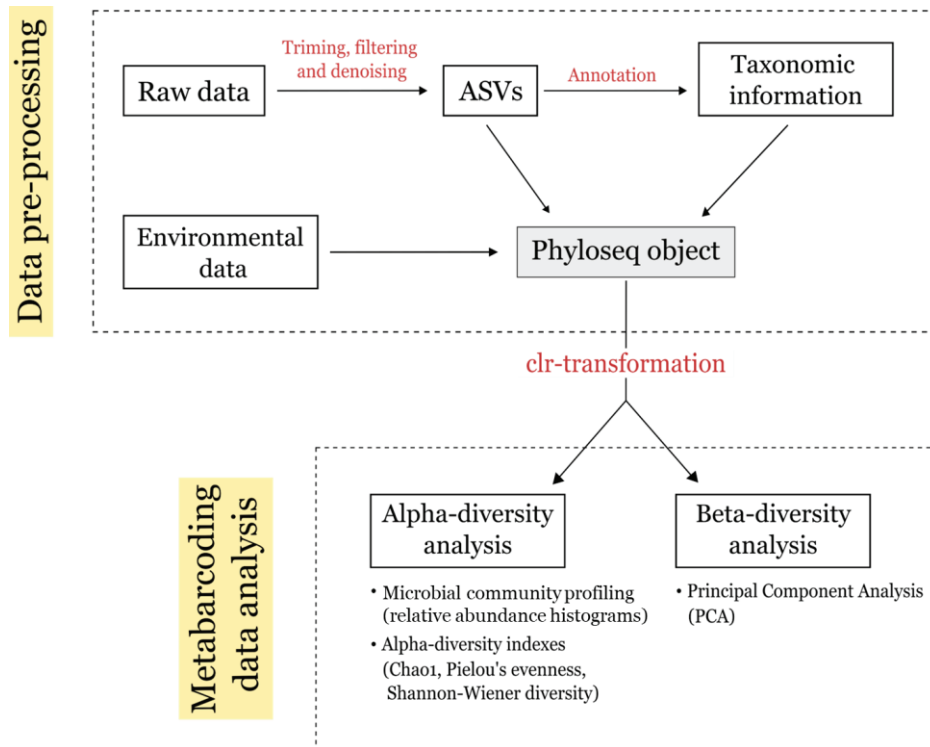


Figure II.4. Workflow for the microbial community analysis. During the data pre-processing, the phyloseq object was obtained using (i) the ASVs outcome file resulting from the trimming, filtering and denoising of the 16S rRNA gene amplicon sequences performed using the DADA2 pipeline, (ii) the taxonomic information of these ASVs obtained after their annotation using the Silva database, and (iii) the environmental data collected during the experiments. The data were then normalized using a clr-transformation. Finally, metabarcoding analyses were performed and the diversity within (alpha-diversity) and between (beta-diversity) samples was studied.

II.7 *Hyphomicrobium* sp. GJ21 transcriptome

II.7.1 Whole-transcriptome sequencing

After ribosomal RNA depletion with the Ribo-Zero Plus Microbiome rRNA depletion kit, a total RNA library was prepared using the Illumina Stranded Total RNA library prep kit and sequenced (2x150 bp paired end) using the Illumina NextSeq 2000 platform (LCSB genomic platform, University of Luxembourg). Multiple RNA-seq reads in fastqsanger format were obtained for each sample and subsequently released to us. The raw data was uploaded to the Galaxy France web platform (usegalaxy.fr; (The Galaxy Community, 2024)), where it was processed and further analysed. The **Figure II.5** summarizes the workflow used for analysing the whole-transcriptome sequencing data, which was adapted from the tutorial “[Reference-based RNA-Seq data analysis](#)” published in the Galaxy Training website.

II.7.2 RNA-seq reads quality control

To assess the quality of the raw RNA-seq reads, we used the FastQC tool (Galaxy version 0.74+galaxy1), to infer whether the reads had any issues to be aware of. The results were aggregated and visualized using the MultiQC tool (Galaxy version 1.11+galaxy1).

Next, based on the quality reports, the RNA-seq reads were trimmed to remove low-quality bases, as well as reads that were of poor overall quality. In our case, we removed all bases with a quality score below 30. To do this, we used the Trimmomatic tool (Galaxy version 0.39+galaxy2) and its “sliding window trimming” operation, cutting the reads when the average quality within a window of 4 nucleotides fell below 30.

II.7.3 RNA-seq reads mapping to the reference genome

The high-quality filtered RNA-seq reads were aligned to the reference genome of *Hyphomicrobium* sp. GJ21 using the HISAT2 tool (Galaxy version 2.2.1+galaxy1). This tool required the input of two datasets: (i) the RNA-seq reads in fastqsanger format (output of the Trimmomatic tool); and (ii) the reference genome of *Hyphomicrobium* sp. GJ21 in fasta format, exported from the MicroScope web platform (mage.genoscope.cns.fr; (Vallenet et al., 2020)). This was followed by the use of the MultiQC tool to aggregate the HISAT2 summary files and check the percentage of the reads mapped to the genome. As over 70% of the reads have mapped in all samples, we proceeded with the analysis.

The main output of the HISAT2 tool was a BAM file per sample. These types of files store the read sequences, whether they have been aligned to the reference sequence, and if so, the position on the reference sequence to which they have been aligned. To visualize the content of the BAM files, we used the Integrative Genomics Viewer (IGV, (Robinson et al., 2011)).

II.7.4 Quantification of number of reads per annotated gene

Stranded RNA-seq libraries preserved information about the strand from which the RNA was transcribed. Using the Infer Experiment tool (Galaxy version 5.0.3+galaxy0), we confirmed that our RNA-seq libraries were reverse stranded. In details, a selected sub-sample of reads from the BAM files were used to determine their genomic coordinates and strands on the reference genome. This tool required the use of two datasets: (i) the BAM files obtained after the mapping (output of the HISAT2 tool); and (ii) the reference genome of *Hyphomicrobium* sp. GJ21 in BED12 format, obtain by conversion of the genome in GTF format using the Convert GTF to BED12 tool (Galaxy version 357). The MultiQC tool was used to check the number of reads identified as sense and antisense. If they were equivalent, the RNA-seq library was non-directional. However, if it was not equivalent, it meant that the library was forward stranded (more sense reads) or reverse stranded (more antisense reads).

Next, to quantify the number of reads per gene, we used the featureCounts tool (Galaxy version 2.0.3+galaxy2), which required: (i) the BAM files obtained after the mapping (output

of the HISAT2 tool); and (ii) the reference genome of *Hyphomicrobium* sp. GJ21 in GFF/GTF format. The strand information (reverse stranded) was specified in the setting, as well as the GFF feature type filter (“genes”; only rows with the matching feature type will be included in the read count), and the GFF identifier (“gene_id” as by default). The main output of this tool was a table per sample with the reads count per gene. Finally, the MultiQC tool helped checking how many reads have been assigned to genes in each sample, with the aim of recovering at least 50% of them to proceed with further differential gene expression analysis.

II.7.5 Analysis of the differential gene expression

To compare the gene expression between the experimental conditions, we used the DESeq2 tool (Galaxy Version 2.11.40.8+galaxy0), which uses the read count files from the different samples obtained from the featureCounts tool, combines them into a table and applies a normalization step for sequencing depth and library composition (Love et al., 2014). In the tool settings, samples category are notified (in our case, there were two categories: oxic and anoxic conditions). The outputs from DESeq2 included a table with the normalized counts for each gene (rows) across the samples (column), along with a graphical summary of the results, with a PCA plot, a heatmap of the sample-to-sample distance matrix and a histogram of the p-values. The output table was used in the Filter tool (Galaxy Version 1.1.1) to extract genes that showed a significant change in expression (adjusted p-value < 0.05) between the two conditions. Additionally, the genes with a fold change (FC) greater than 2 or lower than 0.5 ($\text{abs}(\log_2\text{FC}) > 1$), representing the most differentially expressed genes, were also extracted. Finally, results from the DESeq2 tool were visualized using a volcano plot, which displays statistical significance (p-value) versus fold change (FC). The Volcano Plot tool (Galaxy version 0.0.5) was used to create this scatterplot using the table with the normalized counts obtained from the DESeq2 analysis as input.

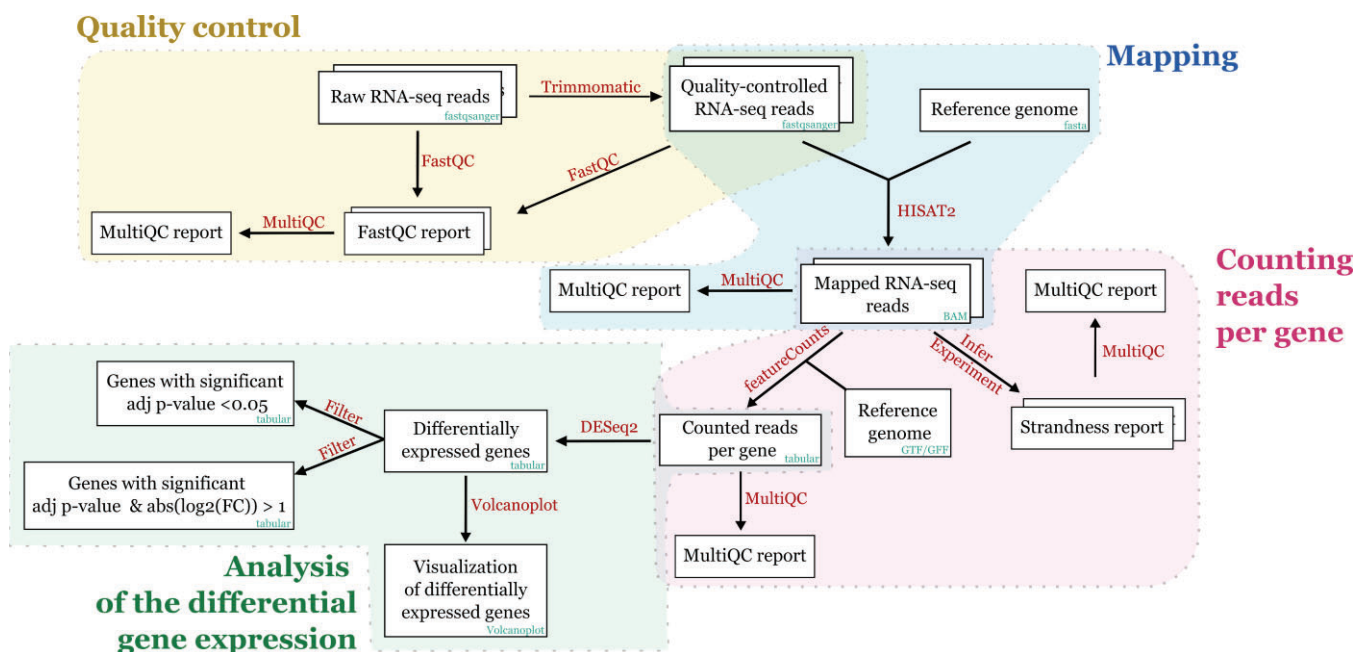


Figure II.5. Workflow for the analysis of the whole-transcriptome sequencing data.

Chapter III

Impact of water content
and oxygen status on
a DCM-degrading microbial community

III.1 Introduction

Dichloromethane (DCM, CH₂Cl₂) is a toxic and persistent industrial solvent that is frequently detected in groundwater, where it can be biodegraded under oxic and anoxic conditions by co-metabolism or serving as carbon and/or electron sources (Hermon et al., 2018). In oxic conditions, the only characterized metabolic pathway that allows bacteria to grow with this compound as their sole source of carbon and energy relies on the activity of the DCM dehalogenase DcmA, a glutathione S-transferase encoded by the highly conserved *dcmA* gene (Muller et al., 2011a) (see details in **section I.1.2.1**). The model strain *Hyphomicrobium* sp. GJ21 can also use this pathway in anoxic conditions, using nitrate as an alternative electron acceptor. In anaerobic conditions, Murdoch and colleagues identified the *mec* cluster and proposed its major role in this type of metabolism, highlighting the potential role of the genes *mecE* and *mecF* during the cleavage of the C-Cl bonds (Murdoch et al., 2022). More recently, Soder-Walz and colleagues demonstrated that, among the genes composing this cluster, the *mecE* and *mecC* genes encode two zinc-dependent methyltransferases which, along with the cobalamin-dependent shuttle protein encoded by *mecB*, are key enzymes in the fermentative degradation of DCM in *Dehalobacterium formicoaceticum* strain EZ94 (Soder-Walz et al., 2024) (see details in **section I.1.2.2**).

In a previous work in laboratory-scale aquifers, Prieto-Espinoza and colleagues showed that DCM dissipation increased upon water level fluctuations when compared to steady-state conditions (95% vs. 42%, respectively) (Prieto-Espinoza et al., 2021). This dissipation was proved to be mainly driven by biodegradation using stable isotope-based methods (compound specific isotope analysis; CSIA) and associated to a change in the microbial community composition. In general, groundwater level fluctuations (GLF) are a natural phenomenon that occur in aquifers due to external factors (Wu et al., 2020). This process is known to impact the microbial communities both directly, through physical disturbance, and indirectly, by altering various physicochemical parameters in the environment (Leira & Cantonati, 2008). Among these, soil moisture and redox conditions have been proposed as one of the most important drivers of the community change during GLF (Rezanezhad et al., 2014; Xu et al., 2004). However, due to the complexity of the systems in which these studies were carried out (lab-soil columns or directly *in situ*), it has been difficult to correlate the direct effects of these parameters on the activity and composition of the microbial community.

The aim of the present study was to examine the individual effects of soil moisture, hereafter referred to as water content, and redox conditions, in particular the oxygen concentration, on the DCM biodegradation and the microbial community composition. Two separate sets of laboratory microcosms were established with (i) three different water contents (33 %, 66% and 100% water content) under oxic conditions; or (ii) four different oxygen status (oxic, anoxic, alternating oxic-anoxic, and alternating anoxic-oxic conditions) under water saturation. DCM was added over time through several pulses and its biodegradation profile was monitored over time by gas chromatography. The microcosms were investigated for their DCM biodegradation

capacity and analysed for their microbial community composition at the beginning and at the end of the experiments. In addition, microcosms were also examined for the presence of biomarker genes for DCM degradation potential (*dcmA* and *mecE-F* genes).

III.2 Materials and Methods

III.2.1 Laboratory microcosms' set up and experimental design

III.2.1.1 Inoculum

To study the impact of water content or oxygen status on the activity and composition of a DCM-degrading microbial community, we used quartz sand inoculum (grain size of 0.4 - 0.6 mm), collected in 2019 from two laboratory-scale aquifers of a previous experiment (Prieto-Espinoza et al., 2021). The sand was stored in two different ways: either it was saturated in contaminated water and kept at 4°C, or it was collected from cores in sterile polyethylene tubes (Ø: 5 cm) coming from the laboratory-scale aquifers and drained from its liquid phases before preservation at -20°C.

III.2.1.2 Laboratory microcosms with different water content

To assess the impact of water content, 15 laboratory microcosms were set up in 160 mL serum bottles. Each laboratory microcosm was filled with 100 ±1 g of the drained sand. To do this, 1.5 kg of sand was homogenised in sterile beakers, and 300 g was separated and sterilised twice at 180°C for 1h30, 24h apart, in a Pasteur oven. Three types of microcosms were then prepared: (i) 3 microcosms were filled with the sterilised sand (abiotic controls); (ii) 6 microcosms were filled with non-sterilised sand and inoculated with the model strain *Hyphomicrobium* sp. GJ21 at the equivalent of 5% (v/v) from a preculture in SGW liquid media (composition detailed in **Table II.2**) with an OD₆₀₀ of 0.1 (biotic controls); (iii) 6 microcosms were filled with non-sterilised sand (environmental samples) (**Figure III.1-a.**). For each type of microcosms, three different water contents (33%, 66% and 100%) were established by adding different volumes of SGW liquid medium (**Figure III.1-b.**; specific volumes in **Table III.1**). In order to monitor the oxygen concentration along the experiment, 11 out of the 15 microcosms had an oxygen sensor spot attached at the inner surface as described in the **section II.4.2**. The 4 microcosms without oxygen sensor spot corresponded to the biotic controls at 33% (1), 66% (1) and 100% (2) of water content. Finally, laboratory microcosms were sealed with grey butyl rubber stoppers and aluminium crimp caps.

The experimental design is summarised in the **Figure III.1-c.** A volume equivalent to 1 mM of DCM was added to the microcosms through their septum using a stock solution at 10 mM of DCM for 3 consecutive pulses (details of added volumes in **Table III.1**). The stock solution was prepared in SGW liquid medium in 54 mL serum bottles, filled completely to eliminate any gas phase, and incubated hermetically at 30°C for at least 24 hours before use to ensure

that DCM became fully miscible in the liquid medium. Once DCM was completely degraded in the biotic controls and environmental samples, a new DCM pulse was applied. Before spiking DCM, the microcosms' gas phase was equilibrated with the atmosphere by opening them in a chemical hood under sterile conditions for 3-5 days. The microcosms were then resealed with new aluminium crimp caps and DCM was added to the microcosms from a freshly prepared stock solution. During the whole experiment, microcosms were incubated at room temperature (approx. 25°C) in the dark. DNA was extracted from the sand matrix at the beginning (T₀) and at the end of the experiment to study the microbial community composition.

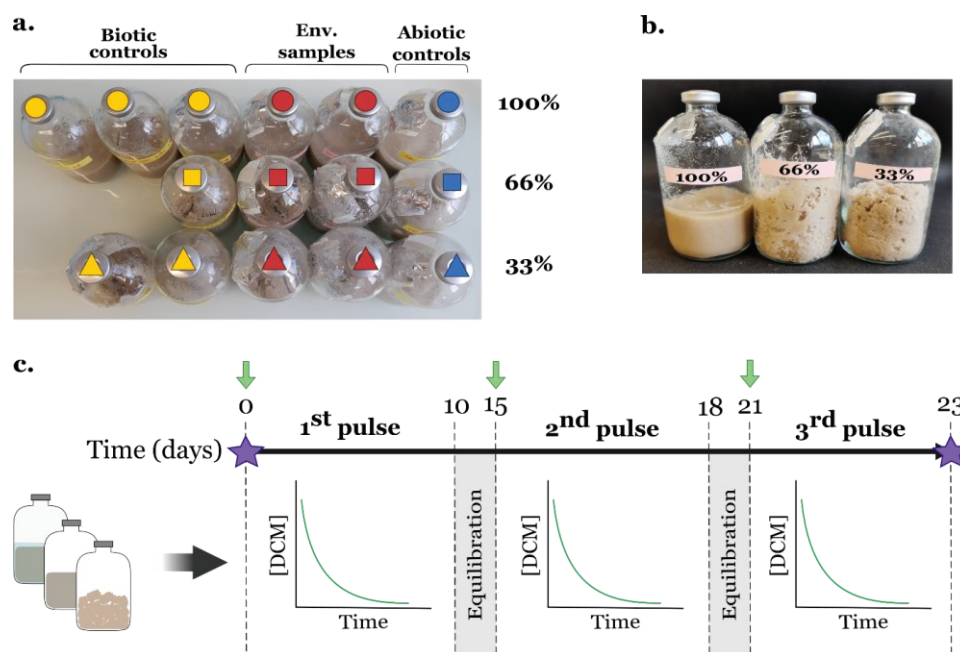


Figure III.1. Experimental set-up to investigate the impact of water content on DCM-degrading microbial populations. **a.** Overview of the laboratory microcosms. The number of replicates is as follows: $n=1$ for abiotic controls (blue), $n=1$ to 3 for biotic controls (yellow), and $n=2$ for environmental samples (Env. samples; red). Water content is indicating by different shapes: triangles for 33%, squares for 66%, and circles for 100%. **b.** Visual display of the different water contents in the laboratory microcosms. **c.** Summary of the experimental design. Green vertical arrows represent the spiking of 1 mM DCM in microcosms on day 0, 15 and 21. The relative concentration of DCM was monitored over time by gas chromatography. When DCM was degraded in the biotic controls and environmental samples, the pulse was stopped and all microcosms were opened under sterile conditions to remove any remaining traces of DCM before re-adding this compound (equilibration step). Purple stars represent the sampling of the sand matrix for DNA extraction at T₀ and at the end of the experiment.

III.2.1.3 Laboratory microcosms with different oxygen status

To assess the impact of oxygen status, 20 laboratory microcosms were set up in 160 mL serum bottles. To do so, 3 kg of a mix of sand saturated with contaminated water and drained sand was homogenised in sterile beakers, and 1 kg was separated and sterilised three times at 180°C for 1h30 in a Pasteur oven with 24h intervals between each cycle. Three types

of microcosms were prepared: (i) 4 microcosms were filled with 80 ± 1 g of sterilised sand (abiotic controls); (ii) 4 microcosms were filled with 80 ± 1 g of sterilised sand inoculated with the strain *Hyphomicrobium* sp. GJ21 at 5% (v/v) from a preculture in SGW liquid media with an OD_{600} of 0.1 (biotic controls); and (iii) 12 microcosms were filled with 120 ± 1 g non-sterilised sand (environmental samples) (**Figure III.2-a.**). To maintain the same air-matrix ratio used in the previous set-up (**section III.2.1.2**), the microcosms were filled with the same volume of sand. Since the sterilised sand was dry and the non-sterilised sand was wet, this volume corresponded to different weights, depending on the initial state of the sand. These differences also affected the amount of SGW liquid medium added to saturate (100%) the sand matrix: 20 mL for the abiotic and biotic controls and 5 mL for the environmental samples (all information in **Table III.1**). For each type of microcosms, 4 oxygen status were established: continuous oxic condition (~ 8 ppm), continuous anoxic condition (< 0.5 ppm), alternating regime going from oxic to anoxic conditions, and alternating regime going from anoxic to oxic conditions. Anoxic conditions were established after sealing the microcosms by replacing the gas phase with a mixture of H_2/N_2 (5%/95%) at 1 atm. In the case of the alternating regime, the oxygen concentration of interest was established before starting a new DCM pulse. The number of replicates per condition was $n=1$ for the abiotic and biotic controls, and $n=3$ for the environmental sample (**Figure III.2-a.**). To monitor the oxygen concentration along the experiment, 12 out of 20 of the microcosms were equipped with an oxygen sensor spot as described in the **section II.4.2**. The 8 microcosms without oxygen sensor spot corresponded to those under continuous oxic conditions (1 abiotic control, 1 biotic control and 3 environmental samples), as well as one of the triplicates of the environmental samples at the other oxygen statuses (1 continuous anoxic, 1 alternating oxic-anoxic and 1 alternating anoxic-oxic). Finally, laboratory microcosms were sealed with grey butyl rubber stoppers and aluminium crimp caps.

The experimental design is summarised in the **Figure III.2-b.** Each microcosm was spiked with 1 mM of DCM as a carbon source through the septum from a stock solution at 10 mM of DCM for 8 consecutive pulses (details of added volumes in **Table III.1**). As before, the stock solution was prepared in SGW liquid medium in 54 mL serum bottles, filled completely to avoid any gas phase, and incubated hermetically at $30^\circ C$ for at least 24 hours before use to ensure that DCM became fully miscible in the liquid medium. Each DCM pulse was done after complete degradation of DCM in the biotic controls and/or environmental samples. From the 1st to the 6th pulse, before each DCM spike, the gas phase was equilibrated with the atmosphere by opening all microcosms, except those under continuous anoxic conditions, in a chemical hood under sterile conditions for 1-2 days. In the case of the microcosms under continuous anoxic conditions, 2 cycles of vacuum- H_2/N_2 filling was applied to directly replace the gas phase by a fresh anoxic atmosphere. After day 56, brief exposure to air was tested. Thus, starting from the 7th pulse, continuous anoxic microcosms were also opened during the equilibration step, applying the anoxic condition back just before the addition of DCM. During the whole experiment, microcosms were incubated at room temperature (approx. $25^\circ C$) in the dark. DNA

was extracted from the sand matrix at the beginning (T₀) and at the end of the experiment to study the microbial community composition.

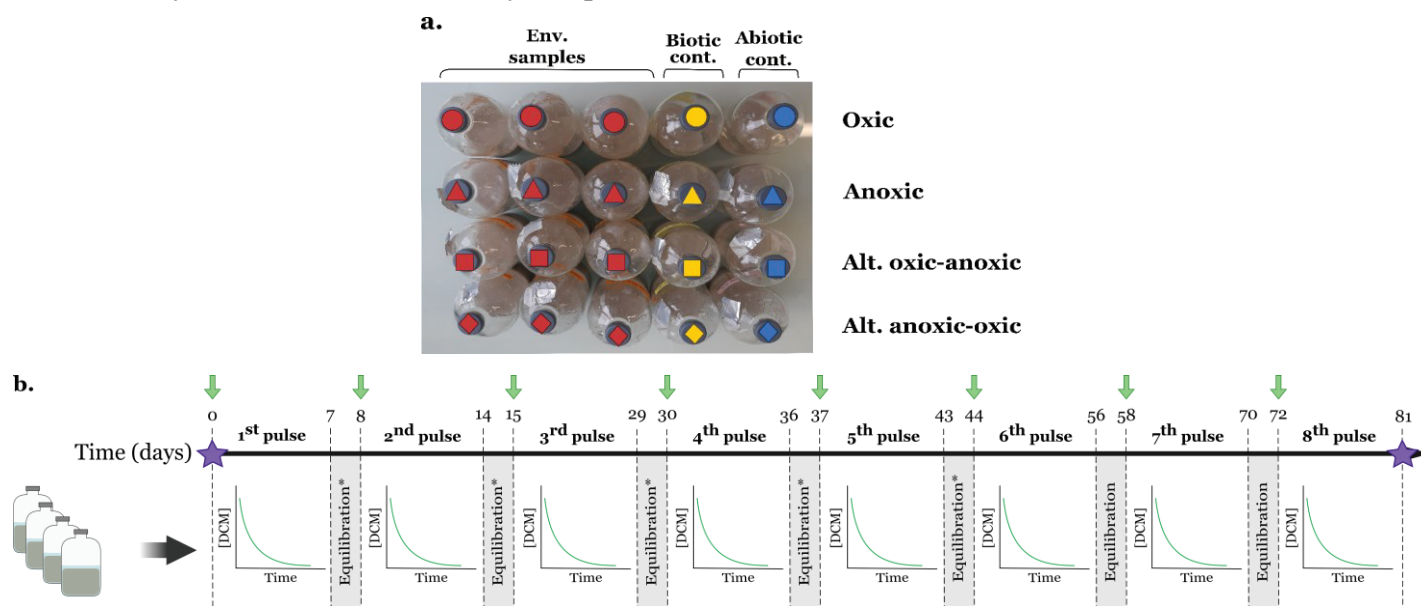


Figure III.2. Experimental set-up to investigate the impact of oxygen concentration on DCM-degrading microbial populations. **a.** Overview of the laboratory microcosms. The number of replicates is as follows: $n=1$ for abiotic controls (Abiotic cont.; blue), $n=1$ for biotic controls (Biotic cont.; yellow), and $n=3$ for environmental samples (Env. samples; red). Oxygen status is indicated by different shapes: circles for continuous oxic conditions (Oxic), triangles for continuous anoxic conditions (Anoxic), squares for alternating conditions starting with oxic (Alt. oxic-anoxic), and rhombus for alternating conditions starting with anoxic (Alt. anoxic-oxic). **b.** Summary of the experimental design. Green vertical arrows represent the spiking of 1 mM DCM in microcosms on day 0, 8, 15, 30, 37, 44, 58, and 72. After the spike, the DCM concentration was monitored over time by gas chromatography. When DCM was degraded in the biotic controls and/or environmental samples, the pulse was stopped, and the microcosms were opened under sterile conditions to remove any remaining traces of DCM before re-adding the compound (equilibration step; * indicates that this procedure was done in all microcosms except those under continuous anoxic conditions). Purple stars represent the sampling of the sand matrix for DNA extraction at T₀ and at the end of the experiment.

III.2.1.4 Summary of the laboratory microcosms' set up

Table III.1 provides specific details of the experimental set up for both experiments, including the origin, quantity, and treatment of the sand matrix, as well as the number of replicates, and volumes of SGW liquid medium and DCM added for each type of microcosm.

Table III.1. Summary of the laboratory microcosms' set up.

	Experiment with different water content			Experiment with different oxygen status		
	Abiotic controls	Biotic controls	Environmental samples	Abiotic controls	Biotic controls	Environmental samples
Sand inoculum			Drained sand (1.5 kg in total)			Mix of sand saturated with contaminated water and drained sand (3 kg in total)
Quantity of sand matrix per microcosm	100 ±1 g	100 ±1 g	100 ±1 g	80 ±1 g	80 ±1 g	120 ±1 g
Sand matrix treatment	Double sterilization at Pasteur oven	Inoculation of GJ21	No treatment	Triple sterilization at Pasteur oven	Triple sterilization at Pasteur oven + inoculation of GJ21	No treatment
Number of replicates	1 per water content	3 at 100% 1 at 66% 2 at 33%	2 per water content	1 per oxygen status	1 per oxygen status	3 per oxygen status
Volume of SGW liquid media per microcosm	35 mL for 100% 23 mL for 66% 11 mL for 33%	13 mL for 100% 8.5 mL for 66% 2 mL for 33%		20 mL		5 mL
Volume of 10 mM DCM stock solution per microcosm and per pulse	3.5 mL for 100% 2.3 mL for 66% 1.1 mL for 33%	1.3 mL for 100% 0.85 mL for 66% 0.2 mL for 33%				2 mL

III.2.2 Monitoring of DCM degradation

DCM concentration was measured from 100 μ L of the microcosms' headspace by GC-FID (Agilent Technologies France SAS) as explained in **section II.4.1.1**. An initial measurement of DCM was made 3 hours after the addition of DCM (T_0). Periodic measurements were then taken over time. The relative DCM concentration at each time point was calculated using the value at the beginning of the experiment (T_0) as the reference of the maximum value (100% of DCM). The final value for each experimental condition was calculated by averaging the relative DCM concentrations of the replicates, with the standard deviation calculated when $n \geq 2$. Values greater than the T_0 were set to 100%. In addition to the relative DCM concentration, the half-life of this compound was also calculated at each pulse using the following equation:

$$\text{DCM half-life}_{X \text{ pulse}}(\text{days}) = \frac{\ln 2}{k}$$

where k is the rate constant of the DCM concentration over time. The period of time before the onset of DCM degradation, hereafter referred to as the 'latency phase', was not considered from the calculation of DCM half-life. The final value for each experimental condition was calculated by averaging the DCM half-life of the replicates, with the standard deviation calculated when $n \geq 2$. When the DCM half-life was greater than the length of the pulse, we considered that DCM was not degraded during that pulse.

III.2.3 Molecular biology analysis

III.2.3.1 DNA extraction from sand matrix

Environmental DNA was extracted from 1 g of the microcosms' sand matrix at the beginning and at the end of the experiment using the "DNeasy PowerWater" kit (Qiagen) according to manufacturer's instructions (see **section II.5.1.1** for detailed protocol). DNA concentrations (ranging from 0.021 - 1.148 ng/ μ L) were determined by fluorometry using the "Qubit[®] dsDNA HS Assay" kit (Thermo Fisher Scientific) as described in **section II.5.1.2**. DNA preparations were stored at -20°C .

III.2.3.2 Primer design

A primer set was designed to amplify the different alleles of the *dcmA* gene by targeting conserved regions of this gene in the isolated strains *M. extorquens* DM4, *Hyphomicrobium* sp. GJ21 and *Hyphomicrobium* sp. MC8b. For this, the respective gene sequences were aligned using ClustalW (Madeira et al., 2024) and primer sets were designed using the Primer3 Input software (primer3.ut.ee; (Kõressaar et al., 2018)). Primer sequences were blasted against the NCBI non-redundant database using the "Nucleotide BLAST" (BLASTn) tool available in the NCBI platform (Camacho et al., 2009) with default parameters to verify their specificity. Finally, the primer set was obtained lyophilized from Eurofins scientific.

Following the same protocol, other sets of primers were developed to ‘universally’ amplify other loci of the *dcm* cluster based on the sequences of the same strains. In particular, primers were designed to amplify the *dcmR*, *dcmB* or *dcmC* genes. Finally, a primer pair specific to the allele of *dcmA* gene in *Hyphomicrobium* sp. MC8b was developed and tested. A summary of the primers developed is provided in **Table III.2**.

Table III.2. Newly designed primer pairs for amplifying the loci of the *dcm* cluster. Primers were designed based on the sequences of the isolated strains *M. extorquens* DM4, *Hyphomicrobium* sp. GJ21, and *Hyphomicrobium* sp. MC8.

Target region		Primer name	Sequences (5'... 3') ^a	Size (bp)	PCR parameters (T _a , polymerase, buffer) ^b
<i>dcmA</i> gene	all known alleles ^c	Forw <i>dcmA</i> Univ	CGCCGACATCTGGATCG	930	58°C, Phusion ^d , GC buffer
		Rev <i>dcmA</i> Univ	YGCGCCCTCYTTCTCAA		
	<i>Hyphomicrobium</i> sp. MC8b	<i>dcmA</i> MC8b uniqueF	GGCAGGCCAGTCTACAGAAG	1086	63°C, Phusion, GC buffer
		<i>dcmA</i> MC8b unique R	TACACGGGCAAACGGAGC		
<i>dcmR</i> gene		Forward <i>dcmR</i>	GAGTGTATTATATTTCCAACCTCG	1070	52°C, Phusion, GC buffer
		Reverse <i>dcmR</i>	CCGATGTGAATGTTTGT		
<i>dcmB</i> gene		Middle 2-f	GTGAGTGCCTGGCAGTA	878	55°C, Phusion, GC buffer
		Middle 2-r	AGGGTAGTACTCTTCAACGAC		
<i>dcmC</i> gene		End-f	AGGCAACAGCTCAATGTACG	979	60°C, Phusion, GC buffer + DMSO
		End-r	GGCCTATCGTTTCGACACC		

^a Nomenclature IUPAC (Y = C or T)

^b T_a: annealing temperature

^c Excepted *dcmA* allele from *Methylophilus* sp DM11, having only 56% identity at the protein level (Vuilleumier et al., 2001)

^d Phusion High-Fidelity DNA Polymerase (2U/μL); Thermo Fisher Scientific

III.2.3.2 Biomarker genes detection and *in silico* analyses

The *dcmA* and *mecE-F* genes were here considered as biomarkers for the potential of DCM degradation under oxic and anoxic conditions, respectively. To test for the presence of these biomarker genes, PCR amplification was performed on the extracted DNA using the following primer sets: (i) Forw *dcmA* Univ and Rev *dcmA* Univ (amplification of *dcmA* gene; **Table III.2**); and (ii) *mecE*-828F and *mecF*-641R (amplification of *mecE-F* gene; **Table II.3**). The used protocol is described in **section II.5.1.3**. The DNA template was used at a final concentration of 0.218 ng/μL in all cases. The DNA bands on the agarose gel corresponding to the PCR products of the gene *dcmA* were recovered and purified using the “NucleoSpin Gel and PCR Clean-Up” kit (Macherey-Nagel) according to the manufacturer’s instructions. The products were quantified by “Qubit® dsDNA HS Assay” kit and sent to sequence with the Sanger method by Eurofins when DNA quantities were sufficient (ranging from 2.78 to 4.18 ng/μL).

The sequences obtained from the amplified fragment of the *dcmA* gene in the different microcosms were compared to the known sequences of this gene using the “Global Alignment tool” in BLAST (Zhang et al., 2000) as explained in **section II.5.1.6**. The sequences were analysed in fasta format using the BLASTn. The phylogenetic tree was constructed using the phylogeny.fr platform (Dereeper et al., 2008). We first performed a multiple alignment using the MUSCLE algorithm. The resulting output was curated with Gblock, leading to the selection of 795 positions, which corresponded to 47% of the full-length *dcmA* gene sequence from *Hyphomicrobium* sp. ATCC51888 (particularly, nucleotide positions 692 to 1486). This curated alignment was then used for tree calculation, using the approximate likelihood-ratio test (aLRT) and the default substitution model (GTR). Tree visualisation was done using TreeDyn, with branches having support values smaller than 50% collapsed.

III.2.3.3 16S rRNA gene amplicon sequencing and data analysis

The hypervariable V3-V4 regions of the 16S rRNA genes were PCR amplified and sequenced as described in **section II.6.1.1**. The resulting sequences from the two experiments (different water content and different oxygen status) were clustered together at 100% identity to obtain the Amplicon Sequence Variants (ASVs). Each ASV was annotated with the QIIME2 platform and the Silva database (version 138, November 2022). The resulting data was released to us.

ASVs were analysed in R (version 4.4.0). Before starting the analyses, singletons (i.e., ASVs that only appeared once across all samples) and doubletons (i.e., ASVs that only appeared twice across all samples) were removed from the data. Alpha-diversity indices (Chao1, Pielou’s evenness, and Shannon-Wiener diversity) were then calculated using the phyloseq R package (McMurdie & Holmes, 2013), as well as the microbial community profiling at the family level using the relative abundance of the ASV sequences. Principal Component Analysis (PCA) based on the Aitchison distance of the clr-transformed data was performed using the microViz R package (Barnett et al., 2021) to visualize dissimilarities between samples. The clr-transformation was done automatically by the microViz R package. To test significance ($p < 0.05$), one-way ANOVA followed by post-hoc Tukey HSD test was conducted.

III.3 Results

III.3.1 DCM degradation kinetics

In each experiment, the DCM degradation kinetics in the different microcosms were assessed by calculating (i) the relative concentration of DCM over time; and (ii) the DCM half-life values in each pulse. As explained in **section II.2.2**, the DCM half-life in each pulse was calculated based on the DCM degradation rate after the latency phase, if present.

III.3.1.1 Impact of water content

DCM degradation was regularly monitored in the set of microcosms exposed to different water contents for 23 days (**Figure III.3**). The oxygen concentration was also measured at the same time points and remained stable at ~8 ppm (i.e., oxic conditions) throughout the whole experiment (**Supplementary figure III.1**).

Dissipation of DCM was minimal in the abiotic controls, indicating that the contribution of the abiotic degradation, adsorption and/or gas leakage was negligible. Therefore, any changes in the concentration of DCM found in the biotic controls and environmental samples that were greater than those found in the abiotic controls were considered as biotic degradation. In the biotic controls, DCM was rapidly degraded from the first pulse at 100% and 66% of water content, and from the second pulse at 33% water content. These results showed, firstly, that the experimental set-up allowed the biodegradation of DCM and, secondly, that the activity of our model strain, *Hyphomicrobium* sp. GJ21, may be sensitive to low water content. Finally, in the environmental samples, DCM was degraded from the first pulse at all water contents, indicating the presence of at least one active DCM-degrading population in these microcosms. However, when comparing the degradation rates among water contents in the environmental samples, DCM degradation was significantly slower (i.e., higher DCM half-life) at 33% of water content during the first DCM pulse ($p < 0.05$; **Table III.3**). This suggests that at lower water contents, the DCM-degrading populations may require some time to adapt before achieving the same degradation activity observed at higher water contents.

The DCM degradation activity of the model strain compared to the dehalogenation activity of the environmental samples mainly showed differences during the first pulse. Indeed, a delay in DCM degradation establishment was observed in the environmental samples compared to the biotic controls. This could be explained by the differences in microcosms setup procedures: the biotic controls were inoculated with a preculture of *Hyphomicrobium* sp. GJ21 on DCM, whereas the environmental samples were established with an environmental inoculum that had been stored at -20°C for 2 years. Therefore, the DCM-degrading microbial populations may have needed some time to start their activity. Furthermore, DCM degradation in the environmental samples was observed at 33% of water content from the first DCM pulse in contrast to the biotic control microcosms, suggesting that some DCM-degrading populations in the environmental samples were less affected by water limitation than our model strain.

Repeated exposure to DCM promoted the degradation of this compound in both the biotic controls and environmental samples at all water contents. Indeed, in the environmental samples, the DCM half-life was significantly slower in the first pulse when compared to the second and third pulses in all experimental conditions (p -value < 0.05 ; **Figures III.3** and **Table III.3**). This effect could be related either to an increase in the size of the microbial populations capable of degrading the DCM or to a shift in their physiological status (e.g., cells coming out of dormancy, adaptation to the conditions imposed by this toxic compound, or the establishment of a stable pool of newly synthesised DCM-degrading enzyme).

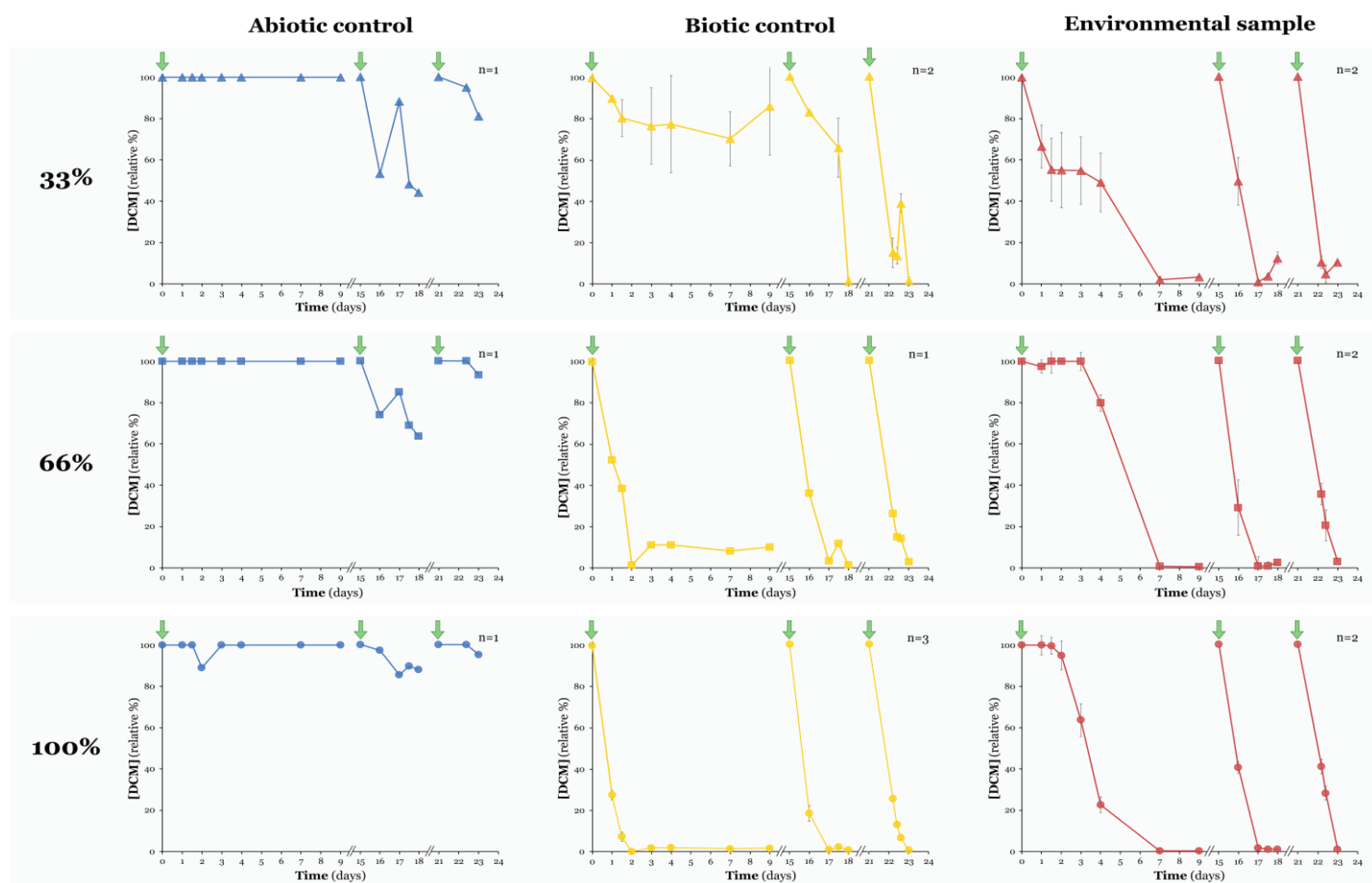


Figure III.3. Impact of the water content on the DCM degradation. The plots show the relative concentration of DCM (%) over time (days). Values higher than 100% have been adjusted to 100%. The blue colour indicates abiotic controls, yellow is for biotic controls, and red for environmental samples. The shape indicates the water content: triangles for 33%, squares for 66%, and circles for 100%. The addition of DCM is indicated by the vertical green arrows. The number of replicates is indicated on the upper right corner of each plot. Standard deviation was calculated from the relative concentrations when $n \geq 2$.

In conclusion, the impact of water content on DCM biodegradation was mainly related to the activation of the function, with DCM-degrading microbial populations in low water content conditions requiring more time to initiate their activity. However, repeated exposure to DCM reduced the influence of this parameter and by the end of the experiment, DCM biodegradation rates were the same irrespective of water content. Translating these findings to the laboratory-scale aquifer scenario, we can hypothesize that periods of reduced water content during the water level fluctuations may initially have slowed down the microbial community's degrading activity. However, over time, the microbial community may have adapted to the new conditions and regain its original function efficiency, especially if in the community included taxa with greater resistance to low water contents.

Table III.3. DCM half-life (days) during each pulse at each tested water content in the abiotic controls (A), biotic controls (B) and environmental samples (E). Water content is indicated by the corresponding percentages (33%, 66% and 100%). Standard deviation was calculated when $n \geq 2$. ‘NOD’ (No Observed Degradation) indicates that the DCM half-life was greater than the duration of the pulse. Two symbols are used to indicate significance ($p < 0.05$): the letter ‘a’ for environmental samples with different water content that exhibited a significantly different DCM half-life within individual DCM pulses; the symbol ‘†’ for cases when the DCM half-life was significantly different across DCM pulses within environmental samples at the same water content.

	DCM half-life (days)		
	1 st pulse	2 nd pulse	3 rd pulse
A - 33 %	NOD	NOD	NOD
A - 66%	NOD	NOD	NOD
A - 100%	NOD	NOD	NOD
B - 33%	NOD	0.65 ±0.13	0.41 ±0.05
B - 66%	0.95	0.40	0.43
B - 100%	0.28 ±0.03	0.29 ±0.01	0.45 ±0.02
E - 33%	1.38 ±0.14 ^{a†}	0.30 ±0.03	0.38 ±0.05
E - 66%	1.04 ±0.01 [†]	0.39 ±0.19	0.43 ±0.03
E - 100%	0.78 ±0.04 [†]	0.36 ±0.04	0.35 ±0.01

III.3.1.2 Impact of oxygen status

DCM degradation was monitored in the set of microcosms exposed to different oxygen status for 81 days (**Figure III.4**). The oxygen concentration was also measured throughout the whole experiment and confirmed that the conditions established at the start of each pulse remained stable (anoxic conditions with $O_2 < 0.5$ ppm, and oxic conditions with $O_2 \sim 8$ ppm; **Supplementary figure III.2**). No dissipation of DCM was observed in the abiotic controls, supporting that the contribution of abiotic degradation, adsorption and/or gas leakage was negligible. Therefore, all changes in DCM concentration in the biotic controls and environmental samples greater than those in the abiotic controls were interpreted as biotic degradation.

In the biotic controls, DCM was degraded from the first DCM pulse in all microcosms. This result was expected since the model strain *Hyphomicrobium* sp. GJ21 is able to degrade this compound under oxic and anoxic (denitrifying) conditions. The observed degradation during this first pulse was similar irrespective of the oxygen status. On the other hand, repeated exposures to DCM improved the performance of the function, whether the regime was

continuous or alternating, indicating that this strain was able to switch from one metabolism to the other one without any detrimental effects on its activity. Additionally, the DCM half-lives were significantly higher in the first pulse than in the rest of the pulses (p-value <0.05), suggesting that, even if *Hyphomicrobium* sp. GJ21 was active from the beginning of the experiment, it required some time to adapt to the microcosm system. Another possibility is that the strain was at the stationary phase in the preculture used for inoculation, and so it needed some time to re-start its activity at the maximum capacity.

In the environmental samples, the degradation profiles differed depending on the oxygen status and pulse. Microcosms under continuous oxic conditions consistently degraded DCM completely within 2 days from the second pulse, whereas those under continuous anoxic conditions did not degrade DCM until the seventh pulse. As noted in **section III.2.1.3**, from day 56 onward (i.e., from the end of the 6th pulse), the continuous anoxic microcosms were exposed to the atmosphere during the ‘equilibration’ step between pulses, after which DCM degradation rates became similar to those observed under the other oxygen statuses (**Table III.4**). With regard to the alternating regime, microcosms starting in oxic conditions showed comparable DCM degradation under oxic conditions to those in the continuous condition. In addition, unlike the microcosms in continuous anoxic conditions, these ones could degrade DCM under anoxic conditions; however, they exhibited a DCM half-life that was at least eight times longer under anoxic conditions compared to oxic conditions (i.e., the shortest half-life in anoxic condition was 2.51 days, while the shortest half-life in oxic conditions was 0.31 days). On the other hand, alternating microcosms starting in anoxic conditions required more pulses and alternations to degrade DCM similarly to the ones in continuous conditions. Additionally, they also degraded DCM under anoxic conditions after 3 DCM pulses. Altogether, these results suggest that, firstly, oxic conditions were more favourable for efficient DCM degradation, and, secondly, that the initial oxygen concentration determined the activity of the DCM-degrading microbial community, which was promoted when first exposed to oxic conditions. The observed drastic differences in DCM degradation between continuous anoxic conditions and any alternating regime were abolished after a brief exposition to the atmosphere during the equilibration step. This suggests that the DCM-degrading populations may require an initial exposure to oxic conditions to become active.

When comparing the activity of the model strain with the environmental samples, significant differences were only observed in the continuous anoxic microcosms (p-value <0.05). Under this condition, *Hyphomicrobium* sp. GJ21 was able to completely degrade DCM from the first pulse, in contrast to the DCM-degrading populations coming from the environmental sample, which, as mentioned above, only degraded this compound from the 7th pulse.

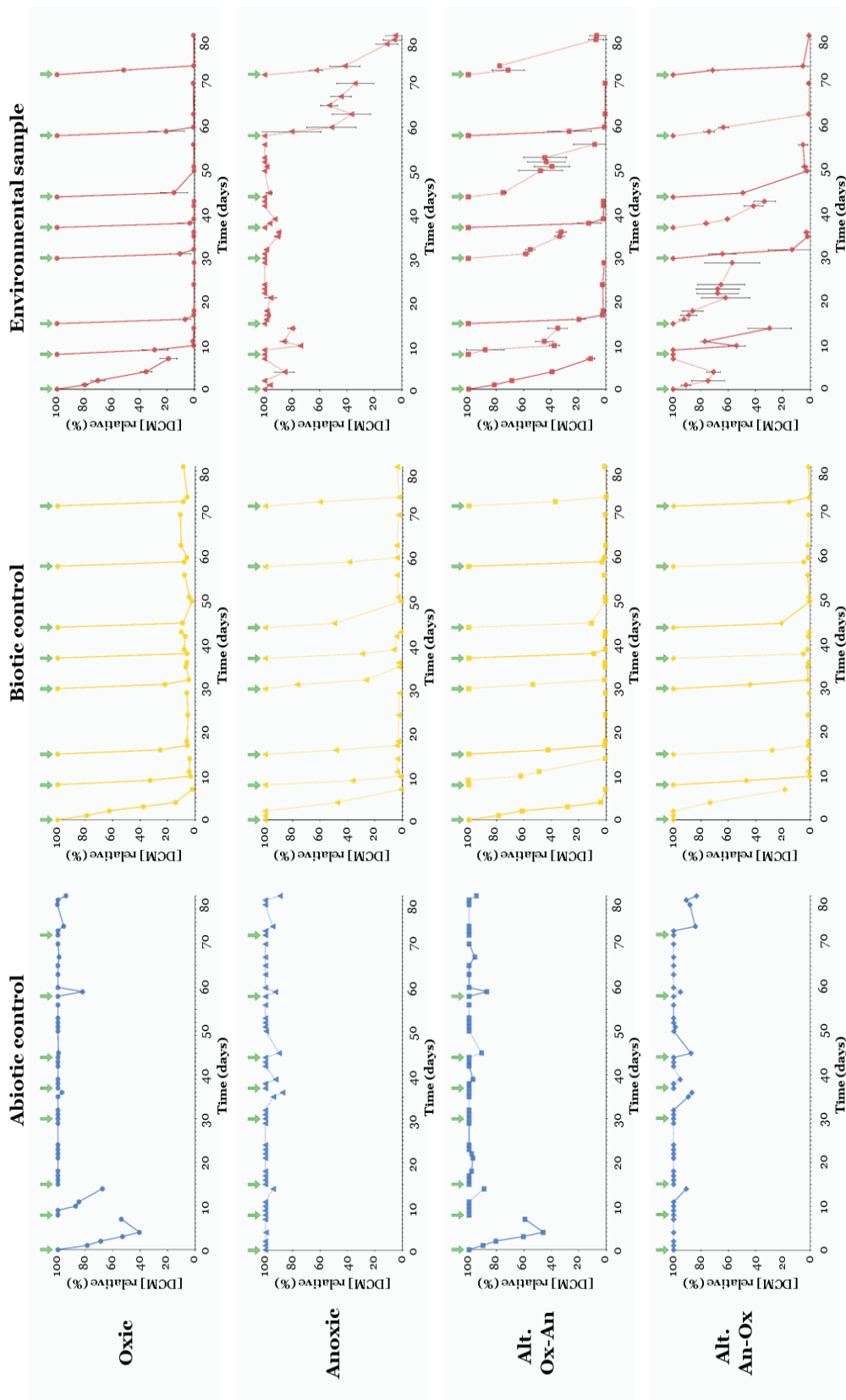


Figure III.4. Impact of the oxygen status on DCM degradation. The plots show the relative DCM concentration (%) over time (days). Values higher than 100% have been adjusted to 100%. The colour indicates the type of microcosms: blue for abiotic controls, yellow for biotic controls, and red for environmental samples. The shape indicates the oxygen status: circles for continuous oxenic conditions, triangles for continuous anoxic conditions, squares for alternating conditions from oxenic to anoxic, and rhombus for alternating conditions from anoxic to oxenic. The addition of DCM is indicated by the green arrow. Standard deviation was calculated from the relative DCM concentrations only for environmental samples (n=3).

In conclusion, the oxygen status significantly impacted the DCM biodegradation function of the microbial community, with oxic conditions generally promoting this activity. Additionally, the initial oxygen concentration to which the alternating microcosms were exposed played a key role on determining their DCM-degradation efficiency throughout the experiment. Interestingly, a short exposure to the atmosphere enhanced DCM biodegradation under anoxic conditions. Translating these findings to the laboratory-scale aquifer scenario, we can hypothesize that the water table fluctuations, which led to an increase in oxygen concentration in the fluctuating area, could have promoted the DCM-degrading activity within the microbial community.

Table III.4. DCM half-life (days) during each pulse depending on the oxygen status in the abiotic controls (A), biotic controls (B) and environmental samples (E). The oxygen status is indicated as follows: ‘Ox’ for continuous oxic conditions, ‘An’ for continuous anoxic conditions, and ‘Alt.’ stands for alternating conditions. The standard deviation was calculated in the environmental samples where n=3. ‘NOD’ (No Observed Degradation) indicates that the DCM half-life was greater than the duration of the pulse. Two symbols are used to indicate significance ($p < 0.05$): the letters (‘a’, ‘b’) for environmental samples with different oxygen status that exhibited a significantly different DCM half-life within individual DCM pulses; the symbol ‘+’ for cases when the DCM half-life was significantly different across DCM pulses within environmental samples at the same oxygen status.

	DCM half-life (days)							
	1 st pulse	2 nd pulse	3 rd pulse	4 th pulse	5 th pulse	6 th pulse	7 th pulse	8 th pulse
A - Ox	NOD	NOD	NOD	NOD	NOD	NOD	NOD	NOD
A - An	NOD	NOD	NOD	NOD	NOD	NOD	NOD	NOD
A - Alt. Ox-An	NOD	NOD	NOD	NOD	NOD	NOD	NOD	NOD
A - Alt. An-Ox	NOD	NOD	NOD	NOD	NOD	NOD	NOD	NOD
B - Ox	1.16	0.40	0.47	0.44	0.24	0.29	0.27	0.28
B - An	1.03	0.31	0.42	0.85	0.49	0.85	0.41	0.37
B - Alt. Ox-An	0.75	0.59	0.29	0.31	0.29	0.75	0.19	0.19
B - Alt. An-Ox	2.68	0.23	0.31	0.33	0.22	0.75	0.22	0.30
E - Ox	3.04 ± 0.55 [†]	0.24 ± 0.05 ^a	0.21 ± 0.01	0.22 ± 0.02	0.19 ± 0.04	0.45 ± 0.11	0.24 ± 0.01	0.22 ± 0.02
E - An	NOD	NOD	NOD	NOD	NOD	NOD	7.10 ± 3.85	3.04 ± 1.16
E - Alt. Ox-An	2.25 ± 0.25	3.18 ± 1.17 ^{ab}	0.37 ± 0.05	3.64 ± 0.42	0.31 ± 0.07	5.20 ± 3.51	0.31 ± 0.05 [†]	2.51 ± 0.66
E - Alt. An-Ox	NOD	6.34 ± 0.82 ^b	NOD	0.56 ± 0.05	4.62 ± 1.24	1.22 ± 0.29	0.74 ± 0.07	1.00 ± 0.37

III.3.2 Presence of biomarker genes for DCM biodegradation

To determine whether the known DCM utilisation pathways were detectable in the different tested conditions, the presence of the *dcmA* and *mecE-F* genes was studied in the microcosms with different water contents or oxygen status. To do this, newly designed primer pairs were used to target all the known sequences for each locus. The different alleles of *dcmA* gene were targeted by using universal primers that allow the amplification of most of the *dcmA* gene sequences (details in **section III.2.3.2**). In contrast, the *mecE-F* genes have only been recently identified, so little is known about their potential diversity in the environment. For instance, the primers used were designed by Murdoch and colleagues using the target gene alleles found in the genome of one DCM degrader, *Dehalobacter* sp. UNSWDHB, and in peat metagenomes (Murdoch et al., 2022).

The results of these amplifications, that were consistent through replicates, are summarized in the **Table III.5-a.** and **b.** The *dcmA* biomarker gene was not detected in the abiotic controls across all experiments, nor in their initial inoculum (To-A). In contrast, it was detected in all biotic controls and environmental samples from both experiments, as well as in both inocula (To-B and To-E), though with weaker amplifications (data not shown). Despite PCR being only a semiquantitative method, these results suggest that the *dcmA*-carrying populations were either eliminated in the sterilized sand of abiotic controls or reduced to levels below the detection limit by the heat treatment. Additionally, the increase in the number of copies of the *dcmA* gene in the biotic controls and environmental samples, irrespective of the experimental conditions, could be explained by either the proliferation of strains carrying the *dcmA* gene during the experiment, or the transfer of the genomic island carrying the *dcmRABC* cluster to new bacterial populations. The *dcmA* genes detected in the biotic controls were phylogenetically similar to the allele of *Hyphomicrobium* sp. GJ21, suggesting that the degradation of DCM observed in these microcosms was mainly performed by the inoculated strain (**Figure III.5**). In the case of the environmental samples, some of the obtained sequences were new allelic versions of the *dcmA* gene that have not been reported in the databases (**Supplementary table III.1**). Overall, the allelic versions found in the environmental samples were phylogenetically close to those of the known strains (**Figure III.5**). The relatively short experimental time (23 days) suggest that the different versions of this gene were already present in the sand samples from the beginning of the experiment, and so they were not the result of a genetic adaptation during the experiment. Interestingly, the allelic versions of *dcmA* clustered together based on water content, while no distinctions were observed regarding oxygen status. This suggests that different bacterial populations may have dominated the DCM-degrading community depending on the water content, with no such selection exerted by the oxygen status.

The biomarker locus *mecE-F* was detected in both environmental inocula (To-E). These results indicate that microbial populations carrying the *mecE-F* genes, recently linked to the DCM utilisation under anoxic conditions, were present in the initial sand inocula. These *mec-*

carrying microbial populations were detected irrespective of the water content or oxygen status. The lack of detection in the abiotic controls of both experiments, as well as in the To-A and To-B and the biotic controls exposed to different oxygen statuses, may be a consequence of the heat-sterilization process, which could have kept the abundance of this gene below the detection threshold. In the case of the biotic controls exposed to different water content, as mentioned in **section III.2.1.2**, the sand inoculum was not sterilized; therefore, the *mecE-F* genes were detected since they were present in the initial sand inoculum. Additionally, while detecting the *mec*-system in oxic conditions may seem surprising, because the *mecE-F* genes were already detected in the initial inocula of both experiments, it does not necessarily mean that the *mec*-carrying populations were active in this condition. Complementary analysis should be carried out to determine whether the pathway to which these genes belong was involved in the degradation of DCM under oxic conditions. Altogether, this demonstrate the importance to search for this newly discovered DCM utilisation system in our experiments and more generally the ubiquity of this system.

Table III.5. Presence of *dcmA* and *mecE-F* genes biomarkers for the DCM degradation in microcosms with different water content (**a.**), or oxygen statuses (**b.**). ‘A’ stands for abiotic controls, ‘B’ for biotic controls, and ‘E’ for environmental samples. The percentage values indicate the water content. ‘Ox’ corresponds to oxic conditions, and ‘An’ to anoxic conditions. ‘Alt.’ stands for alternating conditions. To corresponds to the initial inoculum. ✓ indicates the detection of the gene of interest. ✗ indicates the absence of detection of the gene of interest. Replicates are not shown since the results were consistent.

a.	To-E	A - 100%	A - 66%	A - 33%	B - 100%	B - 66%	B - 33%	E -100%	E -66%	E -33%
<i>dcmA</i>	✓	✗	✗	✗	✓	✓	✓	✓	✓	✓
<i>mecE-F</i>	✓	✓	✓	✓	✓	✓	✓	✓	✓	✓

b.	To - A	To - B	To - E	A - Ox	A - An	A - Alt. Ox-An	A - Alt. An-Ox	B - Ox	B - An	B - Alt. Ox-An	B - Alt. An-Ox	E - Ox	E - An	E - Alt. Ox-An	E - Alt. An-Ox
<i>dcmA</i>	✗	✓	✓	✗	✗	✗	✗	✓	✓	✓	✓	✓	✓	✓	✓
<i>mecE-F</i>	✗	✗	✓	✗	✗	✗	✗	✗	✗	✗	✗	✓	✓	✓	✓

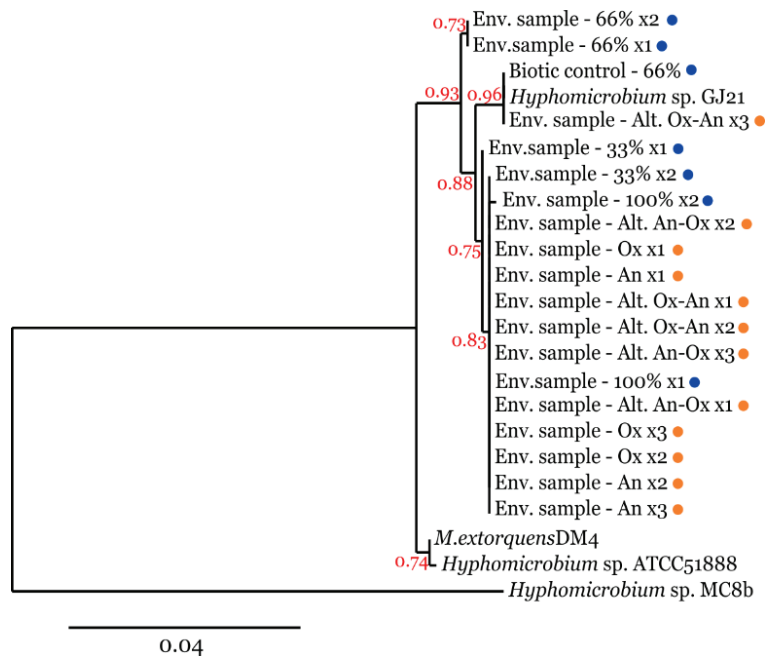


Figure III.5. Phylogenetic tree of the *dcmA* sequences recovered from the microcosms with different water content (blue circle) or oxygen status (orange circle). The phylogenetic tree is based on the estimated maximum likelihood (PhyML) method of an alignment of 795 positions using Phylogenly.fr. The number after the microcosm's name indicates the replicate from which the sequence is derived.

III.3.3 Composition of the microbial community

To characterize the microbial community established in the different microcosms according to the experimental conditions, we analysed the data obtained from the 16S rRNA gene amplicon sequencing analysis performed on the DNA extracted at the beginning (T₀) and at the end of each experiment (different water content or oxygen status). The data from both experiments was clustered together at 100% identity, yielding a total of 2 059 ASVs sequences for taxonomic analysis. Taxonomic assignment was consistent but unexpectedly high across the different taxonomic levels, with 28.6%, 40.7%, 40.7%, 41.8%, 42.6%, and 53.1% of ASVs remaining unassigned at the kingdom, phylum, class, order, family, and genus level, respectively. This suggests an issue during the sequencing process, likely related to the low DNA concentrations recovered from the different microcosms (from 0.0224 to 1.148 ng/ μ L; details in **Supplementary table III.2**), which were below the recommended threshold for the Novogene sequencing platform (10 ng/ μ L). Despite these limitations, we proceeded with the analysis of the obtained data.

III.3.3.1 Microcosms with different water content

Of all the ASVs detected in both experiments, 1 098 ASVs were present in the microcosms exposed to different water contents, with an average of 206 ± 26 ASVs per sample (details in **Supplementary table III.2-a**). In order to explore the dataset and identify any pattern based on the experimental conditions, we first visualized the relative abundance of the different bacterial taxa at T₀ and at the end of the experiment (**Figure III.6**). For the sake of

visibility, the results are displayed at the family taxonomic level. The plot shows families for which the sum of the relative abundances across samples was greater than 0.5%. The rest were grouped in the 'Others' category.

In the abiotic controls, differences in the relative abundance of taxa when compared to the initial inoculum (To) were observed, as well as between the various water contents to which the microcosms were exposed. For example, in the microcosms exposed to water saturation (100%), the *Pseudomonadaceae* family was greatly reduced compared to the To and other water contents (only 6% of the ASVs present), whereas the family *Sphingomonadaceae* was increased in the microcosms exposed to 66% of water content (15% of the ASV vs. $5 \pm 2\%$ in the other abiotic controls and To). However, these abiotic controls were heat-sterilised and did not degrade DCM over time, so these differences may be due to a random sampling effect (Zhou et al., 2013), or to residual carbon sources used by certain heat-resistant taxa, allowing the microbial community to develop differently.

In the biotic controls, although we inoculated them with *Hyphomicrobium* sp. GJ21 at the beginning of the experiment, the family *Hyphomicrobiaceae* was not predominant. On average, this family represented the $5 \pm 2\%$ of the ASVs in each of these microcosms, the majority of which (97-100%) belonged to the genus *Hyphomicrobium*. The most abundant family in all biotic controls regardless of the water content was the family *Pseudomonadaceae* (relative abundance $\geq 43\%$). As the sand matrix was not sterilized before the addition of *Hyphomicrobium* sp. GJ21 in this first experiment, this could have led to its growth limitation by the pre-existing community in the environmental inoculum. Interestingly, the relative abundance of the *Hyphomicrobiaceae* family was slightly, and not significantly, lower at low water contents. As already suggested by the reduced DCM degradation function efficiency in the previous **section III.3.1.1**, this bacterial family may not be adapted to low water contents. Repetition and replication allowing a better statistical testing of the acceptance or rejection of this hypothesis would be necessary.

In the environmental samples, the dominant taxa were globally similar across water contents and replicates, with the exception of the replicate x2 at water saturation. In general, the observed differences across microcosms, which were more important between replicates than between conditions, could be explained either by the intrinsic microcosm heterogeneity or an artefact of random sampling. In detail, as in the initial inoculum, the *Pseudomonadaceae* family was predominant in all conditions (relative abundance $\geq 38\%$), except in the second replicate at water saturation (100% water content) where its relative abundance was 9%. All the detected ASVs in this family belonged to *Pseudomonas* spp., a widespread genus characterized by a high potential for adaptation to different environmental conditions and versatile metabolic capacities (Silby et al., 2011). Previous work have linked some isolates of this genus to the DCM degradation activity in the absence of the *dcmA* gene (Krausova et al., 2006). The *Hyphomicrobiaceae* family was also ubiquitous in all conditions at higher relative abundances than in the initial inoculum (relative abundance of 14-18%), except at 33% of water

content (relative abundance of 2%), consistent with the observation that some members of this family may be poorly adapted to low water content. The ASVs from the *Hyphomicrobiaceae* family belonged mainly to *Hyphomicrobium* spp. (15 out of 20 ASVs), a genus consisting of facultatively methylotrophic strains strongly associated with the degradation of DCM (Muller et al., 2011a), in particular in aquifers (Hermon et al., 2018). The *Caulobacteraceae* family was highly abundant in both replicates at 100% water content (relative abundance of 14-22%). The predominant ASVs in this family belonged to the genus *Brevudimonas*, which includes some strains that have been described in the literature as having the potential to degrade various n-alkanes and polycyclic aromatic hydrocarbons (Guermouche M'rassi et al., 2015), but no association with organochloride compounds has yet been described. Finally, the increase in abundance of the families *Nocardioideaceae* (relative abundance of 1-6%) and *Xanthobacteraceae* (relative abundance of 1-4%) is also noteworthy, as both families contain some members that have already been described as capable of degrading a variety of pollutants, including C1 compounds (Iwabuchi et al., 1998; Travkin et al., 1997; Van Ophem & Duine, 1990). For example, DCM degradation has been observed in the genus *Xanthobacter*, whose gene encoding the DCM dehalogenase DcmA is 98-99% similar to previously isolated DCM dehalogenase genes (Emanuelsson et al., 2009).

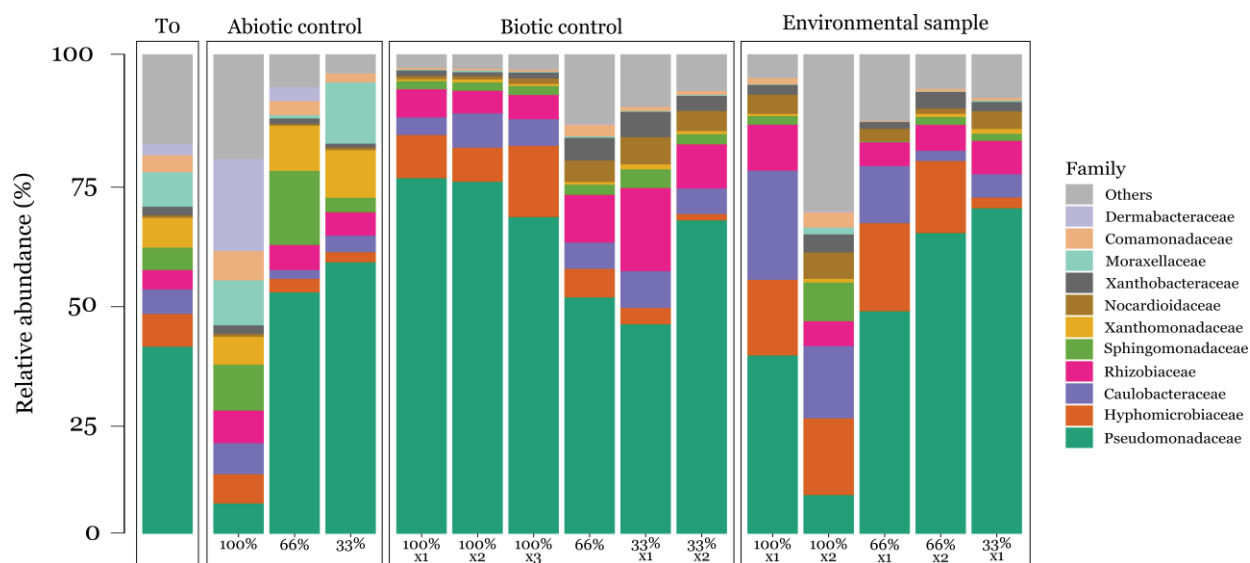


Figure III.6. Family-level relative abundances (in %) at the beginning (To) and at the end of the experiment in microcosms exposed to different water contents. Families with a lower relative abundance than 0.5% are grouped in ‘Others’ category.

To assess the impact of water content on the diversity of the microbial community, we calculated the alpha-diversity metrics at the ASV level in the different microcosms, grouping them by type of inoculum (**Figure III.7-a.**) or by water content in the case of the environmental samples (**Figure III.7-b.**). In general, the microbial community in the initial inoculum presented a higher richness (Chao1), evenness (Pielou’s evenness) and diversity (Shannon-Wiener diversity) when compared to all types of microcosms at the final sampling point. This suggests that during the experiment, starting from a rich inoculum, the biodiversity

of the microbial community was reduced, with certain microbial taxa being selected and favoured under these conditions. In addition, even if the richness of the microbial community in the abiotic controls was similar to the one in the biotic controls and environmental samples, its evenness and diversity was slightly higher, suggesting that the presence of DCM in the samples imposed a positive selection of microbial taxa capable of growing with this compound, which may have become predominant at the end of the experiment.

When focusing on the effect of different water contents in the environmental samples, there was a trend towards higher richness, evenness and diversity in microcosms at water saturation (100% of water content) compared to the other two conditions (**Figure III.7-b.**). This trend was also observed in the abiotic controls (results not shown), which would suggest that it was a general impact that was not limited to the DCM-degrading microbial populations. However, none of these results were significant, in part due to the reduced number of replicates included in this experiment.

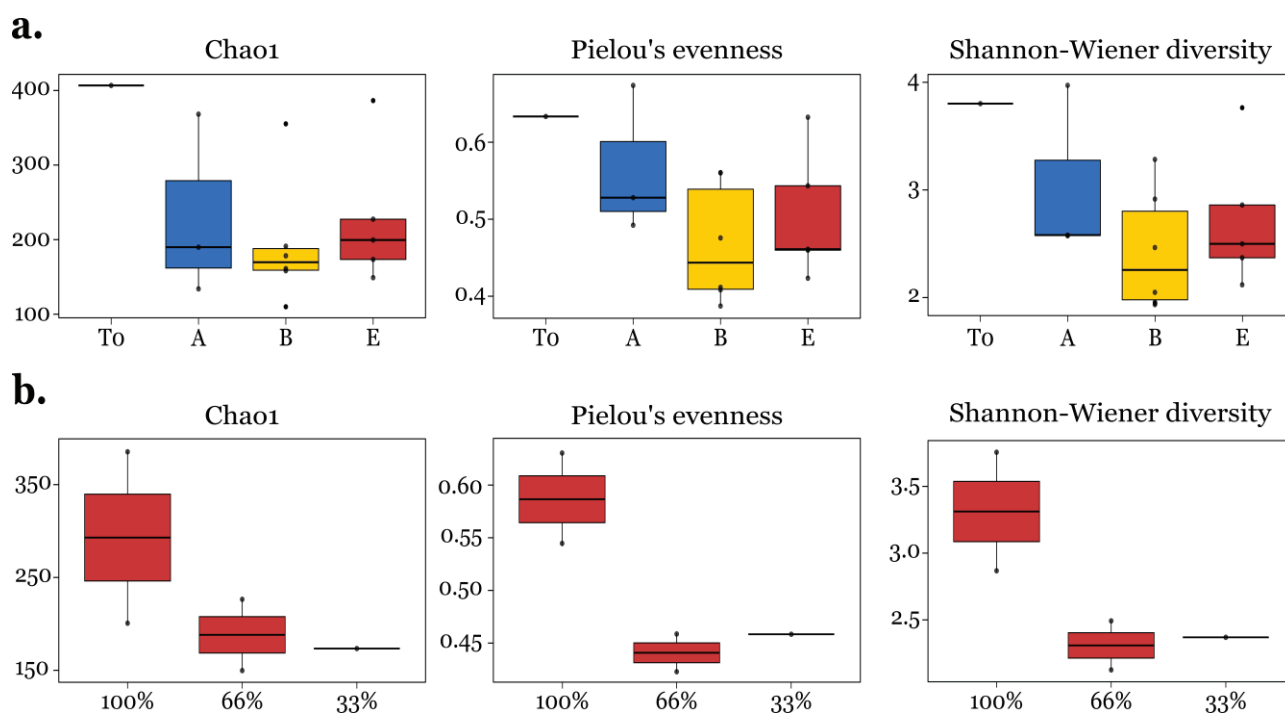


Figure III.7. Microbial community diversity indices of microcosms exposed to different water content. The calculated alpha-diversity metrics were the Chao1 index (i.e. richness estimator), the Pielou's evenness (i.e. how evenly ASVs are distributed), and the Shannon-Wiener diversity index (i.e. it reflects both the number of ASVs and the equality of the distribution). **a.** Alpha-diversity metrics as a function of the inoculum type, with grey for To (n=1), blue for abiotic controls (A, n=3), yellow for biotic controls (B, n=6), and red for environmental samples (E, n=5). **b.** Alpha-diversity metrics in the environmental samples according to water content (100%, 66% or 33%; n=2, except for 33% of water content where n=1). The points in the boxplot correspond to each replicate.

To compare the microbial composition among the environmental samples, a PCA was performed on the clr-transformed abundance data at the genus-level phylotypes (**Figure III.8**). The PCA showed that the first two principal components (PC1 and PC2) accounted for 71.7% of the variation in taxonomic composition between samples. Although 57.5% of the variation was explained by the PC1 only, no clear distribution was observed, which was mainly due to the fact that the variation within the same water content was equivalent to the variation found between different water contents. This indicates that there was no significant impact of this parameter on the composition of the bacterial community during the experiment. The overlaying of DCM half-life information on the plot (green shade) didn't put in evidence any distribution based on this parameter, with a higher score for samples with a lower DCM half-life. Overall, these observations were limited by the lack of replicates and so, new experiments should be carried out to draw stronger conclusions on the potential effect of water content.

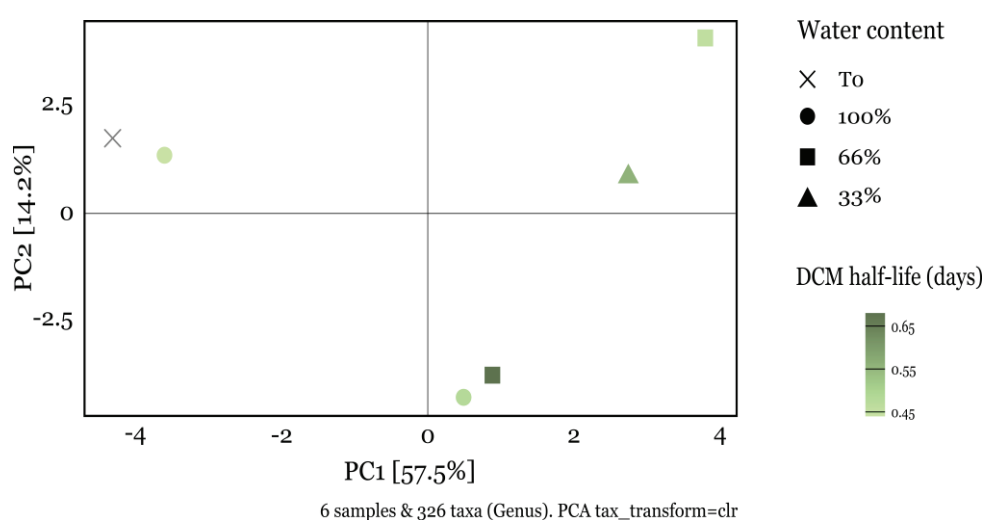


Figure III.8. Principal Coordinate Analysis (PCA) plot derived from clr-transformed abundance data at the genus-level phylotype in the environmental samples exposed to different water contents. The shape indicates the water content: triangles for 33%, squares for 66%, and circles for 100%. The gradient colour is based on the average DCM half-life of each sample during the whole experiment: the darker, the higher the DCM half-life, and vice-versa. The cross corresponds to the initial inoculum (To).

III.3.3.2 Microcosms with different oxygen status

Of all the ASVs detected in both experiments, 1 803 ASVs were present in the microcosms exposed to different oxygen status, with an average of 319 ± 21 ASVs per sample (details in **Supplementary table III.2-b.**). The relative abundance of the different microbial taxa was visualized at the family level at To and at the end of the experiment (**Figure III.9**).

DNA extractions from the abiotic controls resulted in low DNA concentrations, impairing the sequencing of their initial inoculum (To-A). At the end of the experiment, slight differences in the relative abundance of some taxa were observed depending on the oxygen status. For example, the *Rhodobacteraceae* family was more abundant in the alternating conditions than in microcosms exposed to continuous oxygen concentrations. However, as it was the case in

the previous experiment, these abiotic controls were heat-sterilised and did not degrade DCM. Therefore, the observed differences may be due to either random sampling or to residual carbon sources that allow the growth of different heat-resistant taxa depending on the oxygen status.

The biotic controls were established, in this case, using a heat-sterilised sand matrix inoculated with the strain *Hyphomicrobium* sp. GJ21 at the beginning of the experiment. As a result, the *Hyphomicrobiaceae* family, in particular the *Hyphomicrobium* genus, was the dominant taxon in these types of microcosms regardless of the oxygen status (relative abundance of $62 \pm 3\%$). This indicates that the presence of this strain was not dependent on the oxygen concentration or its regime (continuous or alternating). When compared to the initial inoculum used in these microcosms (To-B), a decrease in the relative abundance of this taxon was observed (relative abundance of 92% in the To-B). This observation could be due either to the fact that the culture serving for inoculation might have contained some dead GJ21 biomass whose DNA was degraded through the 81 days of the experiment, or simply because the abundance of some heat-resistant taxa increased during the experiment and consequently the relative abundance of this bacterium in the microbial community decreased.

The microbial community at the family-level in the environmental samples showed similar taxonomic composition and dominant taxa in both the inoculum (To-E) and at the end of the experiment across different oxygen statuses and replicates. These observations contrast with the differences in the DCM degradation function observed between experimental conditions (**section III.3.1.2**). However, since we are working at the DNA level, the presence of a taxon does not necessarily imply that it was actively participating in the function. Nonetheless, a more detailed comparison reveals that the most abundant family in all environmental samples, *Hyphomicrobiaceae*, had a higher relative abundance at the end of the experiment than in the initial inoculum (To-E) (17-33% vs. 7%, respectively). As mentioned above, this family includes several members already associated with DCM degradation, suggesting that it may have been participating in this function during the experiment. Among the taxa significantly more abundant in microcosms under continuous anoxic conditions compared to those starting in oxic conditions (continuous or alternating regime), we found the family *Pseudomonadaceae*. All the ASVs of this family corresponded to the *Pseudomonas* genus, which is mainly composed of strict aerobes, with some exceptions capable of using nitrate as terminal electron acceptor (Arai, 2011; Li et al., 2022). Other taxa associated with anoxic conditions were the families *Rhodocyclaceae* and *Comamonadaceae*, both of which were significantly more abundant in microcosms starting the experiment in anoxic conditions (continuous or alternating regime) compared to those starting under oxic conditions. In the family *Rhodocyclaceae*, the main ASVs were associated to the *Methyloversatilis* genus and the *Dechloromas* genus, that have been previously reported to be involved on the transformation of chlorinated hydrocarbons under oxic and anoxic conditions (Li et al., 2022). In the case of the *Comamonadaceae* family, the majority of ASVs belonged to the genera *Variovorax* and *Acidovorax*, which have been previously associated with the degradation of various chlorinated compounds (e.g. vinyl

chloride, dichlorobenzene), but under oxic conditions (Monferrán et al., 2005; Wilson et al., 2016). Finally, the family *Caulobacteraceae* was significantly more abundant in microcosms starting under oxic conditions compared to those starting under anoxic conditions (continuous or alternating regime). As in the previous experiment, most of the ASVs belonging to this family were associated with the genus *Brevudimonas* (Guermouche M'rassi et al., 2015).

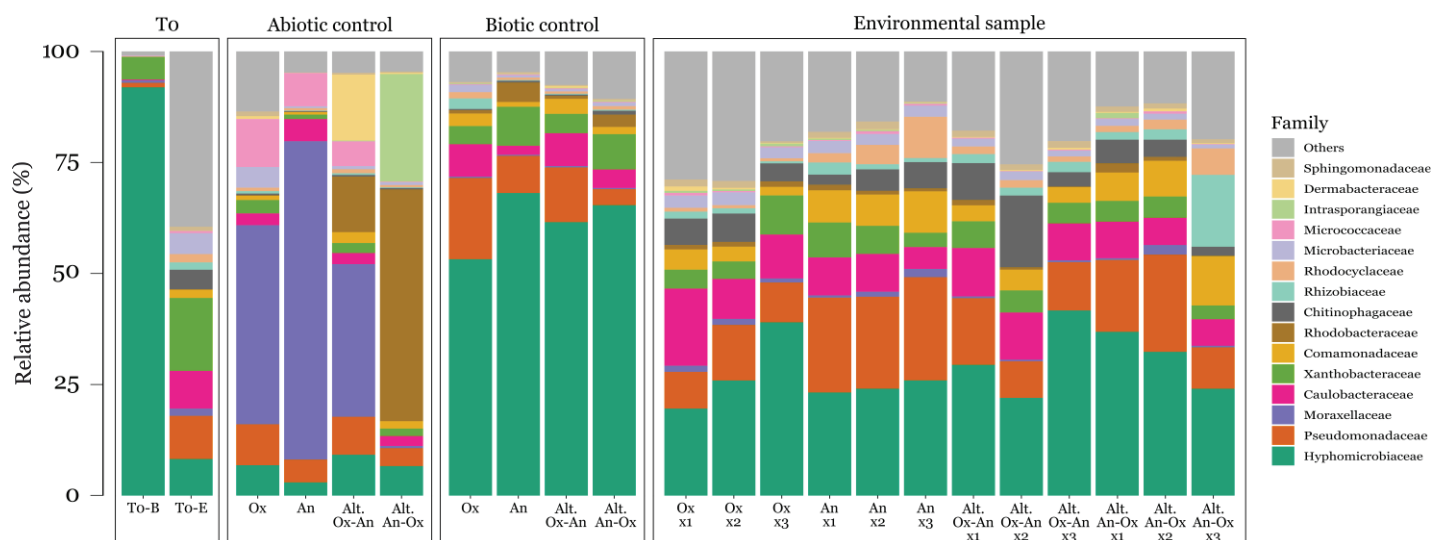


Figure III.9. Family-level relative abundances (in %) at the beginning (To) and at the end of the experiment in microcosms exposed to different oxygen statuses. Families with a lower relative abundance than 0.5% are grouped in ‘Others’ category.

The impact of oxygen status on the diversity of the microbial community was assessed using the alpha-diversity metrics at the ASV level across the different microcosms, based on the type of inoculum (**Figure III.10-a.**) or oxygen status in the case of the environmental samples (**Figure III.10-b.**). As expected, the microbial community in the initial environmental inoculum (To-E) showed higher richness, evenness and diversity than the initial inoculum used in the biotic controls (To-B) (p-value <0.05; **Figure III.10-a.**). This could be explained by the fact that To-B was first heat-sterilised, likely reducing the richness of the inoculum, and then massively inoculated with *Hyphomicrobium* sp. GJ21, which affected the evenness (and consequently diversity) due to the dominance of this single taxon in the microbial community. Similarly, at the end of the experiment, the environmental samples had significantly higher evenness and diversity than the abiotic and biotic controls (p-value <0.05; **Figure III.10-a.**), in link with the higher diversity of the inoculum for these microcosms. Interestingly, the evenness and diversity of the biotic controls were significantly higher than the To-B (p-value <0.05), suggesting that even if the initial inoculum used in these microcosms was heat-sterilized, some taxa were able to resist and develop during the experiment. These taxa may have participated in the degradation of DCM or they could have used some by-products resulting from the activity done by the inoculated strain *Hyphomicrobium* sp. GJ21.

Focusing on the environmental samples, oxygen status had minimal statistical impact on the microbial community indices. Only microbial communities initially exposed to oxic conditions

(continuous or alternating regime) showed a higher richness than those initially exposed to anoxic condition, with samples with the alternating regime being significantly different (p -value < 0.05 ; **Figure III.10-b.**). In general, irrespective of the type of microcosms (A, B or E), microbial communities initially exposed to oxic conditions had a higher richness than those initially exposed to anoxic conditions (results not shown). These observations suggest that the exposure to anoxic conditions may have limited the development of certain taxa and show the importance of the initial oxygen concentration to which microbial communities are exposed at the experiment's onset, which impacts both their activity (**section III.3.1.2**) and composition. Finally, despite no significant differences in the evenness or diversity were observed between conditions in the environmental samples, there was a trend toward higher evenness and diversity in microbial communities exposed to continuous conditions compared to alternating conditions (**Figure III.10-b.**). This suggests that alternating conditions may be more selective, promoting the development of a few taxa that dominated the microbial community.

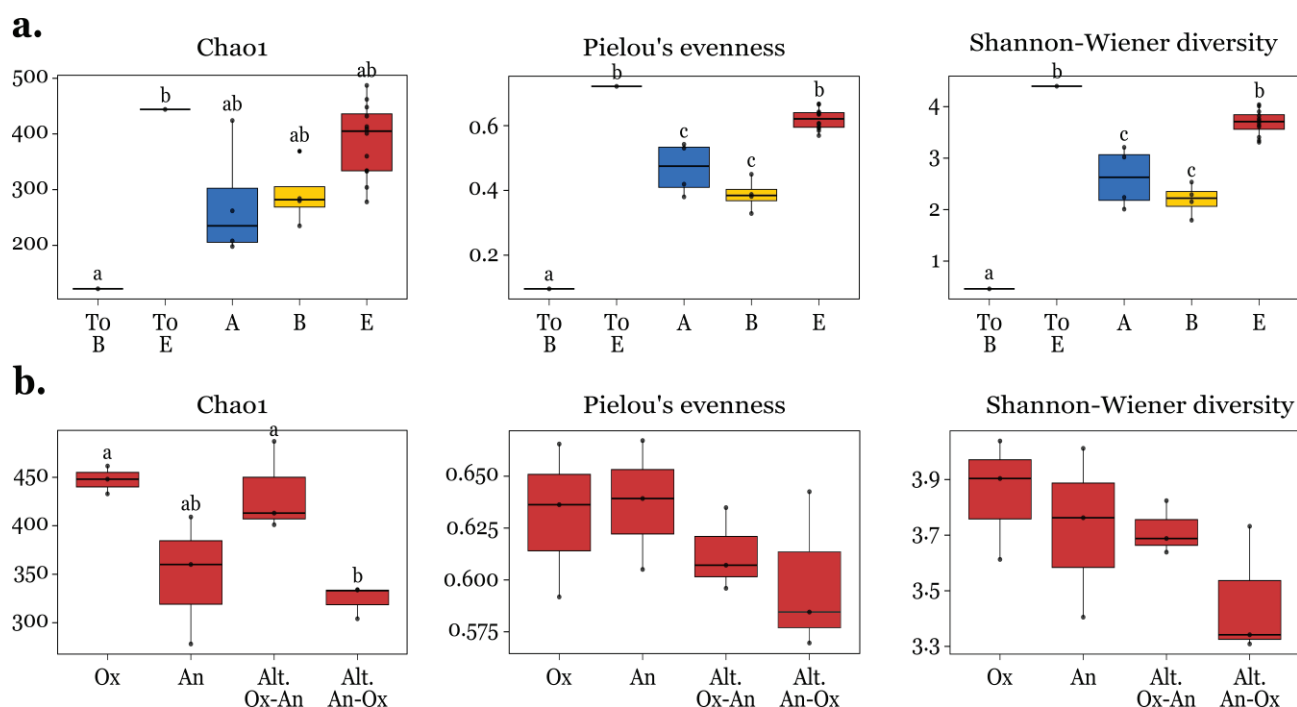


Figure III.10. Microbial community diversity indices of microcosms exposed to different oxygen statuses. The calculated alpha-diversity metrics were the Chao1 index, the Pielou's evenness, and the Shannon-Wiener diversity index. **a.** Alpha-diversity metrics as a function of the type of inoculum. The colours represent the type of microcosms: grey for TO-B ($n=1$) and TO-E ($n=1$), blue for abiotic controls (A, $n=4$), yellow for biotic controls (B, $n=4$), and red for environmental samples (E, $n=12$). The points in the boxplot correspond to each replicate. Letters 'a', 'b' and 'c' show group of significance (p -value < 0.05). **b.** Alpha-diversity metrics in the environmental samples according to oxygen status: continuous oxic (Ox), continuous anoxic (An), alternating oxic-anoxic (Alt. Ox-An), and alternating anoxic-oxic (Alt. An-Ox). The points in the boxplot represent the replicate ($n=3$ per condition). Letter 'a' and 'b' show group of significance (p -value < 0.05).

To further investigate the impact of oxygen status on the microbial composition in the environmental samples, a PCA was performed on the clr-transformed abundance data at the genus-level phylotypes (**Figure III.11**). The PCA showed that the first two principal components (PC1 and PC2) accounted for 37.8% of the variation in taxonomic composition between samples. The PC1 axis distributed the samples according to the oxygen regime to which they were exposed (continuous or alternating), while PC2 axis distributed the samples according to the initial oxygen concentration (continuous anoxic and alternating anoxic-oxic vs. continuous oxic and alternating oxic-anoxic). Interestingly, the initial inoculum To-E, which came from a microoxic sediment, was closer to the anoxic samples according to the PC2. Additionally, samples exposed to an alternating regime are more similar together than with the sample sharing the same starting condition. This suggests that alternating conditions specifically promote or select certain taxa that are capable of developing in an environment where the oxygen concentration is frequently changing. Finally, no clustering was observed on the first 2 principal components as a function of the average DCM half-life (here referred to as degradation efficiency). This may be due to the fact that to calculate this parameter, we took an average of the DCM half-life observed in each pulse along the experiment. Thus, in the case of the microcosms alternating the oxygen status, the lower degradation rate observed under anoxic conditions (**section III.3.1.2**) was probably neutralized by the high rate at which the DCM was degraded under oxic conditions.

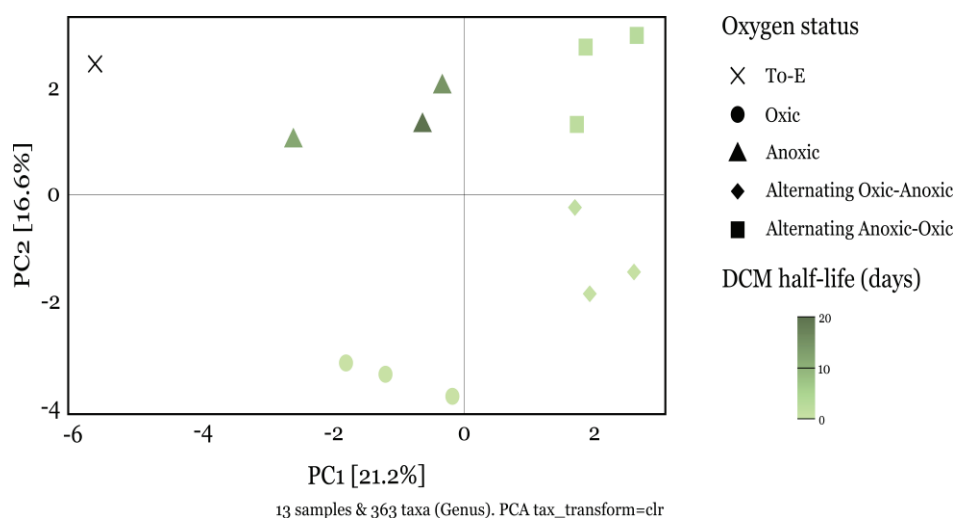


Figure III.11. PCA plot derived from clr-transformed abundance data at the genus-level phylotypes in the environmental samples exposed to different oxygen statuses. The shape indicates the oxygen status: circles for continuous oxic conditions, triangles for continuous anoxic conditions, rhombus for alternating conditions from oxic to anoxic, and squares for alternating conditions from anoxic to oxic. The gradient colour is based on the average DCM half-life of each sample during the whole experiment: the darker, the higher the DCM half-life, and vice-versa. The cross corresponds to the initial inoculum (To-E).

III.4 Discussion

III.4.1 Impact of water content on DCM degradation kinetics and microbial community composition

Soil moisture is an important physicochemical parameter that affects the microbial activity in various ways (Schimel, 2018). Among these, soil moisture determines the water activity (i.e., availability of water for biological reactions) of the soil, which, when reduced, limits microbial physiological functions. Furthermore, it regulates solute transport and gas diffusion, which are positively and negatively correlated with the amount of water, respectively.

In our study, we have observed that microbial communities exposed to low water contents (33%) had a lower degradation rate than those exposed to higher water contents (66% and 100%). These results agree with previous work by Shen and colleagues, which tested 8 water contents from 0% to 100% and showed that the microbial activity responsible for the dechlorination of the volatile perchloroethylene (C_2Cl_4) was significantly positively correlated with the soil water content (Shen et al., 2021). The authors concluded that water content, rather than soil type and inocula, was the predominant rate-limiting parameter in soil for microbial reductive dechlorination. It is important to note that neither the *dcmA* or *mec* pathways are involved in catalysing reductive DCM degradation. In addition, in an experiment investigating the role of water level fluctuations on the biogeochemical functioning of soils, Rezanezhad and colleagues found that soil respiration, measured through CO_2 effluxes, was highest for moisture contents near 60% (Rezanezhad et al., 2014), as it was previously described by Linn & Doran (1984). They proposed that this moisture content maximizes the balance between solute transport and effective soil aeration. In our case, however, we did not observe a significant difference in DCM-degradation between samples with 66% and 100% water content. This absence of difference may be related to the distinct experimental settings used in our study compared to theirs. In particular, they conducted a 75-day experiment in a 45 cm-high soil column with a vertical oxygen gradient, while we did a 24-day experiment in small 160 mL bottles. Another hypothesis to explain this could be that, as the sand used in our experiment came from the saturated zone of a laboratory-scale aquifer, it may have contained microbial populations adapted to the high water content conditions. Thus, their activity may be equally optimal at both 100% and 66% water content. This 'legacy effect' has been described by previous authors who have shown that it is not only the soil moisture *during* the experiment that is important for soil microorganisms and their activity, but also what it *was* before (Banerjee et al., 2016; Preece et al., 2019).

Repeated exposure to DCM promoted the degrading activity, which was similar regardless of the water content. This observation suggests that populations capable of utilising DCM as sole carbon and energy source had a selective advantage during the experiment. The observed acceleration of DCM degradation could thus be related to an increase in the size of the DCM-degrading populations or a change in their physiological state (Wang et al., 2018). In this

regard, it is known that DCM utilization requires a number of adaptations to cope with the genotoxic effects of the by-products, such as hydrochloric acid and formaldehyde, that are formed during the enzymatic transformation of this compound (Firsova et al., 2005; Muller et al., 2011b).

On the other hand, water content did not significantly change the alpha-diversity of the microbial community despite our observation of a trend toward higher richness, evenness and diversity at 100% water content. Schimel (2018) proposed that at low water contents, the microbial community is mainly dominated by a few microorganisms that are able to resist the physiological stress induced by these conditions. In our study, we observed this reduction in the diversity of the microbial community at low water contents, suggesting that under these conditions, few species were indeed dominating the community. The dominant taxon at low water contents was the family *Pseudomonadaceae*, in particular the genus *Pseudomonas* spp.. Notably, soil isolates of *P. putida* have previously been associated with an optimal soil moisture level of 40%, which was below of the water capacity of the soil used in that study (Filonov et al., 1999). However, to confirm our observations, we should repeat the experiment with more replicates, which would allow us to perform statistical analysis. In terms of beta-diversity, water content did not impact the composition of the microbial community, as no clustering was observed in relation to this parameter.

Taken together, our observations suggest that water content may influence the timing of the community function activation, but not its composition. Indeed, in the previous study done by Shen and colleagues, the researchers found that while the perchloroethylene dechlorination activity was positively correlated with soil moisture, the community composition was mainly clustered by soil type (laterite, brown soil and black soil) rather than water content (Shen et al., 2021). Another hypothesis to explain our results is that for changes to occur at the composition level, it would be necessary to perform the experiment over a longer period of time or in an open environment allowing colonisation, as well as to adapt the sampling procedure to observe the population dynamics. Finally, to allow for more robust statistical analyses, it would be necessary to repeat the experiment with a greater number of replicates in order to obtain more conclusive results.

III.4.2 Impact of oxygen status on DCM biodegradation kinetics and microbial community composition

In aquatic environments like aquifers, oxygen concentrations can range from completely anoxic to saturated oxic conditions, which results in the formation of oxygen gradients that may either remain stable or alternate over time, as seen during GLF. In general, these changes in oxygen levels play an important role in regulating the functional interactions, structure and activity of many microbial communities (Fenchel & Finlay, 2008).

In our study, we observed that microbial communities in continuous oxic conditions showed the fastest DCM degradation at the beginning of the experiment. These results suggest that the autochthonous microbial populations in our environmental samples degraded mainly in oxic conditions, an observation consistent with previous studies carried out on groundwater from the same experimental site, the industrial site of Themeroil, which demonstrated an intrinsic DCM biodegradation potential under oxic conditions (Hermon et al., 2018). In contrast, when microbial communities were exposed to continuous anoxic conditions, no degradation was observed. It was only after a short exposure to the atmosphere at day 58, between the 6th and 7th pulses, that DCM degradation started. It was not possible to ascertain whether this observation was due to the aeration of these microcosms, or whether it was simply a matter of chance and that the DCM-degrading populations in continuous anoxic conditions required a longer period of time (58 days) to start the activity. In this regard, Frindte and colleagues observed that variable redox conditions in short periods of time can result in similar soil bacterial activity rates (measured through CO₂, NO₂ and CH₄ fluxes) to the ones observed under constant oxic conditions (Frindte et al., 2013). DeAngelis and colleagues proposed that obligate anaerobes may require episodic occurrence of oxygen in order to regenerate their electron acceptors (DeAngelis et al., 2010). In complement to this, using a multi-phase flow reactive transport *in silico* model, Prieto-Espinoza and colleagues noticed that the presence of CO₂ should favour the metabolic activity of anaerobic DCM degraders (Prieto-Espinoza et al., 2023). They proposed that this could occur either through its utilization by the H₂-consuming partners of *Candidatus* 'Dichloromethanomonas elyunquensis' strain RM, enabling the DCM-oxidation activity of the latter strain, or through its use for carbon assimilation via the Wood-Ljungdahl pathway, in which DCM and CO₂ are used to generate formate and acetate in the strains *Dehalobacterium formicoaceticum* DMC and *Candidatus* 'Formimonas warabiya' DCMF (see details in **Figure I.9**). In summary, in our case, the opening the microcosms may have been sufficient to regenerate or replace the pool of CO₂, thereby promoting the activity of the DCM-degrading microbial populations found in the microcosms exposed to continuous anoxic conditions.

In microcosms where the oxygen concentration alternated, differences were observed depending on the initial oxygen concentration to which they were exposed to. In particular, the degradation of DCM under both oxic and anoxic conditions was enhanced in microcosms that were initially exposed to oxic conditions. This could be due to the fact that initial exposure to oxic conditions facilitated the activation of the DCM-degrading population, in particular facultative anaerobic bacteria capable of degrading this compound in both oxic and anoxic conditions. Consequently, when the oxygen concentration decreased, the microbial population was already ready to degrade this compound. Conversely, a first exposure to anoxic conditions may have limited the development of these types of microbial populations and so, the community would need a longer period of time to become active. Similar observations were reported for a filamentous bacteria of wastewater treatment plant microbial community, where at the single-cell level, 28% of cells exhibited activity (here the assimilation of oleic acids) when

aerobically preconditioned compared to 3% if the cells when anoxically preconditioned (Sheik et al., 2016). However, other work contradicts these observations. Particularly, Vitte and colleagues observed a better removal of polycyclic aromatic hydrocarbons (PAHs) when an anoxic period preceded an oxic period (Vitte et al., 2011). As PAHs are known to be both degraded under oxic and anoxic conditions, the authors suggested that a pre-exposure to anoxic conditions may stimulate the anaerobic metabolism and prepare the conditions for better degradation by aerobic metabolism. Löser and colleagues found no changes in the degradation rate or concentration of residual hydrocarbons in a diesel-fuel-contaminated soil when subjected to aerobic/anaerobic changes (Löser et al., 1998). Conversely, Vieira and colleagues showed that intermittent aeration in a bioreactor setup promoted the biodegradation of diesel oil and gasoline from a contaminated effluent, hypothesizing that this effect was due to the loss of the most volatile hydrocarbons during the aeration stage (Vieira et al., 2009). Altogether, it seems that the responses to oxygen alternations may depend on the specific compounds and the metabolism of the microbial populations in the samples, as well as on the experimental setup. Considering that the DCM-degrading populations in our experiment were mainly active under oxic conditions, this might explain why the pre-exposure to anoxic conditions was detrimental for the DCM degradation activity, though not as deleterious as continuous anoxic exposure. This finding was in line with the previous study carried out in laboratory-scale aquifers, in which we observed that water level fluctuations, which caused an increase in oxygen concentration in the system, promoted the biodegradation of DCM (Prieto-Espinoza et al., 2021). In conclusion, the periodic exposure to either higher oxygen concentrations or the atmosphere may have enhanced the activity of microbial communities in this fluctuating zone.

In addition to impact the DCM degrading activity, the initial oxygen concentration to which microcosms were exposed also significantly impacted the richness of the microbial community, which was lower when starting under anoxic conditions. In particular, alternating microcosms starting in anoxic conditions had the lower richness, evenness and diversity. In terms of the beta-diversity, samples clustered according to the oxygen regime to which they were exposed, demonstrating that this parameter influenced the composition of the bacterial community. Vitte and colleagues also observed a specific adaptation of the microbial communities capable of degrading PAHs to the type of incubation, selecting the most adapted bacteria in each case (Vitte et al., 2011). In addition, in our experiment, samples that experienced anoxic conditions were spatially separated from those that were in continuous oxic conditions throughout the experiment. This suggests that exposure to anoxic conditions, either at the beginning or during the experiment, exerted a selection pressure on the microbial community resulting in a change in its composition in the same direction.

III.4.3 Limitations and improvements of the experimental design

One of the main limitations in the use of the data derived from these experiments is the shortage of replicates in the different types of microcosms (controls and environmental

samples), which meant that most of the analyses were missing statistical power. This was a consequence of the use of a GC requiring manual injection to quantify DCM over time, which limited the number of microcosms that could be measured per time points. Another constraint derived from the same limitation was the inability to explore more combinations of the parameters of interest. In these experiments, we have only tested either different water contents under a single oxic condition, or different oxygen concentrations under water saturation. Consequently, the output of other combinations that do occur in the environment during water level fluctuations, couldn't be tested on DCM degradation activity and microbial community. To overcome these limitations, a more comprehensive experiment was design and was carried out in collaboration with the “Institut Terre et Environnement de Strasbourg” (ITES), having access to an automated GC, which allowed the measurement of up to 60 microcosms per day in an acclimatised room with a constant temperature. This helped prevent the variations in DCM partitioning between the gas and liquid phases within the microcosms observed in the experiments presented in this chapter, which were associated with temperature differences between the incubator (25°C) and the room where the GC-FID was located.

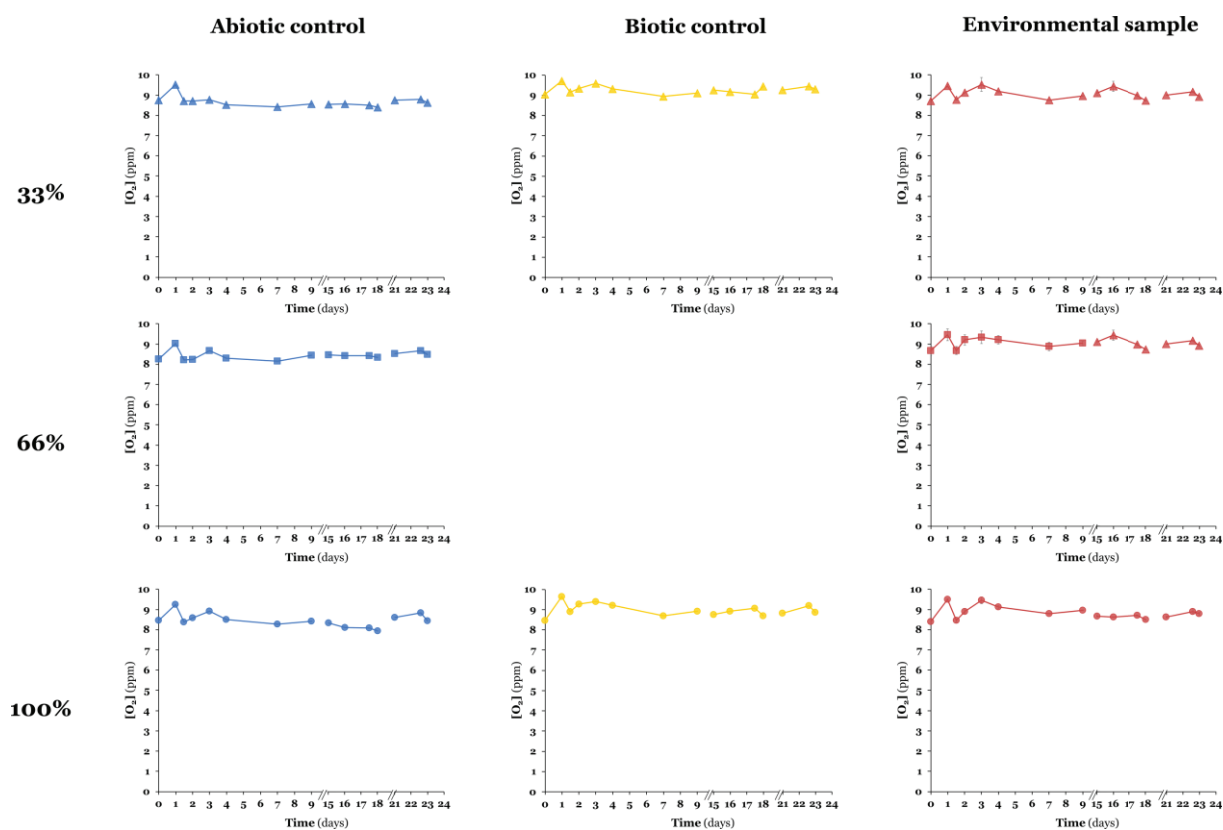
Additionally, the initial inoculum used in each of the experiments presented here was different, making comparisons between them difficult. Despite both inocula were derived from the laboratory-scale aquifers of a previous experiment (Prieto-Espinoza et al., 2021), they were prepared from different phases: drained sand was used for the experiment investigating the impact of water contents, while a mixture of saturated sand with contaminated water and drained sand was used for the experiment on the impact of oxygen status (see details in **section III.2.1**). The consequence of the distinct initial inocula and microbial community composition was clear when comparing the most abundant families per experiment: *Pseudomonadaceae* in the water content experiment, and *Hyphomicrobiaceae* in the oxygen status experiment. Finally, the biotic controls were setup differently in both experiments, as the first analyses demonstrated the poor persistence or colonisation of our model strain in the biotic controls. Altogether, these differences made delicate the comparison between both experiments.

III.5 Conclusion

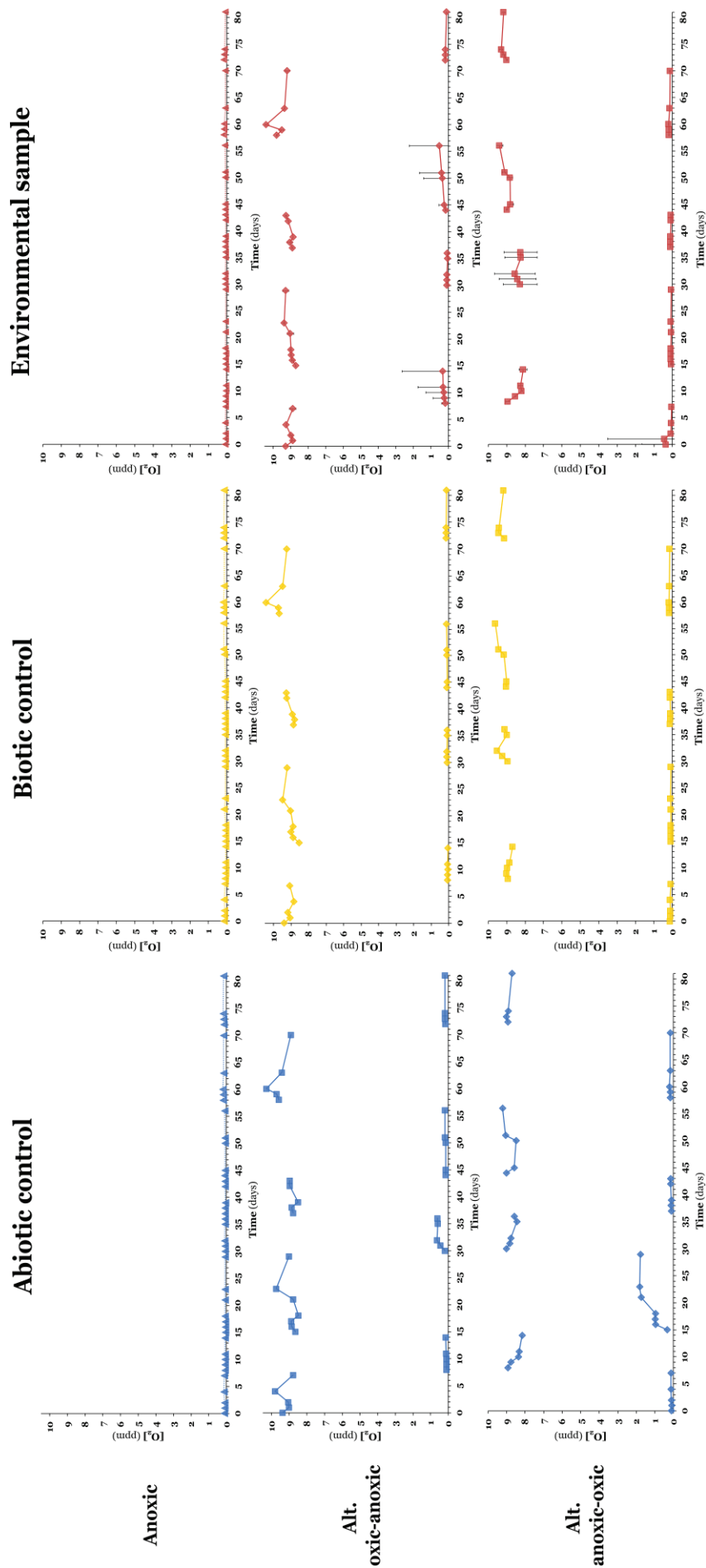
A previous experiment in laboratory-scale aquifers showed that water level fluctuations promoted DCM biodegradation (Prieto-Espinoza et al., 2021). To reduce the complexity of the system, here we investigated in laboratory microcosms the individual impact of two of the parameters altered this phenomenon. Our results showed that both water content and oxygen status impacted the activity and the composition of the DCM-degrading microbial community to different extents. On the one side, the water content mainly impacted on the ‘activation’ of the DCM degradation function, which was faster at water saturation. However, repeated exposure to DCM reduced the influence of this parameter on the biodegradation function. This parameter did not significantly affect the composition of the microbial community, but a trend

towards higher richness and diversity at water saturation was observed. On the other side, oxygen status impacted the overall DCM degradation, which was promoted under oxic conditions, as well as the microbial community composition, which was dissimilar in function of the oxygen concentration regime to which they were exposed. Regarding the alternating conditions, we showed that the initial oxygen concentration to which these types of microcosms were exposed significantly determined the efficiency of this activity during the following pulses. New experiments should be performed to overcome the statistical limitations we have encountered during these experiments, as well to explore new combinations between both parameters that will help us to further understand the role of water content and oxygen status during water level fluctuations.

Supplementary information - chapter III



Supplementary figure III.1. Monitoring of oxygen concentration (ppm) over time (days) in microcosms exposed to different water contents. The colour represents the type of microcosms: blue for abiotic controls, yellow for biotic controls, and red for environmental samples. The shape indicates the water content to which microcosms were exposed: circles for 100%, squares for 66%, and triangles for 33%. Biotic controls with 66% water content were not equipped with oxygen sensor spot.



Supplementary figure III.2. Monitoring of oxygen concentration (ppm) over time (days) in microcosms exposed to different oxygen status. The colour represents the type of microcosms: blue for abiotic controls, yellow for biotic controls, and red for environmental samples. The shape indicates the oxygen status to which microcosms were exposed: triangles for anoxic conditions, squares for alternating regime starting from oxic conditions (Alt. oxic-anoxic), and rhombus for alternating regime starting from anoxic to oxic conditions (Alt. anoxic-oxic). Microcosms under oxic conditions were not equipped with oxygen sensor spots.

Supplementary table III.1.1. Sequence diversity of the *dcmA* gene, encoding the DCM dehalogenase DcmA. Detected single nucleotide polymorphisms (SNPs) in the different microcosms, as well as in the isolated DCM-degrading strains *Hyphomicrobium* sp. ATCC51888 and *Hyphomicrobium* sp. GJ21, compared to the reference strain *M. extorquens* DM4. The strain *Hyphomicrobium* sp. MC8b, whose *dcmA* gene shows 88% of sequence identity and 99 SNPs compared to the reference strain, is not shown due to space limitations. The microcosms replicate number is indicated after the symbol x.

Nucleotide position	C62G	G63C	C62T	G63T	C62T	G82A	C83T	T97G	C114A	T139A	C452A	A385G ^a	T386G	A449G	G532A	A691G	A708G	A746G	A778G	C817T	T829A	A833T	
	A20G	A20V																					
Amino acid position	S10	L15 ω	A20C	A20G	A20V	A27T	A27V	Y32D	P37 ω	S46T	T50N	I128V ^b	I128T	K149R	V176I	T230A	I235M	K248R	S259G	A272V	F276I	K277M	
<i>M. extorquens</i> DM4	C	A	G	C	G	G	C	T	C	T	C	A	T	A	G	A	A	A	A	C	A	T	A
<i>Hyphomicrobium</i> sp. ATCC51888	C	A	G	C	G	A	C	T	C	T	C	A	T	A	G	A	A	A	A	C	A	T	A
<i>Hyphomicrobium</i> sp. GJ21	T	T	T	G	C	G	T	T	C	A	A	A	T	A	G	A	G	G	A	T	A	T	A
Biotic control 66%	T	T	T	G	C	G	T	T	C	A	A	A	T	A	G	A	G	G	A	T	A	T	A
Env. sample 100% x1	C	A	T	G	T	G	T	T	C	A	A	A	G	A	G	A	G	A	A	C	A	T	A
Env. sample 100% x2	C	A	T	G	T	G	T	T	C	A	A	A	G	A	G	A	G	A	A	C	A	T	A
Env. sample 66% x1 and x2	C	A	T	G	T	G	T	T	C	A	A	A	T	A	A	A	G	A	A	T	A	T	A
Env. sample 33% x1 and x2	C	A	T	G	T	G	T	T	C	A	A	A	G	A	G	A	G	A	A	C	A	T	A
Env. sample Ox x1 - x3	C	A	T	G	T	G	T	T	C	A	A	A	T	A	G	A	A	G	A	C	A	T	A
Env. sample An x1 - x3	C	A	T	G	T	G	T	T	C	A	A	A	T	A	G	A	A	G	A	C	A	T	A
Env. sample Alt. Ox-An x1 and x2	C	A	T	G	T	G	T	T	C	A	A	A	T	A	G	A	A	G	A	C	A	T	A
Env. sample Alt. Ox-An x3	T	T	T	G	C	G	T	T	C	A	A	A	T	A	G	A	A	G	A	C	A	T	A
Env. sample Alt. An-Ox x1 - x3	C	A	T	G	T	G	T	T	C	A	A	A	T	A	G	A	A	G	A	T	A	T	A

ω : synonym change in the third position of the codon (wobble pairing)

^a SNP not previously reported (Hermon, 2017; Vuilleumier et al., 2009)

[†] Amino acid change not previously reported (Hermon, 2017; Vuilleumier et al., 2009)

Supplementary table III.2. Information of sequencing processes. **a.** Results for microcosms exposed to different water content. **b.** Results for microcosms exposed to different oxygen status.

a.

Samples	DNA concentration (ng/ μ L)	QC analysis	Sequencing depth
To - E	0.0556	Passed	27 598
A - 100%	0.0404	Passed	
A - 66%	0.0968	Passed	
A - 33%	0.185	Passed	
B - 100% x1	0.143	Passed	
B - 100% x2	0.193	Passed	
B - 100% x3	0.123	Passed	
B - 66%	0.052	Passed	
B - 33% x1	0.182	Passed	
B - 33% x2	0.153	Passed	
E - 100% x1	0.191	Passed	
E - 100% x2	0.36	Passed	
E - 66% x1	0.292	Passed	
E - 66% x2	0.277	Passed	
E - 33% x1	0.221	Passed	
E - 33% x2	0.109	Fail	0

b.

Samples	DNA concentration (ng/ μ L)	QC analysis	Sequencing depth
To - A	0.0224	Fail	0
To - B	0.152	Passed	27 598
To - E	0.399	Passed	
A - Ox	0.029	Passed	
A - An	0.050	Passed	
A - Alt. Ox-An	0.107	Passed	
A - Alt. An-Ox	0.021	Passed	
B - Ox	0.700	Passed	
B - An	0.310	Passed	
B - Alt. Ox-An	0.714	Passed	
B - Alt. An-Ox	0.889	Passed	
E - Ox x1	0.305	Passed	
E - Ox x2	0.226	Passed	
E - Ox x3	0.274	Passed	
E - An x1	0.354	Passed	
E - An x2	0.576	Passed	
E - An x3	1.148	Passed	
E - Alt. Ox-An x1	0.484	Passed	
E - Alt. Ox-An x2	0.450	Passed	
E - Alt. Ox-An x3	0.868	Passed	
E - Alt. An-Ox x1	0.263	Passed	
E - Alt. An-Ox x2	0.414	Passed	
E - Alt. An-Ox x3	0.302	Passed	

Chapter IV

Method development and optimisation

Ce chapitre technique a pour objectif de présenter la stratégie et les étapes d'optimisation qui ont conduit aux choix de configurations expérimentales utilisées dans le **chapitre V**. Ainsi, le but de ce chapitre est de récapituler une partie essentielle du travail réalisé pendant ma thèse et lié à la mise en place expérimentale des 160 microcosmes soumis à 36 conditions expérimentales (**chapitre V**). Ce chapitre est rédigé en française à la demande de l'école doctorale qui exige qu'environ 10% des manuscrits de thèse soit en français, mais aussi pour que ces travaux d'optimisation puissent servir au mieux les futures optimisations de ce type de stratégie expérimentale effectuées au laboratoire.

IV.1 Introduction

Dans l'expérience décrite au **chapitre V**, nous étudions comment la composition et l'activité d'une communauté microbienne dégradant le DCM sont impactées par trois paramètres physicochimiques : la teneur en eau, le statut oxygène, et la granulométrie de la matrice. Afin de dépasser les limitations que nous avons rencontrés pendant l'expérience décrite au Chapitre III, nous avons décidé d'utiliser une chromatographie en phase gazeuse (GC) équipé d'un passeur automatique, ce qui permet d'augmenter le nombre de réplicats par condition expérimentale, ainsi que d'étudier plus de combinaisons entre les paramètres physicochimiques d'intérêt. La stratégie est de mesurer la concentration en DCM présente dans les microcosmes en utilisant le passeur automatique qui prélève directement dans la phase gazeuse des microcosmes sans passer par un vial intermédiaire. Cela est primordial pour limiter le temps dédié à la manipulation et ainsi pouvoir augmenter la fréquence des quantifications. Pour cela, une collaboration avec le laboratoire ITES (Institut Terre et Environnement de Strasbourg, UMR 7063) nous a permis d'utiliser leur équipement (GC-FID-MS, Thermo Fisher Scientifique ; détails dans la **section II.4.1.2**). Cependant, l'utilisation de cet appareil a nécessité une adaptation de la configuration expérimentale afin de travailler avec des fioles de 20 mL, format compatible avec le passeur, au lieu des bouteilles de pénicilline de 160 mL. De plus, en ajoutant la variable 'granulométrie' à notre travail, il a fallu mettre en œuvre une matrice artificielle au lieu du sédiment environnemental utilisé dans le chapitre précédent. N'utilisant plus ce sable déjà inoculé, nous avons donc également dû valider une manière efficace et reproductible d'introduire l'inoculum environnemental dans les microcosmes.

La **Figure IV.1** schématise les principales questions auxquelles nous avons dû répondre avant de commencer l'expérience présentée dans le **chapitre V**. Les sections suivantes présentent les étapes d'optimisation qui ont conduit à valider les paramètres et conditions expérimentales utilisés en **chapitre V**.

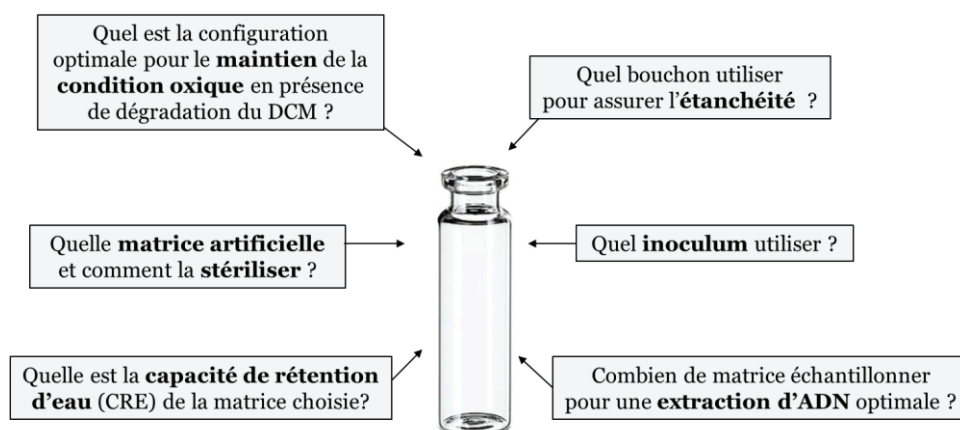


Figure IV.1. Aperçu synthétique des questionnements techniques pour la détermination de la configuration expérimentale de la prochaine expérience (sujet du **chapitre V**).

IV.2 Stabilité des conditions d'oxygénation

Au cours de la prochaine expérience, les microcosmes seront exposés à deux statuts oxiques : la condition oxique ($[O_2] \sim 8$ ppm) ou la condition anoxique ($[O_2] < 0.5$ ppm). Le nouveau système de microcosmes doit donc permettre l'établissement stable de ces conditions expérimentales, i.e. que la consommation de l'oxygène par les microorganismes ne conduise pas à une déplétion de l' O_2 disponible, et que les microcosmes soit assez hermétique pour maintenir les conditions anoxiques durant plusieurs semaines.

IV.2.1 Stabilité de la condition oxique et volume de matrice

Contrainte pas le format des vials compatibles avec le passeur du GC, la verrerie de plus grand volume utilisable pour cette expérience est de vials de 20mL (crimp vials 20mm clear glass 22.5 x 75.5 mm flat bottom - flat top, Interchim). Pour vérifier dans un premier temps que la condition oxique était conservée à l'intérieur des microcosmes de 20 mL scellés et en présence de microorganismes consommant de l'oxygène pour la dégradation du DCM, 2 proportions différentes de phase solide / phase gazeuse ont été testé.

Pour ce faire, nous avons préparé 3 types de microcosmes dans ces vials de 20 mL: (i) un control stérile ($n = 1$), composé d'une matrice de billes de verre de silice en quantité suffisante pour atteindre une hauteur correspondante à 10 mL de liquide, (ii) un essai ($n = 2$), contenant le même volume de billes inoculé avec la souche modèle *Hyphomicrobium* sp. GJ21 (5% (v/v) d'une culture à DO_{600} de 0.1 ou équivalent), et un essai ($n = 2$) contenant seulement 7 mL de billes. Du milieu liquide SGW est ajouté jusqu'à saturation de la matrice laissant respectivement 10 mL et 13 mL de phase gazeuse dans les constructions. 1 mM de DCM a été rajouté dans les échantillons à partir d'une solution stock à 100 mM de DCM dans du SGW. Après 4h d'incubation à 30°C pour permettre la partition du DCM dans des différentes phases, la concentration du DCM dans la phase gazeuse a été suivi par GC. La concentration d'oxygène

dans la phase gazeuse a été mesurée au cours de l'expérience à l'aide de pastilles senseurs d'oxygène placés près du col du vial, comme détaillé dans la **section II.4.2**.

La **Figure IV.2** montre que la concentration d'oxygène est constante et supérieure à 8 ppm dans tous les cas, qu'il y ait ou non dégradation microbienne du DCM. La consommation d'oxygène liée à l'activité microbienne impliquée dans la dégradation du polluant n'est donc pas détectable. De plus, la souche *Hyphomicrobium* sp. GJ21 a dégradé complètement le DCM après 7 jours quel que soit le volume utilisé de matrice (7 ou 10 mL). Ainsi, nous pouvons conclure que l'utilisation des fioles à 20 mL permet de travailler en conditions oxiques. Le développement méthodologique sera poursuivi avec un volume de matrice équivalent à 10 mL afin de maximiser la quantité de matrice utilisable pour la suite des expériences.

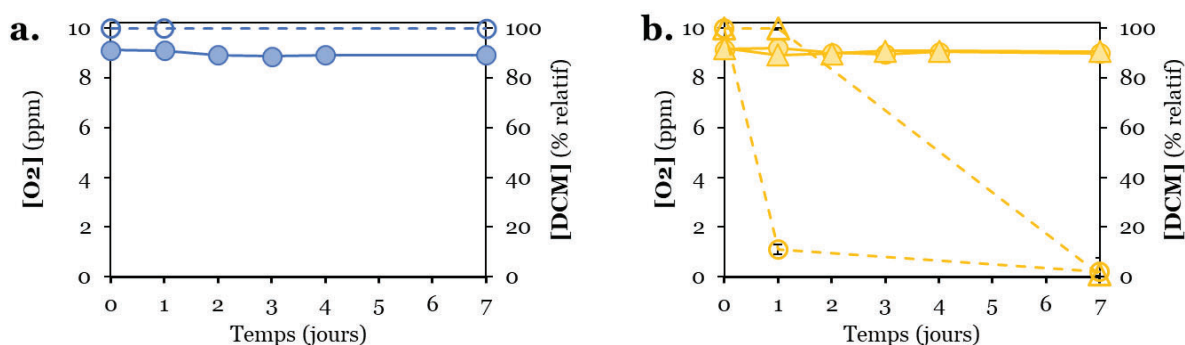


Figure IV.2. Stabilité de la condition oxique dans les vials de 20 mL. Concentration d'oxygène et de DCM au cours du temps **a.** en conditions stériles ou **b.** en présence de *Hyphomicrobium* sp. GJ21. Les lignes continues indiquent la concentration d'oxygène. Les lignes discontinues indiquent la concentration relative en DCM. La couleur bleue correspond aux résultats dans le contrôle stérile ($n = 1$), alors que la couleur jaune correspond aux résultats dans les contrôles positive ($n = 2$, les barres d'erreurs matérialise l'écart-type entre les réplicats). Les cercles correspondent aux fioles avec la matrice à un volume équivalent à 10 mL. Les triangles correspondent aux fioles avec la matrice à un volume équivalent à 7 mL.

IV.2.2 Stabilité de la condition anoxique

Avec les bouteilles sérum utilisées dans la **section III.2.1**, les microcosmes étaient fermés avec des bouchons en caoutchouc de butyle d'une épaisseur de 1 mm et sertis avec des bagues d'aluminium (**Figure IV.3-a.**). Or, la seringue très fine de la GC automatique ne peut pas traverser ce type de bouchons à cause de leur résistance. D'autre part, les bagues d'aluminium utilisées jusqu'ici ne sont pas utilisables avec le système d'échantillonnage automatique car elles ne sont pas magnétiques, ce qui est essentiel pour le prélèvement avec le passeur automatique. Par conséquent, nous avons cherché une nouvelle combinaison de bouchon et bagues de sertissage pour fermer les microcosmes en assurant l'étanchéité des fioles et le maintien des conditions d'anoxie au cours de l'expérience.

Nous avons choisi de tester le bouchon à sertir butyle/PTFE associé à une bague magnétique (**Figure IV.3-b.**) couramment utilisés pour les dosages au GC automatique à l'ITES et dont l'épaisseur est de 0.3 mm. Pour vérifier leur herméticité, des fioles ont été fermés avec le bouchon choisi avant d'induire la condition d'anoxie par remplacement de la phase gazeuse par du N_2/H_2 (cf. **section II.3.1**). La concentration d'oxygène a été suivie au cours du temps à l'aide de pastilles senseurs d'oxygène, comme expliquée à la **section II.4.2**. Que les bouchons restent 'natif' ou que l'on les ai percé plusieurs fois avec une seringue pour mimer le l'échantillonnage, l'anoxie a été rapidement perdue (**Figure IV.3-c.**). L'effet de l'ajout de silicone (de type SG2 Silicon, PreSens GmbH) sur les rebords des fioles, à l'aide d'un cure-dent stérile, a été testé pour son effet sur l'étanchéité. Nous avons observé que l'ajout de silicone est essentiel pour conserver l'étanchéité puisque c'est le seul montage testé conservant l'anoxie au cours du temps ($[O_2] < 0.5$ ppm), et ceux même après plusieurs piqûres à travers le septum (**Figure IV.3-c.**). Par conséquent, la suite des expériences seront réalisées en utilisant du silicone et des bouchons à sertir butyle/PTFE associé à leur bague magnétique.

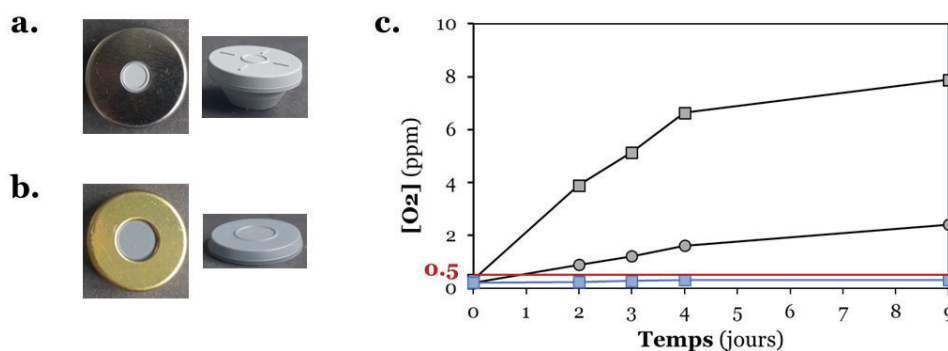


Figure IV.3. Test de maintien des conditions hermétiques en fonction du montage des microcosmes. **a.** Bouchons en caoutchouc butyle sertis avec des bagues d'aluminium utilisés pour l'expérience décrite au **chapitre III**. **b.** Bouchons à sertir butyle/PTFE avec bague magnétique utilisés pour l'expérience au **chapitre V**. **c.** Concentration d'oxygène au cours du temps pour un vial fermé avec un bouchon butyle/PTFE et sa bague magnétique (en gris, $n = 2$) ou avec ajout de silicone sur les rebords du vial avant mise en place du bouchon (en bleu, $n = 2$). Les carrés correspondent aux vials pour lesquels nous avons réalisé plusieurs injections au cours du temps, créant des perforations du bouchon. Les cercles correspondent à une fiole fermée qui n'a pas subi de piqûre d'injections. La ligne rouge à 0.5 ppm représente la limite à ne pas dépasser pour maintenir des conditions d'anoxiques.

IV.3 Sélection de l'inoculum

Dans les travaux décrits dans le **chapitre III**, la matrice et l'inoculum ne faisait qu'un, puisque nous utilisons du sable contenant des microorganismes DCM-dégradant issu d'un projet précédent. Cependant, afin d'inoculer la matrice artificielle de nos microcosmes, nous avons maintenant besoin d'utiliser un inoculum en phase liquide.

Pour ce faire, la capacité de dégrader le DCM de deux types de précultures dérivant de l'expérience sur les aquifères de laboratoire (Prieto-Espinoza et al., 2021) ont été testés pour

servir d'inoculum: (i) un mélange 1 : 1 (v/v) du milieu SGW liquide et la phase liquide des aquifères de laboratoire ; ou (ii) un mélange 1 : 1 (v/p) du milieu SGW liquide et la matrice de sable des aquifères de laboratoire. Nous avons préparé ces cultures dans de bouteilles sérum fermées avec de bouchons en caoutchouc de butyle sertis avec des bagues d'aluminium. En parallèle, un control positif a été préparé en inoculant *Hyphomicrobium* sp. GJ21 dans un mélange 1 : 1 (v/v) du milieu SGW liquide et H₂O ultrapure à l'équivalent de 5% (v/v) d'une culture à DO₆₀₀ de 0.1. L'activité de dégradation du DCM de chaque type de culture pouvant servir d'inoculum potentiel, ainsi que du control positive, a été testée dans des conditions oxygènes et anoxiques (établies comme indiqué à la **section II.3.1**). Pour cela, la concentration du solvant chloré a été suivie par GC au cours du temps après ajout de 1 mM de DCM à partir d'une solution stock de DCM à 100 mM (**Figure IV.4**). Le control positif a complètement dégradé le DCM après 2 et 5 jours dans les conditions oxygènes et anoxiques, respectivement. Cela montre que la souche *Hyphomicrobium* sp. GJ21 a été capable de dégrader ce composé quel que soit la condition d'oxygénation et n'est pas affectée par la dilution au demi du milieu de culture. Aucune dégradation du DCM n'est observé en 30 jours dans les cultures faites à partir de la phase liquide de l'aquifère de laboratoire, indépendamment de la condition d'oxygénation. En revanche, la culture faite à partir du sable a permis la dégradation complète du DCM après 7 jours dans les deux conditions d'oxygénation. En conclusion, les expériences suivantes auront comme inoculum le surnageant récolté d'une préculture faite avec la matrice sable des aquifères de laboratoire. Ainsi, un inoculum contenant une communauté bactérienne active et capable de dégrader le DCM sera utilisée pour toute la procédure expliquée et utilisée dans le **chapitre V**.

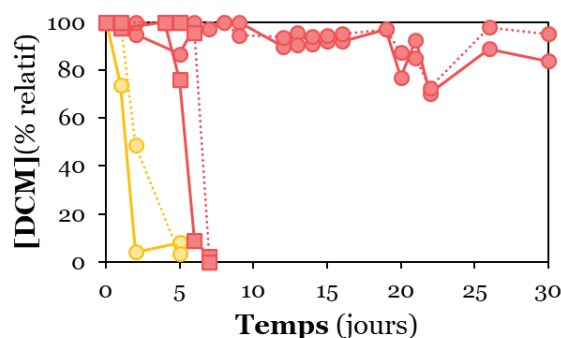


Figure IV.4. Dégradation microbienne du DCM en fonction de l'origine de l'inoculum environnemental. La couleur jaune correspond au microcosme inoculé avec la souche *Hyphomicrobium* sp. GJ21. La couleur rouge correspond aux microcosmes établis avec les échantillons environnementaux issus des aquifères de laboratoire. Les cercles correspondent aux microcosmes réalisés avec la phase liquide de l'aquifère. Les carrés correspondent aux microcosmes établis avec le sable de l'aquifère. La concentration en DCM des microcosmes en conditions oxygènes sont représentées par une ligne continue, et avec ligne discontinue pour ceux en conditions anoxiques.

IV.4 Sélection de la matrice artificielle

IV.4.1 Matrice de billes de verre sodo-calcique

Des billes de verre sodo-calcique lavées à l'acide (Sigma-Aldrich) calibrées aux diamètres 2 mm, 0.42-0.6 mm, et <0.106 mm ont été utilisées pour les premiers tests. Cette matrice a été testée pour savoir si (i) le contact de cette matrice lavée à l'acide induisait des changements de pH du milieu tamponné SGW, et si (ii) le DCM pouvait être dégradé par une communauté bactérienne active en présence de cette matrice.

IV.4.1.1 Maintien du pH

La matrice artificielle achetée étant lavée à l'acide, la stabilité du pH du milieu SGW a été vérifié. Nous avons observé que le pH de milieu SGW a augmenté après contact avec ce type de matrice (**Table IV.1**). La littérature indique que le verre sodo-calcique subit généralement une corrosion au contact de l'eau, ce qui entraîne une libération substantielle d'ions OH⁻ et une augmentation concomitante du pH du milieu (Düffer, 2009).

Table IV.1. pH du milieu SGW avant et après contact avec la matrice artificielle en verre sodo-calcique à différente taille de billes.

	Avant	Après
2 mm	7.95	8.85
0.42 – 0.6 mm		8.13
< 0.106 mm		9.13

Afin de neutraliser cet effet, des essais ont été réalisés en augmentant le pouvoir tampon du milieu SGW. Pour ce faire, nous avons modifié la composition du milieu SGW en ajustant les quantités des 2 composés constituant le tampon phosphate : NaH₂PO₄ et KH₂PO₄. Ainsi, trois milieux SGW 'modifiés' ont été préparés pour neutraliser théoriquement la concentration d'ions hydroxyle correspondant à pH11 (1.1 g/L de NaH₂PO₄ et 0.5 g/L de KH₂PO₄), pH12 (1.71 g/L de NaH₂PO₄ et 1.1 g/L de KH₂PO₄), et pH14 (2.56 g/L de NaH₂PO₄ et 1.9 g/L de KH₂PO₄). Les pH résultants des milieux SGW modifiés sont donc de 7.8, 7.34 et 7.14, respectivement. Nous appellerons par la suite ces milieux SGW11, SGW12 et SGW14. D'autre part, plusieurs lavages à l'eau des 3 types de matrices ont été effectués, jusqu'à ce que le pH de l'eau en contact et sans contact avec les matrices soit le même, avant de sécher les billes à 55°C. Ces matrices ont ensuite été mises en contact avec les 3 milieux SGW modifiés, ainsi qu'avec le milieu SGW classique, et le pH a été suivi au cours du temps (**Figure IV.5**). Au contact avec la matrice, le pH a augmenté, peu importe le pouvoir tampon du milieu. L'augmentation de pH la plus forte a été enregistrée pour la matrice composée par des billes de plus petit diamètre (<0.106 mm). Le milieu classique et le milieu SGW11 n'ont pas permis de conserver le pH en dessous de 8. En revanche, les milieux SGW12 et SGW14 ont neutralisé l'augmentation de pH dû à la matrice

de verre sodo-calcique et conservé le pH en dessous de 8, sauf pour SGW12 avec les plus petites billes. A partir de ces observations, nous avons décidé d'utiliser le milieu SGW14, permettant de maintenir le pH autour de 7.5 avec toutes les matrices après 27 jours.

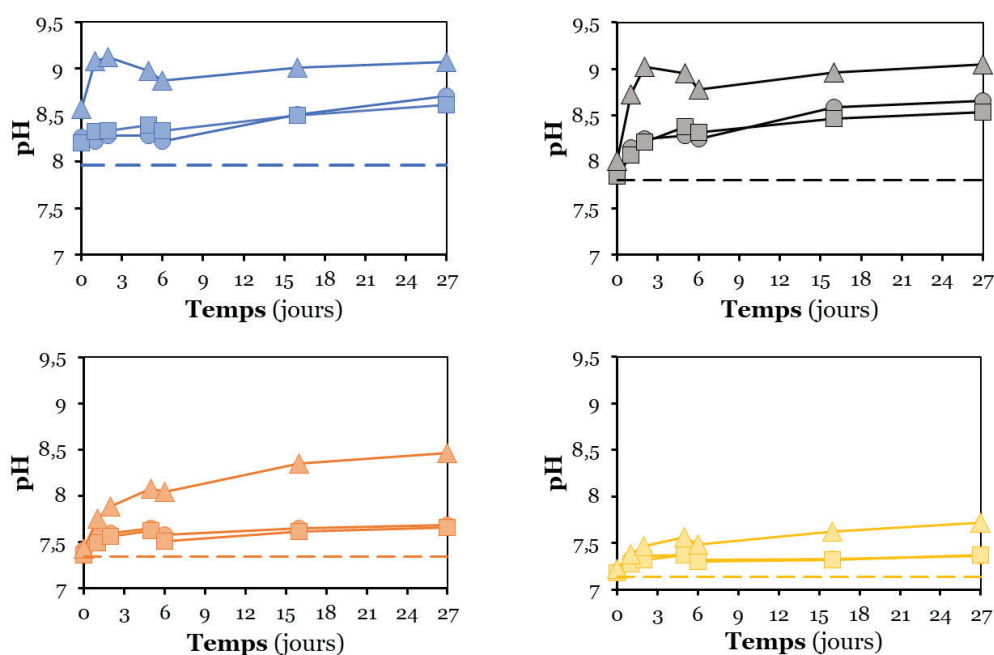


Figure IV.5. Maintien du pH au cours du temps dans les différents milieux SGW après contact avec la matrice artificielle de billes de verre sodo-calcique. La suivie du pH au cours du temps a été fait dans les milieux SGW classique (bleu), modifié pour neutraliser une concentration d'ions hydroxyle correspondant à pH 11 (en gris), à pH12 (en orange), et à pH14 (en jaune). Les formes correspondent à différentes tailles de billes : cercles pour les billes de 2 mm diamètre, carrés pour les billes de 0.42 à 0.6 mm de diamètre, et triangles pour les billes de <0.106 mm de diamètre. La ligne discontinue indique le pH de chaque milieu SGW sans ajout de bille de verre.

IV.4.1.2 Biodégradation du DCM en présence de la matrice artificielle

En utilisant le milieu SGW14, la capacité à dégrader le DCM des populations microbiennes présentes dans l'inoculum environnemental au contact de la matrice artificielle de billes de verre sodo-calcique a été testée.

Ainsi, des vials de 20 mL ont été préparés en les remplissant à moitié avec des billes de chaque diamètre stérilisées au four Pasteur (10 g de billes par vial pour les matrices de 2 mm et 0.42 à 0.6 mm de diamètre, et 8 g par vial pour la matrice de <0.106 mm de diamètre). Ensuite, les matrices ont été saturées avec trois types de phases liquides : (i) un mélange 1 : 1 (v/v) du milieu SGW14 et H₂O pour les contrôle négatives (n = 1 par taille de bille); (ii) un mélange 1 : 1 (v/v) du milieu SGW14 et H₂O inoculé à l'équivalent de 5% (v/v) d'une culture de *Hyphomicrobium* sp. GJ21 à DO₆₀₀ 0.1 pour les contrôles positives (n = 1 par taille de bille) ; (iii) un mélange 1 : 1 de milieu SGW14 et de la phase liquide d'une préculture faite avec la matrice de sable des aquifères de laboratoire pour les échantillons environnementaux (n = 1

par taille de bille). 1 mM de DCM a été rajouté dans tous les vials à partir d'une solution stock à 100 mM et la concentration de ce composé a été mesuré au cours du temps par GC. Le pH a été mesuré à partir d'aliquots prélevés directement de la phase liquide de chaque vial au début (jour 0) et à la fin de l'expérience (jour 10), ainsi qu'aux jours 4 et 7 dans les contrôles positifs et les échantillons environnementaux avec la matrice de billes de taille 2 mm et 0.42-0.6 mm.

Les résultats obtenus sont présentés dans la **Figure IV.6**. Aucune dégradation de DCM n'a été observée dans le control négatif, démontrant que la dégradation abiotique et l'adsorption sur les matériaux était négligeable, et que les fuites de DCM étaient minimales. Dans le cas des contrôles positifs et des échantillons environnementaux, la dégradation complète du DCM est observée en présence des matrices à 0.42 - 0.6 mm et 2 mm de diamètre, alors qu'aucune dégradation n'a été détectée avec la matrice de diamètre <0.106 mm. Ceci peut être un effet de l'augmentation du pH observée dans ce cas (pH environ 10), ce qui a certainement inhibé l'activité des populations dégradantes du DCM dans l'échantillon environnementale, mais aussi de la souche référente *Hyphomicrobium* sp. GJ21.

A la suite de l'échec de cette optimisation, nous avons changé de matrice artificielle.

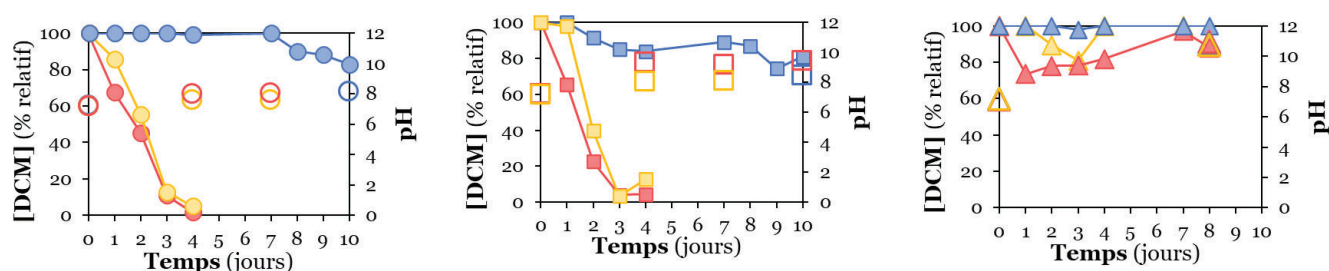


Figure IV.6. Dégradation du DCM au cours du temps en fonction de la granulométrie de la matrice de verre sodocalcique (cercles : 2 mm diamètre ; carrés : 0.42 - 0.6 mm diamètre ; triangles : <0.106 mm diamètre). La couleur bleue correspond au control négatif (n = 1 par taille de bille). La couleur jaune correspond au control positif (n = 1 par taille de bille). La couleur rouge correspond à l'échantillon environnementale (n = 1 par taille de bille). Les marques remplies indiquent la concentration de DCM, et les marques vides indiquent le pH.

IV.4.2 Matrice de billes en verre/zirconium

Comme alternative à la matrice de billes en verre sodocalcique, nous avons acquis des billes en verre/zirconium (Biospec Products) de diamètre 2 mm, 0.5 mm et 0.1 mm. Comme précédemment, nous avons testé (i) la stabilité du pH du milieu tamponné SGW au contact de la matrice ; et (ii) l'activité de biodégradation du DCM en présence de cette matrice.

IV.4.2.1 Maintien du pH

Dans ce cas, l'effet de la matrice de billes en verre/zirconium sur le pH du milieu SGW classique (non modifié) a été testé. En plus, nous avons étudié la stabilité de la matrice en fonction du traitement de stérilisation.

Pour ce faire, nous avons étudié l'impact de deux types de traitement : (i) l'autoclave, qui consiste à la stérilisation du matériel à la chaleur humide (21 min à 120°C), et qui été suivi par un séchage de la matrice à 55°C ; et (ii) le four Pasteur, qui consiste à la stérilisation du matériel à la chaleur sèche (1 h 30 min à 180°C). Les billes en verre/zirconium de différentes tailles stérilisées ont été mises en contact avec du milieu SGW classique. Le pH a été suivi au cours du temps par mesure avec une microsonde directement dans le tube. Indépendamment du traitement de stérilisation, le pH du milieu SGW classique est resté stable autour de 8 points pendant 30 jours quel que soit la granulométrie de matrice (**Figure IV.7**).

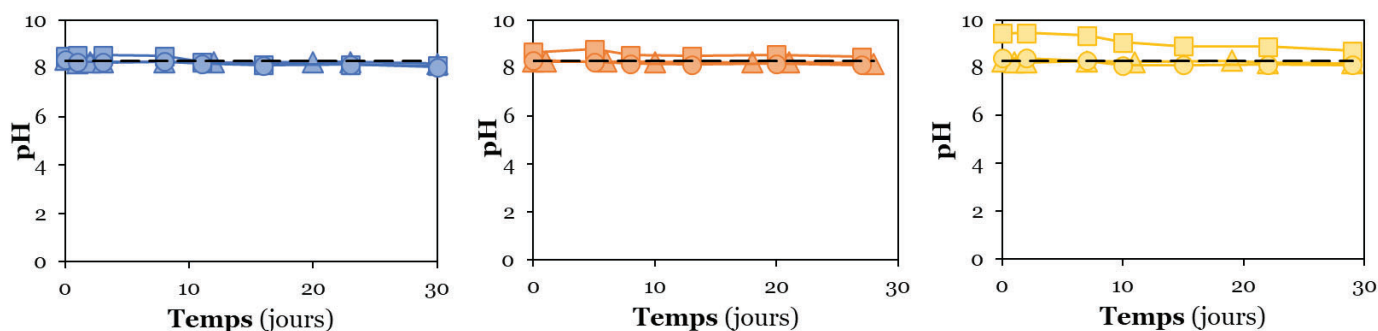


Figure IV.7. Maintien du pH au cours du temps dans les milieux SGW après contact avec la matrice artificielle de billes de verre/zirconium à différente granulométrie (cercles : 2 mm diamètre ; carrés : 0.5 mm diamètre ; triangles : 0.1 mm diamètre). Les couleurs correspondent au traitement de stérilisation (bleu : sans stérilisation ; orange : stérilisée à l'autoclave ; jaune : stérilisée au four paster). La ligne discontinue indique le pH du milieu sans matrice.

IV.4.2.2. Biodégradation du DCM en présence de la matrice artificielle

Finalement, il a fallu tester si la dégradation du DCM par la communauté bactérienne présente dans l'inoculum environnemental était maintenue en présence de cette matrice.

Pour ce faire, nous avons rempli des nouveaux vials de 20 mL avec un volume de billes équivalent à 10 mL, correspondant à 15 g de billes par vial pour chaque granulométrie. Ensuite, les matrices ont été saturées comme précédemment, (i) avec le milieu SGW pour les contrôles négatifs ($n = 1$ par taille de bille) ; et (ii) avec la phase liquide d'une préculture faite avec la matrice de sable des aquifères de laboratoire pour les échantillons environnementaux ($n = 2$ par taille de bille). 1 mM de DCM a été rajouté dans tous les vials à partir d'une solution stock à 100 mM de DCM dans du SGW et la concentration de ce composé a été mesurée au cours du temps par GC. Dans le cas des vials avec les billes à 0.5 mm et 2 mm de diamètre, un second dopage de DCM a été réalisé, en ajoutant à nouveau 1 mM de ce composé après qu'il a été totalement dégradé dans le système. D'autre part, nous avons aussi mesuré le pH dans tous les vials au début, entre chaque pulse, et à la fin de l'expérience.

Sur la **Figure IV.8**, les témoins négatifs indiquent le niveau sous lequel la dissipation du DCM observée est considérée comme de la biodégradation. Dans le cas des échantillons environnementaux, le DCM a été complètement dégradé en présence de toutes les matrices. De plus, le pH a été maintenu de façon stable aux environs de 8 durant toute l'expérience et dans tous les vials. Les matrices de billes en verre/zirconium semblent être un matériel inerte qui ne change ni le pH du milieu, ni n'inhibe la dégradation microbienne du DCM.

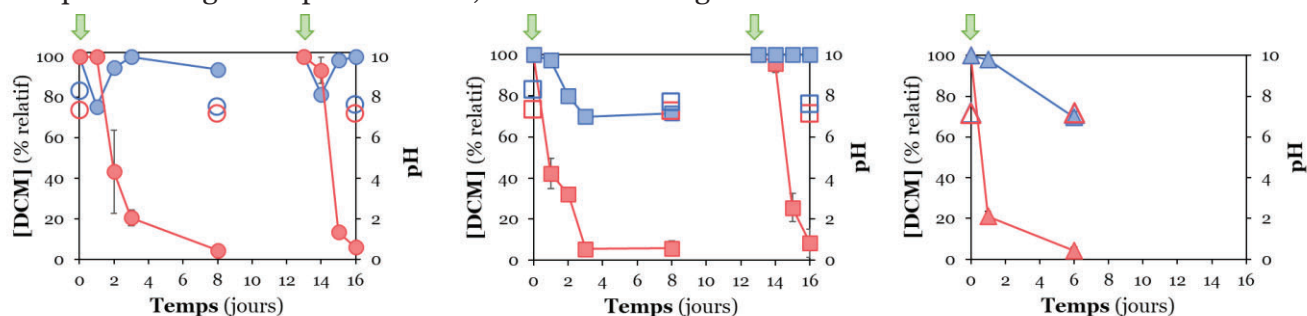


Figure IV.8 Dégradation du DCM au cours du temps en fonction de la granulométrie de la matrice artificielle de verre/zirconium (cercles : 2 mm de diamètre ; carrés : 0.5 mm de diamètre ; triangles : 0.1 mm diamètre). La couleur bleue correspond au control négatif (n = 1 par taille de bille). La couleur rouge correspond à l'échantillon environnemental (n = 2 par taille de bille). Les marques remplies indiquent la concentration de DCM, et les marques vides indiquent le pH. La flèche verte indique l'addition du DCM dans les vials.

IV.5 Détermination de la capacité de rétention d'eau des matrices artificielles en fonction de leur diamètre

La capacité de rétention d'eau (CRE) est une valeur caractéristique d'une matrice qui définit son état hydrique et qui correspond à la quantité d'eau qu'un substrat peut retenir dans et par ses pores contre la force de la gravité. Plus les grains sont de petites tailles, plus la somme des surfaces est grande et plus la force de capillarité pour retenir l'eau est importante. Pour la matrice artificielle sélectionnée pour les expériences suivantes, il nous faut déterminer empiriquement le volume de liquide correspondant la CRE pour chaque taille de bille. Cette information permettra de déterminer le volume de phase liquide à rajouter à chaque matrice pour atteindre la saturation en eau de la matrice, la CRE, et la moitié de la CRE. Pour déterminer la CRE des matrices en fonction de la granulométrie, nous avons utilisé une méthode qui consiste à faire passer un volume connu d'eau à travers une masse déterminée de matrice et à récupérer l'eau traversant cette matrice. Cette méthode est résumée de façon graphique par la **Figure IV.9**. Nous avons mis un filtre en papier, préalablement saturé en eau, dans un entonnoir et nous l'avons rempli avec 150 g de chaque matrice étudiée. Ensuite, l'entonnoir a été placé sur une éprouvette et 100 mL d'eau ont été versés sur la matrice. Après 5-10 minutes, nous avons mesuré le volume d'eau qui a traversé la matrice. La CRE a été ensuite calculée en divisant le volume qui a été retenu par la matrice, calculé en faisant la

soustraction entre le volume rajouté à la matrice et le volume récupéré, par la masse de la matrice utilisée. La valeur de la CRE est donc exprimée ici en mL par g. Nous avons réalisé l'expérience deux fois et nous avons calculé la moyenne pour déterminer la valeur de la CRE de chaque matrice.

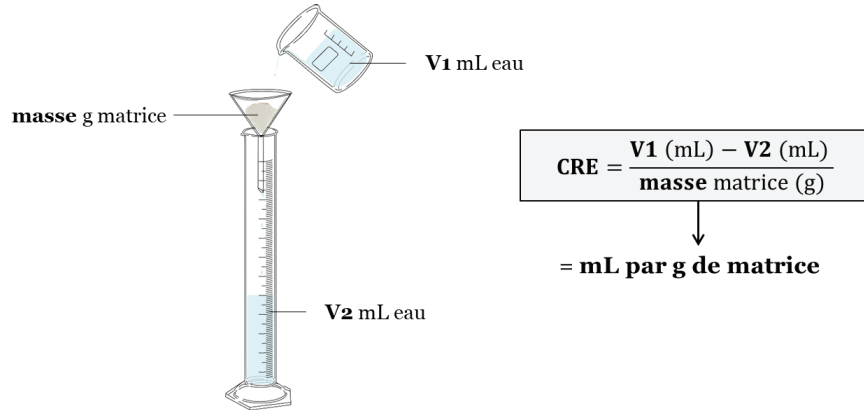


Figure IV.9. Détermination de la capacité de rétention d'eau (CRE) de chaque matrice artificielle.

Quant au volume nécessaire pour saturer la matrice, il a été déterminé visuellement en ajoutant d'eau jusqu'à observer la saturation de la matrice. Dans le cas de la matrice de billes à 0.1 mm de diamètre, la CRE n'est expérimentalement pas distinguable de la saturation de la matrice. Par conséquent, nous avons décidé que pour cette taille de billes, nous travaillerons avec seulement deux contenus en eau : saturation de la matrice et la moitié du volume de la CRE. La **Table IV.2-a.** récapitule la CRE de chaque matrice, et la **Table IV.2-b.** résume les volumes à rajouter dans 15 g de matrice pour arriver aux contenus d'eau d'intérêt en fonction de la taille des billes.

Table IV.2. Récapitulatif des CRE et volumes à rajouter en fonction de la granulométrie de la matrice artificielle. Volumes de liquide correspondant à **a.** la capacité de rétention d'eau (CRE) de chaque matrice ; et **b.** ce qu'il faut ajouter à 15 g de matrice pour atteindre le contenu d'eau d'intérêt en fonction de la taille des grains de la matrice artificielle.

a.

	mL par 100 g
2 mm	16.99
0.5 mm	15.3
0.1 mm	4.3

b.

	2 mm	0.5 mm	0.1 mm
Saturation	2.6 mL	2.6 mL	2.6 mL
CRE	0.6 mL	2.25 mL	
½ CRE	0.3 mL	1.125 mL	1.25 mL

IV.6 Optimisation de la quantité de matrice artificielle à utiliser pour l'extraction d'ADN

Afin d'étudier la communauté microbienne établie dans les différentes conditions expérimentales, des extractions d'ADN d'une portion de matrice seront réalisées à de moments spécifiques de l'expérience. Ainsi, il est nécessaire d'optimiser la quantité de matrice à prélever pour permettre d'obtenir assez d'ADN pour l'analyse par metabarcoding, tout en minimisant la masse de billes récoltées.

Pour l'extraction d'ADN, le kit « DNeasy PowerWater » (Qiagen) a été utilisé comme expliqué en détails dans la **section II.5.1.1** sur 0.5 g, 1.0 g et 1.5 g de matrice. Pour ce faire, des vials contenant chacun 15 g de matrice artificielle pour chaque granulométrie ont été préparés et saturés avec du milieu liquide SGW inoculé à 5% (v/v) avec *Hyphomicrobium* sp. GJ21 à partir d'une culture à $DO_{600} = 0.1$ (ou équivalent). La source de carbone et d'énergie, 1 mM de DCM, a été rajoutée et sa dégradation suivie. Quand le DCM a été totalement dégradé, les différentes matrices ont été échantillonnées aux quantités d'intérêt et soumis à une extraction d'ADN. Les acides nucléiques obtenus ont été quantifiés par le kit « Qubit® dsDNA HS Assay », comme décrit à la **section II.5.1.2**.

Plus la granulométrie de la matrice est élevée, moins la concentration moyenne d'ADN obtenu est élevée (**Figure IV.10**). De plus, l'augmentation de la masse de billes utilisée pour l'extraction permet d'obtenir plus d'ADN, sauf avec la matrice de billes de 0.1 mm de diamètre, qui permet de récolter le maximum d'ADN à partir de 1.0 g de matrice plutôt que de 1.5 g. Ayant besoin de 50 ng d'ADN dans minimum 10 μ L pour le séquençage, et pour minimiser les prélèvements dans des microcosmes de tailles réduite, nous avons décidé d'utiliser 1.0 g de matrice artificielle pour la suite des expériences.

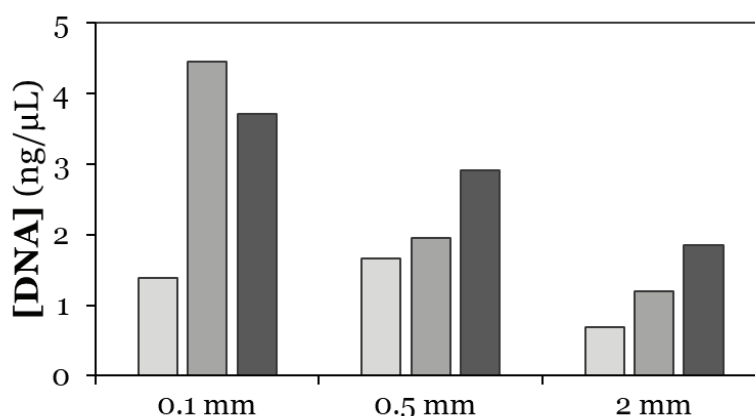


Figure IV.10. Concentration d'ADN (ng/ μ L) extraite pour chaque taille de billes en fonction de la masse de billes échantillonnées. La couleur la plus claire correspond à l'échantillonnage de 0.5 g de matrice. La couleur moyenne correspond à l'échantillonnage de 1.0 g de matrice. La couleur foncée correspond à l'échantillonnage de 1.5 g de matrice.

IV.6 Limites de détection (LOD) et quantification (LOQ)

Les limites de détection (LOD ; concentration minimale détectable) et de quantification (LOQ ; concentration minimale quantifiable avec précision) ont été déterminées dans les différentes conditions expérimentales pour l'équipement nouvellement utilisé pour la quantification du DCM (GC-FID-MS ; Thermo Fisher Scientific). En particulier, les LOD et LOQ ont été calculées en fonction de la taille des grains (2, 0.5 et 0.1 mm) et du contenu en eau de la matrice (saturation en eau, CRE et 1/2 CRE). Comme la concentration d'oxygène n'avait pas d'impact sur le calcul de la LOD ni de la LOQ (résultats non présentés), l'analyse a été réalisée en oxie.

Pour le calcul des LOD et LOQ, des courbes d'étalonnage ont été préparées dans des vials de 20 mL remplies avec 15 g de matrice artificielle de chaque granulométrie (2, 0.5 et 0.1 mm). Chaque courbe d'étalonnage a été préparée avec les concentrations suivantes de DCM : 0 mM - 0.0005 mM - 0.005 mM - 0.05 mM - 0.1 mM - 0.3 mM - 0.5 mM - 1 mM - 1.5 mM. Pour atteindre ces concentrations, le DCM a été rajouté à partir d'une solution stock à 20 mM de DCM dans du SGW. Pour calculer le volume (V) à ajouter par vial à partir de la solution stock, l'équation suivante a été utilisée :

$$V_{\text{DCM}} = \frac{V_{\text{final vial}} \times [\text{DCM}] \text{ courbe étalonnage}}{[\text{DCM}] \text{ solution stock}}$$

où « $V_{\text{final vial}}$ » correspond au volume final de la phase liquide dans la matrice pour chaque contenu en eau (saturation, CRE et 1/2 CRE ; l'information de ces volumes en fonction de la taille des billes est à la **Table IV.2-a.**), « $[\text{DCM}]$ courbe étalonnage » correspond à la concentration d'intérêt dans la courbe d'étalonnage, et « $[\text{DCM}]$ solution stock » correspond à la concentration de DCM dans la solution stock (dans notre cas, 20 mM). Le DCM est ajouté au vial prérempli de leur matrice stérile et de SGW. Le volume de SGW dans chaque vial a été calculé tel que :

$$V_{\text{SGW}} = V_{\text{final vial}} - V_{\text{DCM}}$$

où le « $V_{\text{final vial}}$ » correspond au volume d'intérêt final pour atteindre soit la saturation, soit la CRE ou la 1/2 CRE, et « V_{DCM} » correspond au résultat de l'équation précédente. Les vials ont été fermés avec des bouchons à sertir butyle/PTFE associé à leur bague magnétique après ajout de la silicone dans le rebord des vials. La concentration de DCM a été mesurée directement à travers le septum des vials après 3 heures pour permettre la partition de ce composé dans le système triphasique. Chaque point de la courbe d'étalonnage a été mesuré 3 fois, sauf le point à 0 mM DCM qui a été mesuré 5 fois. Les équations utilisées pour le calcul de la LOD (**a.**) et de la LOQ (**b.**) dans chaque condition expérimentale sont à la page suivante :

a.
$$\text{LOD} = 3.3 \times \frac{\sigma}{S}$$

b.
$$\text{LOQ} = 10 \times \frac{\sigma}{S}$$

où σ correspond à l'écart-type du bruit de fond et S correspond à la pente de la courbe d'étalonnage. L'écart-type du bruit de fond a été calculé à partir de 5 mesures des vials à 0 mM de DCM.

Comme montré dans la **Figure IV.11**, en fonction de la taille de grains et du contenu en eau dans la matrice artificielle, la courbe d'étalonnage et les valeurs de LOD et LOQ changent. Cela semble indiquer une partition différente du DCM dans le système en fonction du volume de phase liquide dans les vials, ceci étant fonction de la taille de billes utilisée. D'autre part, les coefficients R^2 élevés établissent la linéarité de l'air de pic en fonction de la concentration, excepté au-delà de 1 mM de DCM en présence des billes à 0.1 mm de diamètre. Cela indique qu'il ne sera pas possible d'estimer de façon précise les concentrations au-delà de 1 mM, concentration maximale utilisée dans les expériences subséquentes. Concernant les LOQ et LOD, dans la plupart des cas, la LOQ est proche à 1 mM DCM, alors que la LOD reste plus basse. Ces observations suggèrent que cette méthode permet une détection satisfaisante du DCM pour l'étude de nos questions biologiques, mais que la précision de la quantification de ce composé est limitée aux concentrations plus élevées. Face à cet enjeu, nous ajouterons dans l'expérience suivante des « vials étalons » avec des concentrations connues (0 mM et 1 mM) de DCM qui seront utilisés pour normaliser, pour chaque série de mesures au GC, la concentration de DCM présente dans les échantillons. Ces « vials étalon » seront préparés pour chaque combinaison de paramètres expérimentales (taille de billes, contenu en eau et concentration d'oxygène) et suivront le même parcours expérimental que le reste des vials.

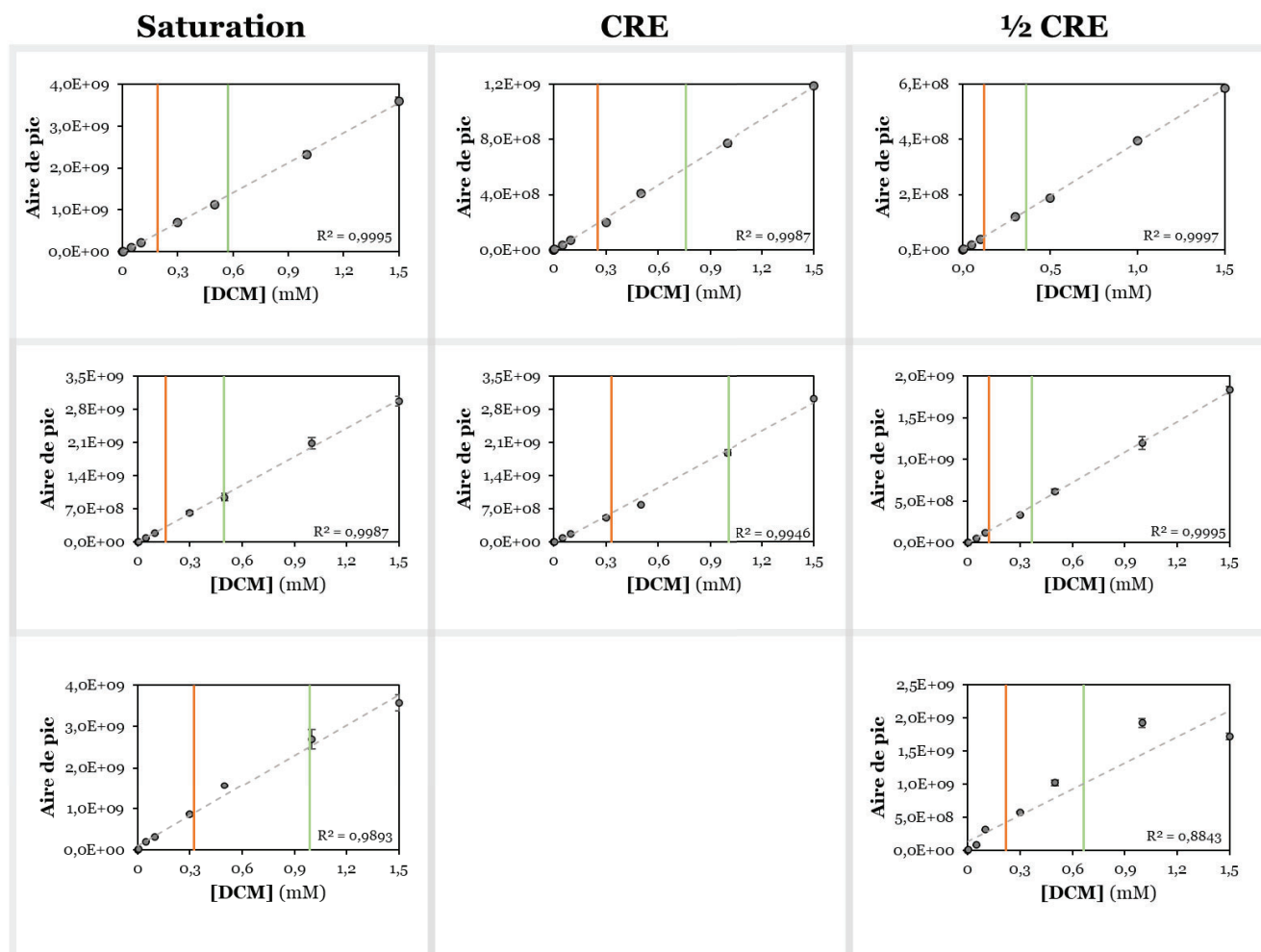


Figure IV.11. Courbes d'étalonnage déterminant les limites de détection (LOD) et quantification (LOQ) par condition expérimentale (taille de billes et contenu en eau). 9 concentrations de DCM ont été utilisées : 0 mM - 0.0005 mM - 0.005 mM - 0.05 mM - 0.1 mM - 0.3 mM - 0.5 mM - 1 mM - 1.5 mM. L'axe des abscisses correspond aux concentrations de DCM et l'axe des ordonnées correspond à l'aire de pic détectée par la GC. Chaque point correspond à la moyenne de 3 mesures consécutives reportée avec son écart type. La ligne discontinue correspond à la courbe de tendance dont le coefficient de détermination R^2 est reporté au bas de chaque graphique. Les lignes orange et verte correspondent à les LOD et LOQ de chaque condition, respectivement.

IV.7. Résumée des paramètres choisis

L'ensemble de ces étapes d'optimisation ont servi à perfectionner les microcosmes utilisés dans les chapitres précédents en proposant une nouvelle configuration expérimentale. Celle-ci est plus adéquate pour étudier l'impact des paramètres physicochimiques d'intérêt (contenue en eau, conditions d'oxygénation, et la taille de bille de la matrice) sur l'activité et la composition d'une communauté microbienne dégradante du DCM, puisqu'elle permet notamment d'augmenter sensiblement le nombre de réplicas. La **Figure IV.12** résume ces choix, et décrit la configuration expérimentale qui sera utilisée dans le **chapitre V**.

En résumé, nous avons vérifié que la condition oxique ($[O_2] \sim 8$ ppm) est maintenue au cours du temps dans les vials de 20 mL que nous utiliserons pour travailler avec la GC automatique. Concernant le maintien de la condition anoxique ($[O_2] < 0.5$ ppm), il faudra rajouter de la colle de silicone sur le rebord supérieur des vials avant de les fermer avec les bouchons en butyle/PTFE pour assurer l'étanchéité du système. D'autre part, nous avons choisi de travailler avec une matrice artificielle de billes de verre/zirconium pour éviter l'augmentation du pH induite par les billes de verre sodocalcique, et nous avons calculé les volumes correspondants aux trois contenus en eau d'intérêt (saturation en eau, CRE et $\frac{1}{2}$ CRE) en fonction de la taille de bille de la matrice artificielle. Comme inoculum environnemental, nous utiliserons la phase liquide issue d'une préculture faite avec le sable des aquifères de laboratoire dans le milieu liquide SGW. Finalement, pour obtenir assez d'ADN à envoyer à séquencer tout en minimisant la quantité de matrice échantillonnée, nous avons prévu de travailler à partir de 1.0 g de matrice.

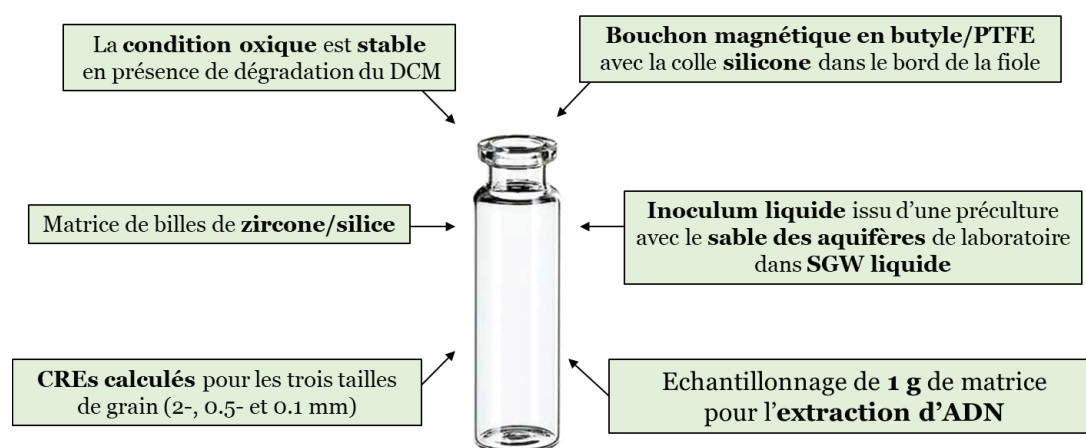


Figure IV.12. Réponses apportées aux questionnements initialement posés suite aux développements méthodologiques présentés dans ce chapitre.

Chapter V

Impact of matrix granulometry on
the response of a DCM-degrading
microbial community
to water content and oxygen status

V.1 Introduction

Groundwater level fluctuations (GLF) are a common environmental disturbance in aquifers, involving changes in the water table caused by external factors. These fluctuations create a transient zone between the continuously saturated and unsaturated area, known as fluctuating zone, characterized by temporal variations in the water saturation, redox conditions (e.g., O₂ concentration), and other parameters, such as nutrient and organic carbon contents (Haberer et al., 2012). The extent of these changes in this fluctuating zone is largely determined by the sediment granulometry, as it governs the water holding capacity (WHC) of the matrix. WHC refers to the amount of water retained by the matrix against gravity when the water table level drops (drainage period). Finer grain sizes result in higher water retention, which in turns lead to a reduced gas diffusion through the matrix. Conversely, larger grains result in lower water retention, allowing for better gas diffusion. These physicochemical changes are expected to impact the microbial community's composition and their metabolic functions. Thus, GLF exerts a selective pressure on the microbial populations, favouring the microorganisms with metabolic plasticity and redox tolerance mechanisms, which become dominant in the fluctuating zone (Wei et al., 2024).

In the context of DCM-polluted aquifers, a previous experiment using laboratory-scale aquifers demonstrated that water level fluctuations enhanced DCM biodegradation and changed the composition of a native microbial community from a multi-contaminated aquifer (Prieto-Espinoza et al., 2021). Following this initial work, we investigated in **chapter III** the individual impact of two key parameters affected during the water level fluctuations (i.e., matrix moisture and oxygen status) on DCM-degrading microbial populations. Our results showed that water content mainly influenced the time necessary for the DCM degradation function to effectively occurs, while oxygen status impacted both the DCM-degrading function and microbial community composition. However, due to technical limitations, we were unable to perform statistical analyses to confirm our observations or explore the combined effect of these two parameters, which would provide a better understanding of the processes occurring during GLF *in situ*.

In this chapter, we investigated the combined impact of water content and oxygen status on a DCM-degrading community using improved experimental settings. Additionally, given the importance of matrix granulometry during GLF *in situ*, we explored the role of this parameter. So the primary goal of the study presented in the current chapter was to investigate the impact of these three key parameters (water content, oxygen status and matrix granulometry) on both the DCM biodegradation kinetics and on the microbial community composition. Moreover, taking advantage of the experimental setting, we assessed the response of the microbial community to changes in oxygen status, and whether this response varied under different experimental conditions. Laboratory microcosms were set up with (i) three different matrices mimicking soil sediments: sand-like (beads of \varnothing 2 mm), silt-like (beads of \varnothing 0.5 mm), and clay-like (beads of \varnothing 0.1 mm), or without matrix; (ii) three different water contents representing the

three aquifer regions: water saturation for the saturated zone, WHC for the fluctuating zone when water table drops, and $\frac{1}{2}$ WHC for the unsaturated zone; and (iii) two different oxygen status: oxic ($[O_2] \sim 8$ ppm), and anoxic ($[O_2] < 0.05$ ppm) conditions. DCM was added over time through several pulses and its degradation kinetics was daily monitored via GC. To study the microbial community's response to a disturbance in oxygen status, oxygen status was shifted after 4 DCM pulses in half of the microcosms, while maintaining the others in their initial condition. The microbial communities established under the different experimental conditions, disturbed and undisturbed microcosms, were evaluated for their DCM biodegradation potential using the biomarker genes for DCM degradation under oxic and anoxic conditions (*dcmA* and *mecE-F* genes, respectively). Finally, the microbial community composition was assessed through 16S rRNA gene amplicon sequencing analysis at the beginning, before the disturbance, and at the end of the experiment.

V.2 Materials and Methods

V.2.1 Set up of laboratory microcosms

The influence of water content, oxygen status and matrix granulometry on the activity and composition of a DCM-degrading microbial community was studied in 160 laboratory microcosms established in 20 mL sterile glass vials. Each microcosm was filled with either 15 g of a sterile artificial matrix, consisting of zirconium/silica beads with diameters of 2 mm ($n=52$), 0.5 mm ($n=52$) or 0.1 mm ($n=36$), or left without any matrix ($n=20$). A liquid environmental inoculum derived from the laboratory-scale aquifers (Prieto-Espinoza et al., 2021) was then added to each microcosm. The rationale for using this type of inoculum on the artificial matrix was explained in **section IV.3**, and the procedure to prepare it was detailed in **section II.3.2**. Briefly, 18 precultures were established in 160 mL serum bottles by mixing, per culture, 40 g of sand derived from the laboratory-scale aquifers and 50 mL of SGW liquid medium. Half of the precultures ($n=9$) were set under oxic conditions and the other half ($n=9$) in anoxic conditions, and 1 mM of DCM was added to each preculture from a DCM stock solution at 100 mM. After complete DCM degradation, the supernatants of the precultures were collected and pooled for further use as the environmental inoculum in this experiment, as validated in **section IV.3**.

Four types of microcosms were established depending on the treatment of this liquid inoculum: in abiotic controls, the inoculum was sterilized by two consecutive filtration steps using a 0.2 μ m membrane (Minisart, Thermo Fisher Scientific); in biotic controls the filtered-sterilized inoculum was inoculated with the model strain *Hyphomicrobium* sp. GJ21 at an equivalent of 5% v/v from a preculture in SGW liquid medium with an OD_{600} of 0.1; in the no-DCM controls and environmental samples the inoculum was used without any treatment (**Figure V.1**). In the abiotic and biotic controls, as well as in the environmental samples, the liquid inoculum was diluted at 1:1 (v/v) with a 2 mM DCM stock solution in SGW medium to

achieve the desired water content, resulting in 1 mM of DCM within each microcosm. In the no-DCM controls, the liquid inoculum was diluted with pure SGW liquid media until reaching the desired water content (see **Table V.1** for details on the final volume per water content and matrix granulometry). In microcosms without any matrix, the total volume was consistently set at 10 mL, comprising 5 mL of liquid inoculum. Finally, the microcosms were sealed with 20 mm magnetic butyl-PTFE crimp caps, with silicon applied on the rims of the vials (optimized in **section IV.2.2**), and they were set under either oxic ($[O_2] \geq 8$ ppm, hereafter referred to as O) or anoxic ($[O_2] < 0.5$ ppm, hereafter referred to as A) conditions. All microcosms were equipped with an oxygen sensor. A summary of all the laboratory microcosms that were set up during the experiment is given in **Table V.1**.

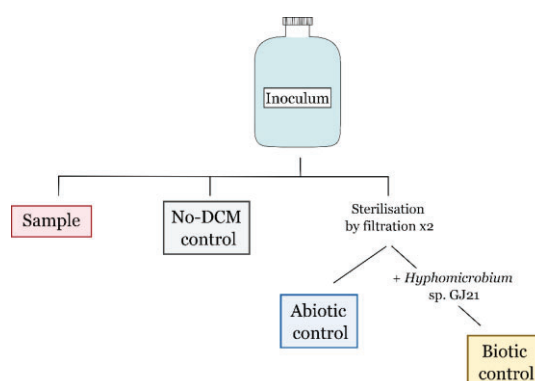


Figure V.1. Preparation of the initial inoculum according to the type of microcosm. The abiotic and biotic controls were prepared using the liquid environmental inoculum sterilised by double filtration, followed by the addition of the strain *Hyphomicrobium* sp. GJ21 in the case of the biotic controls. The environmental samples and no-DCM controls were prepared with the environmental inoculum as it was.

Table V.1. Summary of microcosms' set up according to the initial experimental conditions (n=160). The final volume in each microcosm is indicated for each matrix granulometry and water content on the left of the table. The numbers in each cell correspond to the number of replicates per condition. '-' indicates that no microcosm was established with that particular experimental set up. WHC stands for water holding capacity.

			Abiotic control				Biotic control			No-DCM control			Environmental sample			
			Saturation	WHC	½ WHC		Saturation	WHC	½ WHC	Saturation	WHC	½ WHC	Saturation	WHC	½ WHC	
	2 mm	Saturation= 2.6 mL WHC= 0.6 mL ½ WHC= 0.3 mL	Oxic	2	2	2	2	2	2	2	2	2	4	4	4	
		Anoxic	2	2	2	2	2	2	2	2	2	2	4	4	4	
	0.5 mm	Saturation= 2.6 mL WHC= 2.25 mL ½ WHC= 1.125 mL	Oxic	2	2	2	2	2	2	2	2	2	4	4	4	
		Anoxic	2	2	2	2	2	2	2	2	2	2	4	4	4	
	0.1 mm	Saturation= 2.6 mL ½ WHC= 1.25 mL	Oxic	2	2	-	2	2	-	2	2	-	2	4	-	4
		Anoxic	2	2	2	-	2	2	-	2	2	-	2	4	-	4
no matrix		Saturation= 10 mL	Oxic	2	2	-	-	2	-	-	2	-	-	4	-	-
			Anoxic	2	2	2	-	-	2	-	-	2	-	-	4	-

V.2.2 Experimental design

After setting up the laboratory microcosms, the experiment began directly with the addition of DCM and the sealing of the vials. Subsequent addition of DCM in each microcosm was done using DCM stock solutions at different concentrations depending on the grain size (150 mM for 2 mm and 0.5 mm; 62.5 mM for 0.1 mm; and 250 mM for vials without matrix). The use of different stock solutions aimed to minimize the liquid volume added to the system over time, thereby maintaining as much as possible the initial water content.

A total of four consecutive DCM pulses were performed, each pulse occurring after the complete degradation of DCM in the majority of the biotic controls and environmental samples. At the end of each pulse and before the addition of DCM, the gas phase in the microcosms was renewed by opening them in a chemical hood under sterile conditions for 1-2 days to allow its equilibration with the atmosphere. After the 4th DCM pulse, the oxygen status was changed from oxic to anoxic conditions (OA) and vice versa (AO) in half of the microcosms, while the other half remained in their initial conditions (OO or AA). Finally, three more consecutive DCM pulses were performed before the end of the experiment. Throughout the experiment, the microcosms were kept at 25°C in a temperature-controlled room. DNA was extracted from 1 g of the artificial matrix (or 1 mL of liquid phase for microcosms without matrix and the initial liquid inocula) at three different time points: at the beginning (T₀), before the change in the oxygen status (T_{bef}), and at the end of the experience (T_{end}). Experimental design is summarised in **Figure V.2**.

Due to the limited space in the rack of the automated GC, which could accommodate a maximum of 60 vials, the 160 microcosms and the calibration points (0 and 1 mM of DCM per grain size and water content; discussed in **section IV.6**) were monitored by separate batches. The experiment was divided into three series separated by a time interval to allow other users to pass their samples: (i) microcosms with 2 mm grain size matrix (n=52) + calibration points (n=6) from January 2023 to March 2023, (ii) microcosms with 0.5 mm grain size matrix (n=52) + calibration points (n=6) from September 2023 to November 2023, and (iii) microcosms with 0.1 mm grain size matrix (n=36) and no matrix (n=20) + calibration points (n=6) from January 2024 to March 2024.

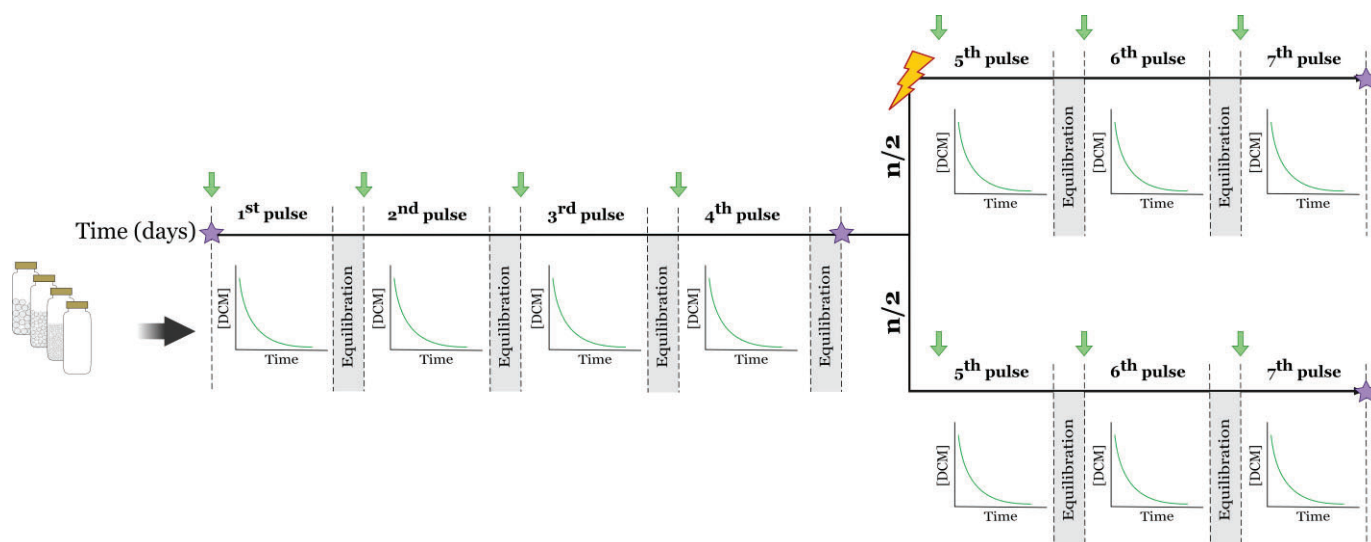


Figure V.2. Experimental design. 1 mM of DCM was added to the microcosms per pulse (indicated by green arrows). During each pulse, DCM concentration was daily monitored by gas chromatography. After 4 DCM pulses, the oxygen status was changed in half of the microcosms. The experiment finished after 3 further DCM pulses. DNA extraction was performed at the beginning (To), before the change in the oxygen status (T-bef), and at the end of the experiment (T-aft), and is indicated by the purple star. The lightning represents the disturbance (change of oxygen status).

V.2.3 Monitoring of DCM concentrations

DCM concentration was measured from 200 μL of the microcosms' headspace, which was automatically sampled by the GC-FID-MS (Thermo Fisher Scientific), as described in **section II.4.1.2**. An initial measurement of DCM was made 3 hours after the addition of DCM (To), based on empirically observations indicating that this time is sufficient for DCM to reach gas-aqueous phase equilibrium. Periodic measurements were then taken over time. Two sterile calibration points in SGW liquid media (0 and 1 mM of DCM) for each water content and granulometry were also included in the measurement series. These points were used to normalize the DCM concentration at each time point and to control for machine drift, as explained in the **section II.4.1.2**. Values greater than the 1 mM calibration point were set to 1 mM.

V.2.3.1 Data treatment

The impact of the experimental conditions on the DCM-degradation kinetics at each pulse was analysed based on the half-life of this compound, calculated using the following equation:

$$\text{DCM half-life}_{\text{X pulse}}(\text{days}) = \frac{\ln 2}{k}$$

where k is the rate constant of the DCM concentration over time. The period of time before the onset of DCM degradation, hereafter referred to as the 'latency phase', was not considered from the calculation of DCM half-life. When the calculated DCM half-life was greater than the

duration of the pulse, we considered that DCM was not degraded in that pulse. To test significance ($p < 0.05$), one-way ANOVA was performed.

V.2.4 Molecular biology analysis

V.2.4.1 DNA extraction

Environmental DNA was extracted from 1 g of the artificial matrix before the change in the oxygen status (T-bef) and at the end of the experiment (T-aft) by directly sampling it from the microcosms with a spatula upon sterile conditions. For microcosms without a matrix, as well as for the liquid inocula used to set up each type of microcosm (To), the extraction was done from 1 mL of each liquid phase. The “DNeasy PowerWater” kit (Qiagen) was used according to manufacturer’s instructions and DNA concentrations (0.028 - 21.6 ng/ μ L) were determined by fluorometry using the “Qubit® dsDNA HS Assay” kit (Thermo Fisher Scientific). DNA preparations were stored at -20°C until further use. Extraction blanks were included in each batch of extraction for quality control.

V.2.4.2 Detection of biomarkers and *in silico* analyses

To test the presence of the *dcmA* and *mecE-F* biomarker genes, PCR amplification was performed on the extracted DNA using the primers sets Forw *dcmA* Univ and Rev *dcmA* Univ (amplification of *dcmA* gene; **Table III.2**), and *mecE* 828F and *mecF* 641R (amplification of *mecE-F* genes; **Table II.3**). The used protocol is described in **section II.5.1.3**. The DNA template was used at a final concentration of 0.218 ng/ μ L in all cases.

V.2.4.3 16S rRNA gene amplicon sequencing and data analysis

The hypervariable V3-V4 regions of the gene encoding the 16S rRNA were PCR amplified and sequenced using the Illumina NextSeq 2000 platform (LCSB genomic platform, University of Luxembourg), as described in **section II.6.1.2**. Demultiplexed raw data were trimmed, filtered, denoised and clustered at 100% identity using the DADA2 pipeline to obtain Amplicon Sequence Variants (ASVs) (see details in **section II.6.1.2**). ASV were then annotated using the Silva reference database (version 138, June 2024).

The resulting ASV abundance matrix was analyzed in R (version 4.4.0). Before starting the analyses, singletons (i.e., ASVs that only appeared once across all samples) and doubletons (i.e., ASVs that only appeared twice across all samples) were removed from the data. Alpha-diversity indices (Chao1, Pielou’s evenness, and Shannon-Wiener diversity) were then calculated using the phyloseq R package (McMurdie & Holmes, 2013), as well as the microbial community profiling at the family level using the relative abundance of the ASV sequences using the microeco R package (Liu et al., 2021). Principal Component Analysis (PCA) based on the Aitchison distance of the clr-transformed data at the genus-level phylotype were performed using the microViz R package (Barnett et al., 2021). To test significance (p -value < 0.05), one-way ANOVA followed by post-hoc Tukey HSD test was conducted. Additionally, to identify the

correlation between the microbial taxa and the physicochemical parameters of interest (grain size, water content and oxygen status) and the DCM degradation rate, a Spearman correlation test was performed using the *microeco* R package. Finally, the ASVs that were ‘indicator species’ (i.e., ASVs whose presence or absence provided information on a particular set of physicochemical parameters) were identified using the *indicspecies* R package (Cáceres & Legendre, 2009).

V.3 Results

V.3.1 DCM degradation kinetics depending on experimental conditions

DCM degradation was monitored in all microcosms for 7 pulses of DCM (corresponding to 84 days, 67 days, 70 days and 70 days for microcosms with 2 mm, 0.5 mm and 0.1 mm grain size matrix and without matrix, respectively; **Figure V.3**). Oxygen status was also measured and remained stable at the concentration of interest in all pulses (A microcosms with $[O_2] < 0.5$ ppm, and O microcosms $[O_2] \sim 8$ ppm; data not shown).

No DCM dissipation was observed in any of the abiotic controls with the 0.5 mm and 0.1 mm grain size matrix, nor in the ones without matrix (except in one of the replicates, but it was not reproducible over time). This indicates that any changes in the DCM concentration found in the biotic controls and environmental samples under these conditions can be considered as biotic degradation. However, in the abiotic controls with the 2 mm grain size matrix, DCM dissipation was observed from the 3rd pulse under both oxic and anoxic conditions. Three hypotheses could explain this observation: (i) there was a DCM leak during the experiment (this seems unlikely as the anoxic condition was kept stable); (ii) the microcosms were not properly sterilized, or at least a DCM-degrading strain was resistant to the sterilization process, for example by producing spores; (iii) there was a cross-contamination probably propagated by the GC needle during gas phase sampling. In all cases, the decrease in DCM concentration observed from the 3rd pulse in these microcosms must be considered for the remaining of the analysis, and any variation in DCM concentration in the biotic controls and environmental samples from that pulse cannot be attributed solely to biotic degradation.

In the biotic controls, DCM was degraded from the first pulse under oxic and anoxic conditions regardless of grain size and water content, except for the microcosms with the 2 mm grain size matrix at WHC and 1/2 WHC, where no or occasional degradation was observed. We hypothesized that this could be a matter of water limitation, as these conditions had the lowest liquid phase volumes of all, with 0.6 mL and 0.3 mL, respectively. As already observed in **chapter III**, the DCM degradation activity of *Hyphomicrobium* sp. GJ21 seems to be susceptible to this parameter. An exception to this behaviour was found during the 1st DCM pulse at WHC under oxic conditions, where DCM degradation was observed. This could be explained by the fact that this strain had just been inoculated from an active preculture, so the

observed degradation may have resulted from its residual activity, which was only maintained during the 1st pulse. Following the change in the oxygen status of half of the microcosms, the DCM-degrading activity was largely maintained in all experimental conditions. This observation was expected since our model strain, *Hyphomicrobium* sp. GJ21, is known to degrade this compound under both oxic and anoxic conditions. Consequently, switching this parameter should not have a persistent effect on its activity. However, despite the function being overall maintained, the half-life of DCM was impacted by this change in some experimental conditions. For example, at 1/2 WHC with the 0.1 mm and the 0.5 mm grain size matrices, the activity was lost in the OA microcosms immediately after the change in oxygen status, and it was only recovered at the last pulse in the microcosms with the 0.5 mm grain size matrix. This may be related to the increased susceptibility of this strain to low water content, which could have hindered its adaptation to the disturbance. Nonetheless, additional replicates would be necessary to perform statistical analyses of the responses to the change in oxygen status based on the experimental conditions. In summary, two main conclusions could be drawn from the biotic controls: (i) the experimental set-up was suitable for studying the degradation of DCM in the environmental samples; (ii) the DCM degradation activity of the model strain is insensitive to grain size or oxygen status but sensitive to low water content.

In the environmental samples before disturbance, DCM degradation was mainly observed under oxic conditions. Indeed, stable anoxic biodegradation of DCM was observed only with the 0.5 mm grain size matrix at water saturation (2 out of 4 replicates) and WHC (2 out of 4 replicates). In addition, occasional anoxic biodegradation was observed in 1 replicate without matrix and in 2 replicates at WHC with the 2 mm grain size matrix during the first two DCM pulses. Furthermore, under oxic conditions, the water content had a significant impact on the DCM degradation kinetics from the 2nd pulse onward. Indeed, in the 0.5 mm and 0.1 mm grain size matrix, DCM degradation was promoted at 1/2 WHC compared to wetter matrices. In the case of the microcosms with the 2 mm grain size matrix, DCM degradation was promoted at WHC. However, as the abiotic controls also degraded DCM in this condition, no firm conclusions can be drawn in this regard. Taken together, these results suggest that, once the DCM-degrading community is established, its optimum activity occurs at different water contents depending on the grain size. This could be related to differences in the gas diffusion and solute transport at different water contents for the same grain size. Finally, it should be noted that no stable and complete DCM degradation was observed at 1/2 WHC with the 2 mm grain size matrix, indicating that the DCM-degrading community coming from the environmental sample was susceptible to low water volume, despite not as drastically as the model strain *Hyphomicrobium* sp. GJ21.

The response of the DCM-degrading community to the disturbance was mainly influenced by the initial oxygen status to which the community was exposed, excepted in a few cases. In details, in most of the OA microcosms, the function was lost after the disturbance. In the few cases where the function was maintained, i.e. microcosms with the 0.5 mm grain size matrix, the microbial communities were considered resilient to the disturbance as they only resumed

the degradation of DCM after three pulses. On the other hand, in the microcosms where the function was lost, e.g. the ones with 0.1 mm grain size matrix or without matrix, the microbial communities were considered to be sensitive to the disturbance. However, the question remains whether the microbial communities established in these microcosms were not able to support the switch in the oxygen status (sensitive) or whether they needed more time to recover the function (resilient). Regarding the OA microcosms with the 2 mm grain size matrix, the function was lost at WHC (sensitive), while it was consistently maintained at water saturation. In this latter case, the microbial community seemed to be resistant to the disturbance and is even enhanced compared to previous pulse and to non-disturbed microcosms. However, cautious interpretations should consider DCM degradation in the abiotic controls, so we couldn't conclude if this behaviour was only related to the experimental set up (i.e. matrix granulometry and water content) or if influenced by potential cross-contamination. On the other hand, the majority of AO microcosms displayed the function emergence after the disturbance, which could be due to the presence of a pool of microbial taxa requiring oxic conditions to carry DCM degradation activity on (latent microbial functional diversity). The microcosms where this behaviour was not observed were the ones with the 2 mm grain size matrix at $\frac{1}{2}$ WHC, which may be explained by the water content limitation, and the ones with the 0.1 mm grain size matrix at all water content. In the case of the latter microcosms, the absence of function could be related to the reduced gas and solutes diffusion at this granulometry, influencing the function and/or composition of the microbial community established under these conditions.

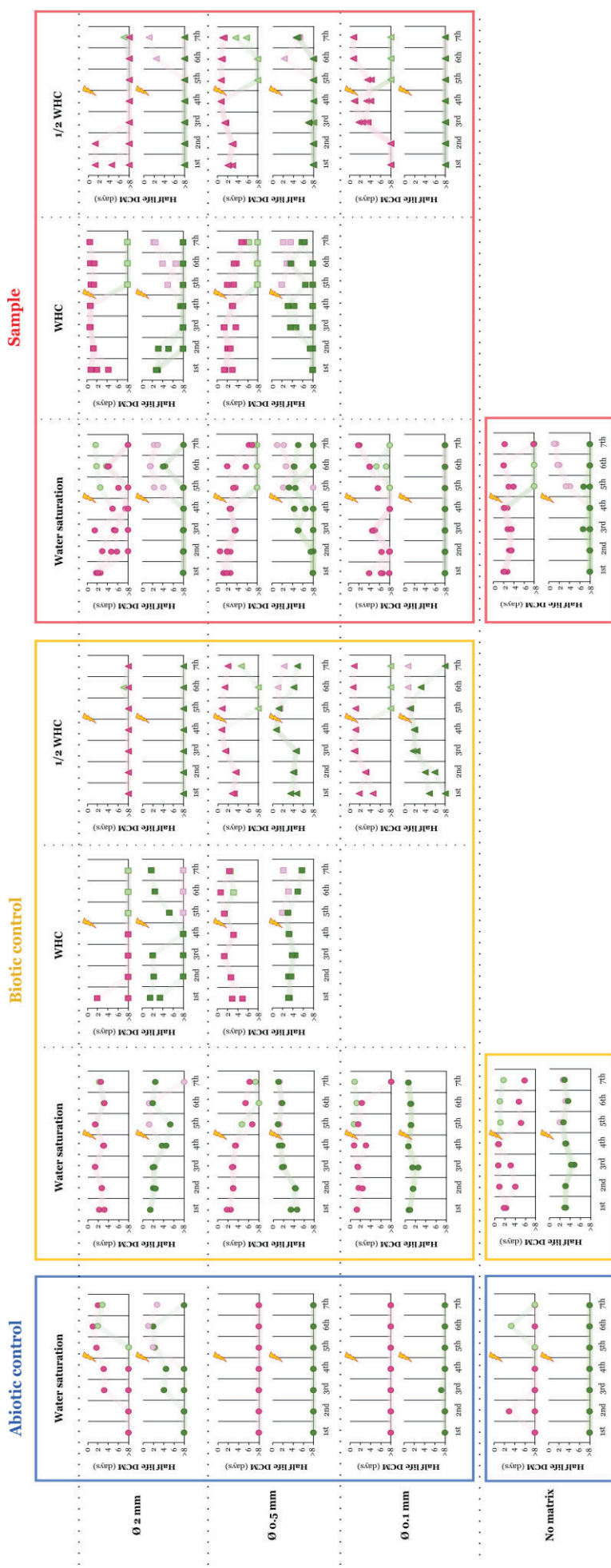


Figure V.3. DCM degradation depending on matrix grain size and water content in different oxic conditions before (1st to 4th pulse) and after the disturbance (5th to 7th pulse). The disturbance, i.e. the change in the oxygen status, was applied to half of the microcosms between 4th and 5th pulses. The X axis represents the successive DCM pulses. The Y axis represents the half-life of DCM (days) in a reversed order. When DCM half-life was superior to 8 days, it was considered as cases of no DCM degradation during that pulse. Per DCM pulse, each point represents a replicate; the same replicate is connected across pulses by a wide translucent line. The colour of the points represents the oxygen status: dark pink for microcosms under oxic conditions, dark green for microcosms under anoxic conditions, light green for microcosms that went from oxic to anoxic conditions (OA), and light pink for microcosms that went from anoxic to oxic conditions (AO). The shape of the points represents the water content: circle for microcosms at water saturation, square for microcosms at WHC, and triangle for microcosms at 1/2 WHC. The 'No DCM' microcosms are not depicted (no detected DCM throughout the experiment). The lightning represents the disturbance (change of oxygen status).

V.3.2 Presence of biomarker genes for DCM biodegradation

The presence of the *dcmA* and *mecE-F* genes was studied in the environmental samples with different grain size, water content and oxygen status before and after the disturbance. As mentioned in **section III.3.2**, the *dcmA* gene was targeted using universal primers, while the primers used for the *mecE-F* genes were specific for the recently described sequences.

Before the disturbance (DNA was extracted at the end of the 4th pulse), *dcmA* was detected in all environmental samples, except at 1/2 WHC with the 2 mm grain size matrix (**Table V.2**). These results suggest that the presence of strains carrying the *dcmA* gene was ubiquitous regardless of the experimental conditions and the DCM degradation efficiency. Indeed, in some microcosms the *dcmA* biomarker was detected while the DCM degradation was not observed (e.g. at 1/2 WHC under anoxic conditions at lower grain size). This could be due to the fact that the strains carrying this gene were either in a dormant state, contributing to the pool of latent functional diversity, or were dead. In any case, these observations showed that the presence of the *dcmA* gene alone was not a sufficiently reliable biomarker for predicting the occurrence of the function. In the case of the microcosms where the *dcmA* gene was not detected, i.e. at 1/2 WHC with the 2 mm grain size matrix, this may be due to the low water volume inoculated leading to undetectable quantity of the *dcmA* biomarker gene..

On the other hand, the *mecE-F* genes were not detected in any of the microcosms tested before the disturbance (**Table V.2**). This suggests that the strains carrying these genes were either present at concentrations below the detection limit or not present at all. Another possibility is that the primers used for the amplification of these genes were too specific, failing to capture their variability in the environment. Future analysis of the DNA extracted from the microcosms with the 0.5 mm grain size matrix, where some microcosms degraded DCM under anoxic conditions, could confirm whether this function was linked to the presence of *mecE-F* genes.

After the disturbance (DNA extracted at the end of the experiment), the *dcmA* and *mecE-F* genes were detected in all tested microcosms, meaning that their presence was independent of the experimental condition (**Table V.3**). Moreover, comparing with what was observed before the disturbance, this also suggests that the strains carrying these genes proliferated throughout the experiment as their reached the detection limit. It should be noted that the *mecE-F* genes, involved in the degradation of DCM in anoxic conditions, were also detected in the microcosms under oxic conditions, although this was not the case before the disturbance. Three main hypotheses could explain these observations: (i) at least one bacterial population carrying the *mecE-F* genes may have utilized another carbon source under oxic conditions, enabling their growth during the experiment; (ii) bacteria carrying the *mecE-F* genes may possess an alternative pathway for metabolizing DCM under oxic conditions (e.g. the *dcmA* pathway), allowing them to thrive under this condition; (iii) the quantity of the bacteria carrying these genes remained constant, but their relative abundance increased due to the decline in other bacterial populations.

Table V.2. Detection of *dcmA* and *mecE-F* biomarkers for DCM degradation before the disturbance (end of the 4th pulse). ✓ indicates the presence of the gene of interest. ✗ indicates the non-detection of the gene of interest. Nd stands for not determined. Replicates (n=4) are not shown since the results were consistent. Empty cells are for conditions that were not set up during the experiment (WHC was similar to water saturation with the 0.1 mm grain size matrix). O and A stands for oxic and anoxic conditions, respectively.

	ø 2 mm		ø 0.5 mm		ø 0.1 mm	
	<i>dcmA</i>	<i>mecE-F</i>	<i>dcmA</i>	<i>mecE-F</i>	<i>dcmA</i>	<i>mecE-F</i>
Saturation O	✓	✗	✓	Nd	✓	✗
Saturation A	✓	✗	✓	Nd	✓	✗
WHC O	✓	✗	✓	Nd		
WHC A	✓	✗	✓	Nd		
1/2 WHC O	✗	✗	✓	Nd	✓	✗
1/2 WHC A	✗	✗	✓	Nd	✓	✗

Table V.3. Detection of *dcmA* and *mecE-F* biomarkers for the DCM degradation at the end of the experiment (end of the 7th pulse). ✓ indicates the presence of the gene of interest. ✗ indicates the non-detection of the gene of interest. Nd stands for not determined. Replicates (n=2) are not shown since the results were consistent. Empty cells are for conditions that were not set up during the experiment (WHC was similar to water saturation with the 0.1 mm grain size matrix). OO and AA correspond to microcosms that were conserved in oxic and anoxic conditions, respectively, throughout the experiment. OA correspond to microcosms that changed from oxic to anoxic conditions. AO correspond to microcosms that changed from anoxic to oxic conditions.

	ø 2 mm		ø 0.5 mm		ø 0.1 mm	
	<i>dcmA</i>	<i>mecE-F</i>	<i>dcmA</i>	<i>mecE-F</i>	<i>dcmA</i>	<i>mecE-F</i>
Saturation OO	✓	Nd	✓	✓	✓	✓
Saturation AA	✓	Nd	✓	✓	✓	✓
Saturation OA	✓	Nd	✓	✓	✓	✓
Saturation AO	✓	Nd	✓	✓	✓	✓
WHC OO	✓	Nd	✓	✓		
WHC AA	✓	Nd	✓	✗		
WHC OA	✓	Nd	✓	✓		
WHC AO	✓	Nd	✓	✓		
1/2 WHC OO	✓	Nd	✓	✓	✓	✓
1/2 WHC AA	✓	Nd	✓	✓	✓	✓
1/2 WHC OA	✓	Nd	✓	✓	✓	✓
1/2 WHC AO	✓	Nd	✓	✓	✓	✓

V.3.3 Analysis of microbial community composition in relation to experimental conditions

To characterize the microbial community established in the different microcosms according to the experimental conditions, we analysed the data obtained from the 16S rRNA gene amplicon sequencing performed on the DNA extracted at the beginning of the experiment (T₀), before the disturbance (T-bef; end of the 4th DCM pulse) and at the end of the experiment (T-aft). It is important to note that the production of amplicons failed for 12 samples, including abiotic controls (2), biotic controls (4), and environmental (6), all of which came from microcosms with the 2 mm grain size matrix at low water contents, preventing further analyses in these cases. Details of the DNA concentration for each sample, as well as the information during data quality treatment, are provided in **Supplementary table V.1**. All reads obtained from the different microcosms were clustered together at 100% identity, yielding a total of 8 940 ASVs for taxonomic analysis. Taxonomic classification left unassigned 0.02%, 0.04%, 1%, 4.2%, 12.5% of the total ASV at the phylum, class, order, family and genus level, respectively.

V.3.3.1 Impact of physicochemical parameters on microbial taxonomical composition

Of all 8 940 ASVs detected, 6 592 ASVs were detected in the microcosms with the 2 mm grain size matrix, 2 355 ASVs in the microcosms with the 0.5 mm grain size matrix, 2 059 ASVs in the microcosms with the 0.1 mm grain size matrix, and 2 194 ASVs in the microcosms without matrix. In order to explore the microbial taxonomical composition in the microcosms depending on the experimental conditions, we visualized the relative abundances of the microbial populations at T₀, T-bef and T-aft in the different microcosms (**Figure V.4** to **V.7**). For the sake of visibility, the results are displayed at the taxonomic level of the family.

In the abiotic controls inoculated with a filter-sterilized inoculum, the predominant taxa before the disturbance (**Figure V.4**) varied with matrix grain size: the family *Rhodocyclaceae* in the presence of the 2 mm grain size matrix (relative abundance of 45 ±1%), the family *Brevibacteriaceae* in the presence of the 0.5 mm grain size matrix (relative abundance of 34 ±3%), and the family *Alcalinagaceae* in the presence of the 0.1 mm grain size matrix and in the absence of matrix (relative abundances of 82 ±5% and 54 ±8%, respectively). Moreover, although the presence of the *Hyphomicrobiaceae* family was generally negligible (classified under the category ‘Others’), its relative abundance was significantly higher in the abiotic controls where DCM was dissipated (i.e., microcosms with the 2 mm grain size matrix from the 3rd pulse; see **Figure V.3**). In this context, even though this family was not a predominant taxon in these microcosms (relative abundance of 4 ±1%), its presence may have contributed to the degradation of DCM, explaining the observed dissipation of this compound. In the abiotic controls where no DCM dissipation was observed, the compositional differences may be due to the ability of some bacteria that resisted sterilization to utilize other available carbon sources in the microcosms (e.g., from dead biomass) or methodological bias (e.g., in some

cases, the recovered DNA concentration was very low for classical amplicon generation; Kennedy et al., 2014). Finally, the change in oxygen status did not lead to any significant changes in the taxonomical composition of the microbial communities in the abiotic controls, regardless of the experimental conditions. This suggests that the differences that were found in the environmental samples after the disturbance were linked to changes in the DCM-degrading microbial populations.

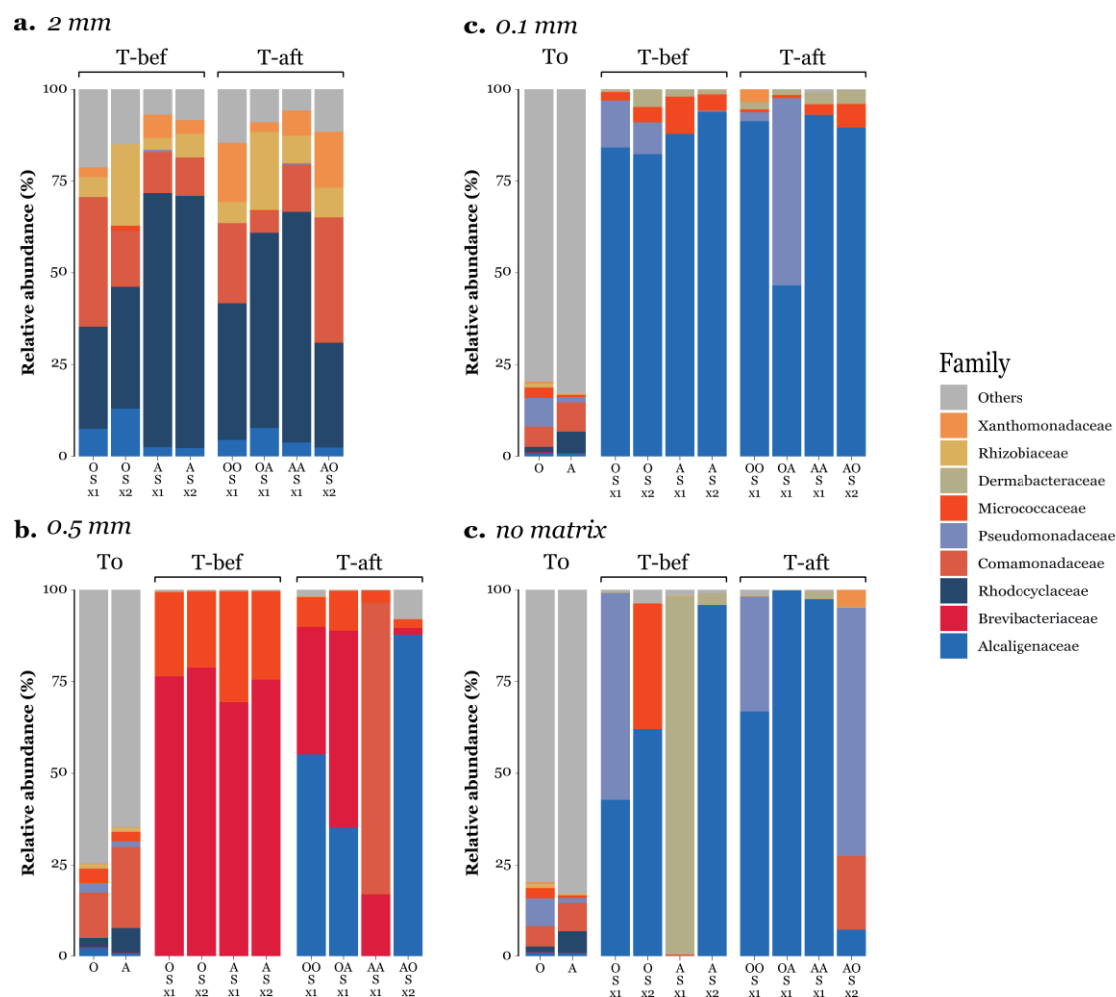


Figure V.4. Relative abundances (in %) at the family-level at To, T-bef and T-aft in the abiotic controls. Families with a relative abundance lower than 0.1% are classified under the ‘Others’ category. The panels show the taxonomical community composition in microcosms with: **a.** 2 mm grain size matrix (To samples are not shown due to unsuccessful sequencing); **b.** 0.5 mm grain size matrix; **c.** 0.1 mm grain size matrix; and **d.** in the absence of matrix. O and A correspond to microcosms that were under oxic and anoxic conditions before the disturbance, respectively (n=2 per granulometry). OO and AA correspond to microcosms that were maintained under oxic and anoxic conditions, respectively (n=1 per granulometry). OA corresponds to microcosms that change from oxic to anoxic conditions after the disturbance (n=1 per granulometry). AO corresponds to microcosms that change from anoxic to oxic conditions after the disturbance (n=1 per granulometry). S indicates ‘water saturation’.

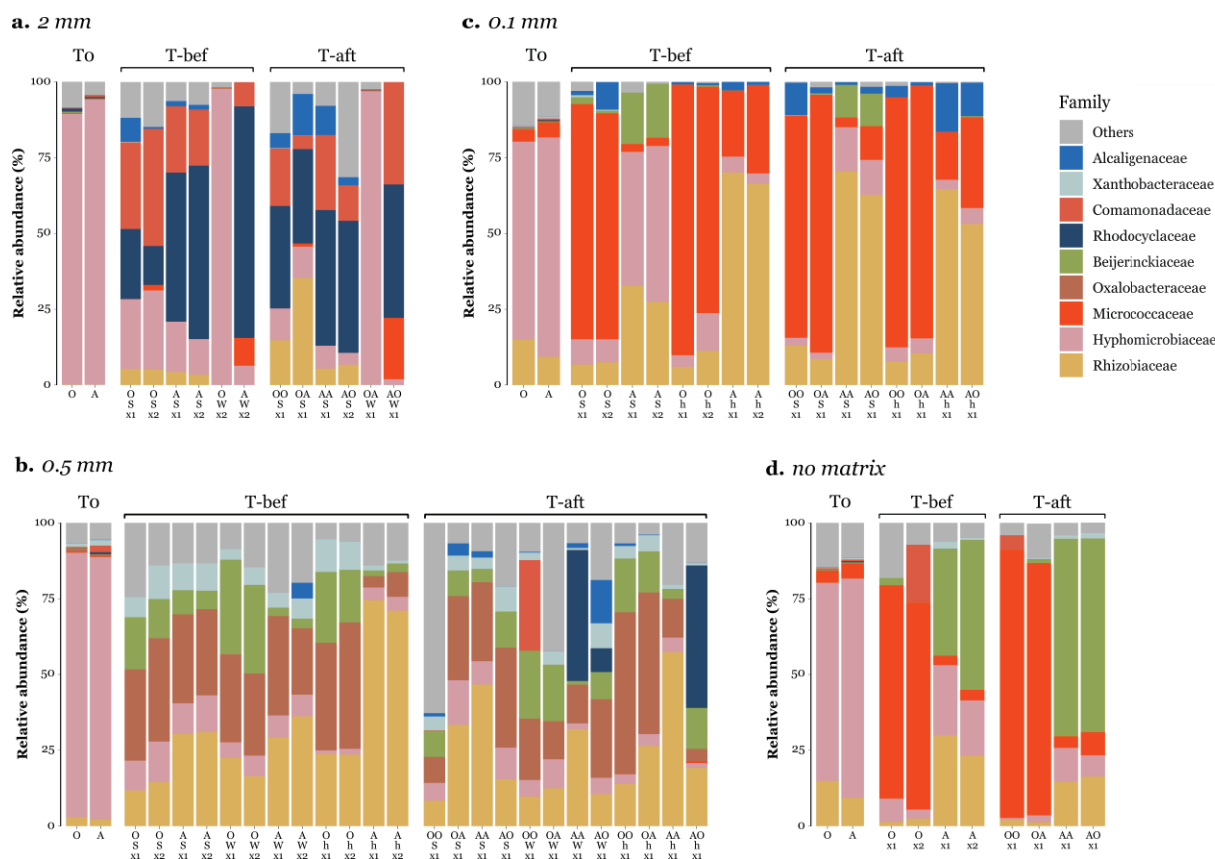


Figure V.5. Relative abundances (in %) at the family level at To, T-bef and T-aft in the biotic controls. Families with a relative abundance lower than 0.1% are classified under the ‘Others’ category. The panels show the taxonomical community composition in microcosms with: **a.** 2 mm grain size matrix (OW_{x1}, AW_{x1}, OOW_{x2} and AAW_{x2} samples are not shown due to unsuccessful sequencing); **b.** 0.5 mm grain size matrix; **c.** 0.1 mm grain size matrix; and **d.** in the absence of matrix. O and A correspond to microcosms that were under oxic and anoxic conditions before the disturbance, respectively (n=2 per water content and granulometry). OO and AA correspond to microcosms that were maintained under oxic and anoxic conditions, respectively (n=1 per water content and granulometry). OA corresponds to microcosms that change from oxic to anoxic conditions after the disturbance (n=1 per water content and granulometry). AO corresponds to microcosms that change from anoxic to oxic conditions after the disturbance (n=1 per water content and granulometry). S indicates ‘water saturation’, W indicates ‘water holding capacity’, and h indicates ‘1/2 water holding capacity’.

In the biotic controls before the disturbance (**Figure V.5**), the relative abundance of the family *Hyphomicrobiaceae* was significantly lower than in the initial inoculum (To) when the strain *Hyphomicrobium* sp. GJ21 was just inoculated, regardless of the experimental conditions (relative abundances of $11 \pm 4\%$ in the biotic controls at T-bef vs. $83 \pm 5\%$ at To). One potential explanation for the decrease in the relative abundance of this family is that some taxa, initially present in the environmental inoculum and resistant to the sterilization step, may have proliferated during the experiment and interfered the development of *Hyphomicrobium* sp. GJ21. Another hypothesis could be that because of the increase in the abundance of these “resistant” taxa from the initial inocula, the relative abundance of the *Hyphomicrobiaceae*

family was reduced, even if the absolute number of cells was constant or slightly increasing. However, despite the low relative abundance of *Hyphomicrobiaceae*, the ASV constituting this family could have played an important role in the degradation of DCM during the experiment. To exemplify this, it is worth to note that unlike in the environmental sample microcosms, DCM degradation occurred in the majority of the biotic controls under anoxic conditions. Considering that the environmental inoculum used to set up both types of microcosms was from the same origin (**Figure V.1**), these differences suggest that the addition of the DCM-degrading strain *Hyphomicrobium* sp. GJ21 contributed to this function in the biotic controls. Finally, the disturbance generated no differences in the relative abundance of this family when comparing the microcosms that changed the oxygen status and those that maintained the initial conditions, which showed that both the DCM degradation function and the model DCM-degrading strain were resistant to the disturbance.

In the environmental samples, the oxic and anoxic inoculum (To) showed similar taxonomical composition, with significant differences in the relative abundance of the families *Rhodocyclaceae* (greater under anoxic conditions) and *Pseudomonadaceae* (greater under oxic conditions), regardless of the matrix grain size. These trends were amplified in the samples collected before the disturbance (**Figure V.6**), with the taxonomical composition primarily influenced by oxygen status, rather than granulometry or water content. This was likely due to the varying development of the DCM-degrading taxa, as oxic conditions promoted DCM degradation, as shown in **section V.3.1**. Among the taxa which relative abundance varied across experimental conditions, the *Pseudomonadaceae* family was significantly more abundant under oxic conditions than under anoxic conditions irrespective of the water content and grain size. All 194 ASVs detected in this family belonged to the genus *Pseudomonas*, which has previously been associated with DCM degradation activity in the absence of the *dcmA* gene (Muller et al., 2011a). This genus is mainly composed of strict aerobes, which may explain its higher relative abundance under oxic condition. Furthermore, the relative abundance of this family was significantly greater in the presence of the 0.1 mm grain size matrix compared to other grain sizes. Another taxon which relative abundance was significantly higher under oxic conditions, regardless of grain size, was the family *Nocardiaceae*. Interestingly, under oxic conditions, this family was significantly more abundant at WHC in the presence of the 2 mm grain size matrix, and at 1/2 WHC with the 0.1 mm grain size matrix, compared to other water contents with the same grain size. Both of these conditions were characterized by rapid degradation of DCM. The majority of the ASVs in this family (95%) were identified as belonging to *Rhodococcus*, a genus of aerobic bacteria. Additionally, *Rhodococcus* sp. has been previously associated with the utilization of DCM as the sole carbon and energy source in absence of the *dcmA* gene (Lee et al., 2010; Muller et al., 2011a), as well as with the aerobic degradation of other chlorinated compounds, such as vinyl chloride (Malachowsky et al., 1994). Finally, the family *Chitinophagaceae* was also significantly more abundant under oxic conditions in all cases, except with the 0.1 mm grain size matrix. The majority of ASVs were not assigned to a particular genus (43%), but among the taxonomically attributed ones, the most frequently

genera were *Asinibacterium* (22%), *Edaphobaculum* (17%), and *Sediminibacterium* (13%), all of which are aerobic bacteria. Notably, *Sediminibacterium* sp. has been previously linked to the aerobic degradation of vinyl chloride (Wilson et al., 2016). Additionally, the *Chitinophagaceae* family was significantly more abundant in the microcosms without a matrix than in the other cases, suggesting that the development of bacteria from this family may be favoured in the planktonic state. In contrast, the family *Rhodocyclaceae* was significantly more abundant under anoxic conditions, except with the 0.1 mm grain size matrix. The majority of the ASVs from this family belonged to the genera *Dechlorosoma* (70%) and *Methyloversatilis* (21%), both of which have been previously reported to degrade chlorinated compounds under both oxic and anoxic conditions (Achenbach et al., 2001; Li et al., 2022). Similarly, the family *Alcalinagaceae* was significantly more abundant under anoxic conditions in the presence of the 2 mm and 0.1 mm grain size matrix at low water content. The majority of ASVs from this family were identified as *Achromobacter* (99%), a genus that includes members capable of degrading chlorotoluene under oxic conditions (Pacholak et al., 2017). Nevertheless, as shown in **section V.3.1**, no DCM degradation was observed in most of the microcosms under anoxic conditions before the disturbance, suggesting that the increase in the abundance of these taxa may result from the utilization of alternative residual carbon sources or from the decline of taxa that were susceptible to anoxic conditions, including some taxa potentially capable of DCM degradation. Moreover, these families were also predominant in the abiotic controls (**Figure V.4**), further supporting the hypothesis that they were not involved in DCM degradation. Lastly, it is interesting to note that the abundance of the family *Hyphomicrobiaceae* significantly decreased from the To in all microcosms, except those without matrix. This suggests that the growth of this family may be promoted in the planktonic state or that taxa that develop in the presence of matrices may interfere with their growth. Furthermore, the *Hyphomicrobiaceae* family was significantly more abundant in the microcosms degrading DCM under anoxic conditions (i.e., 2 replicates at water saturation and 2 at WHC with the 0.5 mm grain size matrix) than in those under the same conditions without observed degradation. This indicates that, even at low abundance, the *Hyphomicrobiaceae* family may have played a role in anaerobic DCM degradation.

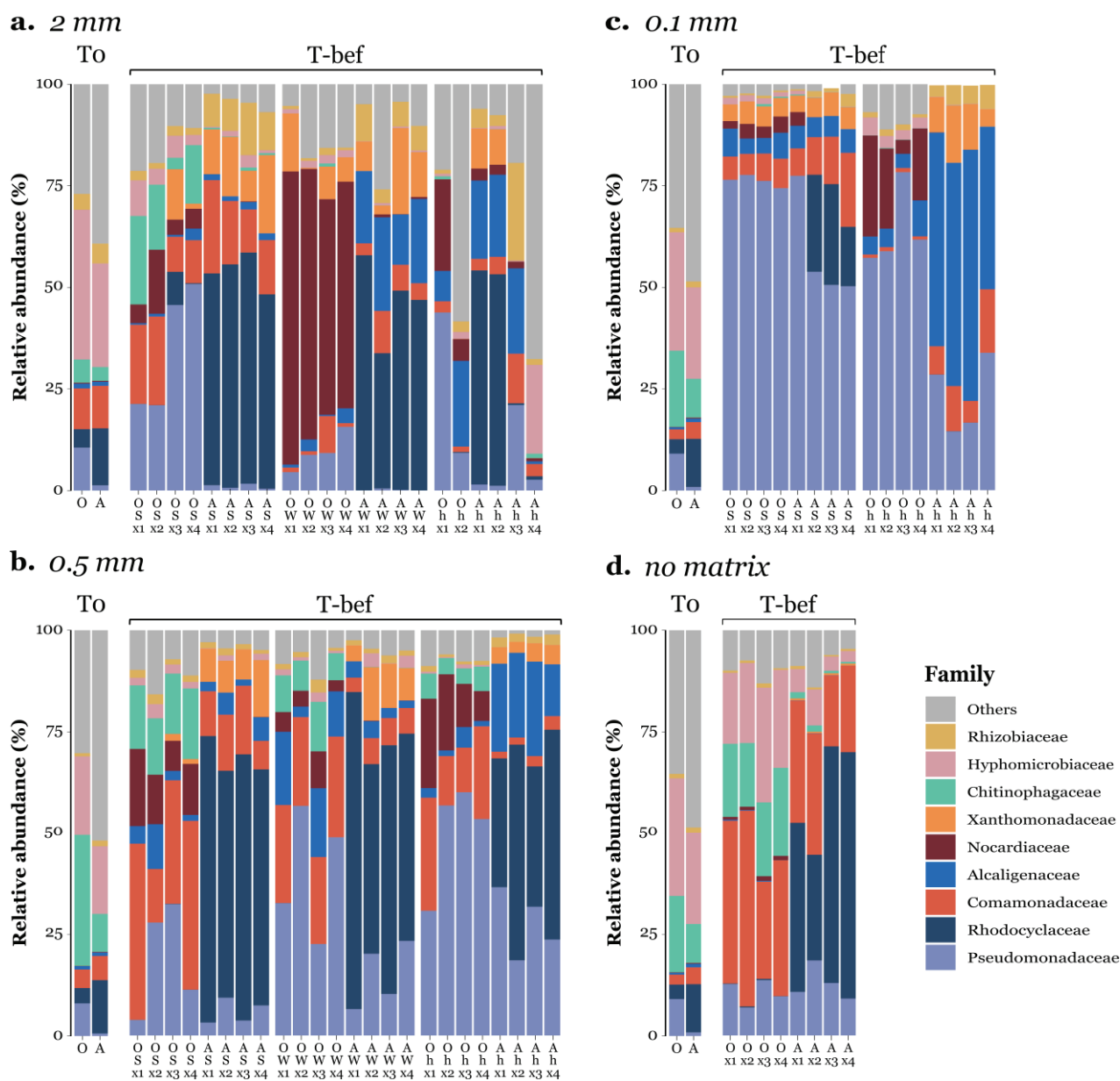


Figure V.6. Relative abundances (in %) at the family level at To and T-bef in the environmental samples before the disturbance. Families with a relative abundance lower than 0.1% are classified under the ‘Others’ category. The panels show the taxonomical community composition in microcosms with: **a.** 2 mm grain size matrix (Ohx3 and Ohx4 samples are not shown due to unsuccessful sequencing); **b.** 0.5 mm grain size matrix; **c.** 0.1 mm grain size matrix; and **d.** in the absence of matrix. O and A correspond to microcosms that were under oxic and anoxic conditions, respectively (n=4 per water content and granulometry). S indicates ‘water saturation’, W indicates ‘water holding capacity’, and h indicates ‘1/2 water holding capacity’.

In the environmental samples after the disturbance, changes in taxa were mainly dependent on the oxygen status to which the microcosms shifted (**Figure V.7**). For example, in OA microcosms, the abundance of the families *Rhodocyclaceae* and *Alcaligenaceae*, previously associated with anoxic conditions, increased significantly in microcosms with the 2 mm, 0.5 mm and 0.1 mm grain size matrices. On the contrary, in the same OA microcosms with the 0.1 mm and 0.5 mm grain size matrices, the abundance of the families *Nocardioaceae* and *Pseudomonadaceae*, previously associated with oxic conditions, significantly decreased. When comparing the OA microcosms where the function was resilient to the disturbance (e.g., microcosms with the 0.5 mm grain size matrix) with those where the function was sensitive to the disturbance (e.g., microcosms at WHC with the 2 mm grain size matrix and at 1/2 WHC with the 0.1 mm grain size matrix), the taxonomical composition did not show any drastic changes. One possible explanation is that the specific taxa responsible for resuming the DCM degradation may require more time to re-start their activity under these conditions. Alternatively, DCM degradation could have been mediated by co-metabolism, a process in which a compound is degraded without being used as carbon source to support microbial growth (Horvath, 1972). In this case, bacteria responsible for DCM degradation would not benefit from its degradation to increase its population. Regarding the AO microcosms, the abundance of the family *Rhodocyclaceae* significantly decreased in all microcosms except those with the 0.1 mm grain size matrix. Conversely, the family *Nocardiaceae* was significantly more abundant in microcosms with the 0.5 mm grain size matrix, as well as at 1/2 WHC with the 2 mm grain size matrix, which may have contributed to the emergence of the DCM degradation activity in these microcosms under oxic conditions. In the microcosms without matrix, the main taxon that showed a significant increase in relative abundance after the disturbance was the *Chitinophagaceae* family, which appeared to be promoted under oxic conditions in the absence of a matrix as noted before the disturbance. Finally, no differences were observed between the AO and AA microcosms with the 0.1 mm grain size matrix, potentially explaining why the DCM-degrading function did not emerge after the disturbance.

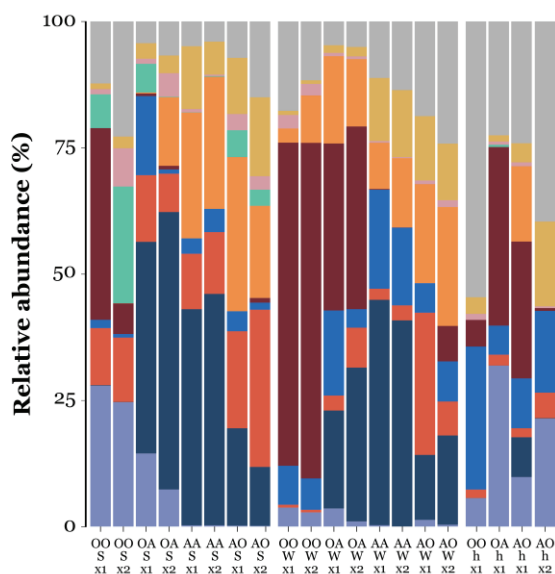
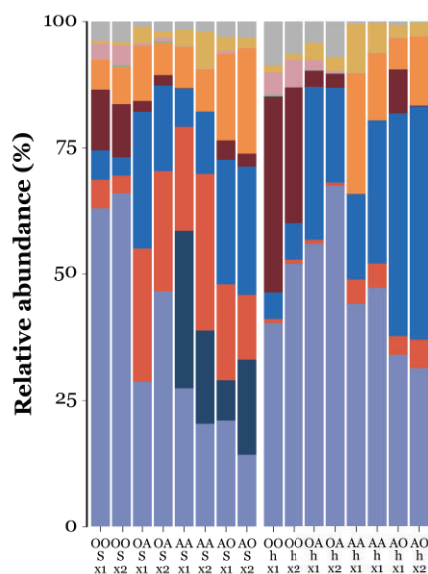
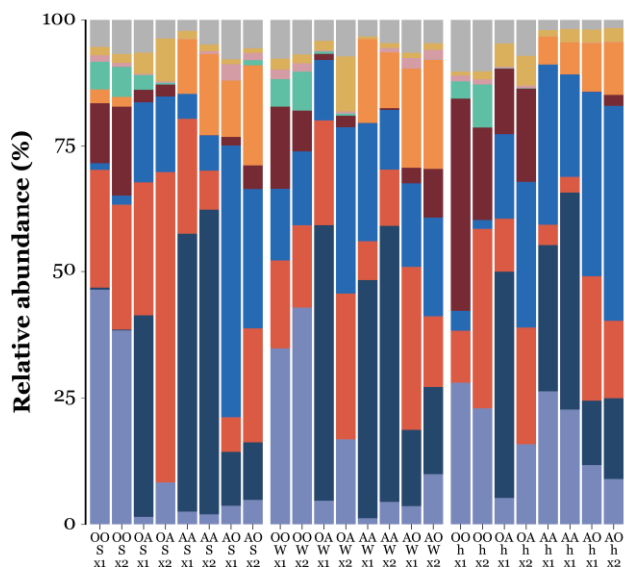
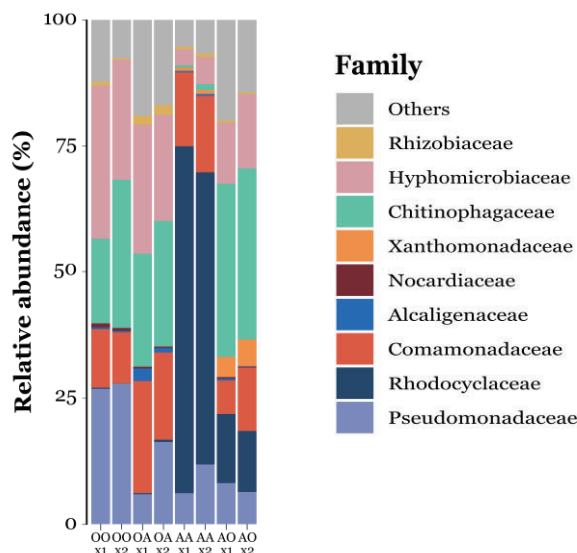
a. 2 mm**c. 0.1 mm****b. 0.5 mm****d. no matrix**

Figure V.7. Relative abundances (in %) at T-aft at the family-level of in the environmental samples after the disturbance. Families with a relative abundance lower than 0.1% are classified under the ‘Others’ category. The panels show the taxonomical community composition in microcosms with: **a.** 2 mm grain size matrix (OOhx2, OAhx2, AAhx1 and AAhx2 samples are not shown due to unsuccessful sequencing); **b.** 0.5 mm grain size matrix; **c.** 0.1 mm grain size matrix; and **d.** in the absence of matrix. OO and AA correspond to microcosms that were maintained under oxic and anoxic conditions, respectively (n=2 per water content and granulometry). OA corresponds to microcosms that change from oxic to anoxic conditions after the disturbance (n=2 per water content and granulometry). AO corresponds to microcosms that change from anoxic to oxic conditions after the disturbance (n=2 per water content and granulometry). S indicates ‘water saturation’, W indicates ‘water holding capacity’, and h indicates ‘1/2 water holding capacity’.

V.3.3.2 Impact of physicochemical parameters on the richness, evenness and diversity

To study the impact of oxygen status, water content and matrix granulometry on microbial community diversity, we first calculated the alpha-diversity metrics at the ASV level in the environmental samples. The analyses were disregarded in both microcosms with filter-sterilized inocula (i.e., abiotic and biotic controls), and those without added DCM (i.e., no-DCM controls). The results showed that matrix granulometry significantly impacted the microbial community diversity. In particular, microbial communities in microcosms with the largest granulometry (i.e., 2 mm grain size) exhibited significantly higher richness, evenness and diversity compared to the other microcosms (p -value < 0.05 ; **Figure V.8**). Conversely, microbial communities in microcosms with the finest granulometry (i.e., 0.1 mm grain size), displayed significantly lower diversity than in the other microcosms (p -value < 0.05).

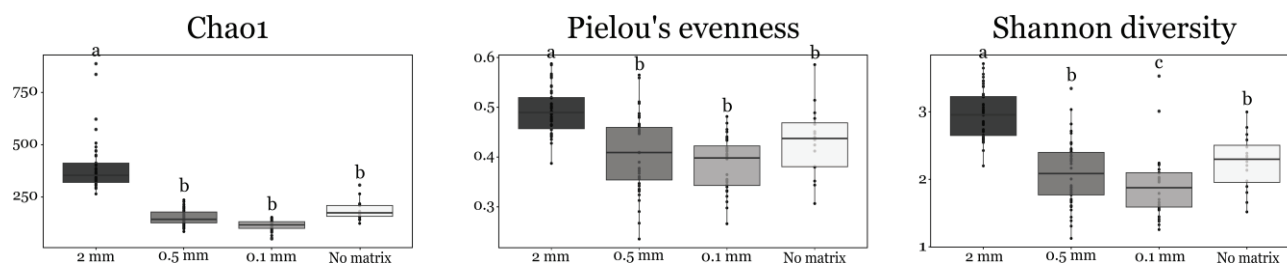


Figure V.8. Microbial community diversity in the environmental samples depending on the grain size matrix. The alpha-diversity metrics used were Chao1 index (i.e. number of ASVs per condition), Pielou's evenness (i.e. how evenly ASVs are distributed), and Shannon-Wiener diversity index (i.e. it reflects both the number of ASVs and the equality of the distribution). We used the data coming from T-bef and T-aft. The points in the boxplot represent each replicate ($n=24$ for the 2 mm and 0.5 mm grain size matrix; $n=16$ for the 0.1 mm grain size matrix; and $n=8$ in absence of the matrix). Letters a, b and c show group of significance (p -value < 0.05).

Before the disturbance, the general trend in the environmental samples, based on oxygen status, was a reduction in the alpha diversity of the microbial communities exposed to anoxic conditions. However, significant differences were only observed with the 0.5 mm grain size matrix. In this case, richness, evenness and diversity were significantly higher under oxic conditions than under anoxic conditions ($p < 0.05$; **Figure V.9**). These results suggest that before the disturbance (4 pulses), oxygen status did not significantly impact the diversity of microbial communities across different matrix grain sizes, except for the 0.5 mm grain size.

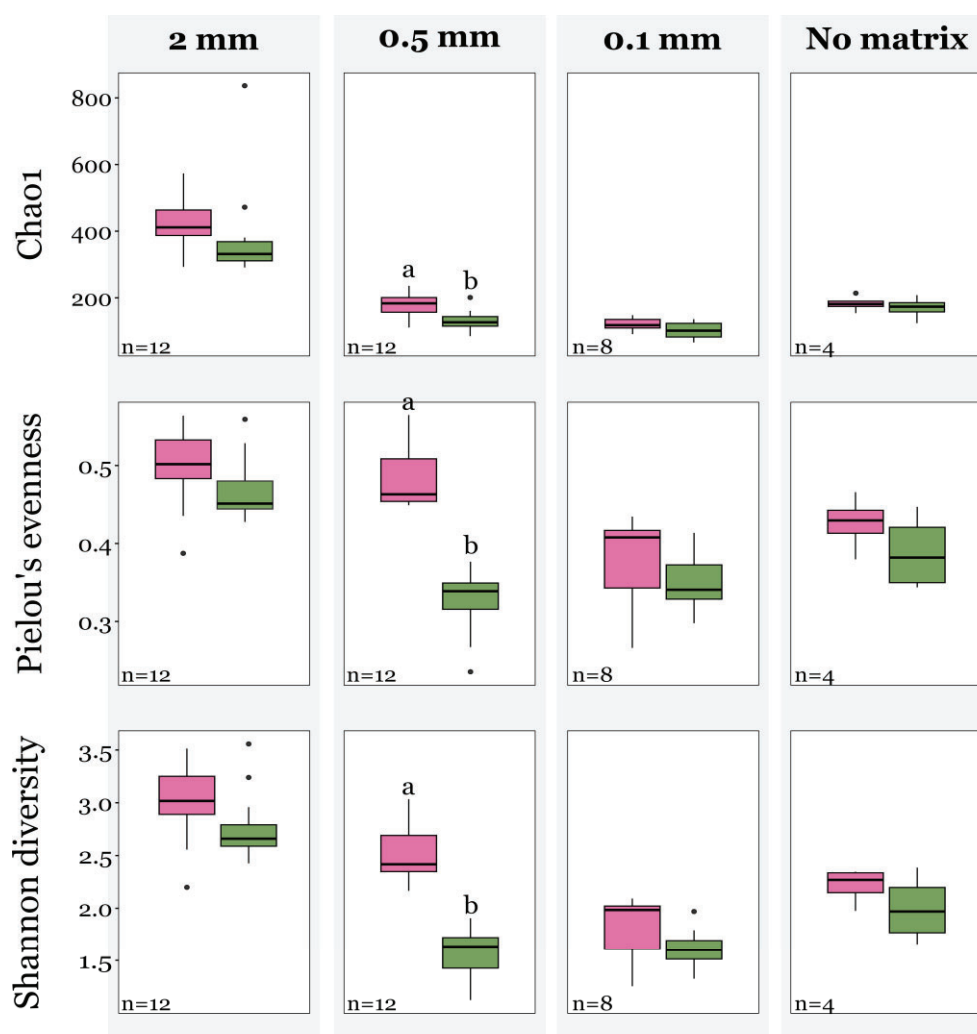


Figure V.9. Microbial community diversity in the environmental samples before the disturbance as a function of oxygen status. The alpha-diversity metrics used were Chao1 index, Pielou's evenness, and Shannon-Wiener diversity index. Dark pink represents the microcosms under oxic conditions and dark green represents the microcosms under anoxic conditions. The number in the left corner corresponds to the number of replicates per oxygen status in each granulometry. Letters a, and b show group of significance (p-value < 0.05).

Following the disturbance, no significant differences were observed between the disturbed (OA and AO) and non-disturbed (OO and AA) microcosms in the presence of the 2 mm and 0.1 mm grain size matrix (**Figure V.10**). However, with the 0.5 mm grain size matrix, richness, evenness and diversity significantly decreased in the OA compared to the OO microcosms, while evenness and diversity significantly increased in the AO compared to the AA microcosms. This result aligns with the previous observation that oxygen status only impacted the diversity of the microbial community in presence of this matrix grain size. Finally, in the absence of matrix, richness significantly increased in the OA microcosms compared to the OO

microcosms, while both evenness and diversity significantly increased in the AO microcosms compared to the AA microcosms.

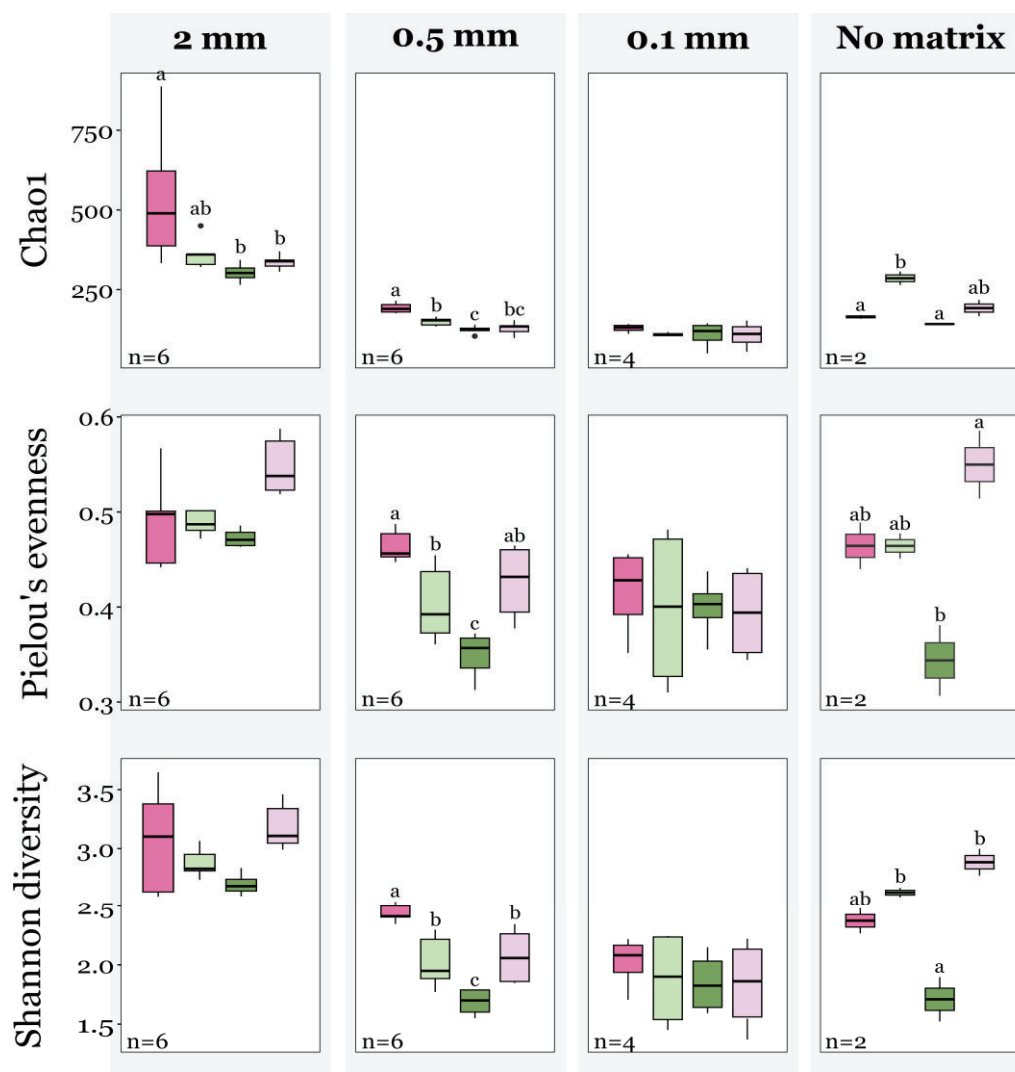


Figure V.10. Microbial community diversity in the environmental samples after the disturbance as a function of oxygen status. The alpha-diversity metrics used were Chao1 index, Pielou's evenness, and Shannon-Wiener diversity index. Dark pink represents OO microcosms, light green represents OA microcosms, dark green represents AA microcosms, and light pink represents AO microcosms. The number in the left corner corresponds to the number of replicates per oxygen status at each granulometry. Letters a, b and c show group of significance (p-value < 0.05).

Finally, the impact of water content varied across different matrix grain sizes. For instance, in the 2 mm grain size matrix, lower water content significantly increased the richness and diversity of microbial communities (**Figure V.11**). However, in finer grain sizes, lower water content led to a significant decrease in the microbial community richness, evenness and diversity. Since in microcosms with the 2 mm grain size matrix no DCM degradation was observed at $\frac{1}{2}$ WHC, the observed differences may not be related to the influence of this parameter on the DCM-degrading populations. On the other hand, considering that oxygen

status did not affect the microbial diversity of microcosms with the 0.1 mm grain size matrix, these results suggest that at finer grain sizes, water content exerts a stronger impact on the microbial community diversity than oxygen status.

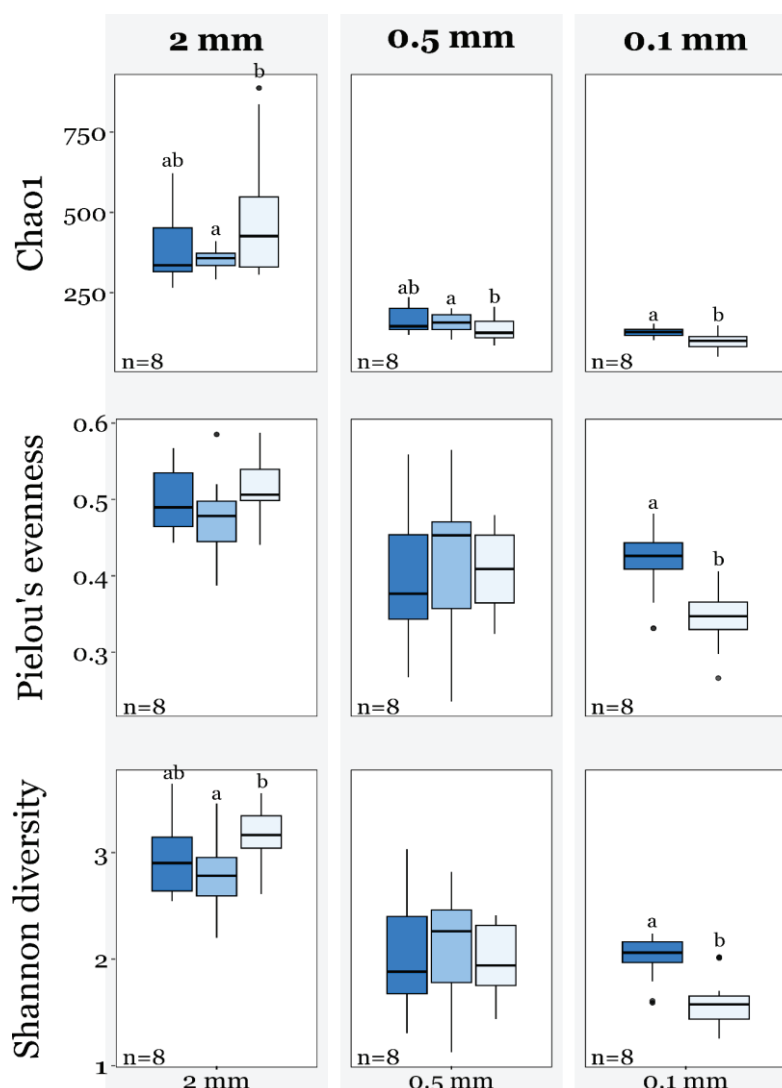


Figure V.11. The alpha-diversity metrics used were Chao1 index, Pielou's evenness, and Shannon-Wiener diversity index. We used the data coming from T-bef and T-aft. Dark blue represents the microcosms at water saturation, medium blue represents the microcosms at WHC, and light blue represents the microcosms at 1/2 WHC. The number in the left corner corresponds to the number of replicates per water content in each granulometry. Letters a and b show group of significance (p -value < 0.05).

V.3.3.3 Impact of physicochemical parameters on beta-diversity

To compare the microbial composition between the environmental sample microcosms as a function of grain size, two PCAs were performed on the clr-transformed abundance data at the genus-level phylotypes at T-bef and T-aft (**Figure V.12**). The PCA for the samples at T-bef showed that the first two principal components (PC1 and PC2) accounted for 39.9% of the variation in taxonomic composition, while in the PCA for the samples at T-aft, the PC1 and PC2

accounted for 32.6% of the variability (**Figure V.12-a.**). Notably, the microbial community compositions of the initial inocula (To) across different grain sizes clustered together, confirming that differences between samples with different grain sizes mainly developed along the experiment. When examining PC3 and PC4 axis, they accounted for around 15% of the variability at T-bef and T-aft (**Figure V.12-b.**). The samples clustered according to the matrix granulometry, except for those without a matrix. Overall, these results suggest that the matrix grain size was not the main parameter explaining the variation in microbial community composition across the different microcosms. However, the observations along the PC3 and PC4 axis indicate that this parameter may have had a subtle influence during the experiment. Alternatively, the observed clustering in the PC3 and PC4 axis could be attributed to a batch effect, given that microcosms with different matrices were setup at different chronologically times along the experiment (2 mm: January 2023 to March 2023; 0.5 mm: September 2023 to November 2023; 0.1 mm and no matrix: January 2024 to March 2024). However, if this was the case, we would expect that microcosms without a matrix to cluster together with those with the 0.1 mm grain size matrix, as they were setup simultaneously.

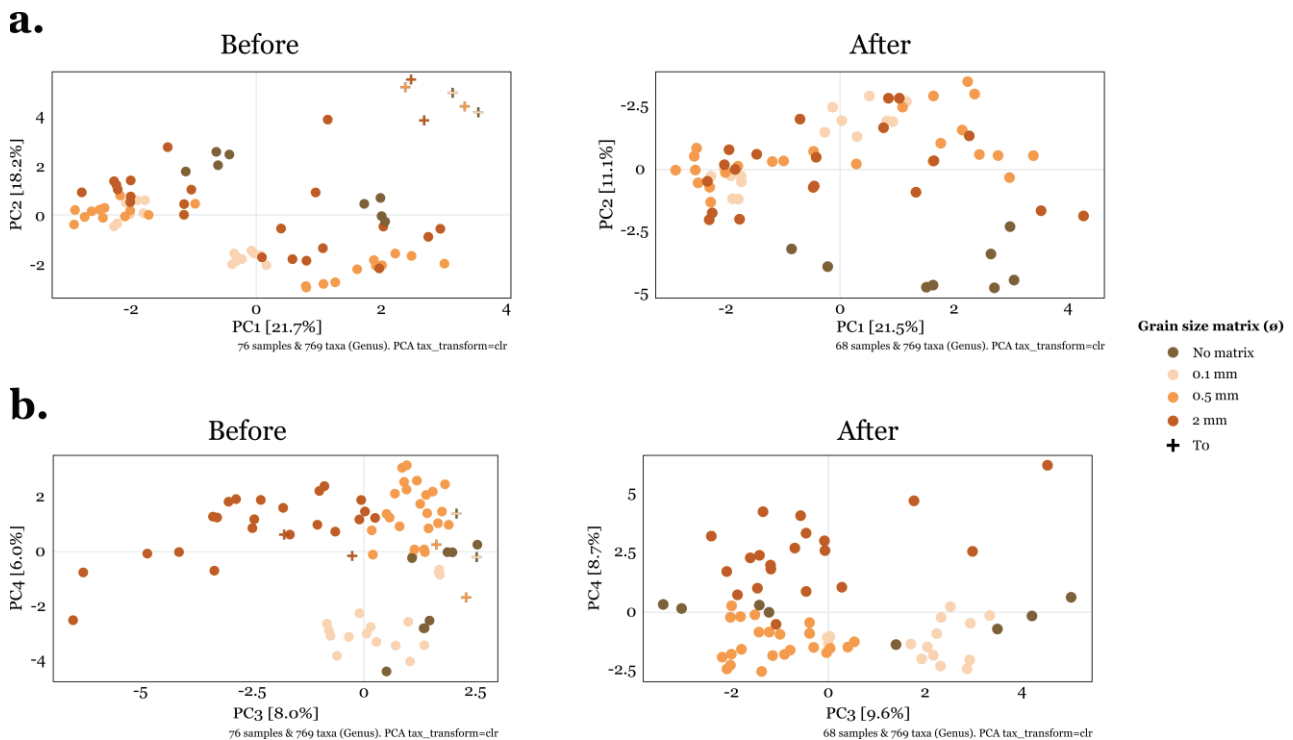


Figure V.12. PCA plot derived from clr-transformed abundance data of the genus-level phylotypes in the environmental samples at the beginning of the experiment and before the disturbance (To and T-bef), and at the end of the experiment (T-aft). The colour indicates the grain size matrix. Circles represent the samples. The cross represents the To samples. The PC1 and PC2 are visualized in **a.**, and the PC3 and PC4 are visualized in **b.**

We then compared the microbial composition between the environmental sample at T-bef as a function of oxygen status and water content across each matrix granulometry (**Figure V.13**). The results showed that the first two components accounted for 46.5%, 70%, 66.2% and 78.9% of the variability for 2 mm, 0.5 mm, and 0.1 mm grain size matrix and in the absence of matrix, respectively. PC1 clustered samples based on their oxygen status. PC2, which explained less than 20% of the variability in all cases, separated samples based on their water content, particularly in oxic microcosms with the 0.5 mm and 0.1 mm grain size matrices. These observations suggest that (i) oxygen status was the main parameter influencing the microbial community composition, regardless of matrix grain size; and (ii) water content had a stronger effect on microbial community composition at finer grain sizes.

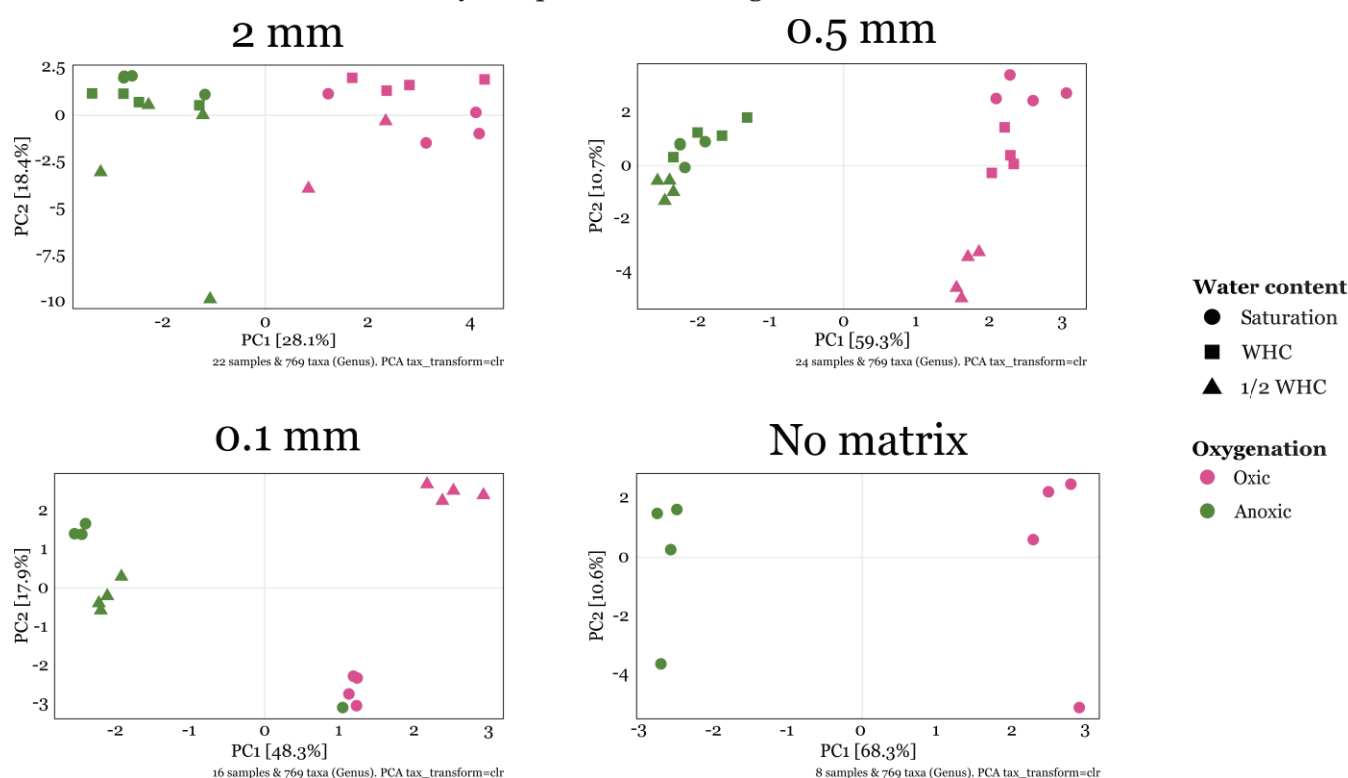


Figure V.13. PCA plot derived from clr-transformed abundance data of the genus-level phylotypes in the environmental samples before disturbance (T-bef) across matrix grain sizes. The colour indicates oxygen status and the shape indicates water content.

Next, to study the dynamics of the microbial community throughout the experiment, we compared the non-fluctuating samples (OO and AA) before the disturbance (T-bef) and at the end of the experiment (T-aft). The results showed no differences over time, suggesting that once the microbial community was established in the microcosms, it remained stable along the experiment (**Figure V.14**).

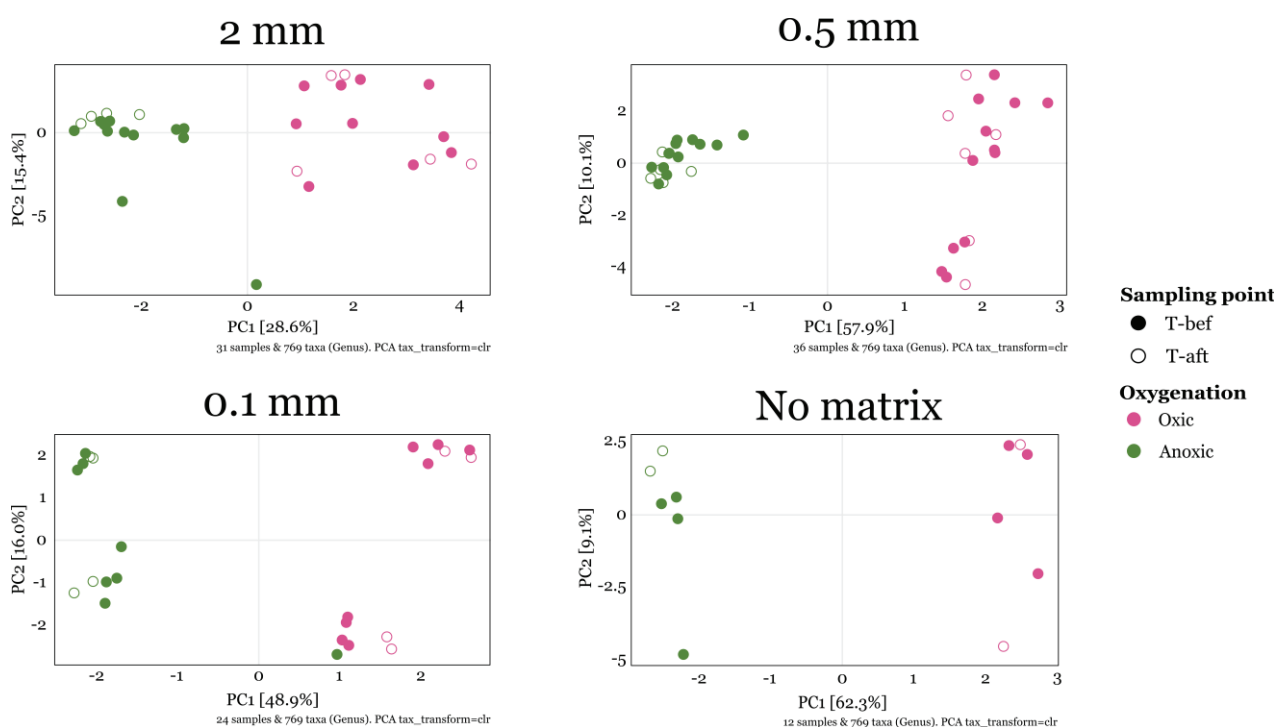


Figure V.14. PCA plot derived from clr-transformed abundance data of the genus-level phylotypes in the OO and AA environmental sample microcosms before disturbance (T-bef) and at the end of the experiment (T-aft) across matrix grain sizes. The colour indicates oxygen status. The filled symbol is from samples at T-bef and empty symbol is from samples at T-aft.

Considering the results above, we can state that all changes in the community composition observed at T-aft in the alternating microcosms can be attributed to the disturbance (**Figure V.14**). For instance, after the change in oxygen status, the microbial community composition of OA microcosms became slightly closer to AA microcosms, whereas in the AO microcosms the effect was the opposite – the microbial community composition became more similar to that of the OO microcosms. However, despite this observed trend, initial oxygen status seems more important than the second oxygen status to explain community composition, particularly at finer grain size. A longer period of time after the disturbance might have shown whether these trends would eventually lead to similar microbial community composition in microcosms with the same post-disturbance oxygen status. Overall, these results suggest that (i) changes in oxygen status did impact the microbial community composition and that the intensity of this effect increased with the matrix grain size; and (ii) the water content affects microbial community differently depending on the grain size, with samples initially under oxic condition more affected by water content at higher grain size, and samples initially under anoxic condition more affected by water content at smaller grain size.

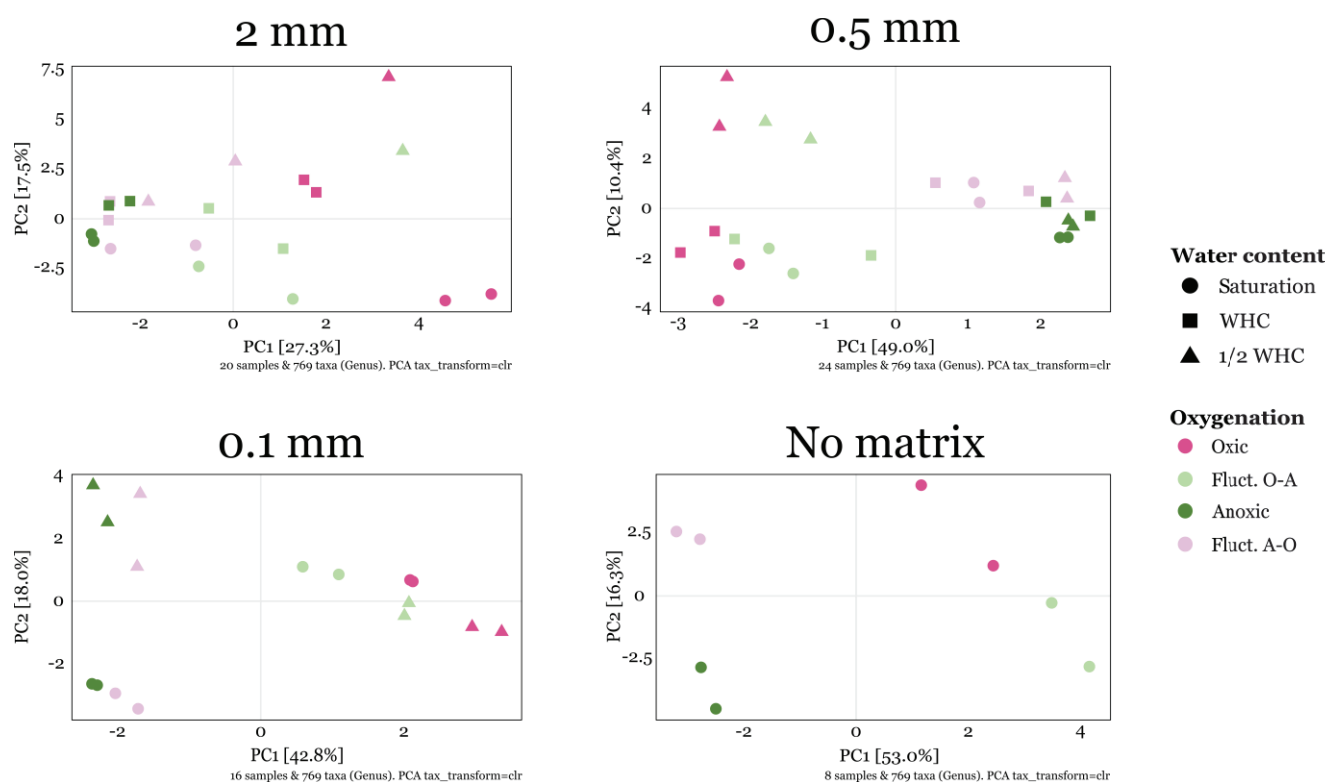


Figure V.15. PCA plot derived from clr-transformed abundance data of the genus-level phylotypes in the environmental samples at the end of the experiment (T-aft) across matrix grain sizes. The colour indicates oxygen status. The shape indicates water content.

V.3.3.4 Correlation between physicochemical parameters and bacterial community composition

The Spearman correlation test was used to identify associations between physicochemical parameters (grain size, oxygen status and water content) or the observed degradation rate, with the relative abundance of particular taxa of the microbial community. This non-parametric test is advantageous because it does not assume linear relationships or a normal data distribution. Moreover, by relying on ranks rather than actual values, it is more robust to outliers and skewed distribution, which are common on microbial data. Additionally, it captures monotonic relationships, which occur when one variable (e.g., a taxon) consistently increases or decreases as other variable (e.g., an environmental parameter) changes, although the rate of change may not be uniform.

We first conducted a Spearman correlation test on the environmental samples before the disturbance, using the microbial relative abundances at the taxonomic level of the genus. In total, 69 genera were correlated with at least one of the physicochemical parameters or the degradation rate. The results are visualized using a heatmap. For clarity, we plotted only the genera that showed significant correlation with the degradation rate (either positive or negative). This resulted in a subset of 47 genera displayed (**Figure V.16**).

The results showed that nearly all genera positively correlated with the degradation rate were also positively correlated with oxygenation (i.e., oxic conditions). This agreed with the previous observation that, before the disturbance, DCM half-life was significantly shorter in oxic conditions. Conversely, with the exception of *Alteribacillus* and *Ralstonia*, the genera that exhibited negative correlation with the degradation rate also aligned with those negatively correlated with oxygenation (i.e., anoxic conditions). Two hypotheses may explain the negative correlation of these genera with both the degradation rate and the oxygenation: (i) the bacteria were obligate anaerobes that thrive solely under anoxic conditions and did not degrade DCM (e.g., the *Proteiniphilum* genus belongs to the family *Dysgonomonadaceae* in which all members are obligate anaerobes); or (ii) the bacteria were aerobes capable of tolerating anoxic conditions and did not degrade DCM. In this case, their relative abundance was enhanced in the absence of DCM-degrading taxa (e.g., the family *Alcaligenaceae*, which includes the genus *Acrhomobacter*, was the most abundant taxa in the abiotic controls with the 0.5 mm grain size matrix, where DCM degradation did not occur (see **Figure V.4**)). Altogether, these results suggest that oxygenation was the main parameter influencing the DCM-degrading taxa before the disturbance.

A fewer number of taxa showed significant correlation with water content. This suggests that the contribution of this parameter to the selection of the DCM-degrading population was less substantial than the oxygen status. Among the genera positively correlated with water content, we found *Hyphomicrobium* of the *Hyphomicrobiaceae* family, which aligns with previous observations indicating that this family may be sensitive to low water content during the experiment. Additionally, the *Hyphomicrobium* genus was positively correlated with both oxygenation and the degradation rate, suggesting its association with the DCM-degrading population in oxic conditions during the experiment. Conversely, among the genera that were positively correlated with the degradation rate but negatively correlated with water content, the genus *Paenarthrobacter*, which belongs to the family *Micrococcaceae*, was the only genus to show a significant negative correlation. This genus has been associated with the biodegradation of atrazine in the literature, but there is no information about its water activity (Jia et al., 2021). Nevertheless, in that work, Jia and colleagues reported an improvement in atrazine removal in the presence of a strain from the genus *Paenarthrobacter* in soil which moisture content was maintained at 30% of its WHC. This aligns with our observation that this genus may be correlated with low water content.

Finally, the matrix grain size was significantly associated to about half of the listed taxa correlating with DCM degradation activity. Interestingly, most genera that negatively correlated with matrix grain size (i.e., more abundant with finer grain sizes) were positively correlated with water content (i.e., more abundant at greater water contents). Considering that these genera were associated with DCM degradation, this suggests that DCM-degrading populations established in finer grain sizes were favoured at higher water contents. It is important to note that this result may be strongly influenced by the inclusion of samples without matrix (value of matrix set to 0), where water content was considered as saturation in

the analysis. This means that it is possible that the genera that were the most negatively correlated to the matrix grain size, i.e., the genus *Sphingoaurantiacus* and *Limnohabitans*, may be linked to planktonic lifestyle. For instance, the genus *Limnohabitans* is described in the literature a common member of the bacterioplankton in freshwater habitats (Grujić et al., 2015). On the other hand, among the genera that were the most significantly positively correlated with matrix grain size (i.e., more abundant at greater grain sizes), we found the genera *Dyadobacter* and *Mycobacterium* (p-value <0.01). These genera were significantly positively correlated to oxygen concentration, while no significant correlation was found with water content. Previous studies have linked some members of this genera with the capacity of biofilm formation (Dow et al., 2020; Muñoz-Egea et al., 2023). Therefore, this trait could have been advantageous in the presence of the larger grain sizes, potentially improving their tolerance to the hydric stress, which may be greater with larger grain sizes.

Lastly, we conducted a Spearman correlation test on the environmental samples after the disturbance, using the microbial relative abundances at the taxonomic level of the genus. In total, 32 genera were correlated with at least one of the physicochemical parameters or the degradation rate. The results are visualized using a heatmap. For consistency with the previous analysis, we plotted only the genera that showed significant correlation with the degradation rate (either positive or negative). This resulted in a subset of 16 displayed genera (**Figure V.17**).

First, there was a decreased in the number of genera that were significantly correlated with the DCM-degradation. One hypothesis is that some of the bacteria previously associated to DCM degradation became inactive after the disturbance due to unfavourable oxygen status. However, in microcosms where the oxygen status remained unchanged, these same taxa continued to degrade DCM. As a result, the strong relationship observed before the disturbance may have been weakened. Among the genera that remained significantly correlated with DCM degradation, 8 genera (i.e., *Rhodoligotrophos*, *Bauldia*, *Galbitalea*, *Hyphomicrobium*, *Reyranella*, *Phenylobacterium*, *Pajaroellobacter*, and *Pseudorhodoplanes*) continued to show positive correlation with this parameter. Among them, the genera *Rhodoligotrophos* (Liu et al., 2019b), *Hyphomicrobium* (Bringel et al., 2017), *Phenylobacterium* (Kanso & Patel, 2004), and *Pseudorhodoplanes* (Tirandaz et al., 2015) include facultatively anaerobic members. The new taxa positively correlated with the degradation rate could be related with the latent microbial functional diversity observed in the AO microcosms.

The same pattern of inconsistent positive correlation before and after disturbance was observed for oxygen status. As hypothesized before, this may be due to the loss of the necessary conditions for these bacterial activities following the shift from oxic to anoxic conditions, while the same bacteria remained active in the non-disturbed microcosms. Finally, no changes were observed in the correlations between these genera and water content or matrix granulometry when compared to their state before the disturbance. This suggests that the association of this

genera with these parameters was independent of the oxygen status or their ability to degrade DCM.

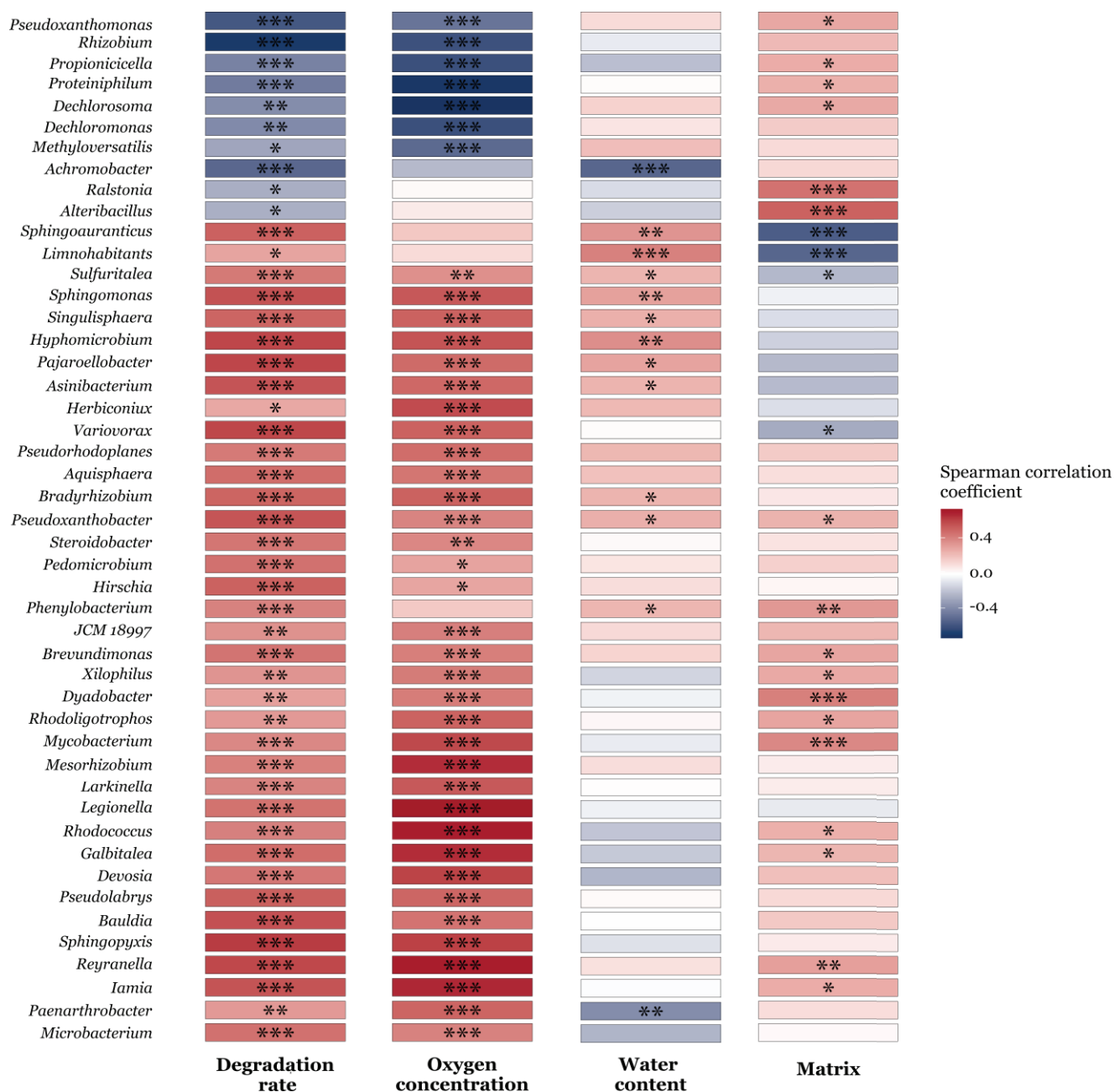


Figure V.16. Heatmap displaying the Spearman correlation coefficients between the relative abundance of specific genera before the disturbance and the physicochemical parameters (oxygen concentration, water content and matrix granulometry) as well as the observed degradation rate. The figure shows the subset of 47 genera (out of 69 genera correlated with at least one parameter) that had a significant positive or negative correlation with the degradation rate. The colour gradient represents the value of the correlation coefficient, with shades of red indicating positive correlation and shades of blue indicating negative correlation. The asterisks represent statistical significance of the correlations: * for p-value < 0.05; ** for p-value < 0.01; and *** for p-value < 0.001.

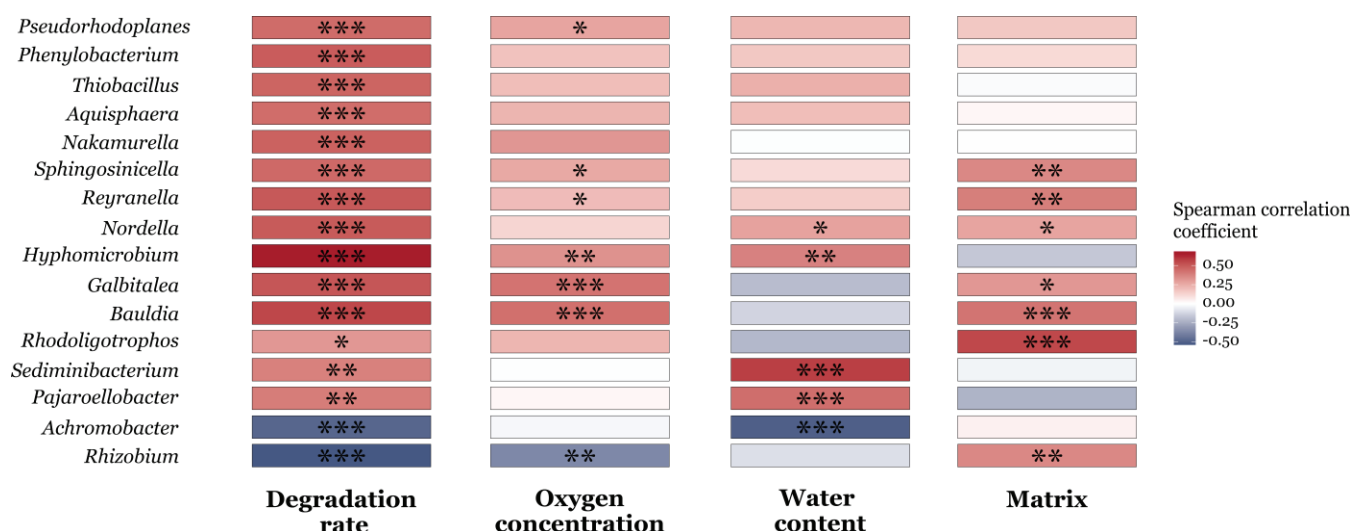


Figure V.17. Heatmap displaying the Spearman correlation coefficients between the relative abundance of specific genera after the disturbance and the physicochemical parameters (oxygen concentration, water content and matrix granulometry) as well as the observed degradation rate. The figure shows the subset of 16 genera (out of 32 genera correlated with at least one parameter) that had a significant positive or negative correlation with the degradation rate. The colour gradient represents the value of the correlation coefficient, with shades of red indicating positive correlation and shades of blue indicating negative correlation. The asterisks represent statistical significance of the correlations: * for p-value < 0.05; ** for p-value < 0.01; and *** for p-value > 0.001.

The Spearman correlation test facilitates the identification of genera potentially associated to the parameters of interest (grain size, oxygen status, water content and degradation rate). However, a limitation of this analysis is that the observed correlations for each genus include the individual correlations of each ASVs within the genus, which may vary along individual ASVs. As a result, distinct correlations at the ASV level may be neutralized or lost. To address this issue, we further perform an analysis at the ASV level to explore the indicator species (i.e., species/ASVs whose status provides information on the overall condition of the ecosystem) that were correlated to specific physicochemical setups. Among these indicator species, we focused on those that were specifically associated with the DCM-degrading function. As a result, 212 ASVs were identified as indicator species in the environmental sample microcosms across the different experimental conditions tested. Among them, 11 ASVs were found as indicator species of DCM-degradation irrespectively of the water content, oxygen status and matrix granulometry. The rest were associated with particular experimental setups. For space reasons, **Table V.4** show the indicator species whose significance was below a p-value of 0.001 (74 ASVs). The complete table is in **Supplementary table V.2**.

Table V.4. Indicator species in the environmental samples along the experiment that correlated with DCM-degradation. Cells marked with the symbol ‘-’ indicate no correlation to a specific value of that respective physicochemical parameter.

ASV	Grain size matrix	Water content	Oxygen status T-bef	Oxygen status T-aft	Genus
ASV1392	No matrix	No matrix	-	-	<i>A4b</i> of unknown genus
ASV843	0.5 mm	-	Oxic	-	<i>Aminobacter</i>
ASV22	No matrix	No matrix	Oxic	-	<i>Asinibacterium</i>
ASV1266	No matrix	No matrix	Oxic	-	<i>Asinibacterium</i>
ASV316	-	-	Oxic	-	<i>Bauldia</i>
ASV631	-	-	Oxic	-	<i>Bauldia</i>
ASV2488	No matrix	No matrix	-	-	<i>Bauldia</i>
ASV453	No matrix	No matrix	Oxic	-	<i>Blastocatellaceae</i> of unknown genus
ASV157	-	-	Oxic	-	<i>Bradyrhizobium</i>
ASV47	-	½ WHC	Oxic	-	<i>Devosia</i>
ASV413	-	-	Oxic	-	<i>Devosia</i>
ASV3102	-	½ WHC	Oxic	-	<i>Devosia</i>
ASV34	-	-	Oxic	-	<i>Edaphobaculum</i>
ASV2342	-	-	Oxic	-	<i>Edaphobaculum</i>
ASV741	2 mm	-	Oxic	-	<i>Gaiellales</i> of unknown family of unknown genus
ASV531	-	-	Oxic	-	<i>Gaiellales</i> of unknown family of unknown genus
ASV630	-	WHC	Oxic	-	<i>Gaiellales</i> of unknown family of unknown genus
ASV1697	No matrix	No matrix	Oxic	-	<i>Gaiellales</i> of unknown family of unknown genus
ASV4262	0.5 mm	-	Oxic	-	<i>Galbitalea</i>
ASV45	2 mm	-	Oxic	-	<i>Galbitalea</i>
ASV850	0.5 mm	-	Oxic	-	<i>Hirschia</i>
ASV457	-	-	Oxic	-	<i>Hyphomicrobium</i>
ASV14	No matrix	No matrix	Oxic	-	<i>Hyphomicrobium</i>
ASV93	-	-	Oxic	-	<i>Iamia</i>
ASV5297	0.5 mm	-	Oxic	-	<i>Iamia</i>
ASV632	-	-	Oxic	-	<i>Ilumatobacteraceae</i> of unknown genus
ASV535	2 mm	-	Oxic	-	<i>Ilumatobacteraceae</i> of unknown genus
ASV2315	2 mm	-	Oxic	-	<i>JCM 18997</i>
ASV1226	-	-	Oxic	-	<i>JG30-KF-CM45</i> of unknown genus

ASV204	-	-	Oxic	-	<i>JG30-KF-CM45</i> of unknown genus
ASV86	2 mm	-	Oxic	-	<i>JG30-KF-CM45</i> of unknown genus
ASV1710	0.5 mm	-	Oxic	-	<i>Lautropia</i>
ASV95	No matrix	No matrix	Oxic	-	<i>Legionella</i>
ASV225	-	-	Oxic	-	<i>Microbacteriaceae</i> of unknown genus
ASV241	0.5 mm	1/2 WHC	Oxic	-	<i>Microbacterium</i>
ASV846	0.5 mm	-	Oxic	-	<i>Microtrichaceae</i> of unknown genus
ASV617	-	-	Oxic	-	<i>Mycobacterium</i>
ASV610	-	-	Oxic	-	<i>Mycobacterium</i>
ASV118	2 mm	Saturation	Oxic	-	<i>Mycobacterium</i>
ASV3014	-	-	Oxic	-	<i>Nakamurella</i>
ASV615	0.5 mm	-	Oxic	-	<i>Nocardioides</i>
ASV199	-	-	Oxic	-	<i>Nordella</i>
ASV71	-	No matrix	Oxic	-	<i>Pajaroellobacter</i>
ASV3029	No matrix	No matrix	Oxic	-	<i>Pajaroellobacter</i>
ASV337	0.5 mm	-	Oxic	-	<i>Pedomicrobium</i>
ASV1765	0.5 mm	-	Oxic	-	<i>Pedomicrobium</i>
ASV304	No matrix	No matrix	-	-	<i>Phenylbacterium</i>
ASV184	0.5 mm	-	Oxic	-	<i>Phreatobacter</i>
ASV313	0.5 mm	-	Oxic	-	<i>Prostheco bacter</i>
ASV4216	0.5 mm	-	-	-	<i>Prosthecomicrobium</i>
ASV122	-	-	Oxic	-	<i>Pseudolabrys</i>
ASV1633	0.5 mm	-	Oxic	-	<i>Pseudomonas</i>
ASV1311	-	-	Oxic	-	<i>Pseudorhodoplanes</i>
ASV67	No matrix	No matrix	-	-	<i>Pseudoxanthobacter</i>
ASV226	-	-	Oxic	-	<i>Reyranella</i>
ASV159	2 mm	-	Oxic	-	<i>Reyranella</i>
ASV298	2 mm	-	Oxic	-	<i>Reyranellaceae</i> of unknown genus
ASV555	0.5 mm	-	Oxic	-	<i>Rhizobiaceae</i> of unknown genus
ASV5	-	-	Oxic	-	<i>Rhodococcus</i>
ASV456	-	1/2 WHC	Oxic	-	<i>Rhodococcus</i>
ASV270	0.5 mm	-	Oxic	-	<i>Rhodococcus</i>
ASV647	-	1/2 WHC	Oxic	-	<i>Rhodococcus</i>

ASV796	2 mm	WHC	Oxic	-	<i>Rhodoligotrophos</i>
ASV3199	No matrix	No matrix	-	-	<i>SC-I-84</i> of unknown genus
ASV160	-	-	Oxic	-	<i>Singulisphaera</i>
ASV82	-	-	Oxic	-	<i>Singulisphaera</i>
ASV1070	0.5 mm	-	Oxic	-	<i>Sphingomonas</i>
ASV112	0.5 mm	-	Oxic	-	<i>Sphingopyxis</i>
ASV248	-	-	Oxic	-	<i>Sphingosinicella</i>
ASV667	0.5 mm	-	Oxic	-	<i>Steroidobacter</i>
ASV735	-	-	-	-	<i>Thiobacillus</i>
ASV1876	-	-	Oxic	-	<i>Thiobacillus</i>
ASV26	0.5 mm	WHC	Oxic	-	<i>Variovorax</i>
ASV916	0.5 mm	WHC	Oxic	-	<i>Variovorax</i>

V.4 Discussion

V.4.1 Impact of physicochemical parameters on DCM degradation kinetics and microbial community composition

During GLF, the physicochemical parameters in the fluctuating zone are significantly impacted, notably the water content and the oxygen status in the area (Chen et al., 2020b). The extent of these changes is closely linked to the granulometry of the aquifer sediment, influencing the WHC (i.e., the amount of water retained in the matrix against gravity) of the sediment during the period of drainage. Previous experiments in laboratory microcosms have shown that water content and oxygen status individually influence the DCM degradation kinetics and microbial community composition (see **chapter III**). In this study, we aimed to integrate these two parameters with varying matrix granulometry to investigate how different combinations of these three factors impacted both the function and composition of a DCM-degrading microbial community.

Our results showed that the principal barrier to DCM degradation activity by the microbial community was water availability. When water content was too low, such as in microcosms at ½ WHC with the 2 mm grain size matrix (i.e., total liquid volume of 0.3 mL), the DCM-degradation activity was not detected, despite a gene encoding this function (*dcmA*) was detectable. This dependence on water content aligns with previous studies, which linked water limitation to nutrient deficiency, limited gas diffusion and restricted motility (Or et al., 2007). Under such conditions, microbial communities either adapt to cope with the physiological stress, such as developing nutrient storage capacity or employing other survival mechanisms (e.g., cell membrane modification, EPS synthesis, osmolyte uptake and/or synthesis), or

experienced a cessation of activity. For example, Uhlířová and colleagues reported a decline in microbial viability and activity when soil microbial communities were exposed to lower water contents, attributing this to water and nutrient deficiency (Uhlířová et al., 2005). Additionally, they observed a shift in the community composition toward more gram positive bacteria, which are inherently more resistant to desiccation due to their rigid cell walls and ability to form spores. In our experiment, the generalized absence of DCM degradation at low water content with the 2 mm grain size matrix suggests that the microbial community we are studying may either require more time to adapt to the physiological stress imposed by low water content or is predominantly sensitive to it.

When water content was not a limiting factor for microbial activity, the main determinant of DCM biodegradation activity was oxygen status. Indeed, before the disturbance, DCM degradation was observed earlier and led to a shorter DCM half-life under oxic conditions, suggesting that the development of the DCM-degrading populations was favoured in this condition. This result was intriguing, as the previous study in laboratory aquifers (Prieto-Espinoza et al., 2021) from which our environmental inoculum was derived, demonstrated the dominance of anaerobic DCM degradation pathways using compound-specific isotope analysis (CSIA). Moreover, under water level fluctuations, which enhanced DCM biodegradation in these laboratory aquifers, the dominant taxa were those typically associated with anoxic DCM degradation, such as the genera *Dehalococcoides*, *Sulfurospirillum*, *Desulfosporosinus* and *Geobacter*. Interestingly, with the exception of *Dehalococcoides*, which was not detected in any case, these genera were found in our initial inocula. Possible explanations for this difference could include: (i) the storage conditions of the environmental inocula, which may not have been suitable for preserving strictly anaerobic bacteria, leading to the loss of these taxa by the time the experiment started; or (ii) the experimental set-up may have lacked some essential elements (e.g., nutrients or electron acceptors) or had different environmental conditions (e.g., no water flow) compared to the laboratory-scale aquifers, impairing the activity or growth of these taxa. In addition, the *mecE-F* genes, which are biomarkers for anaerobic DCM degradation, were not detected prior to the disturbance in any of the environmental sample microcosms tested (**Table V.2**). This finding supports the theory that the relative abundance of taxa capable of this metabolism was too low to be detected.

When DCM degradation occurred under oxic conditions, water content along with matrix grain size exerted a third layer of influence over the activity and composition of the microbial community. Firstly, water content determined the degradation activity intensity - lower water content resulted in shorter DCM half-life in both the environmental samples and in the biotic controls inoculated with *Hyphomicrobium* sp. GJ21. The water conditions associated with the shortest DCM half-life varied depending on the matrix grain size: WHC favoured DCM degradation with the 2 mm grain size matrix, while for the 0.5 mm and 0.1 mm grain sizes, 1/2 WHC seemed more suitable, with the 0.1 mm grain size matrix showing a slightly longer DCM half-life than with the 0.5 mm grain size. This suggests that the optimal DCM degradation with the 0.1 mm grain size matrix could potentially occur at an even lower water content than the

tested conditions. The literature reporting experiments on field soil containing a natural gradient of textures showed a decline in aerobic bacterial activity as soil pore space is filled with water, primarily due to the lower diffusion rate of oxygen in water compared to air (Schjønning et al., 2003). Along with the studies of Skopp and colleagues (Skopp et al., 1990), they proposed a conceptual model that identified an optimum point for microbial activity, occurring when both the diffusion coefficients for nutrients and gases are maximized (**Figure V.18-a.**). This optimum appeared to be influenced by soil texture, being higher in clay-rich soils compared to sandy soils, a difference attributed to the higher gas diffusivity in sandy soil. Using mathematical models, Moyano and colleagues suggested that larger grain sizes increase soil pore space and consequently reduce oxygen diffusion limitations at the same water content (Moyano et al., 2013) (**Figure V.18-b.**). These observations align with our experiment results, where the optimal water content for rapid DCM degradation increased with larger grain sizes. Additionally, the effect of water content on the microbial community composition varied with matrix grain size: finer granulometries showed greater variation between samples at different water contents, i.e. communities at different water contents within the same granulometry were more distinct in finer grain size matrices (**Figure V.13**). One hypothesis to explain these results is that at higher granulometry, the larger pore sizes allow for sufficient oxygen diffusion even at WHC, allowing for microbial activity. As a result, at higher grain size the microbial community composition was less influenced by water content and was mainly driven by differences in oxygen status. In contrast, at finer granulometries, water content at WHC tends to fill the smaller pores, reducing oxygen diffusion. Consequently, water content had a stronger impact on the microbial community composition in these finer granulometry microcosms.

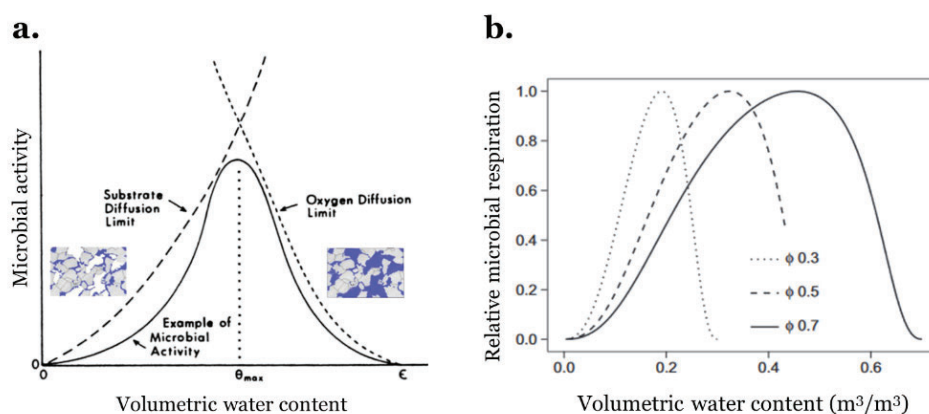


Figure I.18. Relationship between soil water content and microbial activity. **a.** Conceptual plot proposed by Skopp and colleagues (Skopp et al., 1990). The dotted lines represent the theoretical upper limits for either substrate or oxygen diffusion rates. The solid line illustrates the microbial activity that was observed under a given set of environmental conditions in a previous study. θ_{max} corresponds to the water content at maximum activity, and ϵ corresponds to saturated water content. Figure adapted from Or et al. (2007). **b.** Effect of soil pore space on the relationship between microbial respiration activity and volumetric water content. The different lines represent varying soil pore spaces (Φ). Figure adapted from Moyano et al. (2013).

Finally, some differences were observed in the taxonomical composition of the microbial community depending on the matrix grain size, regardless of the water content. For example, the family *Pseudomonadaceae* was significantly more abundant in microcosms with 0.1 mm grain size matrix, while *Chitinophagaceae* was significantly more abundant in microcosms without a matrix (see **section V.3.3.1**). These differences were also evident when plotting the PC3 and PC4 axes in the PCA analysis (**Figure V.12-b.**), which showed clustering of samples based on matrix granulometry. Together, these observations suggest that the matrix exerted some selective influence on specific taxa during the experiment, especially considering that the initial inocula used across the different matrices were compositionally similar (**Figure V.12-a.**). In this regard, previous studies have shown that microbial community structure can indeed be influenced by particle size fractions, correlating specific bacterial taxa with specific sediment grain sizes (Legg et al., 2012; Sessitsch et al., 2001). For example, phyla such as *Firmicutes* and *Alphaproteobacteria* were found to dominate in sandy sediments ($\phi > 0.1$ mm), whereas the phyla *Chloroflexi* and *Deltaproteobacteria* were most abundant in silty sediments ($\phi \leq 0.1$ mm). However, it is important to note that these types of studies have been carried out in natural sediments, where each particle size fraction has distinct mineral composition and surface properties that can also influence microbial community composition (Hemkemeyer et al., 2014). In contrast, our study used the same artificial matrix across the different grain sizes. Therefore, our findings reinforce these previous works by highlighting the direct effect granulometry of the matrix on microbial community. However, our work along with the literature highlighted that pore size and connectivity rather than grain size might be the important factor (Payton et al., 2022). Future research could explore the use of particles of the same size (i.e., equivalent volume or surface), but with varying shapes (e.g., beads of different sphericity, cubes, or rectangular prisms) to create matrices with distinct porosity.

The correlation analyses suggested that oxygen status was the main factor influencing the DCM-degrading microbial taxa, with most genera positively correlated with DCM degradation also showing a positive correlation with oxic conditions. Fewer genera were significantly correlated with either water content or matrix granulometry, indicating that these parameters had a lower contribution to the selection of the DCM-degrading microbial taxa. In general, through these analyses, we were able to identify various genera and individual ASVs significantly correlated with specific physicochemical characteristics. However, it was not possible to directly determine which taxa were responsible for the DCM degradation during the experiment. This limitation arises from working at the DNA-level, as sequencing is performed in DNAs coming from all active and non-active community members. To study the active microbial populations responsible for the DCM-degrading function under the different experimental conditions, further experiments should thus focus on either the gene expression within each microcosm (e.g., metatranscriptomics) or the specific labelling of taxa actively degrading DCM (e.g., DNA-Stable Isotope Probing technique). These approaches will be discussed in the **chapter VII** under the perspectives of my work.

V.4.2 Response of DCM-degrading microbial community to a change in oxygen status

Water level fluctuations cause temporal variations in redox conditions within the fluctuating zone, stimulating microbial activity (Jost et al., 2015). In laboratory-scale aquifers, water level fluctuations resulted in an increase in dissolved oxygen concentration in the fluctuating zone each time the water table rose compared to an aquifer where the water level has not decreased. This increase was attributed to the entrapment of air within the sand matrix during these fluctuations (Prieto-Espinoza et al., 2021). In the work presented in **chapter III**, we found that periodic alternation in oxygen status over time impacted DCM-degrading activity and bacterial community composition. Notably, this impact was highly dependent on the initial oxygen status to which the samples were exposed to (see **section III.4.2**). However, these observations were obtained exclusively at water saturation and required further investigation at other water contents.

Our results here showed that, as observed in **chapter III**, the initial oxygen status influenced the response of the microbial community to the disturbance. When the oxygen status switched from oxic to anoxic conditions, the DCM-degrading function was either maintained (i.e., the microbial community was resilient/resistant to the disturbance) or lost (i.e., the microbial community was sensitive to the disturbance). One hypothesis to explain these findings is that, since the microbial communities were initially exposed to oxic conditions, only DCM-degrading populations capable of surviving in this environment (i.e., aerobic and facultatively anaerobic bacteria) were able to develop and colonize the beads of these microcosms. Consequently, when the oxygen status shifted to anoxic conditions, only a reduced number of taxa could adapt their metabolism to the absence of oxygen (i.e., only taxa with facultatively anaerobic metabolism). In general, the literature indicates that DCM degradation under anoxic conditions is mainly catalysed by strict anaerobic bacteria (Chen et al., 2020a; Holland et al., 2021; Kleindienst et al., 2017). The exception is *Hyphomicrobium* isolates, notably the strain *Hyphomicrobium* sp. GJ21, which are the only isolated representatives known to degrade DCM both anaerobically and aerobically (Bringel et al., 2017; Kohler-Staub et al., 1995). During our experiment, DCM degradation was either immediately lost or, in some cases, took time to recover (indicating resilience) after the change in the oxygen status. This suggests that the facultative anaerobic metabolism was either absent in the DCM-degrading populations in our or that microorganisms with this metabolism required more time to become active after the disturbance. Interestingly, biomarkers genes *mecE-F* for DCM degradation under anoxic conditions were detected in all tested microcosms at T-aft (**Table V.2**), in contrast with at T-bef (**Table V.3**). This finding supports the hypothesis that the DCM-degrading populations with this metabolic pathway were present in the samples but likely needed time to restore activities and/or to reach the relative abundance of detectability. Longer monitoring of microcosms where the function was lost would have been necessary to confirm this hypothesis.

On the other hand, when the oxygen status changed from anoxic to oxic conditions, the DCM-degrading function persisted (i.e., tolerance) in 2 microcosms (i.e., with the 0.5 mm grain size matrix under water saturation and at WHC); it emerged (i.e., latent microbial functional diversity) in 4 microcosms (i.e., with the 2 mm grain size matrix and the 0.5 mm at $\frac{1}{2}$ WHC); and it was still not detected in the 2 other microcosms (i.e., with the 0.1 mm grain size matrix). No case of loss of function (i.e., sensitivity) was reported here. The emergence of the function under oxic conditions suggests the presence of DCM-degrading populations that remained in a dormant state under anoxic conditions and became active only when conditions turned favourable (i.e., in the presence of oxygen). This behaviour has been described in the literature before and is essential for the adaptation and resilience of microbial communities to environmental changes (Shade, 2023; Smith et al., 2022). One hypothesis to explain the absence of DCM degradation function in microcosms with the 0.1 mm grain size matrix, even after the shift to oxic conditions, is that the reduced pore spaces of this matrix constrain oxygen diffusion at any of the tested water contents. Consequently, the DCM-degrading populations either required more time to develop or were not sufficiently exposed to oxygen to become active. This highlights again that pore size and connectivity might be more important than grain size in explaining our observations.

The shift in the microbial community composition after the disturbance appeared to be deterministic in all cases. For instance, the composition in microcosms changing from oxic to anoxic conditions became closer to that observed under anoxic conditions, while the composition of the microcosms changing from anoxic to oxic conditions became closer with those under oxic conditions (**Figure V.12**). No differences were observed based on matrix granulometry or water content, suggesting that the effect of the disturbance was not influenced by these parameters or the differences in microbial community composition arising from them before the disturbance. A longer period of time after the disturbance might have shown whether the disturbed microbial communities would eventually converge with those in the microcosms that were not disturbed.

V.5 Conclusions

Here, we investigated (i) the impact of the water content, oxygen status, and matrix granulometry on the activity and composition of a DCM-degrading microbial community; and (ii) the response of the established microbial community to a disturbance, that is a shift in oxygen status. The results showed that, before the disturbance, water content was the main determinant of DCM-degrading microbial activity. When water content was favourable for the activity to develop, oxygen status became the main parameter influencing both DCM degradation kinetics and microbial community composition. In particular, oxic conditions promoted rapid and stable DCM biodegradation, whereas anoxic conditions limited both function and microbial diversity. Additionally, under oxic conditions, the combination of water content and matrix grain size imposed an additional level of control. Notably, finer the grain

size required lower water content to reach optimal DCM biodegradation, highlighting the potential of matrix pore size over grain size. Finally, the initial oxygen condition to which the microbial community was exposed determined its DCM degradation activity response to the disturbance: when changing from oxic to anoxic conditions, DCM degradation was either maintained or lost, whereas changing from anoxic to oxic conditions led to the emergence of the function in most cases. This highlighted the key role of environmental conditions at controlling the activity of microbial community.

Supplementary information - chapter V

Supplementary Table V.1. DNA concentration and results after the quality control steps. Columns from 4 to 10 correspond to number of reads per sample after (4) filtering, (5) trimming, (6) denoising the forward reads, (7) denoising the reverse reads, (8) merging the forward and reverse reads, (9) removal of the chimeras, and (10) % of reads that remain after the QC steps. For space reasons, the table is found in the following seafire-cloud link: [Supplementary Table V.1](#)

Supplementary Table V.2. Indicator species at the ASV-level in the environmental samples along the experiment. Cells marked with the symbol ‘-’ indicate no correlation to a specific value of that respective physicochemical parameter. The asterisks represent statistical significance of the association: * for p-value <0.05; ** for p-value <0.01; and *** for p-value >0.001. For space reasons, the list is found in the following seafire-cloud link: [Supplementary Table V.2](#)

Chapter VI

Effect of oxygen concentration
on *Hyphomicrobium* sp. GJ21
gene expression

VI.1 Introduction

In aquifers, one of the most common environmental disturbances is groundwater level fluctuations (GLF). They consist of changes in the water table caused by external factors, such as evapotranspiration, precipitation and groundwater withdrawals (Wu et al., 2020). During this process, a fluctuating zone is created between the continuously saturated zone and the continuously unsaturated zone which is characterized by temporal variations not only in water saturation, but also in other physicochemical parameters, such as oxygen concentration. In the fluctuating zone, as the water table rises up (imbibition period), gas diffusion is reduced and results in lower oxygen concentration in the fluctuating zone. Conversely, when the water table drops (drainage period), solute concentrations decrease with water content, while gas exchange is enhanced. These shifts cause changes in the microbial metabolic patterns, as microorganisms either switch to alternative electron acceptors to remain active or enter a dormant state. Thus, microorganisms with metabolic plasticity and redox tolerance mechanisms are usually favoured in regions affected by GLF (Rosenberg & Freedman, 1994), notably denitrifying microorganisms.

Indeed, the most common form of nitrate respiration is denitrification and consists of the reduction of nitrate (NO_3^-) to dinitrogen (N_2) through four sequential reactions ($\text{NO}_3^- \rightarrow \text{NO}_2^- \rightarrow \text{NO} \rightarrow \text{N}_2\text{O} \rightarrow \text{N}_2$). These reactions are catalyzed by the enzymes nitrate reductase, nitrite reductase, nitric oxide reductase, and nitrous oxide reductase, respectively. In general, both the denitrification pathway and aerobic respiration rely on the same core respiratory machinery, which includes NADH dehydrogenase (complex I), a quinone pool (Q), the bc1 complex (complex III), and cytochrome c (cyt.c) (**Figure VI.1**) (Chen & Strous, 2013). However, each pathway also has its own specific modules: aerobic respiration presents a terminal oxidase (complex IV) in charge of the reduction of O_2 to H_2O , while the denitrification pathway comprises four unique modules - the enzymes mentioned above - that are essential for the reduction of NO_3^- to N_2 . The differences in the modules of the electron transport chain result in distinct bioenergetic outcomes: less energy is conserved during the denitrification because fewer protons are translocated to the periplasm in this process (10 H^+ vs. 6 H^+ per electron pair for aerobic respiration and denitrification, respectively).

The family *Hyphomicrobiaceae* is widespread in aquatic and soil environments, including in aquifers (Oren & Xu, 2014). This family of gram-negative bacteria is known for its metabolic, morphological, and ecological diversity. Many members exhibit filamentous hyphae or prosthecae, through which they reproduce by budding. The *Hyphomicrobium* genus, the type genus of this family, consists of facultatively methylotrophic bacteria capable of using C1 compounds, such as methanol and methylamine, as their sole carbon and energy source. While most members of this genus are aerobic chemoorganotrophs, some representatives, including *H. nitratorans*, *H. denitrificans*, and *H. zavarzini* (Martineau et al., 2015), can grow anaerobically via denitrification. In this work, we focused on *Hyphomicrobium* sp. GJ21, a facultative denitrifying bacterium with the unique ability to utilize DCM as its sole carbon and energy source under both oxic and anoxic conditions using the metabolic pathway involving the DCM

dehalogenase DcmA. Due to its metabolic capacity to use DCM under both oxygen and nitrate respiration, *Hyphomicrobium* sp. GJ21 has frequently been used as a model for DCM bioremediation in aquifers (Hermon et al., 2018). Its genome was sequenced and fully annotated by Bringel and colleagues, resulting in a final assembly of 1 circular scaffold comprising 4 contigs, totalling 3.84 Mb in size with a GC content of 60.8% and 4 097 encoded genes (Bringel et al., 2017). However, little is known about its gene expression dynamics, particularly in response to changes in the oxygen concentration, which likely involve the differential expression of key genes from both aerobic and anaerobic respiration pathways (Martineau et al., 2015). Therefore, the aim of our work was to compare the genes expression of *Hyphomicrobium* sp. GJ21 exposed to either oxic ($[O_2] \sim 8$ ppm) or anoxic ($[O_2] < 0.05$ ppm) conditions to identify which genes expressions were impacted by this parameter. To achieve this, total RNA was extracted from mid-exponential phase cultures of *Hyphomicrobium* sp. GJ21 grown under either oxic or anoxic conditions with DCM as sole carbon and energy source. The mRNAs were then sequenced, and differential gene expression was examined and correlated with each oxygen concentration.

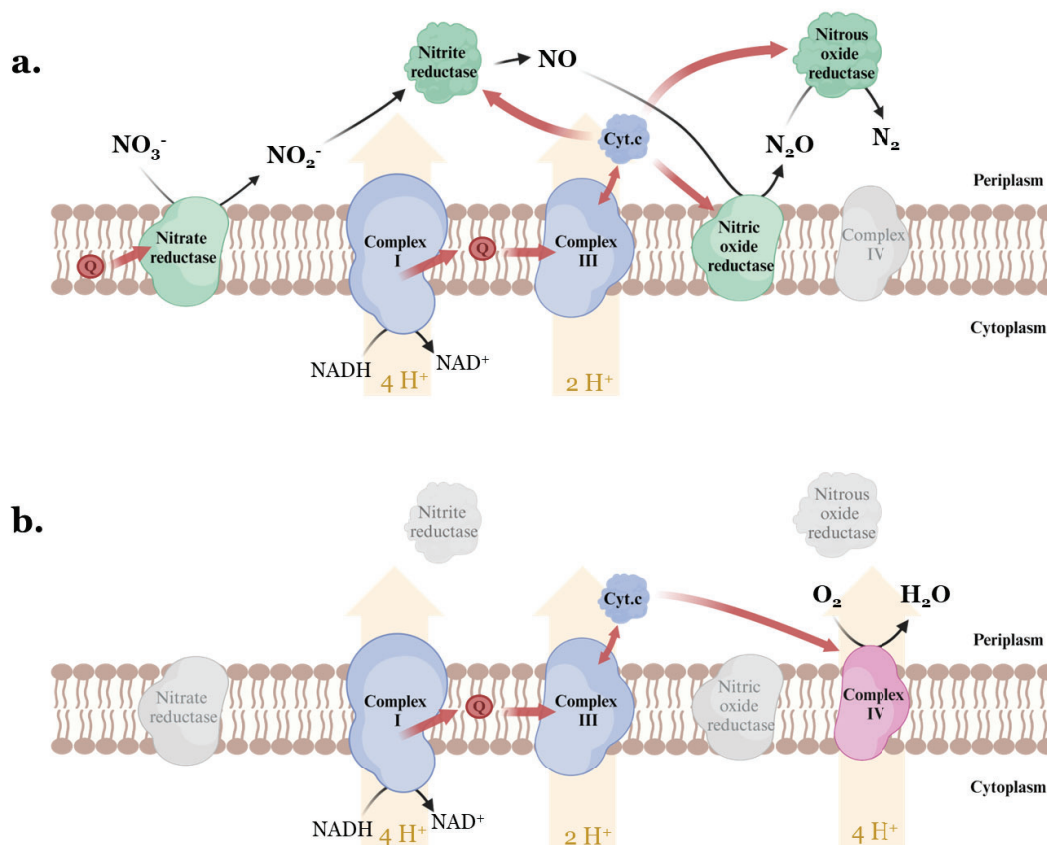


Figure VI.1. Respiratory chains during (a.) denitrification and (b.) aerobic respiration. The common modules among these two respiration pathways are the complex I and III, which consists of the NADH dehydrogenase and the bc1 complex, respectively, and the cytochrome c (cyt.c). Red arrows correspond to electron fluxes and yellow arrows correspond to proton (H^+) transport from the cytoplasm to the periplasm per transported electrons pair. Q corresponds to the quinone pool. Figure adapted from Chen & Strous (2013).

VI.2 Materials and methods

VI.2.1 Cultivation of the model strain *Hyphomicrobium* sp. GJ21

VI.2.1.1 Characterisation of growth

The growth of the model strain *Hyphomicrobium* sp. GJ21 was characterized in oxic ($[O_2] \sim 8$ ppm) and anoxic ($[O_2] < 0.5$ ppm) conditions to identify the different growth phases and determine when the exponential phase occurs to perform RNA extraction.

Cultures were established in 160 mL serum bottles by inoculating *Hyphomicrobium* sp. GJ21 at an OD_{600} of 0.01 in 25 mL of liquid mineral medium M3Clo (composition detailed in **Table II.2**). The cultures were sealed with 20 mm grey butyl rubber stoppers and crimp caps and set under either oxic conditions (n=3; natural atmosphere) or anoxic conditions (n=3). To set up anoxic conditions, the gas phase of the cultures was replaced by a H_2/N_2 (5%/95%) atmosphere at 1 atm, and the cultures were supplemented with 20 mM of KNO_3^- from a stock solution at 1 mM. Next, 8 mM of DCM were injected through the septum of each culture as carbon source from a stock solution at 200 mM of DCM. The cultures were then incubated at 30°C with agitation (120 rpm).

The growth of *Hyphomicrobium* sp. GJ21 was monitored by periodic measurements of the OD_{600} in the cultures. In oxic conditions, the monitoring was carried out over 50 hours, while in anoxic conditions, it was carried out over 72 hours. In both cases, a total of 8 sampling points were made using 1 mL of the cultures per time points as described in **section II.4.4**. Moreover, along the experiment, oxygen concentrations were periodically monitored using non-invasive optical sensor spots attached in the upper part of the cultures as described in **section II.4.2**. The generation time, in hour, associated to each culture was calculated using the following equation:

$$\text{Generation time} = \frac{\ln(2)}{m}$$

where m corresponds to the specific growth rate during the exponential growth phase, and is calculated by extracting the slope of the logarithm of the population size (OD_{600}) over time (hours).

VI.2.1.2 Preparation of cultures for RNA extraction

To study *Hyphomicrobium* sp. GJ21 gene expression, the strain was cultivated in triplicate 160 mL serum bottles under either oxic or anoxic conditions in order to extract the RNA during the exponential phase of its growth. The followed protocol is summarized in the **Figure VI.2**.

Briefly, *Hyphomicrobium* sp. GJ21 'pre-cultures' were prepared in 160 mL serum bottles by adding 1 mL of previous liquid cultures to 49 mL of the liquid mineral medium M3Clo. The pre-cultures were sealed with 20 mm grey butyl rubber stoppers and crimp caps and set under either oxic (n=4) or anoxic (n=4) conditions. 8 mM of DCM was added to each culture as a carbon source

through the septum from a stock solution at 200 mM of DCM and cultures were incubated at 30°C with agitation (120 rpm).

When growth was observed in the pre-cultures ($OD_{600} > 0.1$), new cultures were established in 160 mL serum bottles by inoculating *Hyphomicrobium* sp. GJ21 from the pre-cultures at an OD_{600} of 0.01 in 50 mL of liquid mineral medium M3Clo. The cultures were sealed and set under either oxic ($n=4$) or anoxic ($n=4$) conditions. 8 mM of DCM were added to each culture. 3 cultures were used for RNA extraction in the mid-exponential phase, and the last one was growth monitored until stationary phase to validate the harvesting time point.

In addition to the liquid cultures, two types of solid cultures were used to check the purity of the strain ('Nutrient Agar' (NA) solid media), and whether the growing strain was dechlorinating the DCM (M3Clo solid media with the pH indicator bromophenol blue to detect HCl production). For this purpose, 100 μ L of each pre-culture was used to inoculate the NA and M3Clo solid media. The solid cultures were exposed to 1.4 mM of DCM in glass jars hermetically closed and incubated at 30°C.

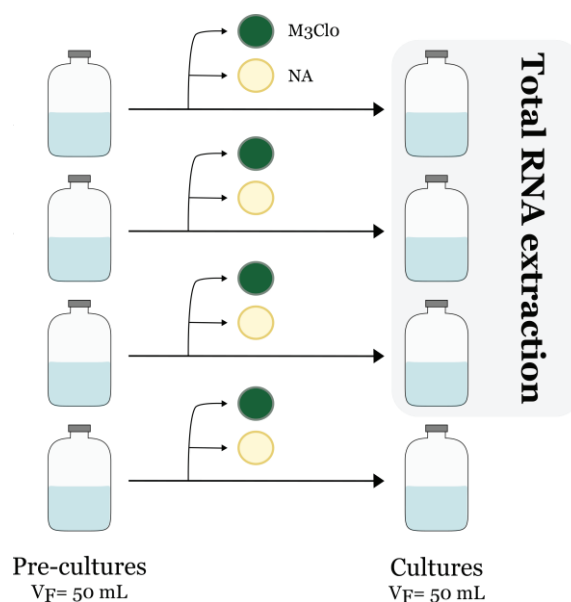


Figure VI.2. Preparation of *Hyphomicrobium* sp. GJ21 cultures for RNA extraction. The same protocol was followed for cultures under oxic and anoxic conditions. Each culture was inoculated with the pre-culture with the required volume to reach an initial OD_{600} of 0.01. To test the purity and the presence of dechlorinating bacteria, NA (yellow circle) and M3Clo (green circle) solid media were inoculated with 100 μ L of each pre-culture. Total RNA extraction was performed in 3 of the 4 cultures. The fourth culture was monitored until the stationary phase to validate the harvesting time.

VI.2.2 Molecular biology analysis

VI.2.2.1 RNA extraction from *Hyphomicrobium* sp. GJ21 cultures

Total RNA was extracted from fresh cell pellet collected in the mid-exponential phase of *Hyphomicrobium* sp. GJ21 cultures. For this, 47 mL of each culture (n=3 per oxygen concentration) were collected at OD₆₀₀ ~0.120 in oxic conditions and OD₆₀₀ ~0.07 in anoxic conditions, and were centrifuged at 8 500 rpm for 20 minutes at room temperature. Total RNA was then extracted from the resulting pellet using the “Monarch Total RNA Miniprep” kit according to the manufacturer’s instructions for “Tough-to-Lyse Samples” (detailed protocol in **section II.5.2.1**). For the cell lysis step, three methods were tested (enzymatic lysis, mechanical lysis, or a combination of both). Among these, we chose to use enzymatic lysis during this work because it resulted in a higher RNA extraction yield. At the end of the protocol, a 5 µL aliquot of the eluted total RNA was stored frozen at -20°C for the characterization analysis. The remainder of the eluted total RNA (~45 µL) was stored frozen at -80°C until depletion, library preparation and sequencing.

VI.2.3 RNA characterization

Prior to sequencing, the total RNA extracted from the *Hyphomicrobium* sp. GJ21 cultures in oxic and anoxic conditions was quantified and quality assessed. Total RNA concentrations were quantified by fluorometry using the “Qubit® RNA HS Assay” kit (Thermo Fisher Scientific). To check for potential DNA contamination in the samples, DNA concentration was also quantified by fluorometry using the “Qubit® dsDNA HS Assay” kit (Thermo Fisher Scientific). Total RNA quality was determined by using the “Agilent RNA 6000 Nano Assay”, according to the manufacturer’s instructions (detailed protocol in **section II.5.2.2**).

VI.2.4 Whole transcriptomics sequencing and data analysis

After ribosomal RNA depletion with the “Ribo-Zero Plus Microbiome rRNA depletion” kit, a total RNA library was prepared using the “Illumina Stranded Total RNA library prep kit” and sequenced (2 x 150 bp paired end) using the Illumina NextSeq 2000 (LCSB genomic platform, University of Luxembourg).

As a result, RNA-seq data were obtained in fastqsanger format, which were processed and further analysed using the Galaxy France web platform (usegalaxy.fr). The complete workflow is described in detailed in **section II.7**. Briefly, the RNA-seq reads were first trimmed using the Trimmomatic tool (Galaxy version 0.39+galaxy2) to remove reads with an average quality below 30. The trimmed RNA-seq reads were mapped to the reference genome of *Hyphomicrobium* sp. GJ21 and were attributed to genomic features using the HISAT2 tool (Galaxy version 2.2.1+galaxy1). The reference genome of *Hyphomicrobium* sp. GJ21, along with its gene coordinates and annotations, was extracted from the MicroScope platform (mage.genoscope.cns.fr). To quantify the number of RNA-seq reads per gene, we used the featureCounts tool (Galaxy version 2.0.3+galaxy2). The resulting files were then used to analyze

the differential gene expression in the strain when exposed to oxic or anoxic conditions by using the DESeq2 tool (Galaxy version 2.11.40.8+galaxy0). A list of genes with the normalized gene counts and the associated p-values testing the null hypothesis, that there is no differential gene expression between conditions, was obtained. The results were visualized using the heatmap2 tool (Galaxy version 3.1.3.1+galaxy0) and the Volcano Plot tool (Galaxy version 0.0.6).

VI.3 Results

VI.3.1 Growth monitoring of *Hyphomicrobium* sp. GJ21

The growth of *Hyphomicrobium* sp. GJ21 was characterized under both oxic and anoxic conditions in order to determine the sampling point in the exponential phase of this strain in our laboratory settings (**Figure VI.3**). The results showed that under oxic conditions, *Hyphomicrobium* sp. GJ21 had a generation time of 10 ± 0.4 hours and was found in the exponential phase from 24 to 47 hours, reaching a maximum OD₆₀₀ of 0.311 ± 0.1 . Under anoxic conditions, the strain had a generation time of 14 ± 0.4 hours and was found in the exponential phase from 18 hours to 44 hours, reaching a maximum OD₆₀₀ of 0.143 ± 0.1 , which was significantly lower than that observed under oxic conditions (p-value <0.05). This may be explained by the lower efficiency at energy production during the anaerobic respiration. Moreover, the absence of a lag phase in cultures under anoxic conditions suggests that the precultures hadn't reached the stationary phase when transferred to the new cultures.

As the monitoring was not done by continuous measurements over time (only 7 sampling points over 50-70 hours), the limits of the exponential phase were not fully determined. However, these results allowed us to establish a time period in which *Hyphomicrobium* sp. GJ21 was in the exponential phase in the settings of interest, which was useful in deciding when to stop the cultures for performing total RNA extraction.

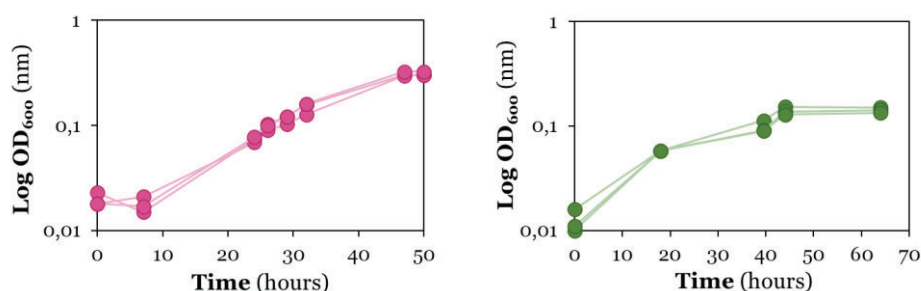


Figure VI.3. *Hyphomicrobium* sp. GJ21 growth curves under oxic (n=3) or anoxic (n=3) conditions. Cultures under oxic conditions (pink colour) and under anoxic conditions (green colour) were maintained at [O₂] ~ 8 ppm around and [O₂] >0.5 ppm, respectively (not shown).

The growth curves of the cultures that were used for total RNA extraction are shown in the **Figure VI.4**. Under oxic conditions, the cultures were stopped after 29 hours of growth when an OD_{600} of 0.120 ± 0.002 was reached, whereas under anoxic conditions, the cultures were stopped after 25 hours of growth when an OD_{600} of 0.069 ± 0.004 was reached. Total RNA concentrations recovered from cultures in oxic and anoxic conditions were 66 ± 2.2 ng/ μ L and 45 ± 5.3 ng/ μ L, respectively, and in both cases DNA contamination was low (6% and 5% of the total volume in oxic and anoxic conditions, respectively). Regarding the Bioanalyzer quality reports, although the Ribosomal Integrity Number (RIN) value was not calculated in some cases, the extracted total RNA displayed clear and well-defined 16S and 23S peaks in all cases, indicating high-quality RNA without signs of degradation (**Supplementary figure VI.1**).

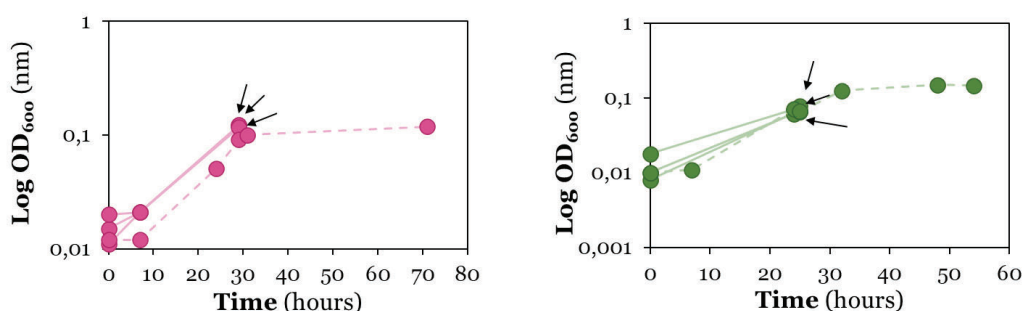


Figure VI.4. Growth curve of the *Hyphomicrobium* sp. GJ21 cultures and harvesting points for total RNA extraction under oxic ($n=4$) and anoxic ($n=4$) conditions. The continuous line corresponds to the cultures where the RNA extraction was performed, and the discontinuous line corresponds to the cultures which were used for growth monitoring over time. The colours indicate the oxygen concentrations: pink for oxic conditions ($[O_2] \sim 8$ ppm), and green for anoxic conditions ($[O_2] < 0.5$ ppm). The arrows report the moment where the liquid phase was collected to pellet the cells.

VI.3.2 Quantification of gene expression

Quality filtered reads of each sample were mapped to each gene of the *Hyphomicrobium* sp. GJ21 genome as a first step to compare gene expression as a function of oxygen concentration. The number of reads aligned to the genome and mapped to specific genes, as well as the initial number of reads before and after trimming, are shown in **Table VI.1**. Under oxic conditions, $86.4 \pm 0.3\%$ of the trimmed reads were aligned to the genome and $83.3 \pm 0.6\%$ of these reads mapped to specific genes. Under anoxic conditions, $85.2 \pm 0.4\%$ of the trimmed reads were aligned to the genome and $82.9 \pm 0.4\%$ of these reads mapped to specific genes. This indicates that a small percentage of reads (less than 4% in the two conditions) was aligned to non-coding regions or genes that may not have been accurately predicted. In addition, no significant differences were found in the number of reads assigned to genes depending on the oxygen concentration, suggesting that the overall number of active genes was relatively stable between the two conditions.

Table VI.1. Summary of reads per sample of reads obtained before and after trimming, reads that aligned to the *Hyphomicrobium* sp. GJ21 genome and reads that mapped to predicted genes.

Sample	Initial reads	Reads after trimming	% ¹	Reads aligned to genome	% ²	Reads mapped to genes	% ³	Mapped genes (out of 4097)
Oxic x1	12 758 344	10 538 581	82.6	9 146 051	86.8	8 852 258	84.0	4072
Oxic x2	12 694 890	10 443 772	82.3	9 052 282	86.7	8 763 091	83.91	4074
Oxic x3	14 402 146	11 881 571	82.5	10 180 999	85.7	9 758 377	82.1	4072
Anoxic x1	16 380 877	13 398 268	81.8	11 523 872	86.0	11 138 392	83.1	4070
Anoxic x2	15 296 119	12 253 822	80.1	10 399 369	84.9	10 212 995	83.3	4059
Anoxic x3	15 906 370	13 070 488	82.2	11 084 850	84.8	10 742 463	82.2	4069

¹Percentage of initial reads remaining after trimming.

²Percentage of trimmed reads that aligned in the genome.

³Percentage of trimmed reads that were assigned to a predicted gene.

VI.3.3 Differential gene expression in response to oxygen concentration

In total, 4 088 genes were found to be expressed across all samples. Out of them, 4 079 genes were expressed in at least one replicate in both conditions, 3 genes were only detected as expressed in oxic conditions, and 6 genes only in anoxic conditions (**Figure VI.5**). In the case of the genes expressed only in oxic conditions, none of them were observed in all three replicates, and when detected, only few reads were associated with them (less than 3 reads per gene), suggesting that these observations may be due to background noise. In the case of the genes which expression was only identified in anoxic conditions, only 2 of them were present in all replicates. These 2 genes were “HYPGJv1_21156”, encoding a protein of unknown function that was geographically closed in the genome to prophage elements (e.g. phage head-tail adaptor, phage major capsid protein), and “HYPGJv1_30359”, encoding another unknown protein encoded near to redox enzymes and proteins (e.g. methanethiol oxidase, cytochrome-c peroxidase, electron transport protein SCO1/SenC). However, since less than 3 reads per gene and per replicate were associated with these two genes, their differential expression was not considered significant. Altogether, these results suggest that, in qualitative terms, the pool of expressed gene was not impacted by the tested growth conditions.

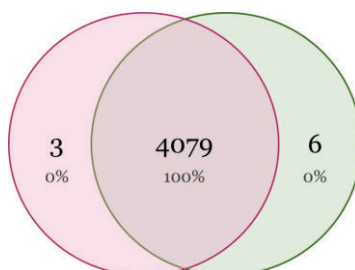


Figure VI.5. Venn diagram of the core and specific transcriptomes (in number of genes) as a function of the oxygen status. Pink represents oxic conditions and green represents anoxic conditions.

While the transcripts detected under both oxic and anoxic conditions were similar, their expression level differed, starting with the most expressed gene under oxic conditions, “HYPGJv1_31561” ($372\,657 \pm 6\,712$ normalized counts (NC)), encoding the DCM dehalogenase DcmA. This gene was the second most expressed under anoxic conditions ($375\,166 \pm 22\,396$ NC). Conversely, under anoxic condition, the most expressed gene was “HYPGJv1_21028” ($492\,272 \pm 26\,083$ NC), encoding the methanol dehydrogenase [cytochrome c] subunit 1 MoxF, which was the second most expressed gene under oxic conditions ($265\,975 \pm 12\,163$ NC). The genes encoding DcmA, DcmB and DcmC, associated with the DCM degradation pathway in *Hyphomicrobium* sp. GJ21, were found among the top 15 most expressed genes regardless of the oxygen concentration, while their transcriptional regulator DcmR (Maucourt et al., 2020) was found as the 50th and 57th most expressed genes in oxic and anoxic condition, respectively. Of the 4 088 detected expressed genes, 38% (1 562 genes) were differentially expressed (adj. p-value <0.05; **Supplementary Table VI.1**). As shown in the **Figure VI.6**, the expression level was consistent through replicates, meaning that the observed differences in the gene expression were mainly dependent on the oxygen status to which the strain was exposed.

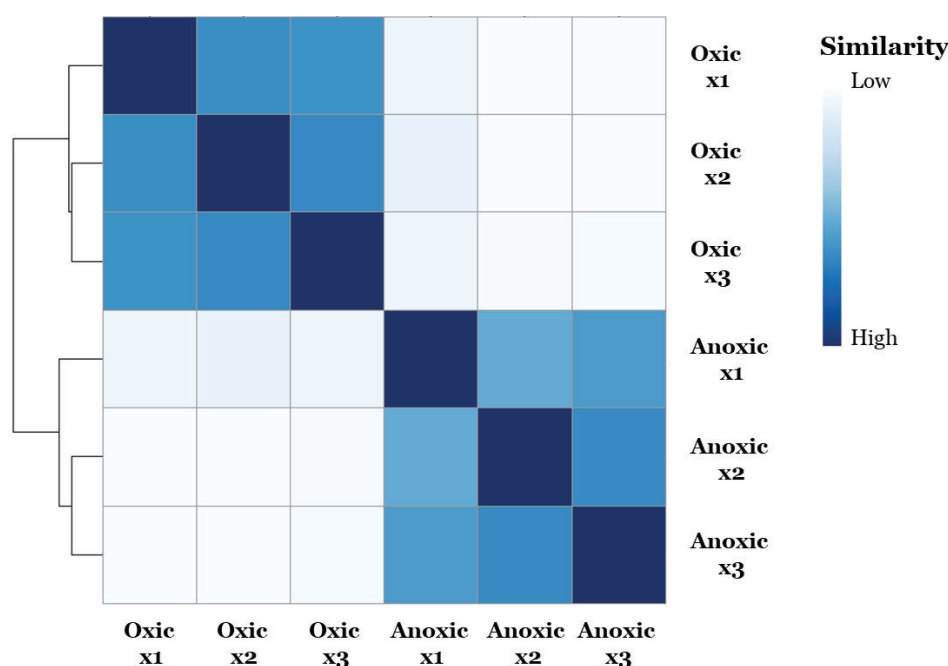


Figure VI.6. Heatmap plot based on the Euclidean distances among samples in terms of gene expression. Samples were hierarchically clustered.

Using the Clusters of Orthologous Groups (COG) classification system to assign transcripts to specific functional groups, we found that 35% of the differentially expressed genes were associated with the category “Metabolism”, 17% were associated with the category “Cellular processes and signalling”, 11% were associated with the category “Information storage and processing”, and the rest (35%) were not associated with any of these categories (**Table VI.2**). Among the COG categories, the most differentially expressed functional groups were the ones related to energy production and nutrient transport in the “Metabolism” category (energy production, inorganic

ion transport, coenzyme transport and amino acid transport), the ones related to cell growth, division and adaptation to stress in the “Cellular processes and signalling” category (cell wall, membrane, envelope biogenesis and signal transduction mechanisms), and the ones related to genetic regulation and protein synthesis in the “Information storage and processing” category (transcription, translation, ribosomal structure and biogenesis).

Table VI.2. Differentially expressed genes in each COG category and functional group.

COG classification	Genes	Functional description	Genes
METABOLISM	547	Energy production and conversion	136
		Inorganic ion transport and metabolism	93
		Coenzyme transport and metabolism	89
		Amino acid transport and metabolism	81
		Lipid transport and metabolism	48
		Carbohydrate transport and metabolism	41
		Nucleotide transport and metabolism	32
		Secondary metabolites biosynthesis, transport and catabolism	27
CELLULAR PROCESSES AND SIGNALING	275	Cell wall/membrane/envelope biogenesis	88
		Signal transduction mechanisms	57
		Posttranslational modification, protein turnover, chaperones	51
		Cell motility	24
		Intracellular trafficking, secretion, and vesicular transport	20
		Defense mechanisms	19
		Cell cycle control, cell division, chromosome partitioning	16
INFORMATION STORAGE AND PROCESSING	179	Transcription	75
		Translation, ribosomal structure and biogenesis	63
		Replication, recombination and repair	40
		RNA processing and modification	1
POORLY CHARACTERIZED	343		
UNKNOWN	218		
Total diff. expressed genes	1562		

Of the 1 562 differentially expressed genes, the expression of 417 genes was at least doubled in one of the conditions (fold change (FC) >2 or FC <0.5; **Supplementary Table VI.2**), representing 26% of the differentially expressed genes. Looking at the COG categories to which these genes belonged, 44% were associated with the category “Metabolism”, 13% were associated with the category “Cellular processes and signalling”, 7% were associated with the category “Information storage and processing” and the remainder (17%) were not associated with any of these categories (**Table VI.3**). Regarding the functional groups, in the “Metabolism” category, the majority of genes were related to energy metabolism and ion regulation (energy production and conversion, inorganic ion transport and metabolism). In the “Cellular processes and signalling”, the majority of genes were related to adaptation mechanisms and signalling pathways (cell wall, membrane and envelop biogenesis, posttranslational modification, protein turnover and chaperones, signal transduction mechanisms). Finally, in the “Information storage and processing” category, the majority of the genes were related to gene expression (transcription).

Table VI.3. Differentially expressed genes whose expression was at least doubled in one of the oxygen concentrations compared to the other one (FC>2 or FC<0.5).

COG classification	Genes	Functional group	Genes
METABOLISM	184	Energy production and conversion	61
		Inorganic ion transport and metabolism	44
		Coenzyme transport and metabolism	21
		Amino acid transport and metabolism	19
		Lipid transport and metabolism	17
		Carbohydrate transport and metabolism	10
		Secondary metabolites biosynthesis, transport and catabolism	8
		Nucleotide transport and metabolism	4
CELLULAR PROCESSES AND SIGNALING	55	Cell wall/membrane/envelope biogenesis	20
		Posttranslational modification, protein turnover, chaperones	10
		Signal transduction mechanisms	10
		Intracellular trafficking, secretion, and vesicular transport	6
		Defense mechanisms	6
		Cell motility	2
		Cell cycle control, cell division, chromosome partitioning	1
INFORMATION STORAGE AND PROCESSING	32	Transcription	23
		Translation, ribosomal structure and biogenesis	6
		Replication, recombination and repair	3
UNKNOWN	71		
Total diff. expressed genes	417		

The plot shown in **Figure VI.7** shows that most of the differentially expressed genes were overexpressed under anoxic conditions compared to oxic conditions.

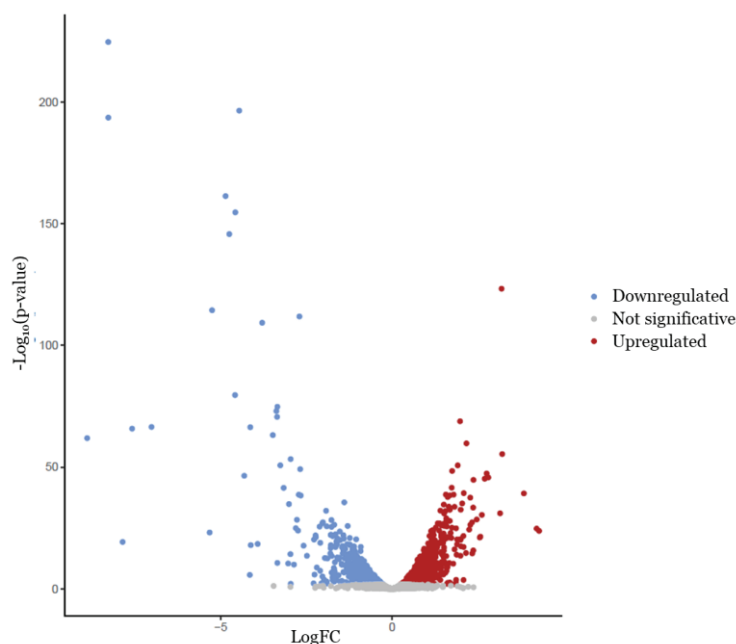


Figure VI.7. Volcano plot of the differentially expressed genes in *Hyphomicrobium* sp. GJ21 when exposed to oxic conditions compared to anoxic conditions. The Y-axis shows the statistical significance (based on the p-value) and the X-axis shows the magnitude of change (based on the fold change - FC). Each point corresponds to one gene. Red points correspond to significantly overexpressed genes in oxic conditions compared to anoxic conditions. Blue points correspond to significantly overexpressed genes in anoxic conditions compared to oxic conditions. Grey points correspond to genes which expression is not statistically significantly different between the two oxygen conditions (p-value >0.05).

Among the top 20 genes that were overexpressed in anoxic conditions, we found the genes encoding for the enzymes and assembly elements participating in the denitrification process, i.e. nitrate reductase, nitrite reductase and nitrous oxide reductase. In addition, some other overexpressed genes were indirectly linked to this process by participating in the biosynthesis and availability of different cofactors, such as the pyrroloquinoline quinone (PQQ) or flavin cofactors. The overexpressed genes list in anoxic conditions also contained transcripts for proteins involved in different metabolic pathways, such as fatty acid biosynthesis, oxidation of methanol, response to oxidative stress, protein folding, membrane transport and integrity, amino acid biosynthesis, nitrogen excretion and degradation of butanol. Additionally, some of them were found in gene clusters. In particular, two groups of genes stood out: one group included genes encoding the nitrate reductase complex (*narI*, *narJ*, *narH* and *narK*), a porin, and a chaperon (**Figure VI.8-a.**), while the other group comprised genes encoding PQQ-related enzymes (*ppqE*, *ppqD*, and protein A) as well as enzymes involved in the fatty acid and serin biosynthesis (**Figure VI.8-b.**). The high expression of these two groups of genes under anoxic conditions suggests that they may be subjected to shared regulation. A summary of these top 20 most downregulated genes in oxic conditions is found in **Table VI.4**.

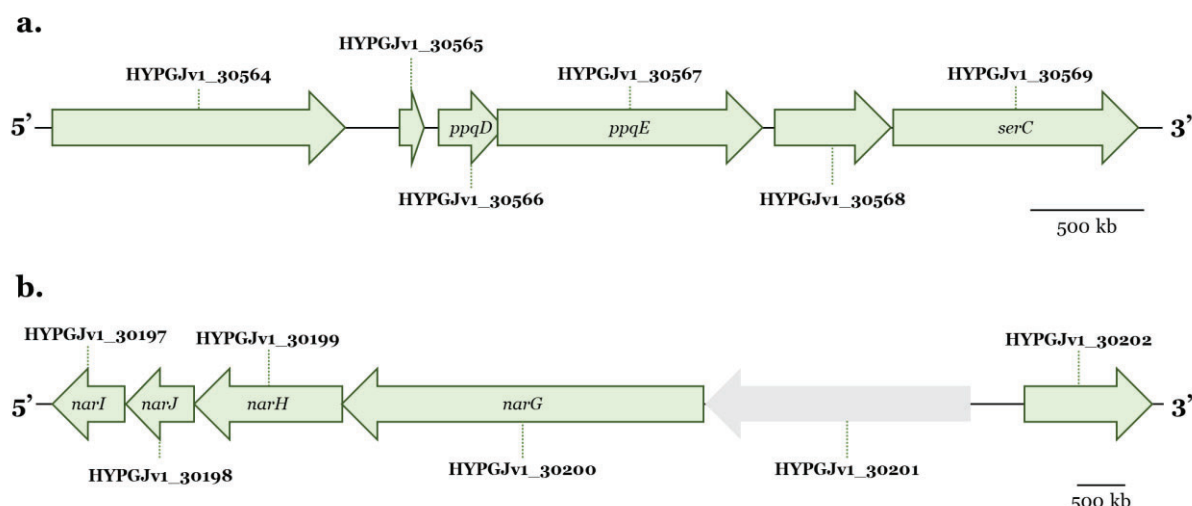


Figure VI.8. Genomic regions containing several genes found in the top 20 most overexpressed genes under anoxic conditions. The codes associated with each gene correspond to their accession numbers in the MAGE platform (mage.genoscope.cns.fr). The names inside the arrows represent the gene names. Further information for each gene is in **Table VI.4**. The grey-coloured gene in **b.** refers to one that was not identified among the top 20 most downregulated genes, but it was among the differentially expressed genes under anoxic conditions.

Table VI.4. Top 20 most overexpressed genes in *Hyphomicrobium* sp. GJ21 under anoxic conditions compared to oxic conditions. Genes are listed in order of decreasing significance. The “ID” and “Description” information was obtained from the MicroScope platform (mage.genoscope.cns.fr).

ID	Description	Function
HYPGJv1_30567	PqqA peptide cyclase	Biosynthesis of pyrroloquinoline quinone
HYPGJv1_30199	Nitrate reductase A subunit beta	Complex nitrate reductase
HYPGJv1_30566	PqqA binding protein	Biosynthesis of the pyrroloquinoline quinone
HYPGJv1_30198	Nitrate reductase 1 molybdenum cofactor assembly chaperone	Complex nitrate reductase
HYPGJv1_30197	Nitrate reductase A subunit gamma	Complex nitrate reductase
HYPGJv1_30564	3-oxoacyl-(acyl-carrier-protein) synthase, KASII	Fatty acid biosynthesis
HYPGJv1_20492	Putative dehydrogenase XoxF	Predicted for methanol oxidation
HYPGJv1_31729	Putative hydrogen peroxide-inducible genes activator	Positive regulator of H ₂ O ₂ inducible genes
HYPGJv1_30526	Copper-containing nitrite reductase	Nitrite reductase
HYPGJv1_30196	Peptidyl-prolyl cis-trans isomerase ppiD	Chaperon for proteins with proline residues
HYPGJv1_30202	Porin_4 domain-containing protein	Transport of nutrients and ions and membrane integrity
HYPGJv1_31859	Catalase KataA	Detoxification of H ₂ O ₂
HYPGJv1_20481	Copper-binding lipoprotein NosL	Complex nitrous oxide reductase
HYPGJv1_30569	Phosphoserine aminotransferase	Biosynthesis of serine
HYPGJv1_20012	Outer membrane protein W precursor	Transport of small molecules and membrane integrity
HYPGJv1_30568	Putative urase oxidase	Nitrogen excretion
HYPGJv1_30200	Nitrate reductase A subunit alpha	Complex nitrate reductase
HYPGJv1_30565	Coenzyme PQQ synthesis protein A	Biosynthesis of the pyrroloquinoline quinone
HYPGJv1_20482	FAD protein FMN transferase	Availability of flavin cofactors
HYPGJv1_31172	1-butanol dehydrogenase (quinone)	Butanol degradation

Among the top 20 genes that were overexpressed in oxic conditions, we found genes that were involved in the aerobic respiration by directly participating in the electron transport chain or indirectly by participating in the availability of cofactors and ions essential for this process. The rest of the most upregulated genes in oxic conditions encoded for proteins participating in iron homeostasis, cell wall biogenesis, signal transduction pathways and amino acids and fatty acids metabolism. Additionally, in this case, we identified only one group of geographically close genes that were overexpressed. This group contains three genes, which are three genes involved in the electron transport chain (**Figure VI.9**). A summary of these top 20 most overexpressed genes in oxic conditions compared to anoxic conditions is found in **Table VI.5**.

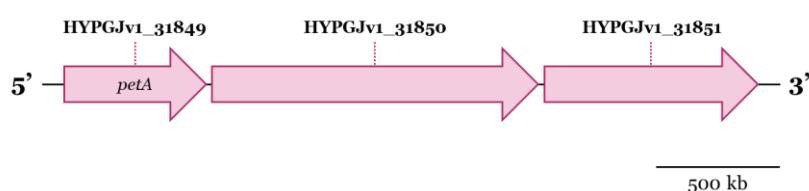


Figure VI.9. Genomic region containing genes found in the top 20 most overexpressed genes under oxic conditions. The codes associated with each gene correspond to their accession numbers in the MAGE platform (mage.genoscope.cns.fr). The names inside the arrows represent the gene names. Further information for each gene is in **Table VI.5**.

Table VI.5. Top 20 most overexpressed genes in *Hyphomicrobium* sp. GJ21 under oxic conditions compared to anoxic conditions. Genes are listed in order of decreasing significance. The “ID” and “Description” information was extracted from the MicroScope platform (mage.genoscope.cns.fr).

ID	Description	Function
HYPGJv1_30613	Ferredoxin-NADP reductase	Production of NADPH
HYPGJv1_30902	Iron-regulated protein A precursor	Iron homeostasis
HYPGJv1_10161	Conserved exported protein of unknown function	Unknown function
HYPGJv1_30055	Cytochrome c domain-containing protein	Component of electron transport chain
HYPGJv1_20847	Sulfite reductase [NADPH] flavoprotein alpha-component	Sulfur metabolism
HYPGJv1_31850	Ubiquinol-cytochrome c reductase, cytochrome B subunit	Component of electron transport chain
HYPGJv1_20233	Cytochrome c oxidase subunit 1 homolog	Component of electron transport chain
HYPGJv1_20828	Copper-sensing transcriptional repressor RicR	Regulator of copper homeostasis
HYPGJv1_20829	Copper-transporting P-type ATPase	Copper homeostasis
HYPGJv1_20361	ErfK/YbiS/YcfS/YnhG family protein	Cell wall biogenesis
HYPGJv1_31403	Cytochrome c homolog	Component of electron transport chain
HYPGJv1_30245	ABM domain-containing protein	Diverse cellular process and metabolic pathways
HYPGJv1_31181	PilZ domain-containing protein	Signal transduction pathway
HYPGJv1_20038	Putative ATPase, AAA family	Diverse cellular process requiring ATP hydrolysis
HYPGJv1_10360	ATP synthase F1 complex subunit alpha	ATP production
HYPGJv1_31849	Ubiquinol-cytochrome c reductase iron-sulfur subunit	Component of electron transport chain
HYPGJv1_31851	Cytochrome c1	Component of electron transport chain
HYPGJv1_31076	Putative signal transduction protein with CBS domains	Signal transduction pathway
HYPGJv1_30244	Putative Intracellular heme transport protein HutX	Iron homeostasis
HYPGJv1_31821	Methylmalonyl-CoA mutase small subunit	Synthesis of propionate

VI.4 Discussion

During groundwater level fluctuations, the aquifer environment is subjected to oxic/anoxic alternations. This dynamic creates an advantageous environment for microorganisms with the metabolic flexibility to switch from electron acceptors. The facultatively anaerobic strain *Hyphomicrobium* sp. GJ21 has the unique ability of degrading DCM in oxic and anoxic conditions, using the same metabolic pathway involving the DCM dehalogenase DcmA, but with different terminal electron acceptors (O_2 or N_2O , respectively). In this study, we investigated the specific genes that are differentially expressed between the aerobic and anaerobic metabolism.

We observed that both conditions lead to the expression of a very similar pool of genes suggesting that variations in oxygen concentration did not lead to significant qualitative changes in the gene transcription in *Hyphomicrobium* sp. GJ21. Notably, the genes involved in the DCM degradation pathway (*dcmA*, *dcmB*, *dcmC*, and *dcmR*) were among the most highly expressed genes in both conditions, with no significant differences in expression levels. This result was expected and somehow can serve as a validation of our analysis.

Although the majority of genes were transcribed both in oxic and anoxic conditions, about 38% of them were differentially expressed, affecting three main functional categories (metabolism, cellular structure and gene and protein production). This suggests that the adaptation of *Hyphomicrobium* sp. GJ21 to a particular oxygen concentration consists of a general response to maintain homeostasis. Among the functional groups, the greatest changes in gene expression were found for genes related to energy production, as expected by the utilisation of different respiration pathways by *Hyphomicrobium* sp. GJ21 (aerobic respiration in oxic conditions and denitrification in anoxic conditions). In support to this, genes involved in the denitrification pathway were among the top 20 most significantly upregulated genes in anoxic conditions, while genes involved in the electron transport chain of aerobic respiration were among the top 20 most significantly upregulated genes in oxic conditions.

In addition to the genes involved in the respiration pathways, there were other genes with significantly different expression levels between conditions that were involved in other cellular processes. Under anoxic conditions, the most overexpressed genes encoded for the PqqA peptide cyclase, which is involved in the biosynthesis of the pyrroloquinoline quinone (PQQ), a redox cofactor essential for bacterial C1-dissimilation (Duine & Frank, 1990). In addition to this gene, 2 other genes among the top 20 most expressed under anoxic conditions were also associated with this process, suggesting that PQQ may play a more significant role in this condition than in oxic conditions. In general, PQQ is considered as a prosthetic group of many redox enzymes, such as the methanol dehydrogenase (MDH) (Duine, 1999). Interestingly, the most highly expressed gene under anoxic conditions, which was significantly more expressed than in oxic conditions, was the MDH MoxF, which uses PQQ as an essential cofactor for its catalytic activity and is involved in the oxidation of methanol to formaldehyde (Anderson et al., 1990). In a previous transcriptomic

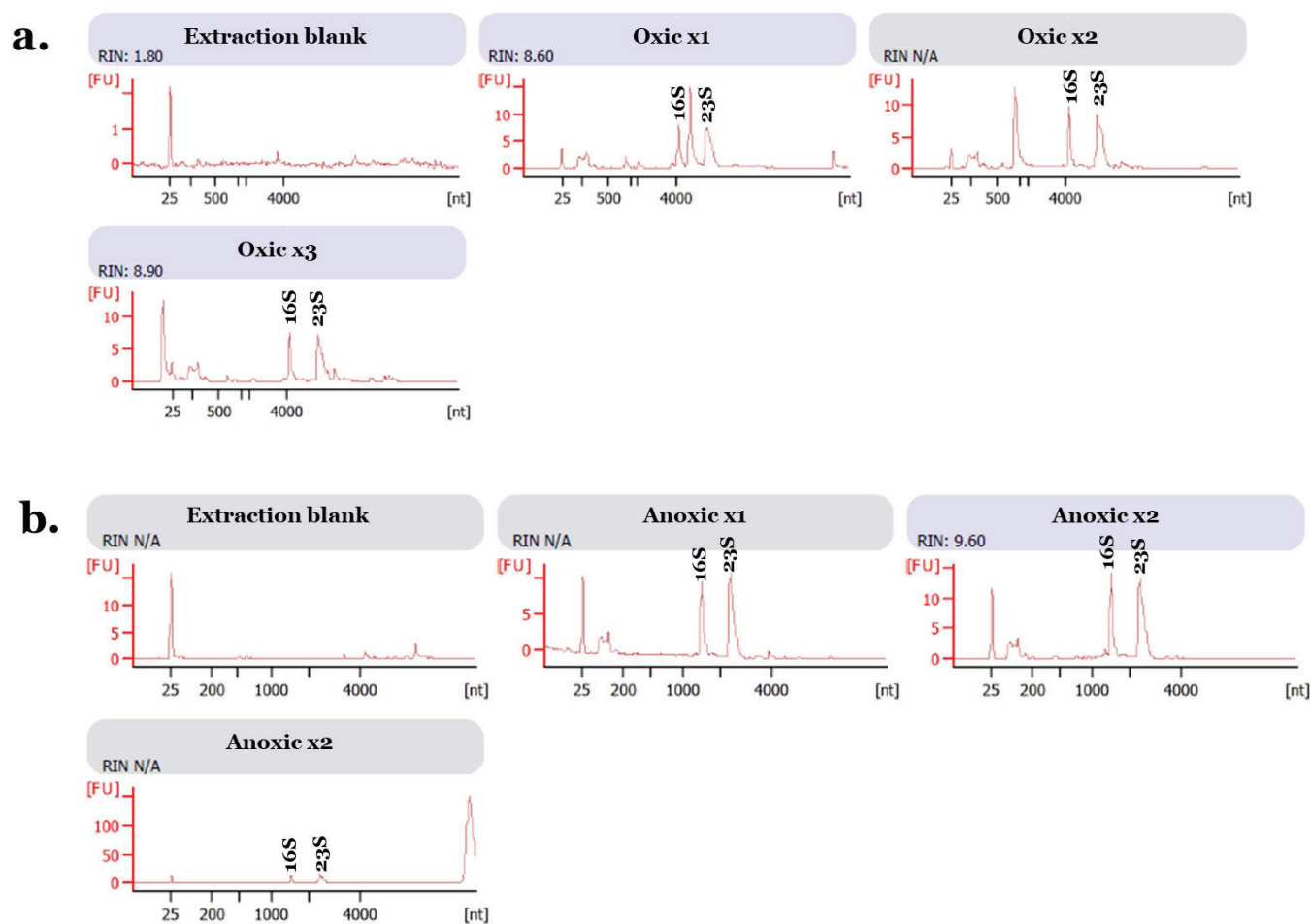
study on the methylotrophic strain *Methylobacterium extorquens*, (Chaignaud et al., 2017) observed high expression of the genes encoding the canonical MDH in this strain, MxaFI, in cultures with methanol or chlorinated compounds, including DCM. The authors proposed that, in the absence of methanol, this enzyme may play a role in the conversion of formaldehyde. Additionally, another overexpressed gene in anoxic conditions was the putative dehydrogenase XoxF. Although its role remains unclear in the literature, XoxF was predicted to be a PQQ-dependent MDH, due to its 50% sequence identity with the periplasmic MDH MxaF. In the laboratory, experiments with the purified XoxF protein from *M. extorquens* AM1 have shown low activity for methanol oxidation (Nakagawa et al., 2012; Schmidt et al., 2010), as well as for formaldehyde oxidation (Yanpirat et al., 2020). However, this enzyme has also been found in non-methylotrophic organisms. Therefore, (Skovran et al., 2011) proposed that XoxF may have a second function, either as an environmental sensor or being involved in the oxidation of another unknown substrate. Finally, another PQQ-dependent dehydrogenase found among the top 20 most overexpressed genes in anoxic conditions was annotated as the 1-butanol dehydrogenase, a periplasmic quinoprotein alcohol dehydrogenase involved in butane degradation (Vangnai & Arp, 2001). The enzyme, maybe misannotated, may play an essential role in helping the bacteria maintain the energy balance and redox state under anoxic conditions. This hypothesis should be further tested by studying the specific role of these proteins in this condition. Other example of genes that were found among the top 20 most upregulated under anoxic conditions were two genes associated with the detoxification of the H_2O_2 , among which we found the one encoding for the catalase KatA. (Su et al., 2014) also reported a higher KatA expression in *Pseudomonas aeruginosa* during anoxic conditions compared to that observed under oxic conditions, and proposed that this enzyme is involved in the protection against NO, a reactive nitrogen species generated during the denitrification process. Finally, other genes involved in the nutrients and small molecules transport and fatty acid biosynthesis were also overexpressed under anoxic conditions, which may be related to the bacterium's response to cope with the stress conditions and the reduced energy production imposed by the anoxic conditions.

Under oxic condition, in addition to the genes directly or indirectly involved in the aerobic respiration and electrons transfer, we identified genes associated with the iron and copper homeostasis among the most overexpressed genes. Both compounds function as cofactors for numerous enzymes, being essential in both aerobic and anaerobic metabolism. However, because of their poor availability and extreme toxicity under oxic conditions, bacteria need to actively regulate the concentration of these compounds to achieve effective homeostasis in this condition (Andrews et al., 2003; Giachino & Waldron, 2020; Rensing & Grass, 2003). In contrast, in anoxic conditions, these compounds are more available and less toxic, which results in the underexpression of these genes compared to conditions with molecular oxygen.

VI.5 Conclusions

In aquifers, GLF induce changes in the redox conditions, such as variations in the oxygen concentration within the fluctuating zone. Microorganisms with metabolic flexibility to switch between oxic and anoxic conditions are thus favoured during this process. In this context, the facultative methylotrophic strain *Hyphomicrobium* sp. GJ21 is frequently used as a model for DCM bioremediation in aquifers due to its unique capacity to use DCM under both oxygen and nitrate respiration. In this work, we investigated the response at the gene expression level of this bacterium when exposed to either oxic or anoxic conditions. The results showed that under both oxic and denitrifying conditions, the pool of expressed genes was similar, indicating that changes in oxygen concentration did not lead to variations in the overall quantity of genes expressed. However, the threshold used to consider a transcript as observed should be revised, particularly to filter out transcripts not found in all triplicates. For this reason, we have focused on analysing the differentially expressed genes by examining the top 20 most overexpressed genes in each condition, presuming that this filtering step would not impact these lists. In this regard, differences were observed in the level of expression of genes involved in the respiratory chain specific to each type of metabolism (aerobic respiration and denitrification). Interestingly, in anoxic conditions, genes related to the biosynthesis of PQQ and those encoding PQQ-dependent alcohol dehydrogenases were among the most overexpressed genes, suggesting their crucial role in the denitrification metabolism. On the other hand, genes related to copper and iron homeostasis were among the most upregulated under oxic conditions, highlighting the importance of maintaining the balance of these compounds in such condition. Further analysis and experiments are necessary to confirm the findings reported here and clarify the role of the most differentially expressed genes in the metabolism of *Hyphomicrobium* sp. GJ21 when exposed to each condition.

Supplementary data - Chapter VI



Supplementary Figure VI.1. Electropherograms of extracted RNAs from the cultures of *Hyphomicrobium* sp. GJ21 grown in **a.** oxic conditions, and **b.** anoxic conditions. Y-axis corresponds to fluorescence units (FU), and X-axis correspond to RNA size in nucleotides. In total, there was 3 replicates per oxygen status, and 1 extraction blank. The first peak corresponds to the marker. The 16S and 23S peaks were automatically determined by the software “2100 Expert Software”, and peak area integrated for the RIN value when possible.

Supplementary Table VI.1. List of genes that were significantly differentially expressed (p-value adj. <0.05) when *Hyphomicrobium* sp. GJ21 was exposed to either oxic or anoxic conditions. The first column lists the genes by their accession numbers from the MicroScope web platform (mage.genoscope.cns.fr). Columns 2 to 4 correspond to the replicates exposed to anoxic conditions, while columns 5 to 7 correspond to the replicates exposed to oxic conditions. In both cases, the values associated to each gene represent the number of reads detected per sample. Columns 8 and 9 provide the gene name and the products it encodes, information compiled from the MicroScope web platform. For space considerations, the table is found in the following seafire-cloud link: [Supplementary Table VI.1](#)

Supplementary Table VI.2. List of differentially expressed genes whose expression was at least doubled in one of the conditions ($FC >2$ or $FC <0.5$) when *Hyphomicrobium* sp. GJ21 was exposed to either oxic or anoxic conditions. The first column lists the genes by their accession numbers from the MicroScope web platform (mage.genoscope.cns.fr). Columns 2 to 4 correspond to the replicates exposed to anoxic conditions, while columns 5 to 7 correspond to the replicates exposed to oxic conditions. In both cases, the values associated to each gene represent the number of reads detected per sample. Columns 8 and 9 provide the gene name and the products it encodes, information compiled from the MicroScope web platform. For space considerations, the table is found in the following seafire-cloud link: [Supplementary Table VI.2](#)

Chapter VII

General conclusions and perspectives

The primary goal of this thesis was to address the following research questions: (i) What is the impact of water content and oxygen status on the activity and composition of a DCM-degrading microbial community? (ii) Can soil granulometry change how water content and oxygen level impact the activity and composition of a DCM-degrading microbial community? (iii) What is the response of a DCM-degrading microbial community to a disturbance, here a change in oxygen concentration? Does this response depend on the environmental conditions? (iv) How does oxygen concentration impact the gene expression of the facultatively anaerobic DCM-degrading strain *Hyphomicrobium* sp. GJ21?

In this final chapter of my PhD dissertation, I will discuss the general conclusions drawn from this work, elaborate on the limitations and then propose short- and long-term perspectives.

VII.1 Conclusions

The main aim of this dissertation was to understand how a microbial community and their DCM-degrading members in particular, might be influenced by its environment. In particular, we decided to focus on three physicochemical parameters that are affected during GLF: water content, oxygen concentration and matrix granulometry. First, we have observed that both water content and oxygen concentration together regulated the activity and composition of the underlying microbial community (**Figure VII.1-(i)**). Water content appeared to act as a first selection barrier, since the community did not degrade DCM when water content was very low. In addition, the onset of the activity was faster at higher water contents. When water content was not a limiting factor, oxygen concentration was the main driving force behind both the activity and composition of the microbial community. In particular, oxic conditions promoted DCM-degrading activity, whereas anoxic conditions generally limited it. In terms of composition, the microbial communities were significantly different depending on the oxygen status. Furthermore, the effect of water content on community composition was observed only under oxic conditions, suggesting that, under anoxic conditions, the community had a more deterministic dynamic. The matrix granulometry influenced the DCM-degrading community activity and composition, but mainly through its control over water content (**Figure VII.1-(ii)**). In particular, finer grain sizes facilitated the maintenance of the activity of the DCM-degrading microbial community at the lowest tested water content (i.e., $\frac{1}{2}$ WHC). A broader range of water contents would have allowed us to more precisely characterize the limits of activity maintenance under low water content in finer granulometries (i.e., 0.5 and 0.1 mm grain size matrices). Regarding the microbial composition, it was also more influenced by water content at finer granulometries. We hypothesized that these observations could be linked with the differences in pore size rather than to grain size. This implies that at finer grain sizes, changes in water content would have a greater impact on the balance between oxygen diffusion and solute transport, and thus have a deterministic role on microbial community composition

and dynamics. Future analyses that separately examine the impact of pore size and grain size would help confirm this hypothesis.

Another aim of this thesis was to study the response of the DCM-degrading microbial community or of a pure strain to different physicochemical conditions. In particular, we focused on (i) microbial community-level response to a disturbance that is a change in oxygen status, examining both the effect on activity and composition, and (ii) whether changes also occurred at the strain level, by assessing transcriptomic changes on a model strain, *Hyphomicrobium* sp. GJ21. This strain was chosen because it can use DCM as a carbon and energy source under both oxic and anoxic conditions, a rare feature in available DCM-degrading isolates. First, the response of the community to the disturbance in oxygen status appeared to depend on the direction of the change (**Figure VII.1-(iii)**). In particular, a change from anoxic to oxic conditions generally led to community gain-of-function, except in cases where water content was limited (i.e., with the 2 mm grain size matrix at 1/2 WHC) or in condition where gas and solutes diffusion was reduced (i.e., with the 0.1 mm grain size matrix, regardless of water content). The opposite disturbance, from oxic to anoxic conditions, led to variable responses, with either function maintenance or loss. A longer observation period after the disturbance could have shown whether the DCM-degrading communities that lost the function were truly sensitive to the disturbance or just needed more time to recover the DCM-degrading activity. Additionally, a change in the oxygen status appeared to be a sufficient disturbance to cause a change in the microbial community composition. Finally, the exposure of *Hyphomicrobium* sp. GJ21 to different oxygen levels revealed major effect at the level of gene expression (**Figure VII.1-(iv)**). Among the impacted genes were the ones that encode proteins related to the respiratory chain, the cofactor PQQ and the homeostasis of essential ions. No differences were observed in the overall number of expressed genes.

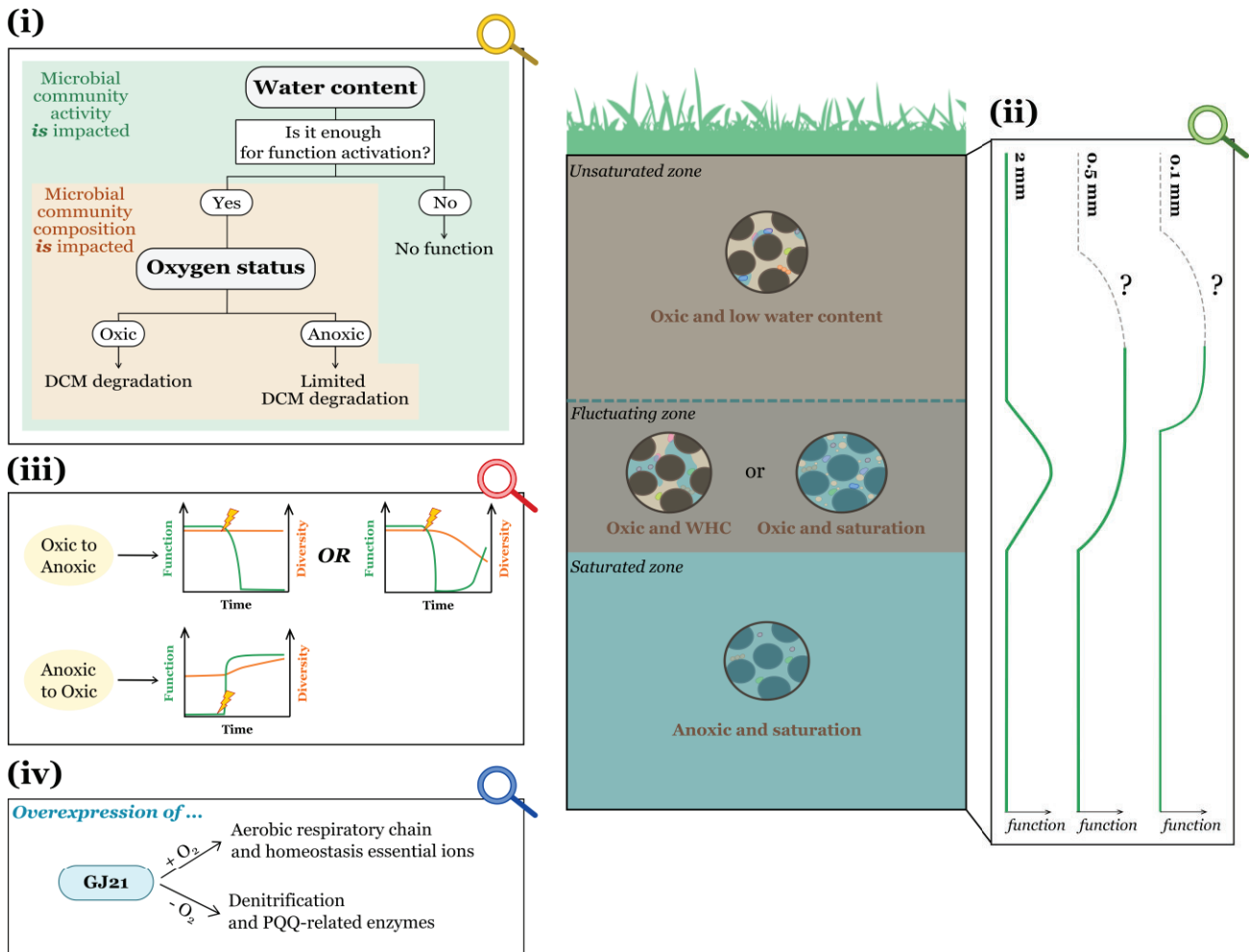


Figure VII.1. Visual summary of the conclusions obtained during this PhD work. The research questions addressed are the following: **(i)** What is the impact of water content and oxygen status on the function and composition of a DCM-degrading microbial community?; **(ii)** Can soil granulometry change how water content and oxygen level impact the activity and composition of a DCM-degrading microbial community?; **(iii)** What is the response of a DCM-degrading microbial community to a disturbance, here a change in oxygen concentration? Does this response depend on the environmental conditions?; and **(iv)** How does oxygen concentration impact the gene expression of the facultatively anaerobic DCM-degrading strain *Hyphomicrobium* sp. GJ21?

VII.2 Experimental limitations

The work described in this thesis relied upon several experimental techniques and decisions, each with their own drawbacks and limitations. For example, the environmental inocula used in chapters III and V had been stored for several years (from 2019 until 2021) in non-sterile environments (bottles and non-sterilized zip bags), and different preservation methods were used (part of the sand was stored dry at -20°C , while the other part was kept water-saturated at 4°C). As a result, we could not be certain that the DCM-degrading microbial communities active during the laboratory-scale aquifers experiment were still present at the start of our own

experiments. In this regard, although Prieto-Espinoza and colleagues showed that the DCM biodegradation in the laboratory-scale aquifers primarily occurred through anaerobic metabolism (Prieto-Espinoza et al., 2023), in our experiment, the DCM biodegradation under anoxic conditions was limited. This suggests that the populations responsible for the anaerobic DCM degradation are either dependent of the waterflow for their activity, or that they have been sensitive to the storage conditions, possibly due to the lack of a consistent anoxic environment. To avoid losing these populations or their activities, we could have used a 'new' environmental inoculum directly sampled from the polluted aquifer site of Themeroil, that might have allowed us to work with a DCM-degrading community more representative of the on-site conditions.

Another limitation encountered in **chapter V**, related to the GC-MS-FID equipment. Despite the advantages provided by this equipment (see **section IV.1**), it was still not possible to analyze more than 60 samples in a series. Thus, we had to process the samples in batches. To do that, we decided to group the samples by the matrix granulometry to (i) simplify the experimental set up, and (ii) reduce the number of calibration points needed for each batch (for each matrix granulometry, we needed from 4 to 6 calibration points). In this context, and given the differences observed based on the matrix granulometry, it raises the question of whether (and how) this decision may have influenced the results, and we wonder if separating the samples differently, such as by water content or mix them randomly, might have been a better approach. Additionally, and related with the space limitations imposed by the methods used in **chapters III** and **V**, the number of replicates in our experiments was limited, which consequently restricted the scope of the statistical analysis and their interpretations.

Regarding the analysis of the microbial community composition, DNA was only extracted at the beginning and end of the experiments (as well as before the disturbance in **chapter V**). Therefore, it was not possible to completely resolve the dynamics of the microbial community or of the different taxa over time. To achieve this, multiple sampling points should have been taken throughout the experiment in the different microcosms. However, in our experiments, sampling without significantly disturbing the environment was challenging and especially in the case of the microcosms **chapter V**, where the amount of matrix was very limited by the microcosms scale-down. In future explorations, these limitations should be considered, and a larger system should be used to allow easier sampling and the collection of a greater matrix volume. This would also help to avoid the DNA concentration limitations that we encountered in both **chapters III** and **V**. Another possibility is the use of a sacrificial method, where multiple microcosms are set up for each experimental condition, and at each sampling point, one of the replicates is entirely used to study the microbial community. The important drawback of the sacrificial method is that we should assume that all replicates have similar compositions and follow the exact same dynamics. From our observation in some conditions (e.g., OA replicates with the 2 mm grain size matrix at water saturation showed different response to disturbance), this assumption is not always applicable.

Finally, another limitation resulting from a methodological decision was the use of the 16S rRNA gene amplicon sequencing to analyze the microbial community, rather than its RNA equivalent or even total RNA sequencing. This choice meant we could not determine which specific taxa was active, or which metabolic activities were expressed under the different experimental conditions. In **chapter V**, we tried to identify taxa/ASVs associated with the DCM-degrading activity through correlation analysis, but we still needed to verify whether these associations were accurate or spurious.

In next section, we will discuss potential approaches to overcome some of these limitations and explore future perspectives for further investigation.

VII.3 Perspectives

As in any scientific work, in the process of addressing our research questions several other ideas arose, notably to overcome some of the limitations highlighted above. Some of these ideas can be future avenues to better understand pollutant(s) fate in aquifers for bioremediation perspectives. In the following sections, these ideas and their feasibility will be discussed.

VII.3.1 Characterisation of ecological niches and DCM-degrading taxa

An ecological niche is described as the set of environmental conditions, including biotic and abiotic factors, that allow a species to persist and carry out its functional role within an ecosystem (Malard & Guisan, 2023). During this PhD work, we have studied a set of abiotic factors (i.e. water content, oxygen level and matrix granulometry) that shaped available ecological niches for the DCM-degrading microbial taxa in our environmental samples. By analysing the taxonomical composition of the microbial communities under these different conditions through 16S rRNA gene amplicon sequencing, we have also somehow started to characterize their ecological niches. However, at that stage, we were unable to determine the overall potential metabolic activities present or identify which taxa, among the ones detected in the DCM-degrading community, were actively degrading this compound in each niche. These are open questions that can set the long- and short-terms perspectives of my work.

To characterize the metabolic activities in each ecological niche, a possibility is to use metatranscriptomics, which enables the identification of actively transcribed genes and gives insights into the metabolic responses of the overall DCM-degrading microbial community to the environmental conditions of interest. To apply this strategy as follow-up of my work, it would first be necessary to decide which combination of physicochemical parameters is the most interesting to start with. Considering that taxonomic composition was primarily impacted by oxygen concentration, I would choose to assess the different metabolic activities established in the microcosms as a function of this parameter. In particular, I would focus on the microcosms at water saturation or WHC with the 0.5 mm grain size matrix, as these cases showed DCM degradation under both oxic and anoxic conditions. The working hypothesis

would be that different activity profiles, associated with different sets of active populations, will arise from different oxygen concentrations. For example, given that the genes *mecE-F* were detected in our environmental inoculum, I would expect the *mec* cassette to be significantly more expressed under anoxic conditions compared to oxic conditions, since this cluster is associated with DCM anaerobic metabolism. In contrast, I would expect the *dcm* island to be more expressed under oxic conditions, although it may still be transcribed under anoxic and denitrifying conditions, as for the facultatively anaerobic strain *Hyphomicrobium* sp. GJ21. In addition, it would also be interesting to study the metabolic activity of these same microcosms just after the change in oxygen concentration and at different time points after the disturbance, to analyze whether the functional response we observed during the experiment is accompanied by a shift in the community's expressed genes. In particular, when resilience was observed, the question would be whether the DCM-degrading function is expressed by the same populations or if functional redundancy allows other populations to take over the DCM degradation process.

To identify the microbial taxa actively degrading DCM in the different ecological niches, the DNA-Stable Isotope Probing (SIP) technique can be used. This method is based on the utilization of ^{13}C -labelled DCM. Microorganisms that actively use this compound as a carbon source will incorporate the heavy isotope (i.e., ^{13}C) into their neosynthesised biomolecules, notably genomic DNA. This will lead to the increased density of their nucleic acids, allowing their separation on an isopycnic gradient. The genomic content of the labelled taxa can then be analysed separately from non-labelled DNA, using either 16S rRNA gene amplicon sequencing or a shotgun metagenomics approach. The application of the DNA-SIP could therefore contribute to the identification of new DCM-degrading taxa that may have developed in the different microcosms and difficult to isolate, as well as new biomarkers for the detection of DCM biodegradation activity *in situ*. During my master's internship, I optimized the separation and purification of the heavy and light DNA fractions. Since, the methods have been applied in a microbial community exposed to micropollutant in a previous PhD work of the group (A. Borreca, 2024). Thus, we could consider this as a short-term perspective of my project. For example, a potential set up to apply this technique would be the microcosms at WHC with the 2 mm grain size matrix under oxic conditions, which showed a high degradation rate of DCM and where the *Rhodococcus* sp. was the dominant taxa. As mentioned in chapter V, this genus has already been linked to the utilization of DCM as a sole carbon and energy source, but in the absence of the *dcmA* gene. Thus, it would be interesting to determine whether *Rhodococcus* sp. was involved in the DCM degradation in these microcosms' setup. If so, we could further study its degradation system in detail in the laboratory, presuming we can isolate this representative. It would also be of interest to perform the DNA-SIP on the microcosms under anoxic conditions, a scenario where our knowledge is still somewhat limited. For instance, the study of the microcosms at WHC with the 0.5 mm grain size matrix under anoxic conditions, where DCM degradation was previously observed, would allow the identification of key taxa for this function. In this context, I propose starting to investigate the

AA microcosm with the 0.5 mm grain size matrix at WHC, which maintained DCM degradation under anoxic conditions until the end of the experiment. These microcosm replicates, like all the microcosms in the experiment, were stored frozen at -20°C at the end of the experiment. We could thus distribute its content into four vials, and spike duplicates of these vials with ^{13}C -DCM, and the other duplicates with ^{12}C -DCM. Based on previous work (Hu, 2021) and to provide enough C to have both DNA strands labelled, we should add at least 6 mM of DCM per microcosm, which means performing at least 6 spikes of 1 mM of DCM each per microcosm. At the end of the incubation, DNA extraction and purification of labelled and unlabelled DNA can be done using the protocol I optimized in the laboratory.

VII.3.2 Importance of matrix grain size vs. porosity and converging to on-site conditions

During this work, we observed that matrix granulometry influenced the composition of the microbial community when exposed to different water content and oxygen status (**Figure VII.2-a.**). We hypothesized that this effect could be attributed to the differences in pore size and connectivity of each matrix, which may impact the balance between gas diffusion and solute transport. However, as Payton and colleagues discussed, the sole use of spherical grains does not allow to separate grain size and matrix porosity contributions (Payton et al., 2022). One way to deconvolute these two contributions is to use grains with a gradient of sphericity, from very angular to rounded particles, or other geometrical shapes for the particles of the matrix, such as cubes, rectangular prisms or pyramids. Hence, grain size (or volume to surface ratio) no longer influences matrix porosity nor connectivity (**Figure VII.2-b.**). This would allow us to determine whether the differences in particles surface area are sufficient for changing the DCM-degrading microbial community or if the effect is related to pores size and connectivity. This study would fall under the long-term perspectives, since it would first be necessary to solve and optimize several parameters, including how to obtain the beads in the desired shape (one possibility to explore would be the 3D-printing of these beads in a material compatible with microbiology and the solvent effect of DCM, or using microfluidic (Alekklett et al., 2018)).

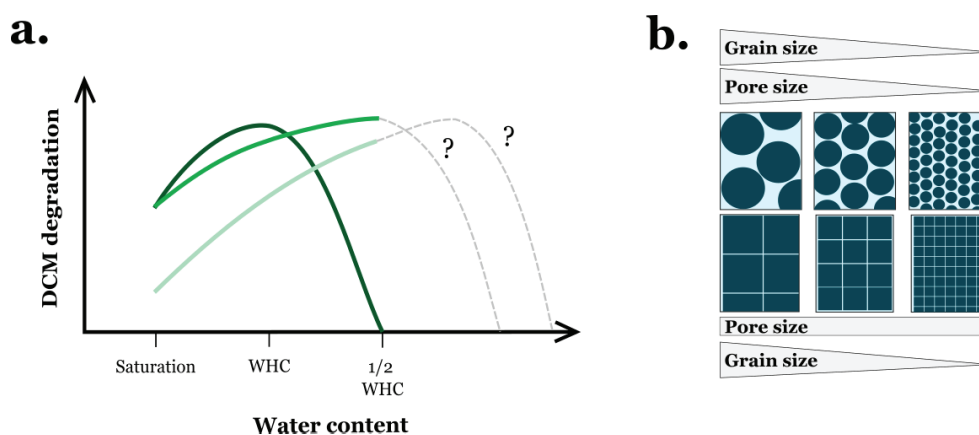


Figure VII.2. Characterisation of matrix impact. **a.** Relationship between DCM degradation activity and water content across the different matrix granulometries observed in **chapter V**. The colour gradient indicates the grain size: dark green for 2 mm grain size matrix, medium green for 0.5 mm grain size matrix, and light green for 0.1 mm grain size matrix. The dashed grey parts of the curves are the water content that were not tested during our experiments **b.** Example of how different grain shapes (spheres and squares) impact the relationship between grain size and pore size. In spherical grains, the pore size decreases as the grain size reduces, while in square grains, the pore size remains unaffected by the reduction in grain size.

On the other hand, a limitation for translating these PhD findings to the on-site scenarii is that the microcosms used are highly simplified representations of the aquifer environment. In particular, the microbial community was exposed to an artificial matrix, composed of an inert material, with only one type of granulometry per microcosm. However, this is not what is typically found *in situ*. Indeed, aquifer sediments comprise a combination of different grain sizes, arising from natural processes, such as sedimentation, erosion, and transport of soil particles, that shape the formation of aquifers over time (Hanshaw & Back, 1979). Thus, if we aim to get closer to on-site conditions, we could try to combine particles of different grain sizes in various proportions and explore the consequences on the microbial community and its activity. In addition, we could also try working with natural soil that would incorporate the variable of different mineral composition associated to each type of particle sediments, which seems to influence the microbial community diversity and composition (Hemkemeyer et al., 2014). In terms of timeline, working with matrices that combine different granulometries can be considered a short-term perspective, as we could use a mixture of the beads of different grain sizes that we already have in the laboratory. However, utilizing a natural soil sediment would require an initial optimization, so this avenue of exploration can be regarded as a longer-term perspective.

VII.3.3 Exploration of the role of PQQ under anoxic conditions

In addition to the expected changes in gene expression related to the nitrate reductase complex in *Hyphomicrobium* sp. GJ21 at different oxygen concentrations, an intriguing finding was the overexpression of PQQ-related genes under anoxic conditions compared to

oxic conditions. These genes included those involved in the PQQ biosynthesis and various PQQ-dependent dehydrogenases. Here, we hypothesized that, considering the bioenergetic differences between aerobic respiration and denitrification, the overexpression of these genes may help maintaining the energy balance and redox state under anoxic condition. To explore the importance and the role of these PQQ-dependent dehydrogenases in the redox state and homeostasis of the bacterial cells under anoxic conditions, classical targets include examining the NADH/NAD⁺ balance and the ATP production. On the one hand, to examine the impact on the redox state, we could use genetically encoded biosensors that, upon binding to NADH, undergo conformational, chemical, or regulatory change coupled to a spectroscopic response. Liu and colleagues followed this strategy by using the redox-responsive bacterial transcriptional factor Rex, coupled to a fluorescent protein, to investigate the effect of removing respiratory chain enzymes on the NADH/NAD⁺ ratio during aerobic respiration in *E. coli* (Liu et al., 2019a). On the other hand, to examine the ATP production, one traditionally used technique is the luciferin/luciferase assay, which relies on the conversion of luciferin by the luciferase in the presence of ATP, resulting on the production of a bioluminescent signal. The main disadvantage of this method is that it requires cell lysis, preventing continuous and real-time intracellular ATP measurements. Deng and colleagues proposed a new strategy using a genetically encoded ATP biosensor, specifically the ATP-sensing *rrnB* P1 promoter coupled with a fluorescent protein, which allows quantitative estimation of intracellular ATP flux in living cells (Deng et al., 2021). Unfortunately, all these strategies requiring genetic manipulations should be considered for the moment as a long-term perspective since we lack proper tools to bioengineer the bacteria of the genus *Hyphomicrobium*.

However, it might be noted that one of the PQQ-dependent dehydrogenases found to be more expressed in anoxic conditions (7th most overexpressed gene) was encoding the MDH XoxF, the first enzyme discovered to use lanthanides as cofactor (Hibi et al., 2011) and a well-studied enzyme in other methylotrophic bacteria (Schmidt et al., 2010). It has notably been associated to stress response (Firsova et al., 2015) and shown to be also expressed in absence of methanol (Chaignaud et al., 2017) and in non-methylotrophic bacteria (Skovran et al., 2011). The in-depth study of this enzyme in alternative model strains can pave the way to understand the role of the PQQ-dependent dehydrogenases in *Hyphomicrobium* sp. GJ21 under denitrifying conditions. Conversely, our observations might help deciphering secondary function of this enzyme, which is apparently not exclusively dedicated to catalysing methanol oxidation.

VII.3.4 Other future perspectives

The above mentioned research ideas could help addressing the major questions arising from the thesis work. However, other questions remain that could serve as a starting point for future research outcomes.

For example, one intriguing question following the findings in Chapter V is whether the microbial communities that ‘gain’ the DCM-degrading activity after changing from anoxic to

oxic condition will maintain this function if exposed to a new disturbance, for example switching them back to the anoxic condition. Considering our observations in Chapter III, where periodic alternations between anoxic and oxic conditions promoted DCM degradation in anoxic conditions, I would speculate that this function will be maintained. If it is indeed maintained, it would be interesting to see whether the microbial community composition also return to its pre-disturbance composition and structure. In this case, I would speculate that it will rather continue progressing developing a microbial community adapted to these alternations, different from stable oxic or stable anoxic microbial community. In contrast, if the microbial community dynamics points toward a more similar composition to the pre-disturbance one, this would suggest that the initial microbial community had the potential for DCM degradation from the beginning, but probably lacked some essential element (component, interactions or time) for the onset of the activity. In this regard, as discussed in Chapter III and as proposed by Prieto-Espinoza and colleagues, this essential element may be CO₂, which seems to promote the metabolic activity of anaerobic DCM degraders (Prieto-Espinoza et al., 2023). During our experiment, the CO₂ that was flushed out at the beginning while establishing the anoxic conditions could have been replenished and dissolved in the liquid phase by the microbial respiration when exposed to oxic conditions. To further investigate the role of CO₂ in this context, we could compare the DCM-degrading function of the microbial community in our environmental inoculum under three conditions: (i) periodic alternation of oxic-anoxic conditions, (ii) periodic addition of CO₂ to the microcosms, and (iii) no opening of microcosms over time. This would allow us to see whether the addition of CO₂ has the same effect on DCM degradation in anoxic conditions as alternating the oxygen concentration.

Another interesting outlook is to explore the relationship between *Hyphomicrobium* sp. GJ21 and the matrix. In Chapter V we observed that the family *Hyphomicrobiaceae*, to which this strain belongs, was significantly more abundant in the absence of the matrix. Thus, we could investigate whether *Hyphomicrobium* sp. GJ21 exhibits different behaviours in the presence versus absence of a matrix, both at the activity- and transcriptomic-level. Since this bacterium is typically considered a reference strain for bioremediation strategies, this study would indicate whether we should reconsider its potential application in aquifers. Moreover, throughout the experiment, we also found that *Hyphomicrobium* sp. GJ21 is sensitive to low water content. In this context, it would be worthwhile to explore the water activity of this strain, which would give useful insights for planning its use in bioremediation strategies. This would necessitate to optimise microcosms size and volume to recover enough biological material, as well as to develop a strategy allowing to collect *Hyphomicrobium* sp. GJ21 biomass in the same physiological status under different water contents for transcriptomics analysis (in comparison to the exponential phase traditionally used in liquid culture). A potential approach to explore would be to measure DCM concentrations in the headspace of the cultures as a proxy of the strain growth. If this holds true, it could help to find the equivalent of the mid-log phase in the microcosms to harvest *Hyphomicrobium* sp. GJ21.

Finally, the data obtained from all these perspectives, along with the exploration of how other physicochemical parameters (e.g., pH, organic matter, etc.) affect DCM-degrading microbial populations, would provide valuable insights for developing more accurate models for the reactive transport of this contaminant in aquifers. In this regard, based on our findings, the incorporation of the grain sizes/pore sizes variable into numerical models that aim at understanding the DCM biodegradation dynamics in polluted aquifers is essential, as it influences both the microbial community behaviour and the physicochemical conditions of the environment. For instance, this parameter is sometimes overlooked or simplified in the literature due to the lack of *in situ* physical characterisation of soil particles at the polluted sites to be modelled, the challenges of incorporate such data, and the increased computation cost in the numerical models (Golparvar et al., 2021). However, despite these difficulties, including the grain size/pore size variable in these models would provide valuable insights into *in situ* processes. Ultimately, this could lead to the design of more effective bioremediation strategies that better account for the prevailing environmental conditions and the specific characteristics of different contaminated sites.

References

- Achenbach, L. A., Michaelidou, U., Bruce, R. A., Fryman, J., & Coates, J. D. (2001). *Dechloromonas agitata* gen. nov., sp. nov. and *Dechlorosoma suillum* gen. nov., sp. nov., two novel environmentally dominant (per)chlorate-reducing bacteria and their phylogenetic position. *International Journal of Systematic and Evolutionary Microbiology*, *51*(2), 527–533.
- Adachi, A., Hamamoto, H., & Okano, T. (2005). Use of lees materials as an adsorbent for removal of organochlorine compounds or benzene from wastewater. *Chemosphere*, *58*(6), 817–822.
- Adachi, A., Ikeda, C., Takagi, S., Fukao, N., Yoshie, E., & Okano, T. (2001). Efficiency of rice bran for removal of organochlorine compounds and benzene from industrial wastewater. *Journal of Agricultural and Food Chemistry*, *49*(3), 1309–1314.
- Agnello, A. C., Bagard, M., van Hullebusch, E. D., Esposito, G., & Huguenot, D. (2016). Comparative bioremediation of heavy metals and petroleum hydrocarbons co-contaminated soil by natural attenuation, phytoremediation, bioaugmentation and bioaugmentation-assisted phytoremediation. *Science of The Total Environment*, *563*, 693–703.
- Aleklett, K., Kiers, E. T., Ohlsson, P., Shimizu, T. S., Caldas, V. E. A., & Hammer, E. C. (2018). Build your own soil: exploring microfluidics to create microbial habitat structures. *The ISME Journal*, *12*(2), 312–319.
- Allison, S. D., McGuire, K. L., & Treseder, K. K. (2010). Resistance of microbial and soil properties to warming treatment seven years after boreal fire. *Soil Biology and Biochemistry*, *42*(10), 1872–1878.
- Allison, V. J., Yermakov, Z., Miller, R. M., Jastrow, J. D., & Matamala, R. (2007). Using landscape and depth gradients to decouple the impact of correlated environmental variables on soil microbial community composition. *Soil Biology and Biochemistry*, *39*(2), 505–516.
- An, M., Western, L. M., Say, D., Chen, L., Claxton, T., Ganesan, A. L., ... & Rigby, M. (2021). Rapid increase in dichloromethane emissions from China inferred through atmospheric observations. *Nature Communications*, *12*(1), 7279.
- An, S., Kim, S. H., Woo, H., Choi, J. W., Yun, S.-T., Chung, J., & Lee, S. (2024). Groundwater-level fluctuation effects on petroleum hydrocarbons in vadose zones and their potential risks: Laboratory studies. *Journal of Hazardous Materials*, *463*, 132837.
- Anderson, D. J., Morris, C. J., Nunn, D. N., Anthony, C., & Lidstrom, M. E. (1990). Nucleotide sequence of the *Methylobacterium extorquens* AM1 *moxF* and *moxJ* genes involved in methanol oxidation. *Gene*, *90*(1), 173–176.

- Andrews, S. C., Robinson, A. K., & Rodríguez-Quiñones, F. (2003). Bacterial iron homeostasis. *FEMS Microbiology Reviews*, 27(2), 215–237.
- Arai, H. (2011). Regulation and function of versatile aerobic and anaerobic respiratory metabolism in *Pseudomonas aeruginosa*. *Frontiers in Microbiology*, 2, 103.
- Armesto, J. J., & Pickett, S. T. A. (1985). Experiments on disturbance in old-field plant communities: impact on species richness and abundance. *Ecology*, 66(1), 230–240.
- Bailón, L., Dopico, Y., Nikolausz, M., Kästner, M., Veiga, M. C., & Kennes, C. (2007). Removal of dichloromethane from waste gases using a fixed-bed biotrickling filter and a continuous stirred tank bioreactor. *Biotechniques for Air Pollution Control II*, 505–514.
- Banerjee, S., Helgason, B., Wang, L., Winsley, T., Ferrari, B. C., & Siciliano, S. D. (2016). Legacy effects of soil moisture on microbial community structure and N₂O emissions. *Soil Biology and Biochemistry*, 95, 40–50.
- Barnett, D. J. m, Arts, I. C. w, & Penders, J. (2021). microViz: An R package for microbiome data visualization and statistics. *Journal of Open Source Software*, 6(63), 3201.
- Bednarz, E. M., Hossaini, R., & Chipperfield, M. P. (2023). Atmospheric impacts of chlorinated very short-lived substances over the recent past – Part 2: Impacts on ozone. *Atmospheric Chemistry and Physics*, 23(21), 13701–13711.
- Benbrahim-Tallaa, L., Lauby-Secretan, B., Loomis, D., Guyton, K. Z., Grosse, Y., El Ghissassi, F., ... & Straif, K. (2014). Carcinogenicity of perfluorooctanoic acid, tetrafluoroethylene, dichloromethane, 1,2-dichloropropane, and 1,3-propane sultone. *The Lancet Oncology*, 15(9), 924–925.
- Bender, E. A., Case, T. J., & Gilpin, M. E. (1984). Perturbation experiments in community ecology: Theory and practice. *Ecology*, 65(1), 1–13.
- Blackman, A. J., Davies, N. W., & Ralph, C. E. (1992). Volatile and odorous compounds from the bryozoan *Biflustra perfragilis*. *Biochemical Systematics and Ecology*, 20(4), 339–342.
- Bougon, N., Aquilina, L., Molénat, J., Marie, D., Delettre, Y., Chancerel, E., & Vandenkoornhuyse, P. (2012). Influence of depth and time on diversity of free-living microbial community in the variably saturated zone of a granitic aquifer. *FEMS Microbiology Ecology*, 80(1), 98–113.
- Brewer, T. E., Aronson, E. L., Arogyaswamy, K., Billings, S. A., Botthoff, J. K., Campbell, A. N., ... & Fierer, N. (2019). Ecological and genomic attributes of novel bacterial taxa that thrive in subsurface soil horizons. *mBio*, 10(5), 10:10.1128/mbio.01318-19.

- Bringel, F., Postema, C. P., Mangenot, S., Bibi-Triki, S., Chaignaud, P., Farhan Ul Haque, M., ... & Vuilleumier, S. (2017). Genome sequence of the dichloromethane-degrading bacterium *Hyphomicrobium* sp. strain GJ21. *Genome Announcements*, 5(30), 10–1128.
- Bro, R., & Smilde, A. K. (2014). Principal component analysis. *Anal. Methods*, 6(9), 2812–2831.
- Bulka, O., Picott, K., Mahadevan, R., & Edwards, E. A. (2024). From *mec* cassette to *rdhA*: a key *Dehalobacter* genomic neighborhood in a chloroform and dichloromethane-transforming microbial consortium. *Applied and Environmental Microbiology*, e00732-24.
- Cáceres, M. D., & Legendre, P. (2009). Associations between species and groups of sites: Indices and statistical inference. *Ecology*, 90(12), 3566–3574.
- Callahan, B. J., McMurdie, P. J., Rosen, M. J., Han, A. W., Johnson, A. J. A., & Holmes, S. P. (2016). DADA2: high-resolution sample inference from Illumina amplicon data. *Nature Methods*, 13(7), 581–583.
- Camacho, C., Coulouris, G., Avagyan, V., Ma, N., Papadopoulos, J., Bealer, K., & Madden, T. L. (2009). BLAST+: Architecture and applications. *BMC Bioinformatics*, 10(1), 421.
- Cardinale, M., Brusetti, L., Quatrini, P., Borin, S., Puglia, A. M., Rizzi, A., ... & Daffonchio, D. (2004). Comparison of different primer sets for use in automated ribosomal intergenic spacer analysis of complex bacterial communities. *Applied and Environmental Microbiology*, 70(10), 6147–6156.
- Cavelan, A., Golfier, F., Colombano, S., Davarzani, H., Deparis, J., & Faure, P. (2022). A critical review of the influence of groundwater level fluctuations and temperature on LNAPL contaminations in the context of climate change. *Science of The Total Environment*, 806, 150412.
- Chaignaud, P., Maucourt, B., Weiman, M., Alberti, A., Kolb, S., Cruveiller, S., Vuilleumier, S., & Bringel, F. (2017). Genomic and transcriptomic analysis of growth-supporting dehalogenation of chlorinated methanes in *Methylobacterium*. *Frontiers in Microbiology*, 8, 1600.
- Chen, G., Fisch, A. R., Gibson, C. M., Erin Mack, E., Seger, E. S., Campagna, S. R., & Löffler, F. E. (2020a). Mineralization versus fermentation: evidence for two distinct anaerobic bacterial degradation pathways for dichloromethane. *The ISME Journal*, 14(4), 959–970.
- Chen, G., Kleindienst, S., Griffiths, D. R., Mack, E. E., Seger, E. S., & Löffler, F. E. (2017). Mutualistic interaction between dichloromethane- and chloromethane-degrading bacteria in an anaerobic mixed culture. *Environmental Microbiology*, 19(11), 4784–4796.

- Chen, J., & Strous, M. (2013). Denitrification and aerobic respiration, hybrid electron transport chains and co-evolution. *Biochimica et Biophysica Acta (BBA)-Bioenergetics*, *1827*(2), 136–144.
- Chen, M., Al-Maktoumi, A., Al-Mamari, H., Izady, A., Reza Nikoo, M., & Al-Busaidi, H. (2020b). Oxygenation of aquifers with fluctuating water table: a laboratory and modeling study. *Journal of Hydrology*, *590*, 125261.
- Claxton, T., Hossaini, R., Wilson, C., Montzka, S. A., Chipperfield, M. P., Wild, O., ... & Lunder, C. (2020). A synthesis inversion to constrain global emissions of two very short lived chlorocarbons: dichloromethane, and perchloroethylene. *Journal of Geophysical Research: Atmospheres*, *125*(12), e2019JD031818.
- Cruz-Martínez, K., Rosling, A., Zhang, Y., Song, M., Andersen, G. L., & Banfield, J. F. (2012). Effect of rainfall-induced soil geochemistry dynamics on grassland soil microbial communities. *Applied and Environmental Microbiology*, *78*(21), 7587–7595.
- Curiel-Alegre, S., Velasco-Arroyo, B., Rumbo, C., Khan, A. H. A., Tamayo-Ramos, J. A., Rad, C., Gallego, J. L. R., & Barros, R. (2022). Evaluation of biostimulation, bioaugmentation, and organic amendments application on the bioremediation of recalcitrant hydrocarbons of soil. *Chemosphere*, *307*, 135638.
- DeAngelis, K. M., Silver, W. L., Thompson, A. W., & Firestone, M. K. (2010). Microbial communities acclimate to recurring changes in soil redox potential status. *Environmental Microbiology*, *12*(12), 3137–3149.
- Declercq, I., Cappuyns, V., & Duclos, Y. (2012). Monitored natural attenuation (MNA) of contaminated soils: state of the art in Europe—A critical evaluation. *Science of The Total Environment*, *426*, 393–405.
- Dekant, W., Jean, P., & Arts, J. (2021). Evaluation of the carcinogenicity of dichloromethane in rats, mice, hamsters and humans. *Regulatory Toxicology and Pharmacology*, *120*, 104858.
- Deng, Y., Beahm, D. R., Ionov, S., & Sarpeshkar, R. (2021). Measuring and modeling energy and power consumption in living microbial cells with a synthetic ATP reporter. *BMC Biology*, *19*(1), 101.
- Dereeper, A., Guignon, V., Blanc, G., Audic, S., Buffet, S., Chevenet, F., ... & Gascuel, O. (2008). Phylogeny.fr: robust phylogenetic analysis for the non-specialist. *Nucleic Acids Research*, *36*(suppl_2), W465–W469.
- DeWeerd, K. A., Flanagan, W. P., Brennan, M. J., Principe, J. M., & Spivack, J. L. (1998). Biodegradation of trichloroethylene and dichloromethane in contaminated soil and groundwater. *Bioremediation Journal*, *2*(1), 29–42.

- Diks, R. M. M., Ottengraf, S. P. P., & Vrijlnad, S. (1994). The existence of a biological equilibrium in a trickling filter for waste gas purification. *Biotechnology and Bioengineering*, 44(11), 1279–1287.
- Dilling, W. L., Tefertiller, N. B., & Kallos, G. J. (1975). Evaporation rates and reactivities of methylene chloride, chloroform, 1,1,1-trichloroethane, trichloroethylene, tetrachloroethylene, and other chlorinated compounds in dilute aqueous solutions. *Environmental Science & Technology*, 9(9), 833–838.
- DiVincenzo, G. D., & Kaplan, C. J. (1981). Uptake, metabolism, and elimination of methylene chloride vapor by humans. *Toxicology and Applied Pharmacology*, 59(1), 130–140.
- Dobson, R., Schroth, M. H., & Zeyer, J. (2007). Effect of water-table fluctuation on dissolution and biodegradation of a multi-component, light nonaqueous-phase liquid. *Journal of Contaminant Hydrology*, 94(3), 235–248.
- Doronina, N. V., Trotsenko, Y. A., Tourova, T. P., Kuznetsov, B. B., & Leisinger, T. (2001). *Albibacter methylovorans* gen. nov., sp. nov., a novel aerobic, facultatively autotrophic and methylophilic bacterium that utilizes dichloromethane. *International Journal of Systematic and Evolutionary Microbiology*, 51(3), 1051–1058.
- Dow, L., Morrissey, K. L., Willems, A., & Kroth, P. G. (2020). Complete genome sequence of *Dyadobacter* sp. 32, isolated from a culture of the freshwater diatom *Cymbella microcephala*. *Marine Genomics*, 52, 100720.
- Düffer, P. F. (2009). Glass surface corrosion and protective interleaving systems. In *69th Conference on Glass Problems: Ceramic Engineering and Science Proceedings, Volume 30, Issue 1* (pp. 181–188). Hoboken, NJ, USA: John Wiley & Sons, Inc..
- Duine, J. A. (1999). The PQQ story. *Journal of Bioscience and Bioengineering*, 88(3), 231–236.
- Duine, J. A., & Frank, J. (1990). The role of PQQ and quinoproteins in methylophilic bacteria. *FEMS Microbiology Reviews*, 7(3–4), 221–225.
- El Fantroussi, S., & Agathos, S. N. (2005). Is bioaugmentation a feasible strategy for pollutant removal and site remediation? *Current Opinion in Microbiology*, 8(3), 268–275.
- Elsner, M., & Imfeld, G. (2016). Compound-specific isotope analysis (CSIA) of micropollutants in the environment—Current developments and future challenges. *Current Opinion in Biotechnology*, 41, 60–72.
- Emanuelsson, M. A. E., Osuna, M. B., Ferreira Jorge, R. M., & Castro, P. M. L. (2009). Isolation of a *Xanthobacter* sp. degrading dichloromethane and characterization of the gene involved in the degradation. *Biodegradation*, 20(2), 235–244.

- Ergas, Sarina. J., Kinney, K., Fuller, M. E., & Scow, K. M. (1994). Characterization of compost biofiltration system degrading dichloromethane. *Biotechnology and Bioengineering*, *44*(9), 1048–1054.
- Fenchel, T., & Finlay, B. (2008). Oxygen and the spatial structure of microbial communities. *Biological Reviews*, *83*(4), 553–569.
- Feng, Y., Bie, P., Wang, Z., Wang, L., & Zhang, J. (2018). Bottom-up anthropogenic dichloromethane emission estimates from China for the period 2005–2016 and predictions of future emissions. *Atmospheric Environment*, *186*, 241–247.
- Fierer, N., Schimel, J. P., & Holden, P. A. (2003a). Influence of drying-rewetting frequency on soil bacterial community structure. *Microbial Ecology*, *45*(1), 63–71.
- Fierer, N., Schimel, J. P., & Holden, P. A. (2003b). Variations in microbial community composition through two soil depth profiles. *Soil Biology and Biochemistry*, *35*(1), 167–176.
- Filonov, A. E., Puntus, I. F., Karpov, A. V., Gaiazov, R. R., Kosheleva, I. A., & Boronin, A. M. (1999). Growth and survival of *Pseudomonas putida* strains degrading naphthalene in soil model systems with different moisture levels. *Process Biochemistry*, *34*(3), 303–308.
- Firsova, J. E., Doronina, N. V., & Trotsenko, Yu. A. (2010). Analysis of the key functional genes in new aerobic degraders of dichloromethane. *Microbiology*, *79*(1), 66–72.
- Firsova, Y. E., Torgonskaya, M. L., Doronina, N. V., & Trotsenko, Yu. A. (2005). Effects of DNA-damaging agents on aerobic methylobacteria capable and incapable of utilizing dichloromethane. *Applied Biochemistry and Microbiology*, *41*(5), 480–485.
- Firsova, Yu. E., Torgonskaya, M. L., & Trotsenko, Yu. A. (2015). Functionality of the *xoxF* gene in *Methylobacterium dichloromethanicum* DM4. *Microbiology*, *84*(6), 796–803.
- Freedman, D. L., Smith, C. R., & Noguera, D. R. (1997). Dichloromethane biodegradation under nitrate-reducing conditions. *Water Environment Research*, *69*(1), 115–122.
- Frindte, K., Eckert, W., Attermeyer, K., & Grossart, H.-P. (2013). Internal wave-induced redox shifts affect biogeochemistry and microbial activity in sediments: a simulation experiment. *Biogeochemistry*, *113*(1–3), 423–434.
- Giachino, A., & Waldron, K. J. (2020). Copper tolerance in bacteria requires the activation of multiple accessory pathways. *Molecular Microbiology*, *114*(3), 377–390.
- Gloor, G. B., Macklaim, J. M., Pawlowsky-Glahn, V., & Egozcue, J. J. (2017). Microbiome datasets are compositional: and this is not optional. *Frontiers in Microbiology*, *8*, 2224.

- Golparvar, A., Kästner, M., & Thullner, M. (2021). Pore-scale modeling of microbial activity: What we have and what we need. *Vadose Zone Journal*, 20(1), e20087.
- Graham, E. B., Averill, C., Bond-Lamberty, B., Knelman, J. E., Krause, S., Peralta, A. L., ... & Contributor Consortium. (2021). Toward a generalizable framework of disturbance ecology through crowdsourced science. *Frontiers in Ecology and Evolution*, 9, 588940.
- Green, T. (1997). Methylene chloride induced mouse liver and lung tumours: an overview of the role of mechanistic studies in human safety assessment. *Human & Experimental Toxicology*, 16(1), 3-13.
- Gribble, G. W. (2023). Naturally occurring organohalogen compounds—a comprehensive review. In *Naturally Occurring Organohalogen Compounds*, pp. 1-546, Springer.
- Grujčić, V., Kasalický, V., & Šimek, K. (2015). Prey-specific growth responses of freshwater flagellate communities induced by morphologically distinct bacteria from the genus *Limnohabitans*. *Applied and Environmental Microbiology*, 81(15), 4993–5002.
- Guermouche M'rassi, A., Bensalah, F., Gury, J., & Duran, R. (2015). Isolation and characterization of different bacterial strains for bioremediation of n-alkanes and polycyclic aromatic hydrocarbons. *Environmental Science and Pollution Research*, 22(20), 15332–15346.
- Gupta, P. K., Yadav, B., & Yadav, B. K. (2019). Assessment of LNAPL in subsurface under fluctuating groundwater table using 2D sand tank experiments. *Journal of Environmental Engineering*, 145(9), 04019048.
- Haberer, C. M., Rolle, M., Cirpka, O. A., & Grathwohl, P. (2012). Oxygen transfer in a fluctuating capillary fringe. *Vadose Zone Journal*, 11(3), vzj2011-0056.
- Hamdi, S., Chevallier, T., Ben Aïssa, N., Ben Hammouda, M., Gallali, T., Chotte, J.-L., & Bernoux, M. (2011). Short-term temperature dependence of heterotrophic soil respiration after one-month of pre-incubation at different temperatures. *Soil Biology and Biochemistry*, 43(9), 1752–1758.
- Hanshaw, B. B., & Back, W. (1979). Major geochemical processes in the evolution of carbonate—aquifer systems. *Journal of Hydrology*, 43(1), 287–312.
- Hashmi, M., Dechert, S., Dekant, W., & Anders, M. W. (1994). Bioactivation of [¹³C]dichloromethane in mouse, rat, and human liver cytosol: ¹³C nuclear magnetic resonance spectroscopic studies. *Chemical Research in Toxicology*, 7(3), 291–296.

- Hayoun, K., Geersens, E., Laczny, C. C., Halder, R., Lázaro Sánchez, C., Manna, A., ... & Vuilleumier, S. (2020). Dichloromethane degradation pathway from unsequenced *Hyphomicrobium* sp. MC8b rapidly explored by pan-proteomics. *Microorganisms*, 8(12), 1876.
- Hellal, J., Barthelmebs, L., Bérard, A., Cébron, A., Cheloni, G., Colas, S., ... & Vuilleumier, S. (2023). Unlocking secrets of microbial ecotoxicology: Recent achievements and future challenges. *FEMS Microbiology Ecology*, 99(10), fiad102.
- Hemkemeyer, M., Pronk, G. J., Heister, K., Kögel-Knabner, I., Martens, R., & Tebbe, C. C. (2014). Artificial soil studies reveal domain-specific preferences of microorganisms for the colonisation of different soil minerals and particle size fractions. *FEMS Microbiology Ecology*, 90(3), 770–782.
- Henry, B. M. (2010). Biostimulation for anaerobic bioremediation of chlorinated solvents. In *In Situ remediation of chlorinated solvent plumes* (pp. 357-423). New York, NY: Springer New York.
- Hermon, L. (2017). *Diagnostic microbiologique de sites contaminés par les solvants chlorés* (Doctoral dissertation, University of Strasbourg).
- Hermon, L., Denonfoux, J., Hellal, J., Jouliau, C., Ferreira, S., Vuilleumier, S., & Imfeld, G. (2018). Dichloromethane biodegradation in multi-contaminated groundwater: insights from biomolecular and compound-specific isotope analyses. *Water Research*, 142, 217–226.
- Hibi, Y., Asai, K., Arafuka, H., Hamajima, M., Iwama, T., & Kawai, K. (2011). Molecular structure of La³⁺-induced methanol dehydrogenase-like protein in *Methylobacterium radiotolerans*. *Journal of Bioscience and Bioengineering*, 111(5), 547–549.
- Holland, S. I., Ertan, H., Montgomery, K., Manefield, M. J., & Lee, M. (2021). Novel dichloromethane-fermenting bacteria in the *Peptococcaceae* family. *The ISME Journal*, 15(6), 1709-1721.
- Holland, S. I., Vázquez-Campos, X., Ertan, H., Edwards, R. J., Manefield, M. J., & Lee, M. (2022). Metaproteomics reveals methyltransferases implicated in dichloromethane and glycine betaine fermentation by ‘*Candidatus Formimonas warabiya*’ strain DCMF. *Frontiers in Microbiology*, 13, 1035247.
- Horvath, R. S. (1972). Microbial co-metabolism and the degradation of organic compounds in nature. *Bacteriological Reviews*, 36(2), 146–155.
- Hossaini, R., Chipperfield, M. P., Montzka, S. A., Leeson, A. A., Dhomse, S. S., & Pyle, J. A. (2017). The increasing threat to stratospheric ozone from dichloromethane. *Nature Communications*, 8(1), 15962.

- Hu, M. (2021). *Discovery of diverse dichloromethane-degrading bacteria and related genes/proteins from novel taxa*. (Doctoral dissertation, UNSW Sydney).
- Huang, J.-C., & Shang, C. (2006). Air stripping. In *Advanced physicochemical treatment processes* (pp. 47-79). Totowa, NJ: Humana Press.
- Iwabuchi, T., Inomata-Yamauchi, Y., Katsuta, A., & Harayama, S. (1998). Isolation and characterization of marine *Nocardioides* capable of growing and degrading phenanthrene at 42°C. *Journal of Marine Biotechnology*, 6, 86–90.
- Jansa, J., Mozafar, A., Kuhn, G., Anken, T., Ruh, R., Sanders, I. R., & Frossard, E. (2003). Soil tillage affects the community structure of mycorrhizal fungi in maize roots. *Ecological Applications*, 13(4), 1164–1176.
- Jia, W., Li, N., Yang, T., Dai, W., Jiang, J., Chen, K., & Xu, X. (2021). Bioaugmentation of atrazine-contaminated soil with *Paenarthrobacter* sp. strain AT-5 and its effect on the soil microbiome. *Frontiers in Microbiology*, 12, 771463.
- Jost, D., Haberer, C. M., Grathwohl, P., Winter, J., & Gallert, C. (2015). Oxygen transfer in a fluctuating capillary fringe: Impact of microbial respiratory activity. *Vadose Zone Journal*, 14(5), 1–14.
- Kanso, S., & Patel, B. K. C. (2004). *Phenylobacterium lituiforme* sp. nov., a moderately thermophilic bacterium from a subsurface aquifer, and emended description of the genus *Phenylobacterium*. *International Journal of Systematic and Evolutionary Microbiology*, 54(6), 2141–2146.
- Kawata, H., Nakayama, C., Sakamoto, M., Ikatsu, H., Miyoshi, S., Tomochika, K., & Shinoda, S. (2000). Isolation of dichloromethane-degrading bacteria from drainage water. *Journal of Health Science*, 46(3), 187–191.
- Kayser, M. F., Stumpp, M. T., & Vuilleumier, S. (2000). DNA polymerase I is essential for growth of *Methylobacterium dichloromethanicum* DM4 with dichloromethane. *Journal of Bacteriology*, 182(19), 5433–5439.
- Kayser, M. F., Ucurum, Z., & Vuilleumier, S. (2002). Dichloromethane metabolism and C1 utilization genes in *Methylobacterium* strains. *Microbiology*, 148(6), 1915–1922.
- Keith, L., & Telliard, W. (1979). ES&T special report: priority pollutants: Ia perspective view. *Environmental Science & Technology*, 13(4), 416–423.
- Kennedy, K., Hall, M. W., Lynch, M. D., Moreno-Hagelsieb, G., & Neufeld, J. D. (2014). Evaluating bias of Illumina-based bacterial 16S rRNA gene profiles. *Applied and Environmental Microbiology*, 80(18), 5717–5722.

- Kensa, V. M. (2011). Bioremediation - an overview. *Journal of Industrial Pollution Control*, 27(2), 161–168.
- Kim, B.-R., Shin, J., Guevarra, R. B., Lee, J. H., Kim, D. W., Seol, K.-H., ... & Isaacson, R. E. (2017). Deciphering diversity indices for a better understanding of microbial communities. *Journal of Microbiology and Biotechnology*, 27(12), 2089–2093.
- Kleindienst, S., Higgins, S. A., Tsementzi, D., Chen, G., Konstantinidis, K. T., Mack, E. E., & Löffler, F. E. (2017). ‘*Candidatus* Dichloromethanomonas elyunquensis’ gen. nov., sp. nov., a dichloromethane-degrading anaerobe of the *Peptococcaceae* family. *Systematic and Applied Microbiology*, 40(3), 150–159.
- Koenig, J., Lee, M., & Manefield, M. (2015). Aliphatic organochlorine degradation in subsurface environments. *Reviews in Environmental Science and Bio/Technology*, 14, 49–71.
- Kohler-Staub, D., Frank, S., & Leisinger, T. (1995). Dichloromethane as the sole carbon source for *Hyphomicrobium* sp. strain DM2 under denitrification conditions. *Biodegradation*, 6(3), 229–235.
- Kolusu, S. R., Schlünzen, K. H., Grawe, D., & Seifert, R. (2017). Chloromethane and dichloromethane in the tropical Atlantic Ocean. *Atmospheric Environment*, 150, 417–424.
- Kolusu, S. R., Schlünzen, K. H., Grawe, D., & Seifert, R. (2018). Determination of chloromethane and dichloromethane in a tropical terrestrial mangrove forest in Brazil by measurements and modelling. *Atmospheric Environment*, 173, 185–197.
- Kõressaar, T., Lepamets, M., Kaplinski, L., Raime, K., Andreson, R., & Remm, M. (2018). Primer3_masker: integrating masking of template sequence with primer design software. *Bioinformatics*, 34(11), 1937–1938.
- Krausova, V. I., Robb, F. T., & González, J. M. (2006). Biodegradation of dichloromethane in an estuarine environment. *Hydrobiologia*, 559(1), 77–83.
- Layer, O. (1988). *Montreal protocol on substances that deplete the ozone layer final act 1987*. Link: [Montreal protocol](#). Accessed on 22/10/2024.
- Lee, E.-H., Kim, J., Cho, K.-S., Ahn, Y. G., & Hwang, G.-S. (2010). Degradation of hexane and other recalcitrant hydrocarbons by a novel isolate, *Rhodococcus* sp. EH831. *Environmental Science and Pollution Research*, 17(1), 64–77.
- Legg, T., Zheng, Y., Simone, B., Radloff, K. A., Mladenov, N., González Peña, A., ... & Nemergut, D. R. (2012). Carbon, metals, and grain size correlate with bacterial community structure in sediments of a high arsenic aquifer. *Frontiers in Microbiology*, 3, 82.

- Leira, M., & Cantonati, M. (2008). Effects of water-level fluctuations on lakes: an annotated bibliography. *Ecological effects of water-level fluctuations in lakes*, 171-184.
- Leisinger, T., Bader, R., Hermann, R., Schmid-Appert, M., & Vuilleumier, S. (1994). Microbes, enzymes and genes involved in dichloromethane utilization. *Biodegradation*, 5(3), 237–248.
- Li, C., Chen, R., Liu, H., Huang, Y., Yu, J., Ouyang, W., & Xue, C. (2022). Response of chlorinated hydrocarbon transformation and microbial community structure in an aquifer to joint H₂ and O₂. *RSC Advances*, 12(36), 23252–23262.
- Linn, D. M., & Doran, J. W. (1984). Effect of water-filled pore space on carbon dioxide and nitrous oxide production in tilled and nontilled soils. *Soil Science Society of America Journal*, 48(6), 1267–1272.
- Liu, C., Cui, Y., Li, X., & Yao, M. (2021). microeco: An R package for data mining in microbial community ecology. *FEMS Microbiology Ecology*, 97(2), fiae255.
- Liu, Y., Landick, R., & Raman, S. (2019a). A regulatory NADH/NAD⁺ redox biosensor for bacteria. *ACS Synthetic Biology*, 8(2), 264–273.
- Liu, Y., Sun, Y., Yu, J., Xia, X., Ding, A., & Zhang, D. (2022). Impacts of groundwater level fluctuation on soil microbial community, alkane degradation efficiency and alkane-degrading gene diversity in the critical zone: evidence from an accelerated water table fluctuation simulation. *Environmental Science and Pollution Research*, 29(55), 83060–83070.
- Liu, Y.-L., Meng, D., Li, R.-R., Gu, P.-F., Fan, X.-Y., Huang, Z.-S., Du, Z.-J., & Li, Q. (2019b). *Rhodoligotrophos defluvii* sp. nov., isolated from activated sludge. *International Journal of Systematic and Evolutionary Microbiology*, 69(12), 3830–3836.
- Löser, C., Seidel, H., Zehnsdorf, A., & Stottmeister, U. (1998). Microbial degradation of hydrocarbons in soil during aerobic/anaerobic changes and under purely aerobic conditions. *Applied Microbiology and Biotechnology*, 49(5), 631–636.
- Louca, S., Polz, M. F., Mazel, F., Albright, M. B. N., Huber, J. A., O'Connor, M. I., ... & Parfrey, L. W. (2018). Function and functional redundancy in microbial systems. *Nature Ecology & Evolution*, 2(6), 936–943.
- Love, M. I., Huber, W., & Anders, S. (2014). Moderated estimation of fold change and dispersion for RNA-seq data with DESeq2. *Genome Biology*, 15(12), 550.
- Lv, H., Su, X., Wang, Y., Dai, Z., & Liu, M. (2018). Effectiveness and mechanism of natural attenuation at a petroleum-hydrocarbon contaminated site. *Chemosphere*, 206, 293–301.

- Mabey, W., & Mill, T. (1978). Critical review of hydrolysis of organic compounds in water under environmental conditions. *Journal of Physical and Chemical Reference Data*, 7(2), 383–415.
- Macdonald, C. A., Clark, I. M., Zhao, F.-J., Hirsch, P. R., Singh, B. K., & McGrath, S. P. (2011). Long-term impacts of zinc and copper enriched sewage sludge additions on bacterial, archaeal and fungal communities in arable and grassland soils. *Soil Biology and Biochemistry*, 43(5), 932–941.
- Madeira, F., Madhusoodanan, N., Lee, J., Eusebi, A., Niewielska, A., Tivey, A. R. N., Lopez, R., & Butcher, S. (2024). The EMBL-EBI Job Dispatcher sequence analysis tools framework in 2024. *Nucleic Acids Research*, gkae241.
- Mägli, A., Messmer, M., & Leisinger, T. (1998). Metabolism of dichloromethane by the strict anaerobe *Dehalobacterium formicoaceticum*. *Applied and Environmental Microbiology*, 64(2), 646–650.
- Mägli, A., Wendt, M., & Leisinger, T. (1996). Isolation and characterization of *Dehalobacterium formicoaceticum* gen. nov. sp. nov., a strictly anaerobic bacterium utilizing dichloromethane as source of carbon and energy. *Archives of Microbiology*, 166(2), 101–108.
- Malachowsky, K. J., Phelps, T. J., Teboli, A. B., Minnikin, D. E., & White, D. C. (1994). Aerobic mineralization of trichloroethylene, vinyl chloride, and aromatic compounds by *Rhodococcus* species. *Applied and Environmental Microbiology*, 60(2), 542–548.
- Malard, L. A., & Guisan, A. (2023). Into the microbial niche. *Trends in Ecology & Evolution*, 38(10), 936–945.
- Martineau, C., Mauffrey, F., & Villemur, R. (2015). Comparative analysis of denitrifying activities of *Hyphomicrobium nitratorans*, *Hyphomicrobium denitrificans*, and *Hyphomicrobium zavarzinii*. *Applied and Environmental Microbiology*, 81(15), 5003–5014.
- Maucourt, B. (2019). *Régulation in labo et in situ de l'expression de génomes de souches bactériennes méthylotrophes dégradant le dichlorométhane* (Doctoral dissertation, University of Strasbourg).
- Maucourt, B., Vuilleumier, S., & Bringel, F. (2020). Transcriptional regulation of organohalide pollutant utilisation in bacteria. *FEMS Microbiology Reviews*, 44(2), 189–207.
- McCulloch, A. (2017). Dichloromethane in the environment. *A Note Prepared for the European Chlorinated Solvents Association (ECSA) and the Halogenated Solvent Industry Alliance (HSIA)*. Link: [Note](#). Accessed on 22/10/2024.

- McGuire, T. M., Newell, C. J., Looney, B. B., Vangelas, K. M., & Sink, C. H. (2004). Historical analysis of monitored natural attenuation: a survey of 191 chlorinated solvent sites and 45 solvent plumes. *Remediation Journal*, *15*(1), 99–112.
- McKew, B. A., Taylor, J. D., McGenity, T. J., & Underwood, G. J. C. (2011). Resistance and resilience of benthic biofilm communities from a temperate saltmarsh to desiccation and rewetting. *The ISME Journal*, *5*(1), 30–41.
- McMurdie, P. J., & Holmes, S. (2013). phyloseq: An R package for reproducible interactive analysis and graphics of microbiome census data. *PLOS ONE*, *8*(4), e61217.
- Michener, J. K., Camargo Neves, A. A., Vuilleumier, S., Bringel, F., & Marx, C. J. (2014). Effective use of a horizontally-transferred pathway for dichloromethane catabolism requires post-transfer refinement. *eLife*, *3*, e04279.
- Miyake-Nakayama, C., Ikatsu, H., Kashihara, M., Tanaka, M., Arita, M., Miyoshi, S., & Shinoda, S. (2006). Biodegradation of dichloromethane by the polyvinyl alcohol-immobilized methylotrophic bacterium *Ralstonia metallidurans* PD11. *Applied Microbiology and Biotechnology*, *70*(5), 625–630.
- Monferrán, M. V., Echenique, J. R., & Wunderlin, D. A. (2005). Degradation of chlorobenzenes by a strain of *Acidovorax avenae* isolated from a polluted aquifer. *Chemosphere*, *61*(1), 98–106.
- Moyano, F. E., Manzoni, S., & Chenu, C. (2013). Responses of soil heterotrophic respiration to moisture availability: an exploration of processes and models. *Soil Biology and Biochemistry*, *59*, 72–85.
- Mueller, O., Lightfoot, S., & Schroeder, A. (2004). RNA integrity number (RIN)–standardization of RNA quality control. *Agilent application note*, *1*, 1-8.
- Mulder, I., Huber, S. G., Krause, T., Zetzsch, C., Kotte, K., Dultz, S., & Schöler, H. F. (2013). A new purge and trap headspace technique to analyze low volatile compounds from fluid inclusions of rocks and minerals. *Chemical Geology*, *358*, 148–155.
- Muller, E. E. L., Bringel, F., & Vuilleumier, S. (2011a). Dichloromethane-degrading bacteria in the genomic age. *Research in Microbiology*, *162*(9), 869–876.
- Muller, E. E. L., Hourcade, E., Louhichi-Jelail, Y., Hammann, P., Vuilleumier, S., & Bringel, F. (2011b). Functional genomics of dichloromethane utilization in *Methylobacterium extorquens* DM4. *Environmental Microbiology*, *13*(9), 2518–2535.
- Muñoz-Egea, M.-C., Akir, A., & Esteban, J. (2023). *Mycobacterium* biofilms. *Biofilm*, *5*, 100107.

- Murdoch, R. W., Chen, G., Kara Murdoch, F., Mack, E. E., Villalobos Solis, M. I., Hettich, R. L., & Löffler, F. E. (2022). Identification and widespread environmental distribution of a gene cassette implicated in anaerobic dichloromethane degradation. *Global Change Biology*, *28*(7), 2396–2412.
- Nakagawa, T., Mitsui, R., Tani, A., Sasa, K., Tashiro, S., Iwama, T., Hayakawa, T., & Kawai, K. (2012). A catalytic role of XoxF1 as La³⁺-dependent methanol dehydrogenase in *Methylobacterium extorquens* strain AM1. *PLoS One*, *7*(11), e50480.
- Nikolausz, M., Kappelmeyer, U., Nijenhuis, I., Ziller, K., & Kästner, M. (2005). Molecular characterization of dichloromethane-degrading *Hyphomicrobium* strains using 16S rDNA and DCM dehalogenase gene sequences. *Systematic and Applied Microbiology*, *28*(7), 582–587.
- Noyer, M., Bernard, M., Verneau, O., & Palacios, C. (2023). Insights on the particle-attached riverine archaeal community shifts linked to seasons and to multipollution during a Mediterranean extreme storm event. *Environmental Science and Pollution Research*, *30*(17), 49685–49702.
- Or, D., Smets, B. F., Wraith, J. M., Dechesne, A., & Friedman, S. P. (2007). Physical constraints affecting bacterial habitats and activity in unsaturated porous media – a review. *Advances in Water Resources*, *30*(6–7), 1505–1527.
- Oren, A., & Xu, X.-W. (2014). The family *Hyphomicrobiaceae*. *The Prokaryotes*, *247*, 281.
- Osuna, M. B., Sipma, J., Emanuelsson, M. A. E., Carvalho, M. F., & Castro, P. M. L. (2008). Biodegradation of 2-fluorobenzoate and dichloromethane under simultaneous and sequential alternating pollutant feeding. *Water Research*, *42*(14), 3857–3869.
- Ottengraf, S. P. P., Meesters, J. J. P., van den Oever, A. H. C., & Rozema, H. R. (1986). Biological elimination of volatile xenobiotic compounds in biofilters. *Bioprocess Engineering*, *1*(2), 61–69.
- Pacholak, A., Smulek, W., Jesionowski, T., & Kaczorek, E. (2017). The ability of *Achromobacter* sp. KW1 strain to biodegrade isomers of chlorotoluene. *Journal of Chemical Technology & Biotechnology*, *92*(8), 2134–2141.
- Parsons Engineering Science Inc Denver Co. (2009). Field-scale evaluation of monitored natural attenuation for dissolved chlorinated solvent plumes. Link: [Document](#). Accessed: 22/10/2024.
- Payton, R. L., Chiarella, D., & Kingdon, A. (2022). The influence of grain shape and size on the relationship between porosity and permeability in sandstone: A digital approach. *Scientific Reports*, *12*(1), 7531.

- Peralta, A. L., Ludmer, S., Matthews, J. W., & Kent, A. D. (2014). Bacterial community response to changes in soil redox potential along a moisture gradient in restored wetlands. *Ecological Engineering*, *73*, 246–253.
- Plante, C. J. (2017). Defining disturbance for microbial ecology. *Microbial Ecology*, *74*(2), 259–263.
- Preece, C., Verbruggen, E., Liu, L., Weedon, J. T., & Peñuelas, J. (2019). Effects of past and current drought on the composition and diversity of soil microbial communities. *Soil Biology and Biochemistry*, *131*, 28–39.
- Prieto-Espinoza, M., Roupert, R. D. C., Muller, E. E. L., Vuilleumier, S., Imfeld, G., & Weill, S. (2023). Combining multi-phase flow and pathway-specific reactive transport modeling to investigate the impact of water table fluctuations on dichloromethane biodegradation. *Advances in Water Resources*, *180*, 104519.
- Prieto-Espinoza, M., Weill, S., Belfort, B., Muller, E. E. L., Masbou, J., Lehmann, F., Vuilleumier, S., & Imfeld, G. (2021). Water table fluctuations affect dichloromethane biodegradation in lab-scale aquifers contaminated with organohalides. *Water Research*, *203*, 117530.
- Pritchard, P. H., & Bourquin, A. W. (1984). The use of microcosms for evaluation of interactions between pollutants and microorganisms. In *Advances in Microbial Ecology* (pp. 133-215). Boston, MA: Springer US.
- Pronk, G. J., Mellage, A., Milojevic, T., Smeaton, C. M., Engel, K., Neufeld, J. D., Rezanezhad, F., & van Cappellen, P. (2020). Carbon turnover and microbial activity in an artificial soil under imposed cyclic drainage and imbibition. *Vadose Zone Journal*, *19*(1), e20021.
- Quinn, T. P., Erb, I., Richardson, M. F., & Crowley, T. M. (2018). Understanding sequencing data as compositions: an outlook and review. *Bioinformatics*, *34*(16), 2870–2878.
- Radding, S. B., Liu, D. H., Johnson, H. L., & Mill, T. (1977). *Review of the environmental fate of selected chemicals* (p. 147). National Technical Information Service.
- Ranjard, L., Poly, F., Combrisson, J., Richaume, A., Gourbière, F., Thioulouse, J., & Nazaret, S. (2000). Heterogeneous cell density and genetic structure of bacterial pools associated with various soil microenvironments as determined by enumeration and DNA fingerprinting approach (RISA). *Microbial Ecology*, *39*(4), 263–272.
- R Core Team (2020). R language and environment for statistical computing, R foundation for statistical. *Computing*.

- Reitz, R. H., Mendrala, A. L., Park, C. N., Andersen, M. E., & Guengerich, F. P. (1988). Incorporation of *in vitro* enzyme data into the physiologically-based pharmacokinetic (PB-PK) model for methylene chloride: implications for risk assessment. *Toxicology Letters*, *43*(1), 97–116.
- Rensing, C., & Grass, G. (2003). *Escherichia coli* mechanisms of copper homeostasis in a changing environment. *FEMS Microbiology Reviews*, *27*(2–3), 197–213.
- Rezanezhad, F., Couture, R.-M., Kovac, R., O’Connell, D., & Van Cappellen, P. (2014). Water table fluctuations and soil biogeochemistry: An experimental approach using an automated soil column system. *Journal of Hydrology*, *509*, 245–256.
- Robinson, J. T., Thorvaldsdóttir, H., Winckler, W., Guttman, M., Lander, E. S., Getz, G., & Mesirov, J. P. (2011). Integrative genomics viewer. *Nature Biotechnology*, *29*(1), 24–26.
- Rosenberg, D. B., & Freedman, S. M. (1994). Temporal heterogeneity and ecological community structure. *International Journal of Environmental Studies*, *46*(2–3), 97–102.
- Rudolph, J., Khedim, A., Koppmann, R., & Bonsang, B. (1995). Field study of the emissions of methyl chloride and other halocarbons from biomass burning in Western Africa. *Journal of Atmospheric Chemistry*, *22*(1), 67–80.
- Rykiel Jr, E. J. (1985). Towards a definition of ecological disturbance. *Australian Journal of Ecology*, *10*(3), 361–365.
- Schimel, J. P. (2018). Life in dry soils: Effects of drought on soil microbial communities and processes. *Annual Review of Ecology, Evolution, and Systematics*, *49*(1), 409–432.
- Schjønning, P., Thomsen, I. K., Moldrup, P., & Christensen, B. T. (2003). Linking soil microbial activity to water- and air-phase contents and diffusivities. *Soil Science Society of America Journal*, *67*(1), 156–165.
- Schlosser, P. M., Bale, A. S., Gibbons, C. F., Wilkins, A., & Cooper, G. S. (2015). Human health effects of dichloromethane: key findings and scientific issues. *Environmental Health Perspectives*, *123*(2), 114–119.
- Schmidt, S., Christen, P., Kiefer, P., & Vorholt, J. A. (2010). Functional investigation of methanol dehydrogenase-like protein XoxF in *Methylobacterium extorquens* AM1. *Microbiology*, *156*(8), 2575–2586.
- Schwandner, F. M., Seward, T. M., Gize, A. P., Hall, K., & Dietrich, V. J. (2013). Halocarbons and other trace heteroatomic organic compounds in volcanic gases from Vulcano (Aeolian Islands, Italy). *Geochimica et Cosmochimica Acta*, *101*, 191–221.

- Sessitsch, A., Weilharter, A., Gerzabek, M. H., Kirchmann, H., & Kandeler, E. (2001). Microbial population structures in soil particle size fractions of a long-term fertilizer field experiment. *Applied and Environmental Microbiology*, 67(9), 4215–4224.
- Shade, A. (2023). Microbiome rescue: Directing resilience of environmental microbial communities. *Current Opinion in Microbiology*, 72, 102263.
- Shade, A., Peter, H., Allison, S. D., Baho, D., Berga, M., Bürgmann, H., ... & Handelsman, J. (2012). Fundamentals of microbial community resistance and resilience. *Frontiers in microbiology*, 3, 417.
- Shade, A., Read, J. S., Welkie, D. G., Kratz, T. K., Wu, C. H., & McMahon, K. D. (2011). Resistance, resilience and recovery: aquatic bacterial dynamics after water column disturbance. *Environmental Microbiology*, 13(10), 2752–2767.
- Sheik, A. R., Muller, E. E. L., Audinot, J.-N., Lebrun, L. A., Gysan, P., Guignard, C., & Wilmes, P. (2016). *In situ* phenotypic heterogeneity among single cells of the filamentous bacterium *Candidatus Microthrix parvicella*. *The ISME journal*, 10(5), 1274–1279.
- Shen, R., Yu, L., Xu, P., Liang, Z., Lu, Q., Liang, D., ... & Wang, S. (2021). Water content as a primary parameter determines microbial reductive dechlorination activities in soil. *Chemosphere*, 267, 129152.
- Sheng, Y., Li, G., Dong, H., Liu, Y., Ma, L., Yang, M., Liu, Y., Liu, J., Deng, S., & Zhang, D. (2021). Distinct assembly processes shape bacterial communities along unsaturated, groundwater fluctuated, and saturated zones. *Science of The Total Environment*, 761, 143303.
- Shestakova, M., & Sillanpää, M. (2013). Removal of dichloromethane from ground and wastewater: a review. *Chemosphere*, 93(7), 1258–1267.
- Shusterman, D., Quinlan, P., Lowengart, R., & Cone, J. (1990). Methylene chloride intoxication in a furniture refinisher: a comparison of exposure estimates utilizing workplace air sampling and blood carboxyhemoglobin measurements. *Journal of Occupational Medicine*, 32(5), 451–454.
- Silby, M. W., Winstanley, C., Godfrey, S. A. C., Levy, S. B., & Jackson, R. W. (2011). *Pseudomonas* genomes: Diverse and adaptable. *FEMS Microbiology Reviews*, 35(4), 652–680.
- Simmonds, P. G., Manning, A. J., Cunnold, D. M., McCulloch, A., O'Doherty, S., Derwent, R. G., ... & Prinn, R. G. (2006). Global trends, seasonal cycles, and European emissions of dichloromethane, trichloroethene, and tetrachloroethene from the AGAGE observations at Mace Head, Ireland, and Cape Grim, Tasmania. *Journal of Geophysical Research: Atmospheres*, 111(D18).

- Skopp, J., Jawson, M. D., & Doran, J. W. (1990). Steady-state aerobic microbial activity as a function of soil water content. *Soil Science Society of America Journal*, 54(6), 1619–1625.
- Skovran, E., Palmer, A. D., Rountree, A. M., Good, N. M., & Lidstrom, M. E. (2011). XoxF is required for expression of methanol dehydrogenase in *Methylobacterium extorquens* AM1. *Journal of Bacteriology*, 193(21), 6032–6038.
- Smith, H. J., Zelaya, A. J., De León, K. B., Chakraborty, R., Elias, D. A., Hazen, T. C., ... & Fields, M. W. (2018). Impact of hydrologic boundaries on microbial planktonic and biofilm communities in shallow terrestrial subsurface environments. *FEMS Microbiology Ecology*, 94(12), fiy191.
- Smith, T. P., Mombrikotb, S., Ransome, E., Kontopoulos, D.-G., Pawar, S., & Bell, T. (2022). Latent functional diversity may accelerate microbial community responses to temperature fluctuations. *eLife*, 11, e80867.
- Soder-Walz, J. M., Deobald, D., Vicent, T., Marco-Urrea, E., & Adrian, L. (2024). MecE, MecB, and MecC proteins orchestrate methyl group transfer during dichloromethane fermentation. *Applied and Environmental Microbiology*, 90(10), e00978-24.
- Stewart, R. D., & Dodd, H. C. (1964). Absorption of carbon tetrachloride, trichloroethylene, tetrachloroethylene, methylene chloride, and 1, 1, 1-trichloroethane through the human skin. *American Industrial Hygiene Association Journal*, 25(5), 439–446.
- Stres, B., Philippot, L., Faganeli, J., & Tiedje, J. M. (2010). Frequent freeze–thaw cycles yield diminished yet resistant and responsive microbial communities in two temperate soils: A laboratory experiment. *FEMS Microbiology Ecology*, 74(2), 323–335.
- Stucki, G., Gälli, R., Ebersold, H.-R., & Leisinger, T. (1981). Dehalogenation of dichloromethane by cell extracts of *Hyphomicrobium* DM2. *Archives of Microbiology*, 130, 366-371.
- Su, S., Panmanee, W., Wilson, J. J., Mahtani, H. K., Li, Q., VanderWielen, B. D., ... & Hassett, D. J. (2014). Catalase (KatA) plays a role in protection against anaerobic nitric oxide in *Pseudomonas aeruginosa*. *PLoS One*, 9(3), e91813.
- Takahashi, S., Tomita, J., Nishioka, K., Hisada, T., & Nishijima, M. (2014). Development of a prokaryotic universal primer for simultaneous analysis of bacteria and archaea using next-generation sequencing. *PLoS One*, 9(8), e105592.
- The Galaxy Community. (2024). The Galaxy platform for accessible, reproducible, and collaborative data analyses: 2024 update. *Nucleic Acids Research*, 52(W1), W83–W94.

- Tirandaz, H., Dastgheib, S. M. M., Amoozegar, M. A., Shavandi, M., de la Haba, R. R., & Ventosa, A. (2015). *Pseudorhodoplanes sinuspersici* gen. nov., sp. nov., isolated from oil-contaminated soil. *International Journal of Systematic and Evolutionary Microbiology*, *65*(12), 4743–4748.
- Torgonskaya, M. L., Doronina, N. V., Hourcade, E., Trotsenko, Y. A., & Vuilleumier, S. (2011). Chloride-associated adaptive response in aerobic methylotrophic dichloromethane-utilising bacteria. *Journal of Basic Microbiology*, *51*(3), 296–303.
- Travkin, V. m, Jadan, A. p, Briganti, F., Scozzafava, A., & Golovleva, L. a. (1997). Characterization of an intradiol dioxygenase involved in the biodegradation of the chlorophenoxy herbicides 2,4-D and 2,4,5-T. *FEBS Letters*, *407*(1), 69–72.
- Trueba-Santiso, A., Fernández-Verdejo, D., Marco-Rius, I., Soder-Walz, J. M., Casabella, O., Vicent, T., & Marco-Urrea, E. (2020). Interspecies interaction and effect of co-contaminants in an anaerobic dichloromethane-degrading culture. *Chemosphere*, *240*, 124877.
- Tyagi, M., da Fonseca, M. M. R., & de Carvalho, C. C. C. R. (2011). Bioaugmentation and biostimulation strategies to improve the effectiveness of bioremediation processes. *Biodegradation*, *22*(2), 231–241.
- Uhlířová, E., Elhottová, D., Tříška, J., & Šantrůčková, H. (2005). Physiology and microbial community structure in soil at extreme water content. *Folia Microbiologica*, *50*(2), 161–166.
- Vallenet, D., Calteau, A., Dubois, M., Amours, P., Bazin, A., Beuvin, ... & Médigue, C. (2020). MicroScope: an integrated platform for the annotation and exploration of microbial gene functions through genomic, pangenomic and metabolic comparative analysis. *Nucleic Acids Research*, *48*(D1), D579–D589.
- Van Ophem, P. W., & Duine, J. A. (1990). Different types of formaldehyde-oxidizing dehydrogenases in *Nocardia* species 239: Purification and characterization of an NAD-dependent aldehyde dehydrogenase. *Archives of Biochemistry and Biophysics*, *282*(2), 248–253.
- Vangnai, A. S., & Arp, D. J. (2001). An inducible 1-butanol dehydrogenase, a quinohaemoprotein, is involved in the oxidation of butane by ‘*Pseudomonas butanovora*’. *Microbiology*, *147*(3), 745–756.
- Vieira, P. A., Vieira, R. B., Faria, S., Ribeiro, E. J., & Cardoso, V. L. (2009). Biodegradation of diesel oil and gasoline contaminated effluent employing intermittent aeration. *Journal of Hazardous Materials*, *168*(2), 1366–1372.

- Vitte, I., Duran, R., Jézéquel, R., Caumette, P., & Cravo-Laureau, C. (2011). Effect of oxic/anoxic switches on bacterial communities and PAH biodegradation in an oil-contaminated sludge. *Environmental Science and Pollution Research*, *18*(6), 1022–1032.
- Vuilleumier, S. (2002). Coping with a halogenated one-carbon diet: aerobic dichloromethane-mineralising bacteria. In *Biotechnology for the Environment: Strategy and Fundamentals* (pp. 105-130). Dordrecht: Springer Netherlands.
- Vuilleumier, S., Chistoserdova, L., Lee, M. C., Bringel, F., Lajus, A., Zhou, Y., ... & Lidstrom, M. E. (2009). *Methylobacterium* genome sequences: a reference blueprint to investigate microbial metabolism of C1 compounds from natural and industrial sources. *PLoS One*, *4*(5), e5584.
- Vuilleumier, S., Ivoš, N., Dean, M., & Leisinger, T. (2001). Sequence variation in dichloromethane dehalogenases/glutathione S-transferases. *Microbiology*, *147*, 611–619.
- Wang, H., Zhang, S., Pratush, A., Ye, X., Xie, J., Wei, H., Sun, C., & Hu, Z. (2018). Acclimation of culturable bacterial communities under the stresses of different organic compounds. *Frontiers in Microbiology*, *9*, 225.
- Ward, D. B., Tizaoui, C., & Slater, M. J. (2005). Continuous extraction and destruction of chloro-organics in wastewater using ozone-loaded Volasil™245 solvent. *Journal of Hazardous Materials*, *125*(1), 65–79.
- Warholm, M., Alexandrie, A.-K., Högberg, J., Sigvardsson, K., & Rannug, A. (1994). Polymorphic distribution of glutathione transferase activity with methyl chloride in human blood. *Pharmacogenetics and Genomics*, *4*(6), 307.
- Wasmund, K., Trueba-Santiso, A., Vicent, T., Adrian, L., Vuilleumier, S., & Marco-Urrea, E. (2023). Proteogenomics of the novel *Dehalobacterium formicoaceticum* strain EZ94 highlights a key role of methyltransferases during anaerobic dichloromethane degradation. *Environmental Science and Pollution Research International*, *30*(33), 80602–80612.
- Watts, R. J., & Teel, A. L. (2006). Treatment of contaminated soils and groundwater using ISCO. *Practice Periodical of Hazardous, Toxic, and Radioactive Waste Management*, *10*(1), 2–9.
- Wei, Y., Chen, Y., Cao, X., Xiang, M., Huang, Y., & Li, H. (2024). A critical review of groundwater table fluctuation: formation, effects on multifeilds, and contaminant behaviors in a soil and aquifer system. *Environmental Science & Technology*, *58*(5), 2185–2203.

- White, P. S., MacKenzie, M. D., & Busing, R. T. (1985). Natural disturbance and gap phase dynamics in southern Appalachian spruce–fir forests. *Canadian Journal of Forest Research*, *15*(1), 233–240.
- Whittaker, R. H. (1972). Evolution and measurement of species diversity. *Taxon*, *21*(2–3), 213–251.
- Wickham, H., & Wickham, H. (2016). *Data analysis* (pp. 189–201). Springer International Publishing.
- Wilson, F. P., Liu, X., Mattes, T. E., & Cupples, A. M. (2016). *Nocardioides*, *Sediminibacterium*, *Aquabacterium*, *Variovorax*, and *Pseudomonas* linked to carbon uptake during aerobic vinyl chloride biodegradation. *Environmental Science and Pollution Research*, *23*(19), 19062–19070.
- Wu, S. J., Hu, Z. H., Zhang, L. L., Yu, X., & Chen, J. M. (2009). A novel dichloromethane-degrading *Lysinibacillus sphaericus* strain wh22 and its degradative plasmid. *Applied Microbiology and Biotechnology*, *82*(4), 731–740.
- Wu, W.-Y., Lo, M.-H., Wada, Y., Famiglietti, J. S., Reager, J. T., Yeh, P. J.-F., Ducharme, A., & Yang, Z.-L. (2020). Divergent effects of climate change on future groundwater availability in key mid-latitude aquifers. *Nature Communications*, *11*(1), 3710.
- Xu, L., Baldocchi, D. D., & Tang, J. (2004). How soil moisture, rain pulses, and growth alter the response of ecosystem respiration to temperature. *Global Biogeochemical Cycles*, *18*(4).
- Yanpirat, P., Nakatsuji, Y., Hiraga, S., Fujitani, Y., Izumi, T., Masuda, S., ... & Tani, A. (2020). Lanthanide-dependent methanol and formaldehyde oxidation in *Methylobacterium aquaticum* strain 22A. *Microorganisms*, *8*(6), 822.
- Yerke, A., Fry Brumit, D., & Fodor, A. A. (2024). Proportion-based normalizations outperform compositional data transformations in machine learning applications. *Microbiome*, *12*(1), 45.
- Yu, J., Cai, W., Cheng, Z., & Chen, J. (2014). Degradation of dichloromethane by an isolated strain *Pandoraea pnomenusa* and its performance in a biotrickling filter. *Journal of Environmental Sciences*, *26*(5), 1108–1117.
- Yu, J., Chen, J., & Wang, J. (2006). Removal of dichloromethane from waste gases by a biotrickling filter. *Journal of Environmental Sciences*, *18*(6), 1073–1076.
- Zhang, M., Geng, S., & Ustin, S. L. (1998). Quantifying the agricultural landscape and assessing spatio-temporal patterns of precipitation and groundwater use. *Landscape Ecology*, *13*(1), 37–54.

- Zhang, Z., & Furman, A. (2021). Soil redox dynamics under dynamic hydrologic regimes—A review. *Science of The Total Environment*, 763, 143026.
- Zhang, Z., Schwartz, S., Wagner, L., & Miller, W. (2000). A greedy algorithm for aligning DNA sequences. *Journal of Computational Biology*, 7(1–2), 203–214.
- Zhou, J., Jiang, Y.-H., Deng, Y., Shi, Z., Zhou, B. Y., Xue, K., Wu, L., He, Z., & Yang, Y. (2013). Random sampling process leads to overestimation of β -diversity of microbial communities. *mBio*, 4(3), 10.1128/mbio.00324-13.
- Zhou, J., Xia, B., Treves, D. S., Wu, L.-Y., Marsh, T. L., O'Neill, R. V., Palumbo, A. V., & Tiedje, J. M. (2002). Spatial and resource factors influencing high microbial diversity in soil. *Applied and Environmental Microbiology*, 68(1), 326–334.
- Zhou, P., Wang, G., & Duan, R. (2020). Impacts of long-term climate change on the groundwater flow dynamics in a regional groundwater system: Case modeling study in Alashan, China. *Journal of Hydrology*, 590, 125557.
- Zoeteman, B. C. J., Harmsen, K., Linders, J. B. H. J., Morra, C. F. H., & Slooff, W. (1980). Persistent organic pollutants in river water and ground water of the Netherlands. *Chemosphere*, 9(4), 231–249.

Annexe I

Annexe II

Scientific communications

Oral presentations

- **Lázaro Sánchez, C.**, Prieto-Espinoza, M., Vuilleumier, S., Imfeld, G., Muller, E. E. L. (2021). Dichloromethane degradation by microbial communities of polluted aquifers is affected by water and oxygen contents - Online flash presentation for EcotoxicomicYR webinar, 22nd of November 2021.
- **Lázaro Sánchez, C.**, Imfeld, G., Vuilleumier, S., Muller, E. E. L. (2023). Groundwater level fluctuations impact the dichloromethane bacterial community structure by governing oxygen tension - Flash presentation for Doctoral School Days of the University of Strasbourg, 20th of April 2023.
- **Lázaro Sánchez, C.**, Imfeld, G., Vuilleumier, S., Muller, E. E. L. (2023). Dichloromethane biodegradation in groundwater is mainly impacted by changes in oxygen tension caused by water table fluctuations - Online oral presentation for EcotoxicomicYR webinar, 13th of November 2023.
- **Lázaro Sánchez, C.**, Imfeld, G., Vuilleumier, S., Muller, E. E. L. (2024). Bacterial degradation of dichloromethane in aquifers depends on matrix granulometry - Oral presentation for Séminaire de Microbiologie de Strasbourg, 4th of April 2024.
- Lázaro Sánchez, C., Imfeld, G., Vuilleumier, S., **Muller, E. E. L.** (2024). Bacterial degradation of the halogenated solvent dichloromethane in microcosms of aquifer: impact of physico-chemical disturbances - Oral presentation for Microbes, Congrès national de la Société Française de Microbiologie à Lille, 7-9th of October 2024.

Poster presentations

- **Lázaro Sánchez, C.**, Prieto-Espinoza, M., Vuilleumier, S., Imfeld, G., Muller, E. E. L. (2022). Impact of oxic conditions and water content on a dichloromethane-degrading microbial community - Poster presented for Séminaire de Microbiologie de Strasbourg, 24th of March 2022.
- **Lázaro Sánchez, C.**, Imfeld, G., Vuilleumier, S., Muller, E. E. L. (2023). Impact of abiotic conditions on a dichloromethane-degrading microbial community - Poster presented for Séminaire de Microbiologie de Strasbourg, 23rd of March 2023.
- **Lázaro Sánchez, C.**, Imfeld, G., Vuilleumier, S., Muller, E. E. L. (2023). Dichloromethane biodegradation in groundwater is mainly impacted by changes in oxygen tension caused by water table fluctuations - Poster presented for Bageco congress at Copenhagen, 26-30th of June 2023.

- Lázaro Sánchez, C., Imfeld, G., Vuilleumier, S., **Muller, E. E. L.** (2023). Bacterial degradation of the toxic halogenated solvent dichloromethane in aquifer microcosms: impact of disturbances in physico-chemical parameters - Poster presented for International Conference in Microbial Ecotoxicology at Gothenburg, 12-14th of November 2024.

Publications

- Hayoun, K., Geersens, E., Laczny, C. C., Halder, R., **Lázaro Sánchez, C.**, Manna, A., Bringel, F., Ryckelynck, M., Wilmes, P., Muller, E. E. L., Alpha-Bazin, B., Armengaud, J., & Vuilleumier, S. (2020). Dichloromethane degradation pathway from unsequenced *Hyphomicrobium* sp. MC8b rapidly explored by pan-proteomics. *Microorganisms*, 8(12), 1876. (see in **Annexe 1**).
- In preparation: publication involving the work here presented at **chapter V**.

Supervision

- Clothilde HUTER (1st year of BTS)
Co-supervision with Emilie MULLER

PhD trainings

- Introduction to R
- Advanced programming in R
- Introduction à la statistique
- Modéliser en 2D avec Inkscape
- Effective reading
- Identifying your skills : An introduction to the “portfolio approach”

Microbial degradation of dichloromethane in aquifers: diversity, community dynamics and stability of the function in response to changes in physicochemical parameters

Résumé

Le dichlorométhane (DCM, CH_2Cl_2) est un solvant industriel persistant et toxique fréquemment détecté dans les eaux souterraines. Des études précédentes réalisées sur des aquifères de laboratoire ont révélé que la biodégradation microbienne du DCM, qui peut se produire en conditions oxiques et anoxiques, était plus marquée dans les aquifères subissant des battements de nappe. Ici, j'ai étudié comment l'activité et la composition d'une communauté microbienne dégradant le DCM étaient influencées par trois paramètres physicochimiques clés affectés par les battements de nappe : le contenu en eau, le statut oxique et la granulométrie de la matrice. Les résultats ont montré que le contenu en eau agit comme un premier filtre de sélection, contrôlant l'activité de la communauté dégradant le DCM. Lorsque la teneur en eau n'est pas un facteur limitant, la présence d'oxygène devient le principal facteur influençant à la fois la cinétique de dégradation du DCM et la composition de la communauté microbienne. La granulométrie de la matrice influence également l'activité et la composition de la communauté DCM-dégradante, mais principalement à travers son contrôle sur la teneur en eau. Dans un second temps, l'impact d'un changement d'exposition à l'oxygène a été évalué sur la communauté microbienne dégradant le DCM, ainsi que sur la souche anaérobie facultative, *Hyphomicrobium* sp. GJ21, au niveau transcriptionnel. Les résultats ont montré que ce dérangement a impacté l'activité et la composition de la communauté microbienne et que le maintien ou la perte de l'activité était dépendante du statut initial en oxygène. D'autre part, en réponse au statut oxique, la souche modèle dégradant le DCM *Hyphomicrobium* sp. GJ21 a différenciellement exprimé des gènes liés aux chaînes respiratoires, au cofacteur PQQ et à l'homéostasie des ions. Des recherches futures, sur l'identification des populations microbiennes et des taxons dégradant activement le DCM dans différents scénarios, ainsi qu'autour de la caractérisation de l'importance relative de la taille des grains et des pores de la matrice, amélioreront notre compréhension de la dégradation microbienne du DCM dans les aquifères. L'ensemble de ces connaissances seront nécessaire à la conception de stratégies de bioremédiation plus efficaces prenant mieux en compte les conditions biotique et abiotique dominantes, ainsi que les spécificités hydrogéologiques des différents environnements contaminés.

Mots clés : Battement de nappe, Dérangement, Statut oxique, Conteneur en eau, Granulométrie de la matrice

Abstract

Dichloromethane (DCM, CH_2Cl_2) is a persistent and toxic industrial solvent frequently detected in groundwater. Previous work with laboratory-scale aquifers demonstrated that DCM biodegradation, that occurs under both oxic and anoxic conditions, was more pronounced during groundwater level fluctuations. In this work, I investigated how the activity and composition of a DCM-degrading microbial community are impacted by three key physicochemical parameters affected by groundwater level fluctuations: water content, oxygen status, and soil matrix granulometry. Results showed that water content acted as a primary selection barrier, controlling the activity of the DCM-degrading community. When water content was not a limiting factor, oxygen status became the main parameter shaping both the DCM degradation kinetics and microbial community composition. Matrix granulometry also influenced the activity and composition of the DCM-degrading community, but mainly through its control over water content. Subsequently, the impact of a change in oxygen status was examined on the DCM-degrading microbial community and on the facultative anaerobic strain *Hyphomicrobium* sp. GJ21 at the transcriptomic level. Results showed that this disturbance influenced both the activity and composition of the microbial community, and that the maintenance or loss of the DCM-degrading activity depended on the initial oxygen status. In the case of the DCM-degrading model strain *Hyphomicrobium* sp. GJ21, its response to oxygen status involved the differential expression of genes related to the respiratory chain, the cofactor PQQ, and ion homeostasis. Future investigations, including the identification of microbial populations and specific taxa actively degrading the DCM under different scenarios, as well as further characterizing the relative importance of the matrix' grain sizes and pore sizes, will improve our understanding of microbial degradation of DCM in the aquifer environment. This knowledge will be essential for designing more effective bioremediation strategies that take better account of the prevailing biotic and abiotic conditions, as well as the hydrogeological characteristics of the various contaminated environments.

Keywords: Groundwater level fluctuations, Disturbance, Oxygen status, Water content, Matrix granulometry